

DTIC FILE COPY

AD-A200 627

AFGL-TR 88-0120

Analysis of Coordinated Observations in the
Region of the Day Side Polar Cleft

D.L. Carpenter
C.R. Clauer

Stanford University
Space, Telecommunications
and Radioscience Laboratory
Stanford, CA 94305

April 1988

Final Report
Period Covered: 23 October 1985 - 22 October 1987

APPROVED FOR PUBLIC RELEASE: DISTRIBUTION UNLIMITED

AIR FORCE GEOPHYSICS LABORATORY
AIR FORCE SYSTEMS COMMAND
UNITED STATES AIR FORCE
HANSCOM AIR FORCE BASE, MASSACHUSETTS 01731-5000

DTIC
ELECTE
OCT 18 1988
S H D

88 10 18 103

AD-A200 627

REPORT DOCUMENTATION PAGE

1a. REPORT SECURITY CLASSIFICATION Unclassified			1b. RESTRICTIVE MARKINGS			
2a. SECURITY CLASSIFICATION AUTHORITY			3. DISTRIBUTION / AVAILABILITY OF REPORT Approved for public release; Distribution unlimited			
2b. DECLASSIFICATION / DOWNGRADING SCHEDULE						
4. PERFORMING ORGANIZATION REPORT NUMBER(S)			5. MONITORING ORGANIZATION REPORT NUMBER(S) AFGL-TR-88-0120			
6a. NAME OF PERFORMING ORGANIZATION Stanford University		6b. OFFICE SYMBOL (If applicable)	7a. NAME OF MONITORING ORGANIZATION Air Force Geophysics Laboratory			
6c. ADDRESS (City, State, and ZIP Code) Space, Telecommunications and Radioscience Laboratory Stanford, CA 94305			7b. ADDRESS (City, State, and ZIP Code) Hanscom AFB Massachusetts 01731-5000			
8a. NAME OF FUNDING / SPONSORING ORGANIZATION		8b. OFFICE SYMBOL (If applicable)	9. PROCUREMENT INSTRUMENT IDENTIFICATION NUMBER F19628-85-K-0001			
8c. ADDRESS (City, State, and ZIP Code)			10. SOURCE OF FUNDING NUMBERS			
			PROGRAM ELEMENT NO 61102F	PROJECT NO. 2311	TASK NO G2	WORK UNIT ACCESSION NO. HG
11. TITLE (Include Security Classification) Analysis of Coordinated Observations in the Region of the Day Side Polar Cleft						
12. PERSONAL AUTHOR(S) D. L. Carpenter, C. R. Clauer						
13a. TYPE OF REPORT FINAL REPORT		13b. TIME COVERED FROM 10/23/85 TO 10/22/87		14. DATE OF REPORT (Year, Month, Day) 1988 April		15. PAGE COUNT 124
16. SUPPLEMENTARY NOTATION						
17. COSATI CODES			18. SUBJECT TERMS (Continue on reverse if necessary and identify by block number)			
FIELD	GROUP	SUB-GROUP	Ionospheric currents; Magnetosphere; Ionospheric plasma convection; Ionosphere coupling Solar wind; Polar cleft.			
19. ABSTRACT (Continue on reverse if necessary and identify by block number) We summarize the results of a data analysis and modeling effort supported at the Stanford University by AFGL Contract F19628-85-K-0001. The objective of the research effort has been to develop electrodynamic models of the connectivity of the dayside high latitude ionosphere with the magnetosphere and solar wind. This is accomplished through the coordinated analysis of a variety of electrodynamic observations utilizing correlative satellite and ground data acquired in the vicinity of the polar cleft. We find very strong evidence for a direct electrical connection between the solar wind and high latitude ionosphere. A model based upon this electrical connection utilizing large scale field-aligned currents in the cleft region reproduces many of the time varying features in the observed high latitude ionospheric electric fields and plasma convection. We examine also the small-scale current structures and expected ionospheric signatures from localized coupling which would be expected from flux transfer events. Analysis of high latitude magnetic data from an array of magnetometers around Sondre Stromfjord (OVER)						
20. DISTRIBUTION / AVAILABILITY OF ABSTRACT <input type="checkbox"/> UNCLASSIFIED/UNLIMITED <input checked="" type="checkbox"/> SAME AS RPT <input type="checkbox"/> DTIC USERS			21. ABSTRACT SECURITY CLASSIFICATION Unclassified			
22a. NAME OF RESPONSIBLE INDIVIDUAL Irving Michael			22b. TELEPHONE (Include Area Code)		22c. OFFICE SYMBOL AFGL/PHG	

220 200 100

CONT OF BLOCK 18:

Field-aligned currents
Flux transfer events

CONT OF BLOCK 19:

Greenland show impulsive events. These magnetic signatures are shown to result from pairs of small scale field-aligned current filaments moving tailward at about 4 Km/sec over the array of stations. These events, however, are inconsistent with present models of FTE current systems. *Keywords: → field-aligned*

TABLE OF CONTENTS

I.	Introduction	1
II.	Large Scale High Latitude Current Systems	5
	Theoretical Introduction	5
	Observations, Analysis and Model Simulations	7
III.	Coordinated Analysis of Satellite and Ground Based Measurements	19
	March 07, 1984: Pre Noon Hours	19
	March 16, 1984: Pre Noon Hours	20
	March 20, 1984: Pre Noon Hours	25
	March 07, 1984: Post Noon Hours	25
	March 16, 1984: Post Noon Hours	37
	Summary	37
IV.	Small Scale Coupling Phenomena	37
V.	References	43
VI.	Appendix 1	47



iii

Accession For	
NTIS GRA&I	<input checked="" type="checkbox"/>
DTIC TAB	<input type="checkbox"/>
Unannounced	<input type="checkbox"/>
Justification	
By _____	
Distribution/	
Availability Codes	
Dist	Avail and/or Special
A-1	

INTRODUCTION

It is now understood that the sun's outer atmosphere, the solar corona, expands supersonically to become the solar wind and that this solar wind carries the solar magnetic field with it into interplanetary space. Upon reaching the Earth, the solar wind plasma and magnetic field interact with the Earth's magnetic field and through this interaction, solar wind energy is coupled to the Earth's magnetosphere and ionosphere. Roughly a few percent of the kinetic power carried by the solar wind plasma impinging on the dayside magnetopause (between 10^{11} and 10^{12} W) enters the magnetosphere to drive currents, energize plasma, and produce a complex pattern of plasma convection (e.g., Hill, 1983; Baker et al., 1985). Much of the extracted solar wind energy is thought to be ultimately dissipated as heat in the Earth's upper atmosphere, while another portion of the extracted energy is thought to be returned to the solar wind by plasmoids which are ejected down the magnetotail during intervals of substorm activity.

The coupling processes which occur at the magnetopause can be divided roughly into two categories. The first is electromagnetic coupling which involves interactions between the solar wind magnetic field and the geomagnetic field (e.g. magnetic reconnection). The second coupling is non magnetic and is generally referred to as a "viscous interaction" (e.g. Kelvin-Helmholtz and impulsive plasma penetration). It appears that electromagnetic coupling provides the major momentum exchange between the solar wind and the magnetosphere (Lee and Roederer, 1982; Podgorny et al., 1978), though there remains considerable debate regarding the possibility that the viscous interactions could be an important or dominant coupling mechanism under some conditions [Reiff and Burch, 1978; Heikkila, 1986 and references therein].

A consequence of the energy coupling at the magnetopause is a system of field-aligned currents whose strength, polarity and configuration vary with the strength and orientation of the interplanetary magnetic field (IMF). These currents provide the electrical coupling between the solar wind MHD dynamo, the magnetosphere, and the conducting ionosphere. The high latitude region 1 currents observed at the polar edge of the auroral zone connect to the boundary layer near the magnetopause. These currents are thought to be driven by the solar wind MHD dynamo electric field and also by polarization electric fields produced by the boundary layer flow. The region 2 currents are thought to connect the equatorward side of the auroral electrojets to the charged Alfvén layers of the inner magnetosphere ring current region. This view of the topology of the region 1 and 2 currents is common and is shown schematically in Figure 1. Recently, however, studies suggest that the dayside and nightside sections of the region 1 and 2 currents may be separated and may be produced by different sources (Friis-Christensen et al., 1985; Spence et al., 1987). On the dayside, a variable system of currents flows in the vicinity of the polar cleft. The cleft system has been modeled as two independent currents controlled respectively by the Y and Z components of the interplanetary magnetic field. These two systems are responsible for producing the well

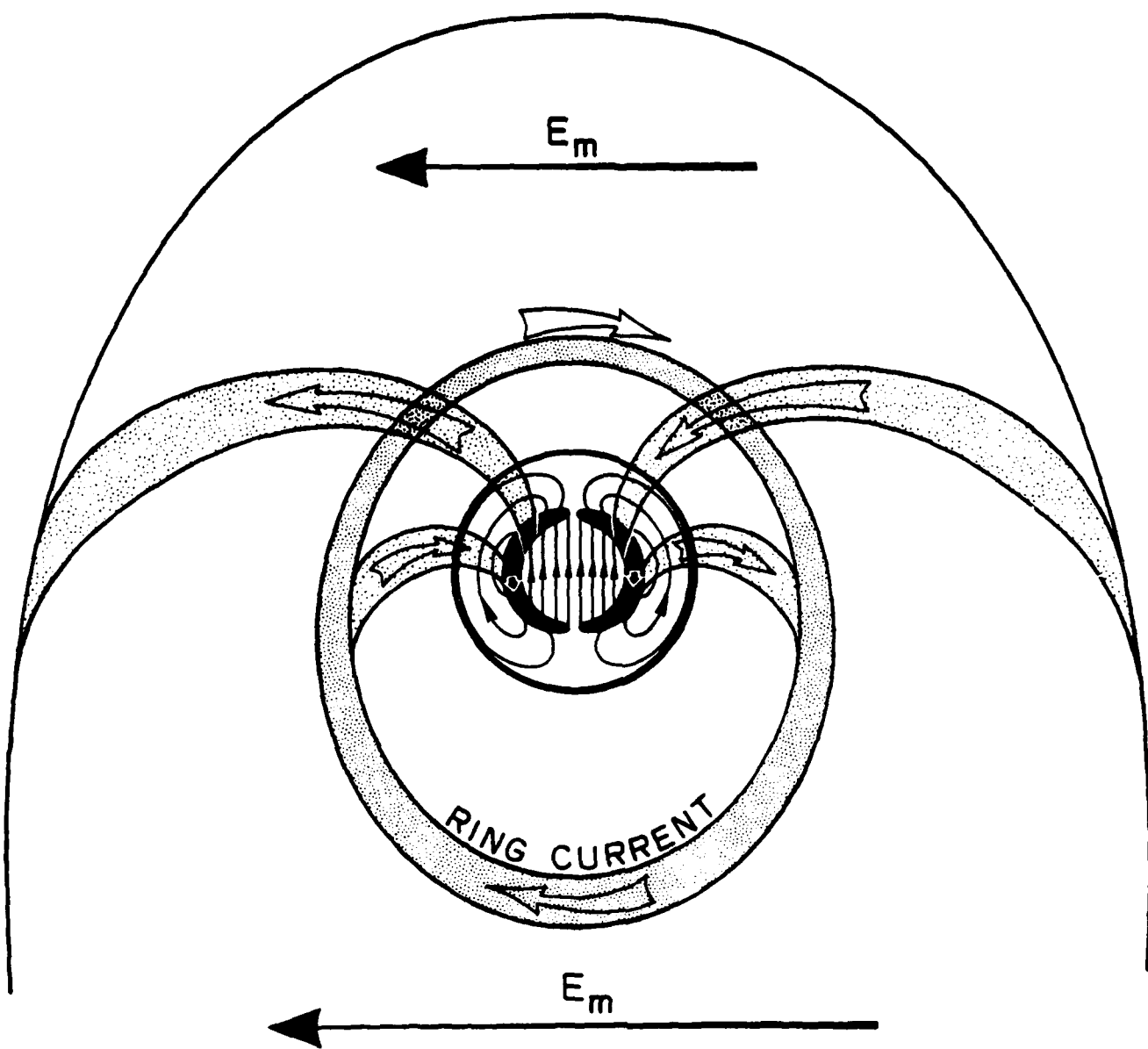
described *DPY* and *DPZ* ground magnetic perturbations which result from the ionospheric Hall currents associated with these systems (D'Angelo, 1980; Banks et al., 1984; Clauer and Banks, 1986; Clauer and Friis-Christensen, 1988). These cleft currents are thought to be driven through a direct electrical connection to the solar wind MHD dynamo at the magnetopause.

Apart from this system of large scale currents, systems of small scale currents are suspected to be associated with other coupling processes which are sporadic, localized, and in some cases, impulsive. These processes include the so called Flux Transfer Events associated with brief, localized reconnection at the magnetopause (Russell and Elphic, 1978; 1979; Paschmann et al, 1982; Saunders et al., 1984) or impulsive plasma penetration in which bursts of plasma penetrate into the magnetopause boundary layer (Heikkila, 1979; Lemaire, 1978). The relative importance of such processes, in addition to Kelvin Helmholtz interactions, is currently an area of controversy and vigorous investigation. For example, recent theoretical work (Southwood, 1987; Lee, 1986) as well as some experimental evidence (Cowley, 1982) suggests that localized reconnection or FTEs at the dayside magnetopause may play a key role in the electrodynamic coupling between the solar wind and the magnetosphere and the ionosphere.

The magnetospheric polar cleft is a dayside topological feature of the magnetosphere through which magnetosheath plasma may penetrate to low altitudes along magnetic field lines which thread the entry and boundary layers of the magnetopause. This is illustrated schematically in Figure 2. The cleft is a latitudinally narrow and longitudinally extended region of solar plasma entry to ionospheric altitudes.

Scientific appreciation of the unique role of the cleft within the magnetosphere - ionosphere system is reflected in the wide variety and increasing numbers of ground-based, rocket, balloon, and satellite investigations which are each contributing new information about the various different physical processes which occur within this relatively small portion of the dayside auroral region and polar cap. Within the overall context of magnetospheric research, studies of the cleft and the phenomena associated with it are beginning to elucidate the full complexity of the interaction of the solar wind with the magnetosphere. There is substantial evidence that the observations within the cleft provide the most direct information about the electrodynamics of the solar wind - magnetosphere - ionosphere interaction since current systems and electric fields within this region appear to respond directly, with little time delay, to variations in the solar wind (Clauer et al., 1984; Clauer and Banks, 1986; Clauer and Friis-Christensen, 1988).

For these reasons, our research efforts have focused upon the coordinated analysis of a variety of electrodynamic observations utilizing correlative satellite and ground data acquired in the vicinity of the polar cleft. In this report, we summarize the results of a three-year analysis and modeling effort supported by AFGL Contract F19628-85-K-0001. The acquisition of the data utilized in



SOLAR WIND-MAGNETOSPHERE DYNAMO AND DP2 EQUIVALENT CURRENT

Figure 1: Schematic representation of region 1 and region 2 currents driven by the solar wind imposed emf E_m . Alfvén layer electric field shielding gives rise to the potential drop between the magnetopause boundary layer and the ring current inner edge. The ionospheric Hall currents which result are similar to the DP2 equivalent current pattern.

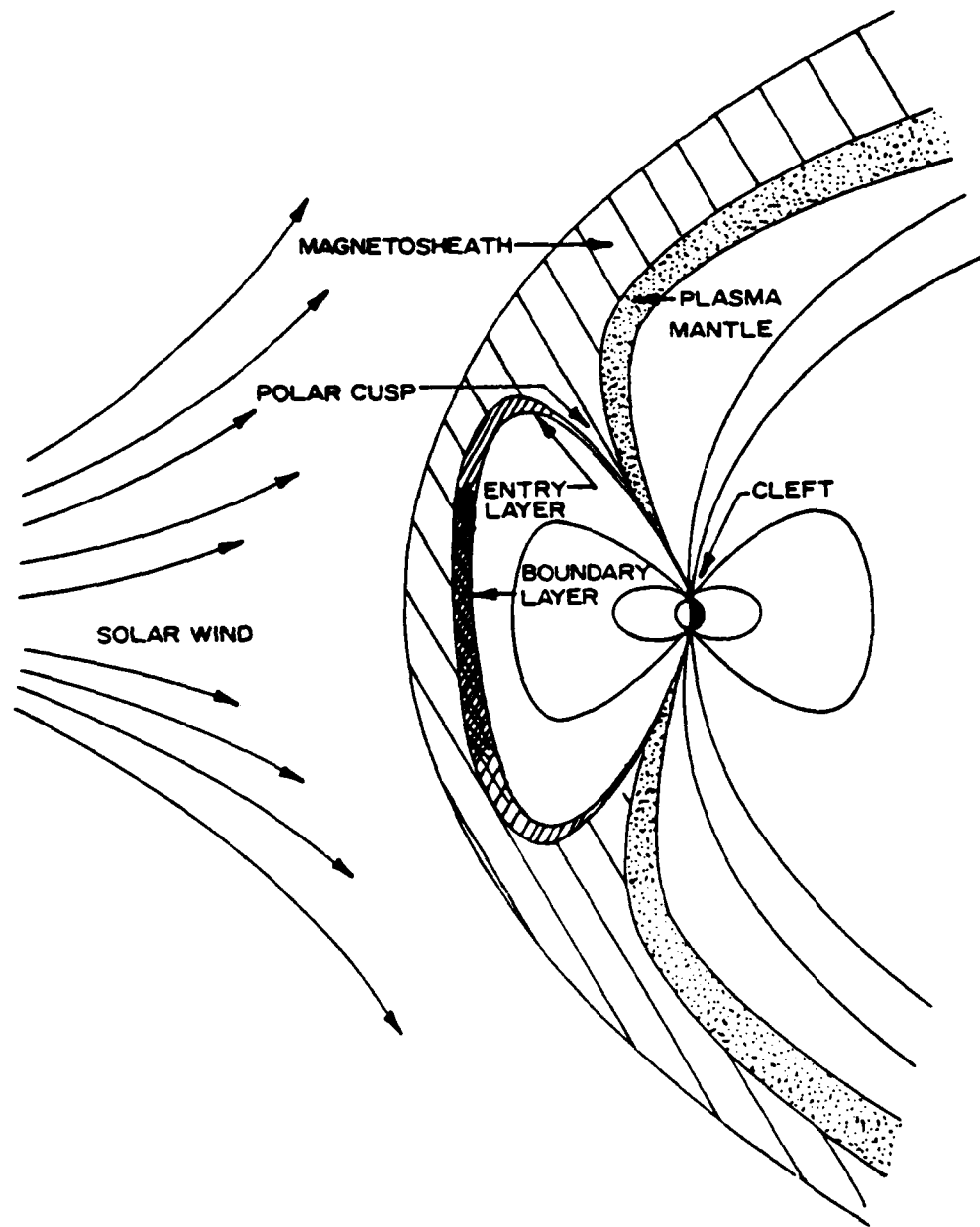


Figure 2: Schematic view of the cusp regions and associated connections to the ionosphere

these investigations has been supported by other sources. The AFGL Contract F19628-85-K-0001 supported the coordinated analysis of these data. The objective of the research effort has been to develop an electrodynamic model of the connectivity of the dayside high latitude ionosphere with the solar wind and magnetosphere. To reach these objectives, our research has been directed along three major divisions: 1) Observations and model simulations of the dayside large scale high latitude current systems, 2) Detailed coordinated analysis of combined satellite and ground based data to elucidate current strengths and configurations under particular solar wind conditions, and 3) The investigation of small scale coupling phenomena through a detailed examination of phenomena occurring in the vicinity of the dayside high latitude convection reversal boundary which we feel are the ionospheric manifestations of processes occurring at the magnetopause and within the entry and boundary layers. Progress within these three areas of investigation are discussed in detail in the following sections.

LARGE SCALE HIGH LATITUDE CURRENT SYSTEMS

THEORETICAL INTRODUCTION

The origin of the polar cap electric field is generally described in terms of two dominant mechanisms acting at the outer edges of the magnetosphere. The first of these is magnetic merging at the dayside magnetopause, a process which depends strongly upon the interplanetary magnetic field (IMF) orientation. The second mechanism is related to a viscous-like interaction at the magnetospheric boundary layer and is responsible for the two-cell convection pattern encompassing the night side polar cap and auroral zone. This process is much less dependent upon the IMF orientation. A number of studies [Friis-Christensen and Wilhelm, 1975; Maezawa, 1976; Friis-Christensen, 1979; Wilhelm et al., 1978; Sergeev and Kuznetsov, 1981; and others] demonstrate the separability of the two mechanisms and provide information about their dependence upon the IMF and solar wind velocity as well as their relationship to the polar cap and auroral zone. The results of these studies indicate that the magnetic field-aligned currents associated with merging are concentrated near the dayside cleft region. Those arising from the boundary mechanism extend towards the midnight sector along the sides of the auroral oval and have been identified as the region 1 currents.

Banks et al., [1984] suggest a model in which the pattern of dayside high latitude field-aligned currents and ionospheric plasma convection is directly determined by the interplanetary electric field (IEF). This model is the result of a synthesis of a variety of observations and the recognition that, due to the geometrical properties of the magnetosphere, the east-west component of the IEF could drive field-aligned currents which connect to the ionosphere at points lying on either side of local noon, while currents associated with the north-south component of the IEF will connect the two polar caps as sheet currents centered at local noon. Figure 3 from Banks et al., [1984] shows a schematic description of these currents and their relationship to the solar wind velocity, magnetic field, and motional electric field.

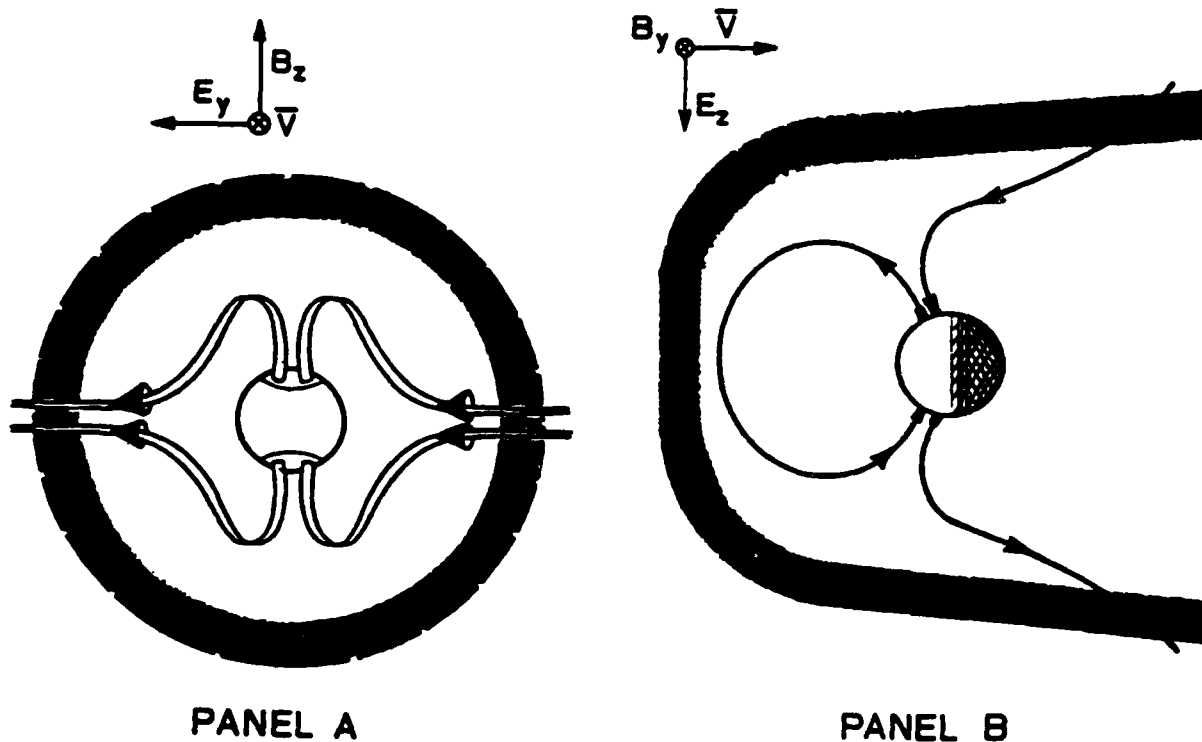


Figure 3: A general view of the way cleft currents driven by the interplanetary electric field connect across the magnetosphere. In Figure 3A, line currents arising from E_y connect from the flanks of the magnetosphere to two discrete zones on either side of local noon. The direction of the current is determined by the sign of B_z , and the case for $B_z > 0$ is shown. In Figure 3B, currents arising from E_z connect to each cleft through sheet currents centered at local noon. Completion of the current circuit through the opposite hemisphere is accomplished by means of a sheet current along closed field lines lying at or near the magnetopause. The direction of currents shown here corresponds to $B_y < 0$. Oppositely directed current would result for $B_y > 0$. After *Banks et al.*, [1984].

This model has guided our research effort to determine the configuration of large scale current systems at high latitudes on the dayside of the magnetosphere and their control by solar wind parameters. These currents, according to the model, are driven by the solar wind emf imposed across the magnetopause. The model follows a simple decomposition of the dayside high latitude field-aligned currents into systems which are separately controlled by the IMF B_y and B_z components (recalling that apart from the solar wind velocity, these are equivalent to the IEF E_z and E_y components).

These field-aligned current systems (shown in Figure 3) are referred to as the *DPY* and *DPZ* current systems as they are associated with the ionospheric systems which have originally been labeled with these names [Friis-Christensen and Wilhelm, 1975]. Here, however, we modify slightly the definition of the *DPZ* disturbance. In the original definition, the *DPZ* disturbance included the entire two-cell current system also known as DP2. We now limit the definition of the *DPZ* system to the more local two-cell pattern observed on the dayside at times when $|B_z| \gg |B_y|$. This system corresponds to the cusp currents statistically described by Iijima and Potemra, [1976] for IMF B_z southward and to the system observed by Araki et al., [1984] and termed NPZ currents by Iijima et al., [1984], Zanetti et al., [1984], and Iijima and Shibaji, [1987]. The *DPY* system is a single ionospheric system produced by Hall currents flowing between a pair of oppositely directed field-aligned current sheets oriented longitudinally across and centered near the noon meridian, as observed by Wilhelm et al., [1978].

OBSERVATIONS, ANALYSIS, AND MODEL SIMULATIONS

Our investigation of the large scale electrodynamic current coupling between the dayside high latitude ionosphere and the solar wind has taken two approaches. Both rely upon high latitude electrodynamic measurements from the Sondre Stromfjord, Greenland incoherent scatter radar as the primary data set.

The first approach uses a numerical computer model to examine the ionospheric electric fields produced by different field-aligned current distributions in the cleft [Rich and Kamide, 1983; Banks et al., 1984]. The model can then, in turn, be compared with measures of ionospheric electric fields obtained by high latitude radars. In our research, we have adapted the computer model used by Banks et al., [1984] to adjust the strength, direction, and location of the *DPY* and *DPZ* field-aligned currents in the polar cleft based upon IMF measurements obtained by the IMP-8 satellite upstream in the solar wind. Then, through a series of steady state calculations, we simulate the temporally varying ionospheric convection pattern produced by the model during a particular interval of time. The simulated convection is then directly compared with the actual convection measured by the Sondre Stromfjord, Greenland radar. Results obtained from the first approach have been presented in two papers, Clauer and Banks [1986] and Clauer and Friis-Christensen

[1988] which are attached in Appendix 1. A brief summary of the results presented in these papers follows.

The initial investigations presented by Clauer and Banks [1986] utilized a distribution of currents which are static in location but changed in strength and direction according to measurements of the IMF B_y and B_z components. Figure 4 shows a polar projection of these field-aligned current distributions in the northern hemisphere. The current distribution includes the region 1 and region 2 currents using the approximate statistical distribution and spatial arrangement from Iijima and Potemra [1976] and the suggested *DPY* and *DPZ* field-aligned currents in the polar cleft from Banks et al., [1984]. This figure shows the current flow directions for the case when $B_z > 0$ and $B_y > 0$. When $B_z = B_y = 0$ no cleft currents would flow and for $B_z < 0$ and $B_y < 0$ the polarities of the cleft currents would reverse. The region 1 and 2 currents are constant in strength and location.

For each measurement time at the Sondre Stromfjord radar, we take the measured IMF at IMP-8 using the appropriate delay time determined from the actual solar wind conditions during the event. Based upon these IMF values, we adjust the strength and direction of the *DPY* and *DPZ* currents and compute the hemispheric electric field distribution. Using the computed electric field, the $\mathbf{E} \times \mathbf{B}$ drift at the radar measurement points are determined and the simulated convection velocity pattern is plotted.

Plates 3, 4, and 5 in Clauer and Banks [1986] attached in Appendix 1 show measured and simulated high latitude ionospheric convection on three days which were investigated. The corresponding IMF measurements obtained by IMP-8 are shown in Figures 5, 6, and 7 of that same paper. The first of these days, April 25, 1983, shows a changes in sign for the IMF B_y component from negative to positive to negative which results in changes in the direction of the high latitude ion drift from eastward to westward and back to eastward. The model reproduces this change in drift associated with the change in sign of B_y .

The second interval, March 16, 1984, is particularly interesting because of an extended region of poleward flow from 1300 UT through 14:45 UT. This interval of strong poleward flow is associated with a large southward IMF. The simulation reproduces the observed poleward flow at high latitudes suggesting that strong *DPZ* currents similar to those in the model exist during strong southward IMF conditions. At lower latitudes, around 75 degrees invariant, the simulation disagrees with the observed convection strength and direction. This suggests a different configuration of the region 1 and 2 currents in this region under these circumstances. In addition, the interval following the strong southward IMF is an interval of strong northward IMF and this, also, is not modeled well.

The third interval, July 24, 1983, shows a variety of complex temporal variations. From 12:30 UT through 13:30 UT a region of strong poleward flow associated with strong southward IMF

FIELD ALIGNED CURRENT

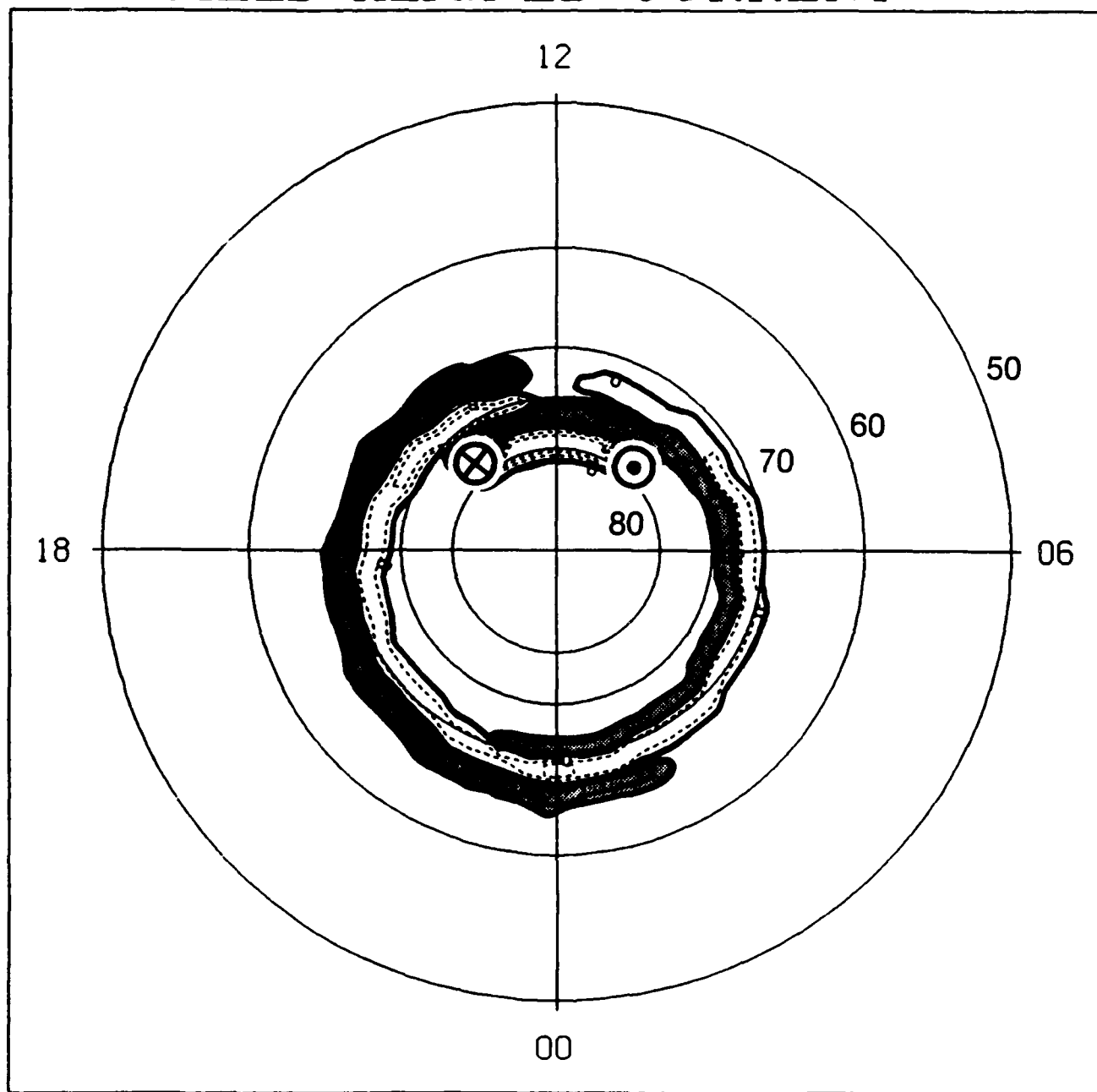


Figure 4: Polar plot of the distribution of field-aligned current used in the computer model. Three regions of current are shown: (1) the region 1 and region 2 currents around the auroral oval with inward current denoted by shading, (2) the DPY sheet currents centered at local noon and lying on and poleward of the region 1 currents, and (3) the DPZ line currents at the longitudinal ends of the DPY currents. The polarities of the currents in this illustration correspond to the case of IMF $B_y > 0$ and $B_z > 0$.

is observed and is similar to the previous example. However, examination of the timing of the southward variation and the onset of poleward flow reveals a problem.

Clauer et al., [1984] and Clauer and Banks, [1986] show that the dayside high latitude ionospheric electric field generally responds to polarity changes in the IMF B_y and B_z components within about 10 to 15 minutes. On July 24, 1983, however, the poleward flow observed at 12:30 UT is associated with a southward turning of the IMF B_z component which occurs at 11:15 UT. The expected delay time between IMP-8 and the magnetopause is about 8 to 12 minutes. Thus, the time delay from when the southward fluctuation is expected to encounter the magnetopause and the onset of observed poleward flow in the ionosphere is over 50 minutes.

We propose two possible explanations for this observation. Examination of the IMF observations indicate that B_y was large and positive at the time B_z turned southward. B_y became nearly 0 at about 13:00 UT. This suggests the possibility that the relative magnitudes of B_y and B_z may be important in determining the ionospheric effects of the DPY and DPZ currents. Alternatively, perhaps the effects of the DPZ current were not observed until around 12:30 UT because of a shift in the spatial distribution of the DPZ currents. It is interesting, however, that the simulation of ion velocity measurements agrees very well with the observations. The interval of poleward flow between 1230 and 1330 UT is reproduced. Since the locations of the currents are constant in the simulation, this suggests that adjusting the relative strengths of the DPY and DPZ currents is sufficient to explain the observations. We also note that following 1330 UT the simulated and observed convection velocities do not agree. This is during an interval of strongly northward IMF. While the results of the Clauer and Banks, [1984] paper show that a remarkably simple model can account for much of the observed high latitude dayside convection observations, further refinement is required to better address the situation for IMF B_z northward and for the auroral electrojet region near local magnetic noon. Therefore, to address more carefully the situation for both IMF B_z northward and southward, Clauer and Friis-Christensen, [1988] have refined the field-aligned current distributions. The new distributions of field-aligned current proposed by Clauer and Friis-Christensen are shown in Figure 5 and their corresponding ionospheric electric potential patterns are shown in Figure 6.

The modified distributions of current better reflect our understanding of the dayside high latitude currents and our ideas regarding the origins of these current systems. We hypothesize that the region 1 currents map to the vicinity of the inner edge of the low latitude boundary layer and the region 2 currents map to the ring current region of the inner magnetosphere. Since the field-aligned current is observed to be continuous in the observations of low altitude polar satellites, this implies that the current is continuous throughout the region of the magnetosphere between the ring current and the low latitude boundary layer. During periods of northward IMF, the region 1 and region 2 currents diminish substantially in strength and are located at higher latitudes. Near local noon, where

Ionospheric Distribution of Field-Aligned Current

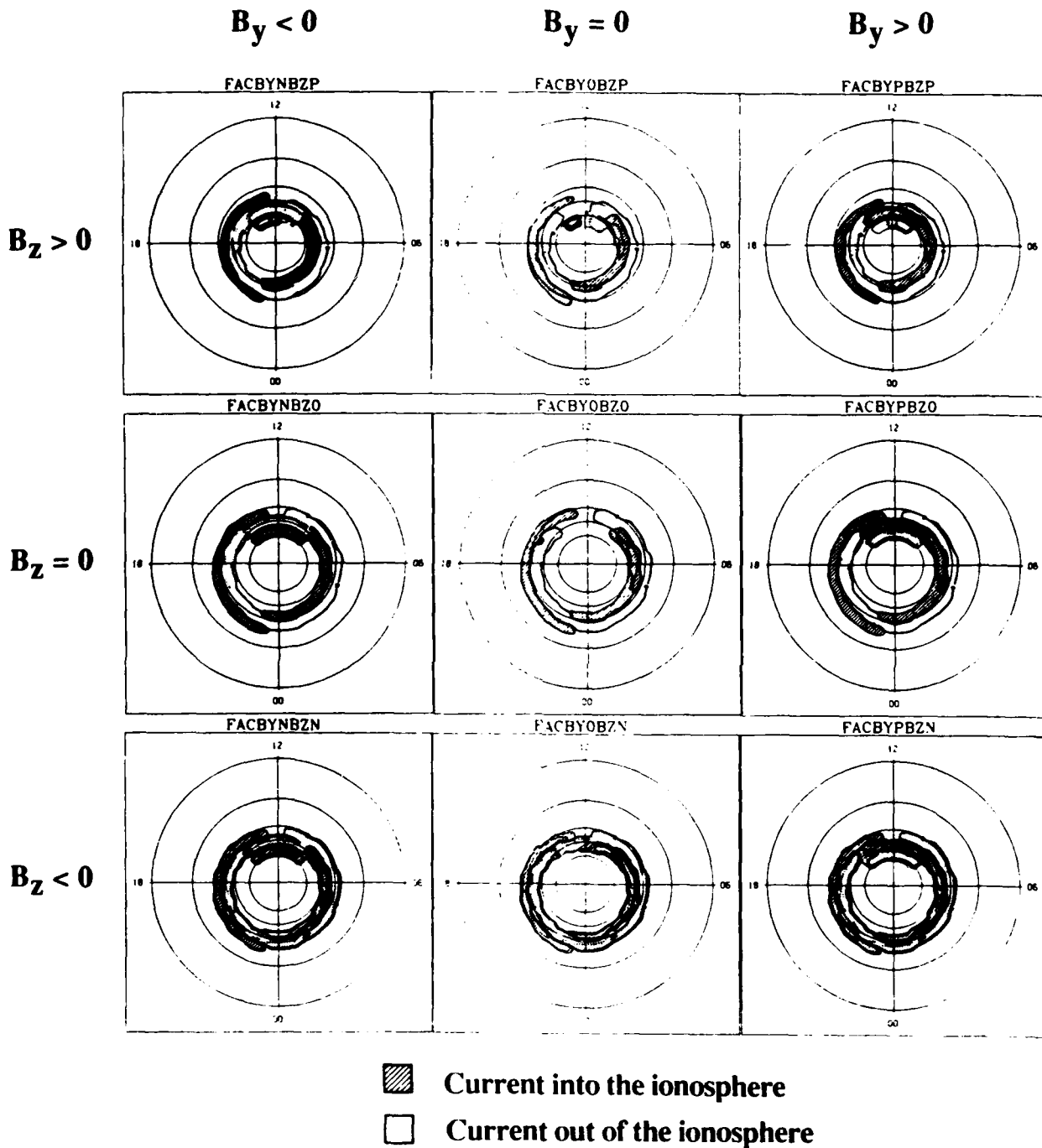


Figure 5: Polar plot of the distribution of field-aligned current used in the revised computer model. The shaded region with solid contours indicates current into the ionosphere and the unshaded region with dashed contours indicates current out of the ionosphere in the northern hemisphere. The contour interval is a 0.5 microamps per square meter.

Ionospheric Electric Potential Pattern

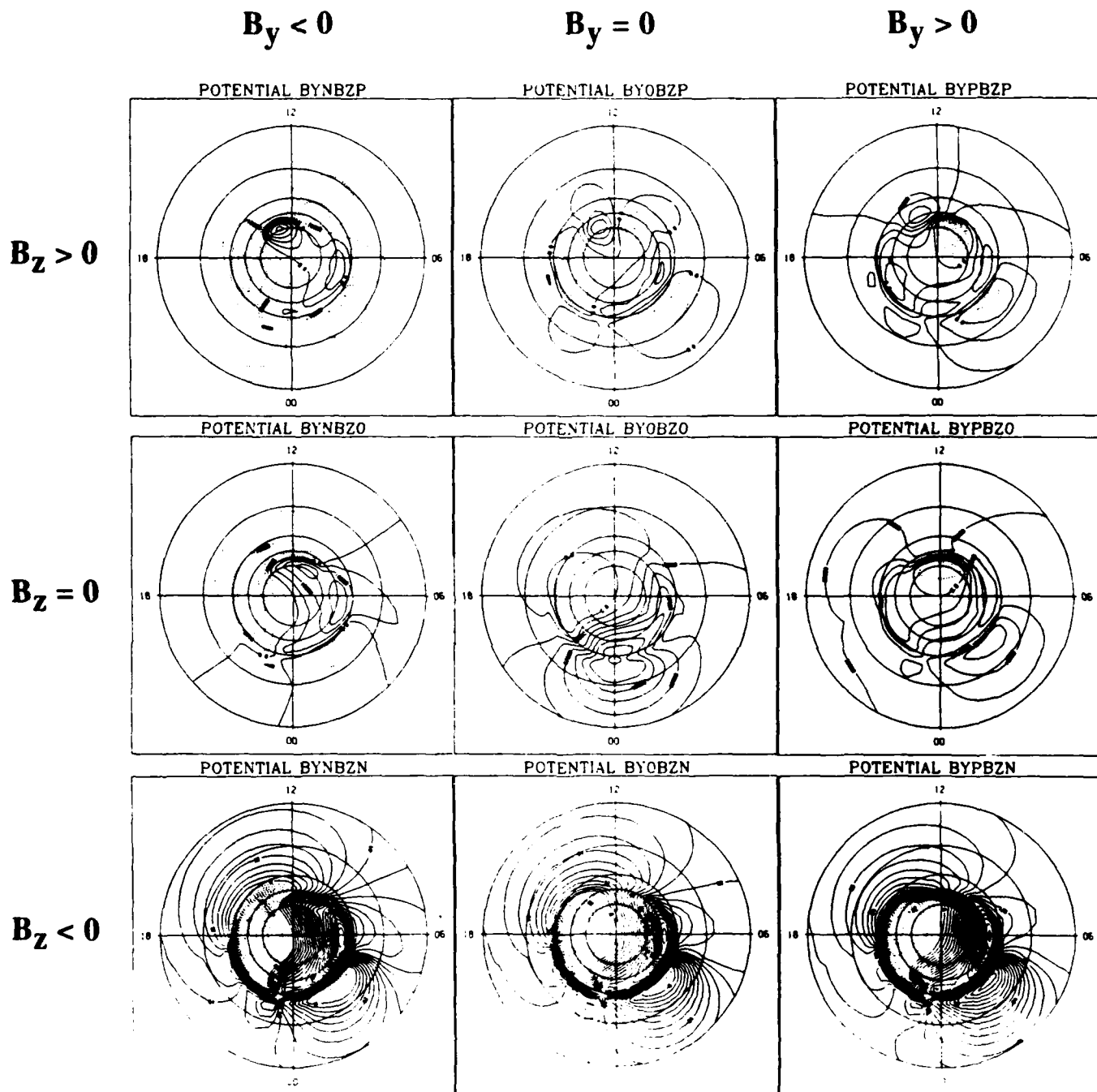


Figure 6: Polar plot of the ionospheric electric potential distribution associated with each of the current distributions shown in Figure 5. The contour interval is 8 kilovolts. The zero potential curve crosses the center of the polar cap and solid contours indicate positive values and dashed contours indicate negative values.

the low latitude boundary layer is quite thin and the boundary layer flow is small, the primary contribution to the region 1 current system are the *DPY* and *DPZ* currents which result from a direct electrical connection between the solar wind and the magnetosphere. We do not address how this electrical connection is accomplished but feel that it is consistent with the variety of magnetic merging models discussed in the literature.

The *DPY* and *DPZ* field-aligned currents are each separately controlled by the IMF B_y and B_z components (or equivalently by the interplanetary electric field E_z and E_y components as discussed by Banks et al., [1984] and D'Angelo, [1980]). The *DPY* ground magnetic disturbance is produced by the ionospheric Hall current flowing between a pair of oppositely directed field-aligned current sheets oriented longitudinally across and centered near the noon meridian. One of the current sheets is collocated with the region 1 currents and the other current sheet is located poleward of the region 1 currents. During northward IMF the *DPY* currents are located at higher latitudes but maintain their relationship relative to the region 1 currents. The poleward sheet lies on field lines near the poleward boundary of the polar cleft and the equatorward sheet which partially forms the noon sector region 1 currents lies near the equatorward boundary of the cleft. Associated with the IMF B_y component is an E_z electric field which drives the *DPY* currents.

For southward IMF (negative B_z) the *DPZ* current system is a field-aligned current wedge with current flowing from the vicinity of the prenoon equatorial magnetopause into the ionosphere at the latitude of the region 1 current and out of the ionosphere in the postnoon region 1 current along field lines which extend to the vicinity of the postnoon equatorial magnetopause. During northward IMF the *DPZ* system (or NBZ system as discussed by some researchers) is a similar current wedge with opposite current direction but located on field lines near the poleward boundary of the polar cleft and thus collocated with the poleward sheet of the *DPY* current system. Associated with the IMF B_z component is an E_y electric field which drives the *DPZ* currents at the longitudinal ends of the cleft.

The latitudinal changes in the currents agree better with observations and are more consistent with the theoretical notions regarding merging on lobe field lines poleward of the cleft for northward IMF and merging on field lines equatorward of the cleft for southward IMF [Dungey, 1963; Crooker, 1979; Reiff, 1982; Luhmann et al., 1984; Chiu et al., 1985, and references therein].

Clauer and Friis-Christensen, [1988] examine the consequences of the new distributions of current and compare with observations on July 23, 1983. During this day, the IMF turns strongly northward for several hours. The observations on this day represent an extreme case and therefore are very interesting for investigation.

Perhaps one of the most noteworthy observations presented in the Clauer and Friis-Christensen

paper is the rapid, almost immediate, response of the dayside high latitude ionospheric currents to the northward turning of the IMF. The IMF (Figure 7) was unusually large on July 23, 1982, having total field values of about 22 nT or larger for much of the day. At 10:15 UT the field measured at IMP-8 turns strongly northward with B_z becoming about 20 nT. It remains northward for several hours. The B_y component of the field is much smaller than B_z from 10:18 until about 13:10 UT. The magnitude of B_y becomes larger than B_z at 13:30 UT. The time delay between IMP-8 and the magnetopause is estimated to be 8 minutes indicating that the northward B_z polarity change would encounter the magnetopause at 10:23 UT. The change in the high latitude currents is observed to occur at the Greenland high latitude magnetic observatories Thule (THL), Kuvdlorssuaq (KUV) and Upernavik (UPN). Station locations are shown in Table 1 in Clauer and Friis-Christensen, [1988] in Appendix 1. The D component of the magnetic field measurements are shown in Figure 8. The response of the currents is seen to begin 3 minutes following the northward IMF encountering the magnetopause and to develop over a period of about 22 minutes.

The observed ionospheric convection pattern is shown in Figure 9. To create this figure we have used the radar measured ionospheric convection data plus the magnetic data from the three magnetic observatories THL, KUV, and UPN. The magnetic data are 15 minute averages and the total horizontal field component is rotated 90 degrees counter clockwise to give the equivalent convection direction. The magnetic measurements are not calibrated with the radar velocity measurements so the magnitude of the vectors is only roughly proportional to the velocity.

From 0800 to 1300 UT, the convection reversal boundary appears to be located between 73 and 75 degrees invariant latitude. The anti-sunward convection observed at latitudes above this boundary is thought to be tailward convection on polar cap field lines. The low latitude of the boundary indicates an expanded polar cap and is consistent with the several intervals of large southward IMF prior to 1015 UT. Extending the convection measurements further poleward using magnetic data, we see a sunward rotation of the convection following 10:15 UT. The sunward convection is restricted to very high latitudes.

Figure 10 shows the model simulation based upon the current distributions shown in Figure 9. Figure 10 can be directly compared with Figure 9. The convection reversal boundary is located at about the same location in both figures. The simulated high latitude vectors at the magnetometer measurement points at dawn and dusk are aligned more east-west than the measured vectors, however, this is likely due to skewing of the magnetometer vectors due to conductivity gradients and the associated field-aligned currents. The highest latitude vectors measured by THL are well reproduced by the simulation. The rotation is seen at 1030 UT in both sets. The measurements at KUV, the next highest latitude vectors, are not as well simulated at 1030 UT but are fairly well modeled after 1100 UT. Thus, the spatial arrangement of the high latitude currents only approximates the actual distribution, but the agreement is quite reasonable and the time variations match

IMP-8 Magnetic Field
23-JUL-83 TO 24-JUL-83
00:00:00 00:00:00

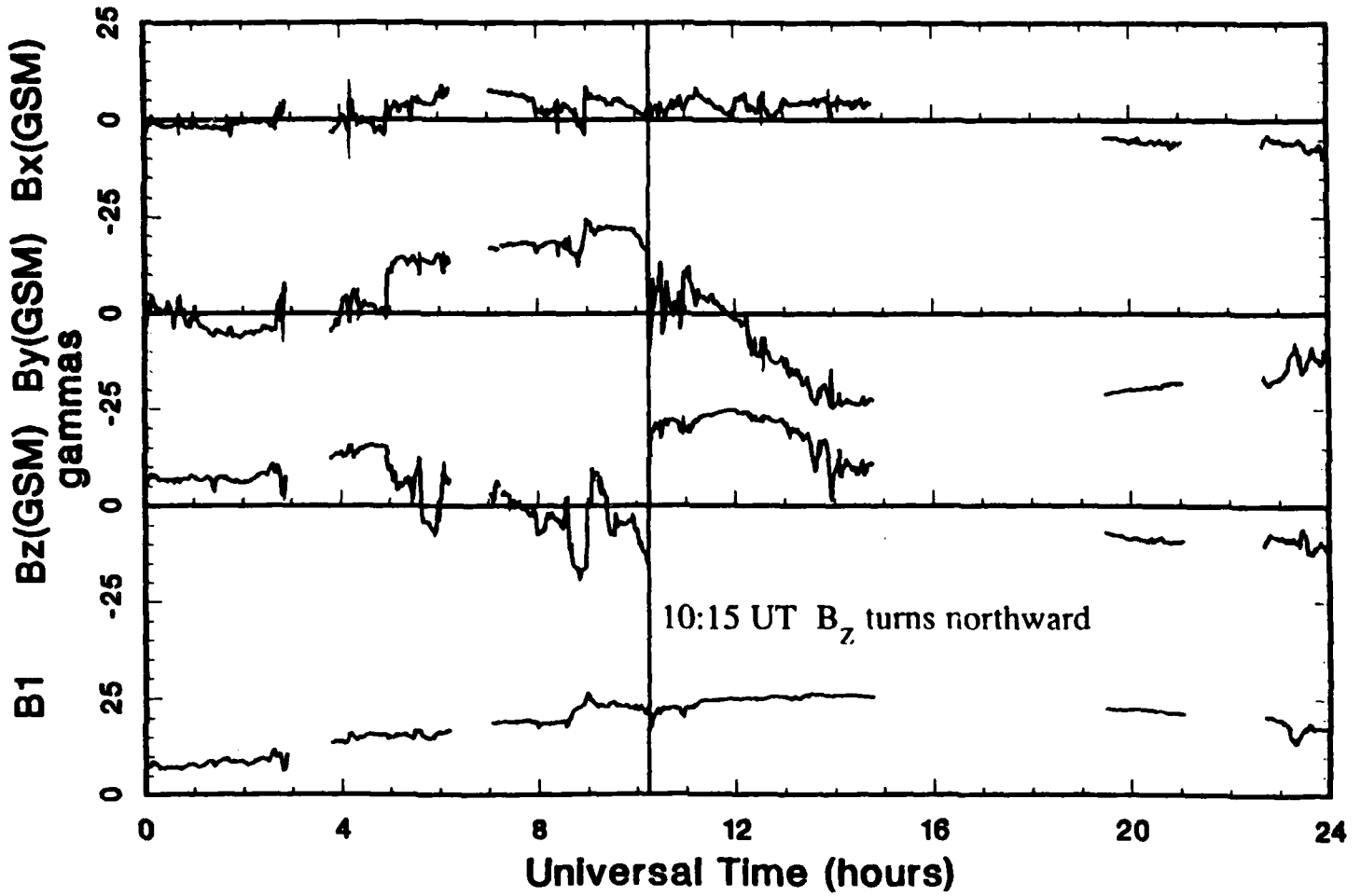


Figure 7: Interplanetary magnetic field measured by the IMP-8 spacecraft during July 23, 1983 shown in GSM coordinates.

Greenland Magnetometer Data

23-JUL-83
10:00:00 TO 12:00:00

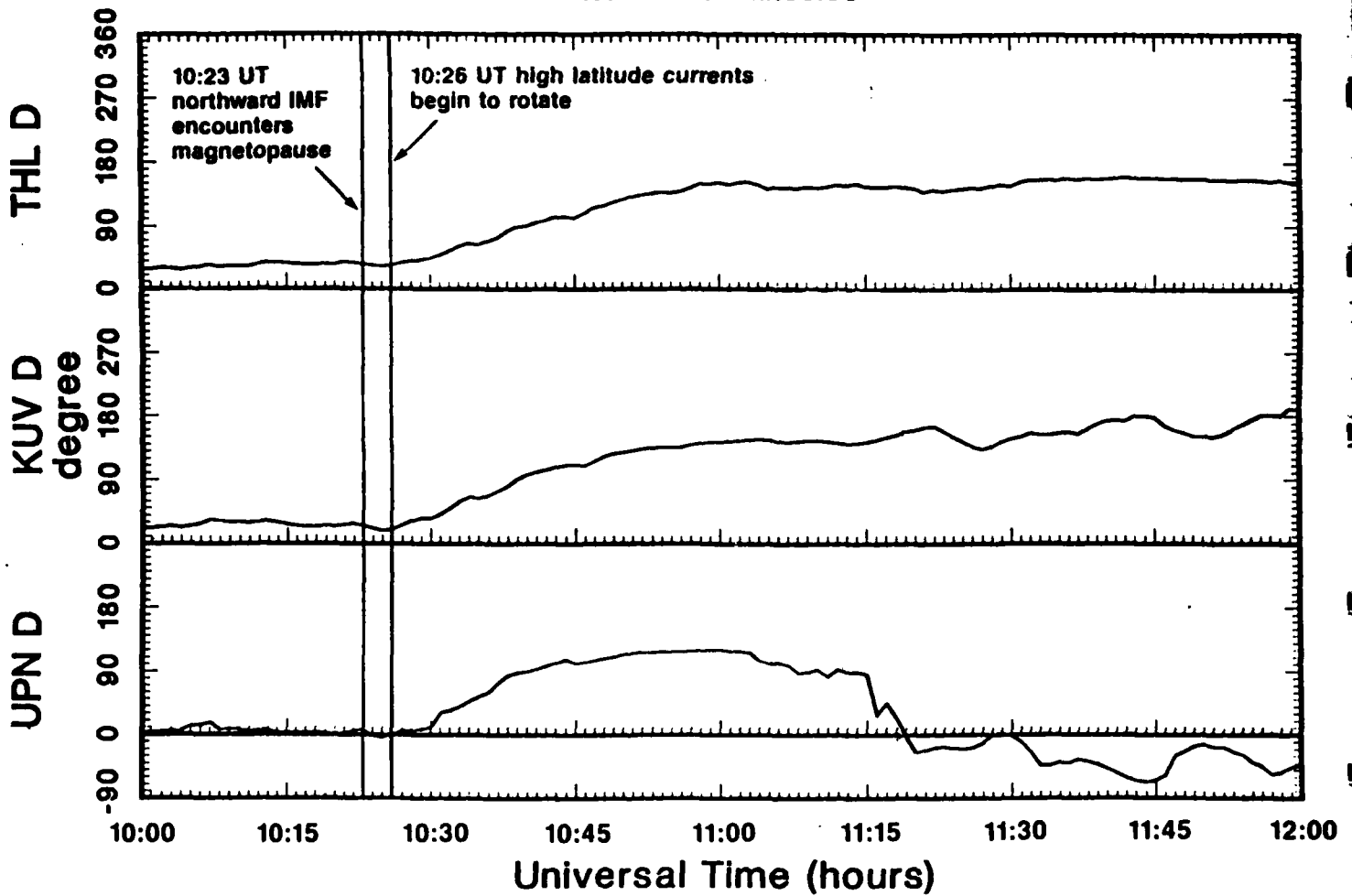


Figure 8: Horizontal magnetic field declination variations measured relative to the average declination at Thule (top), Kuvdlorssuaq (middle) and Upernavik (bottom). At 10:23 UT the northward IMF is estimated to encounter the magnetopause and at 10:26 UT the field at THL and KUV begins a 120° rotation.

MEASURED ION VELOCITY

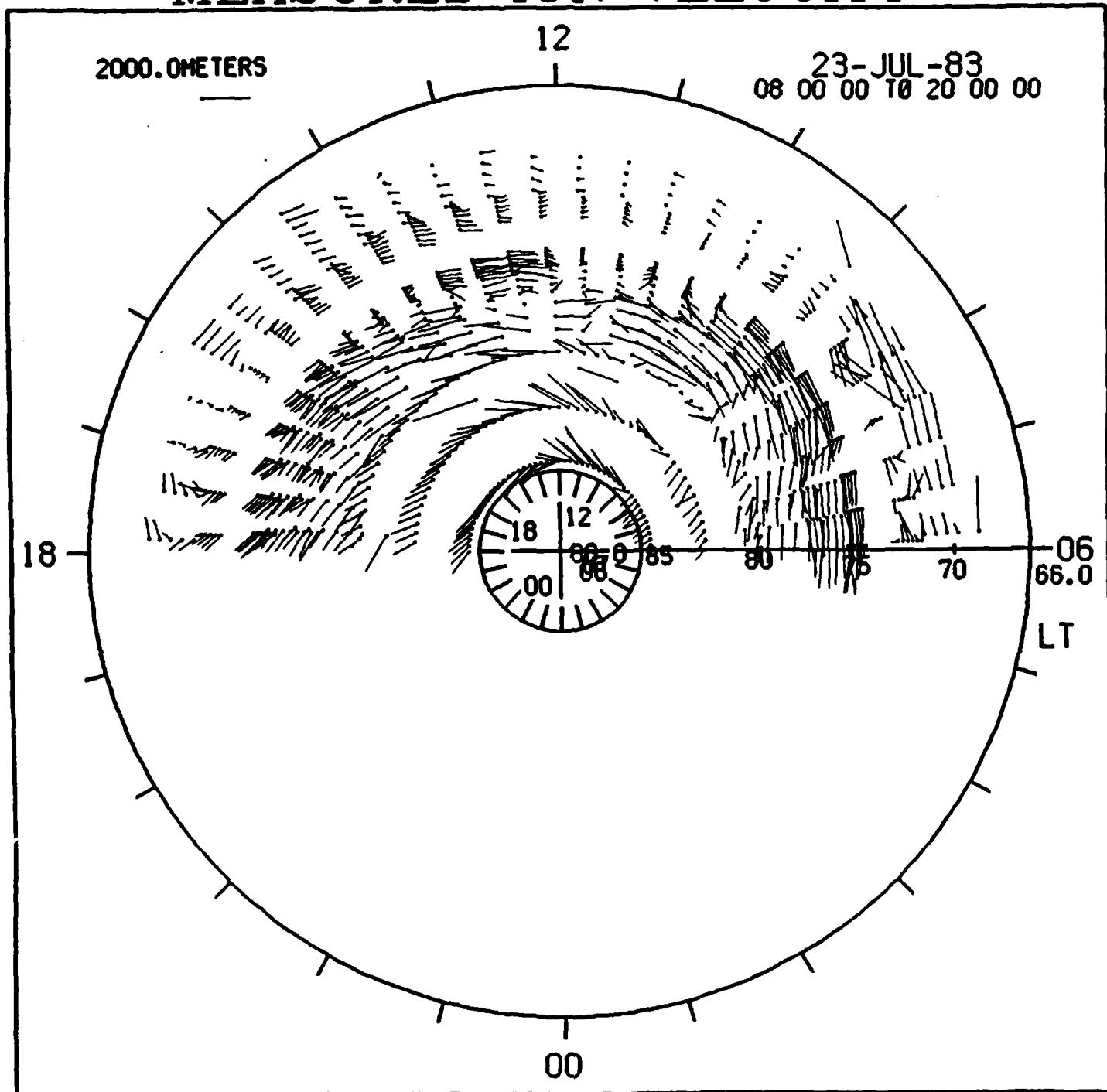


Figure 9: Polar plot showing F-region ion convection velocity vectors as a function of latitude and local time for July 23, 1983. Local time is indicated around the outer circumference of the plot and universal time is indicated around the inner circumference of the plot. Local magnetic noon is at the top of the plot. The three complete rows of highest latitude vectors are convection velocities inferred from ground magnetometer data. The other vectors in the plot are obtained using the Sondre Stromfjord, Greenland incoherent scatter radar.

SIMULATED ION VELOCITY

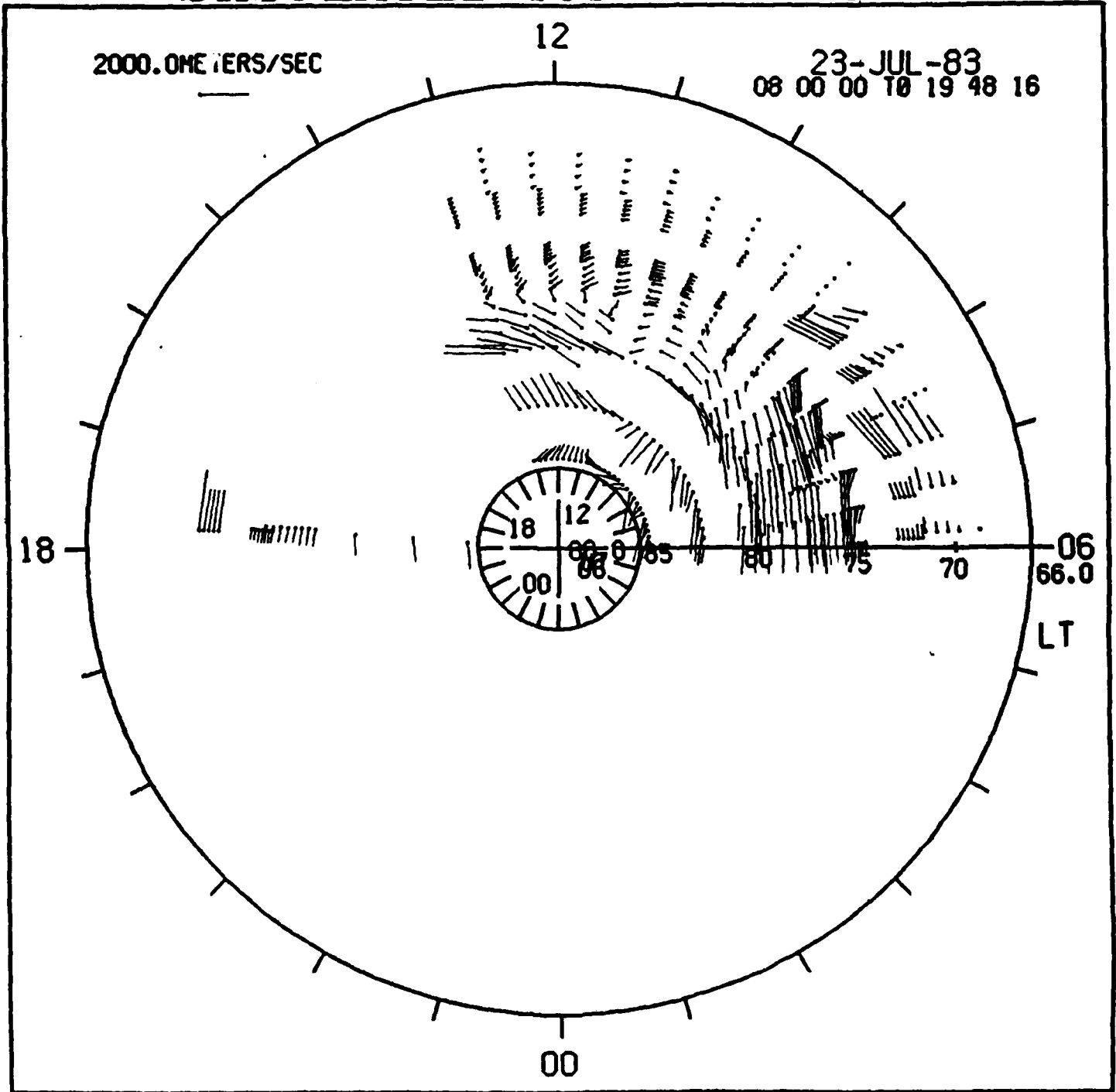


Figure 10: Simulated F-region ion convection velocity vectors for July 23, 1983.

well. Between 12 and 13 UT the magnitudes of the vectors equatorward of the convection reversal boundary are smaller than observed. This has been a consistent feature in most of the simulations shown here and those that have not been published. We intend to examine the conductivity measurements in this region to determine if that is the source of the disagreement.

A more thorough discussion of these data and the results is available in the paper by Clauer and Friis-Christensen attached in Appendix 1.

COORDINATED ANALYSIS OF SATELLITE AND GROUND BASED MEASUREMENTS

The second approach to our investigation of the large scale dayside high latitude current systems uses the coordinated analysis of simultaneous measurements of ionospheric convection obtained by the Sondre Stromfjord radar and *in situ* observations of field-aligned currents, particle precipitation and plasma drift obtained by low altitude polar satellites nearly conjugate with the radar measurements. This work has been discussed in our quarterly progress reports, has been presented in papers at some professional meetings, and is still in progress. Papers are presently in preparation and we will discuss our results as of the completion of our contract. Results from the analysis of these coordinated simultaneous measurements should aid us in setting parameters more accurately in the model current systems discussed above. A variety of coordinated data are available for analysis of dayside high latitude electrodynamic during March 7, 16 and 20, 1984. We have conducted an number of studies of the coordinated electrodynamic parameters measured by the Sondre Stromfjord, Greenland incoherent scatter radar together with *in situ* measurements from low altitude polar satellites. Measurements in the pre-noon sector have utilized the DMSP F7 satellite and measurements in the post-noon sector have utilized the HILAT satellite. During these days, we have a variety of different plasma convection patterns corresponding to IMF $B_z > 0$ and < 0 and IMF $B_y > 0$ and < 0 .

MARCH 7, 1984: Pre Noon hours.

A DMSP satellite pass occurred at 1130 UT which was nearly conjugate with Sondrestrom. DMSP magnetometer data show 2 sheets of current with the equatorward sheet being outward and the poleward sheet directed inward. Figure 11 shows the DMSP magnetometer data together with the derived current density. Sketched along the top of the plot is a schematic indication of the type of particle precipitation observed by the plasma instrument. In Figure 12 we show the ionospheric convection measured by the Sondrestrom radar at the time of the DMSP pass. We have also indicated schematically the locations of the DMSP observed currents and particle precipitation. The region marked "oval" represents the region of hard auroral precipitation consisting of energies of about 1 KeV. The "cusp" region consists of high fluxes of low energy (50 eV) particles, and the "polar cap" region consists of very small fluxes. We note that the cusp plasma is observed in a

region of sunward flowing convection and the electric field is rather strong (long vectors).

Figures 13 and 14 show data obtained from an elevation scan made by the Sondrestrom radar. Figure 13a shows the electron density and Figure 13b shows the ion temperature. In Figure 13a there is a density enhancement located at about 100 km north of the radar at 150 km altitude. This E-region enhancement is due to the 1 KeV oval precipitation. Poleward of this, in the region of the large fluxes of low energy cusp precipitation, the ionospheric density drops to very low values. The cusp precipitation is not producing an ionospheric density enhancement in the F-region as might be expected. Figure 13b provides some insight as to why. Very high ion temperatures are measured in the cusp precipitation region. These high temperatures are the result of joule heating due to the high electric fields and large convection velocities. The consequence of the high temperatures is that the recombination rate is increased and the ionization is eliminated.

These observations occur during an interval of IMF $B_y < 0$ and the IMF observations measured by IMP-8 are shown in Figure 14. A summary of the observations superposed upon a schematic of the global convection pattern assumed for IMF $B_y < 0$ is shown in Figure 15. The features which we show on the figure include, the cusp plasma observed primarily in the poleward region of the upward (region 2) but spreading slightly into the inward region 1 current. The hard oval precipitation lies in the equatorward portion of the region 2 current. The region 1 current lies in the region of primarily polar cap precipitation.

The lack of F-region ionization observed in the region of cusp precipitation is a curious observation since ionosonde observations have often been utilized to identify the polar cusp. If this observation is a general feature, then those ionosonde observations which have claimed to identify the cusp could really be oblique reflections from the strong E-region enhancement at lower latitudes. This is something which should be investigated more thoroughly through the analysis of additional data.

MARCH 16, 1984: Pre Noon hours.

On March 16, 1984, the DMSP pass at 11:50 UT is nearly conjugate with the observations of the Sondrestrom radar. The DMSP magnetometer on this pass observed 3 sheets of current; the equatorward and poleward sheets being outward and the middle sheet being inward. This is shown in Figure 16 using the same format as Figure 11. A summary of the particle observations is schematically shown along the top of Figure 16. In contrast with the observations on March 7, 1984, the region 2 current is entirely associated with 1 KeV oval precipitation and the soft cusp precipitation occurs across the entire region 1 current and into the poleward cusp current sheet. The boundary between sunward convection and anti-sunward convection lies at the boundary between the region 1 and region 2 currents and is shown in the Sondrestrom convection measurements made

March 7, 1984
DMSP Magnetic Field

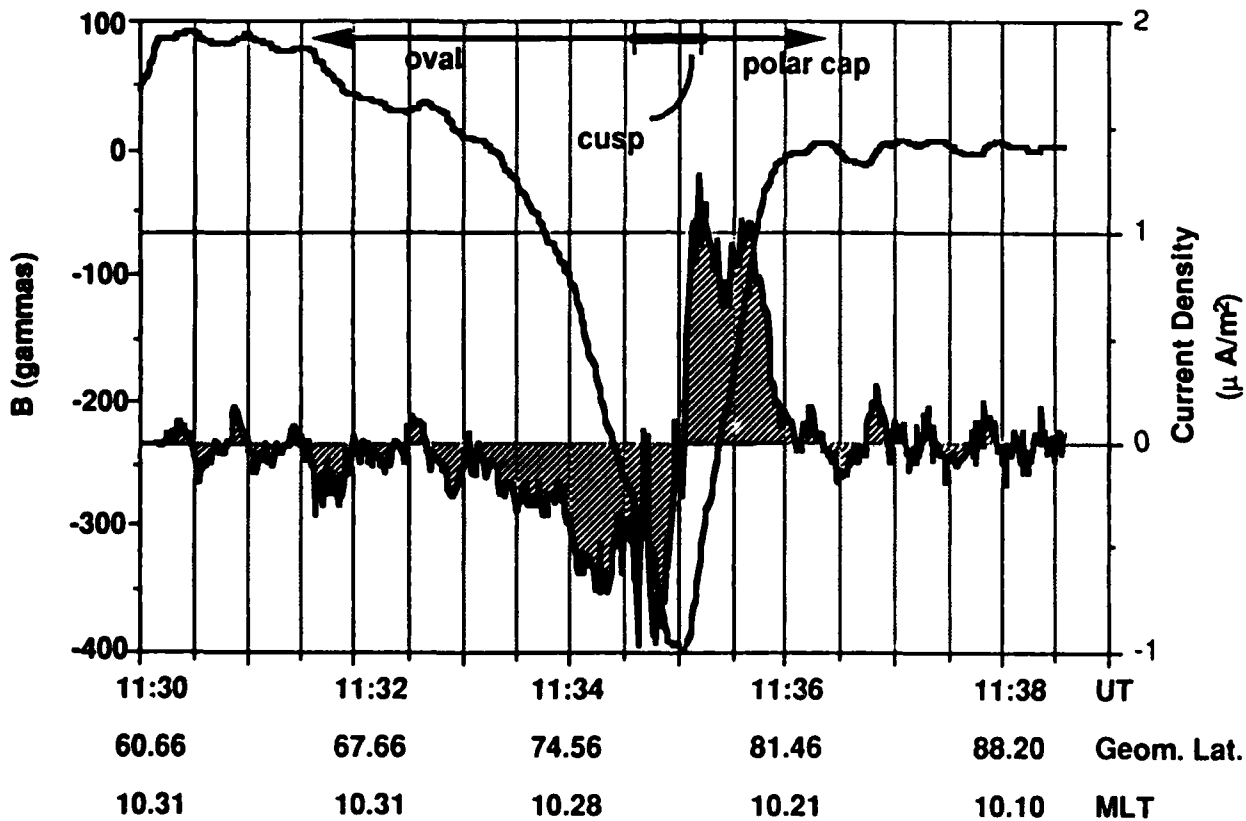


Figure 11: Magnetic field measurements and derived field-aligned current density (shaded curve) obtained by the DMSP polar satellite during a northern hemisphere pass beginning at 11:30 UT on March 7, 1984. UT, Geomagnetic Latitude and Magnetic Local Time are shown along the horizontal axis, magnetic field strength on the left axis, and current density in $\mu A/m^2$ on the right axis. Along the top of the plot is a schematic representation of the particle precipitation measured by the plasma instruments on the satellite. The oval represents fluxes of KEV energy particles, the cusp is a region of enhanced fluxes of low (few eV) energy particles, and the polar cap is a region of low precipitation fluxes. Current directed into the ionosphere is positive, outward current is negative.

SONDRESTROM ION VELOCITY

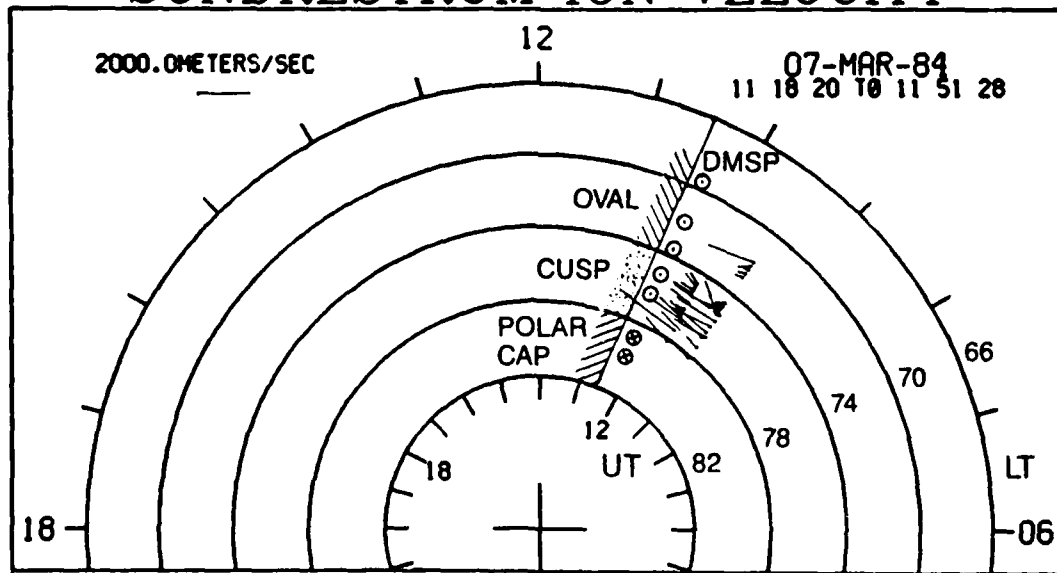


Figure 12: Measurements of ionospheric plasma convection obtained by the Sondre Stromfjord, Greenland radar during the period of the March 7, 1984, 11:30 UT DMSM satellite pass. The location of the DMSM track is indicated on the plot along with a schematic representation of the field-aligned current direction and plasma precipitation regions.

March 7, 1984
11:32 - 11:37 UT
Electron Density

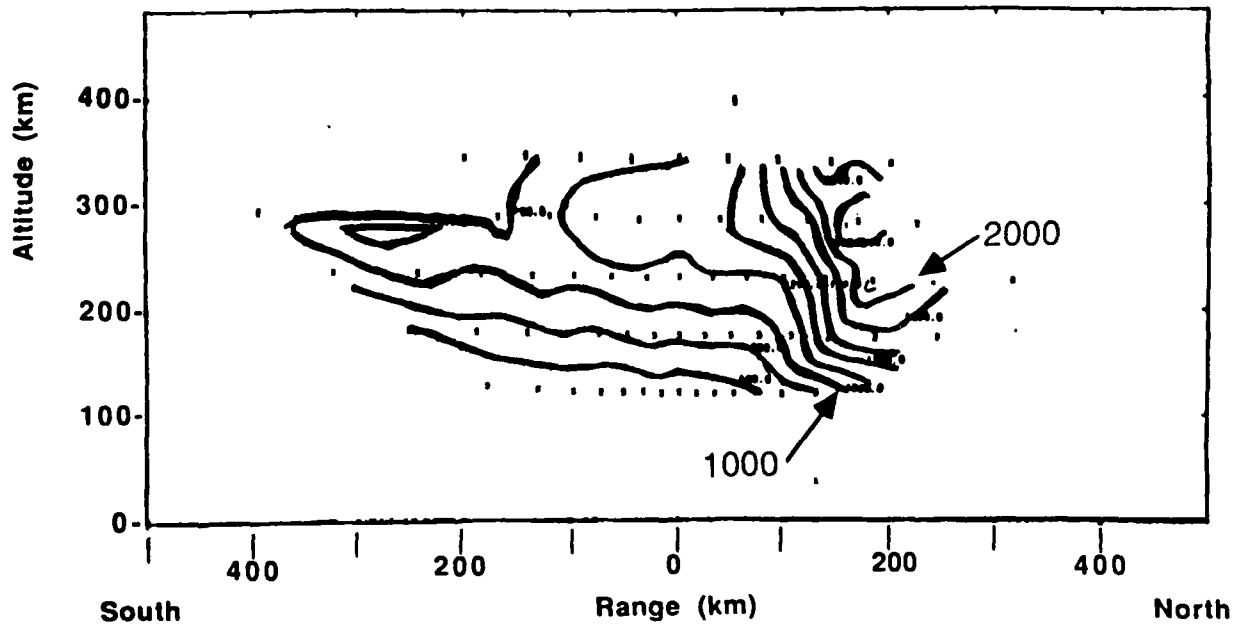
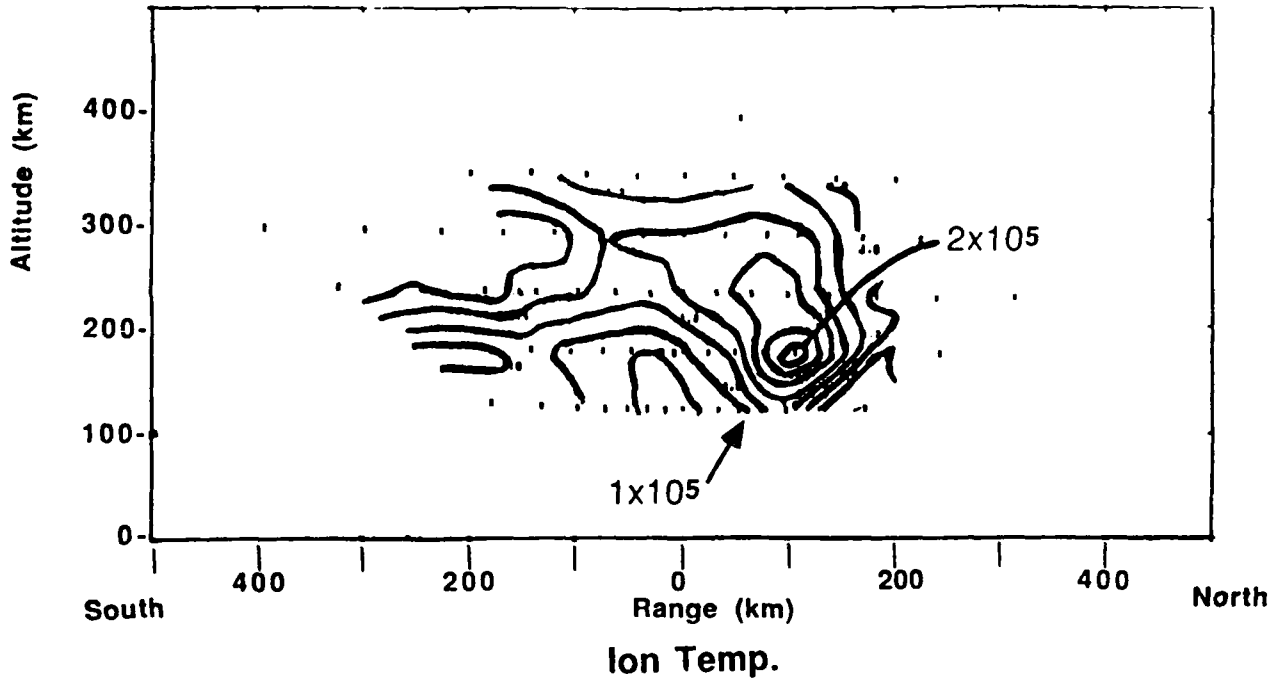


Figure 13 a) Measurements of the ionospheric electron density along the Sondrestrom magnetic meridian obtained during the interval 11:32 - 11:37 UT on March 7, 1984. A density enhancement of $2 \cdot 10^5$ electrons/cc is observed at E-region altitudes about 100 km north of the radar. b) ion temperature measurements obtained during the same meridian scan. A F-region temperature enhancement is observed poleward of the density enhancement measured in panel a).

IMP-8 magnetic field
07-MAR-84 TO 08-MAR-84
00:00:00 00:00:00

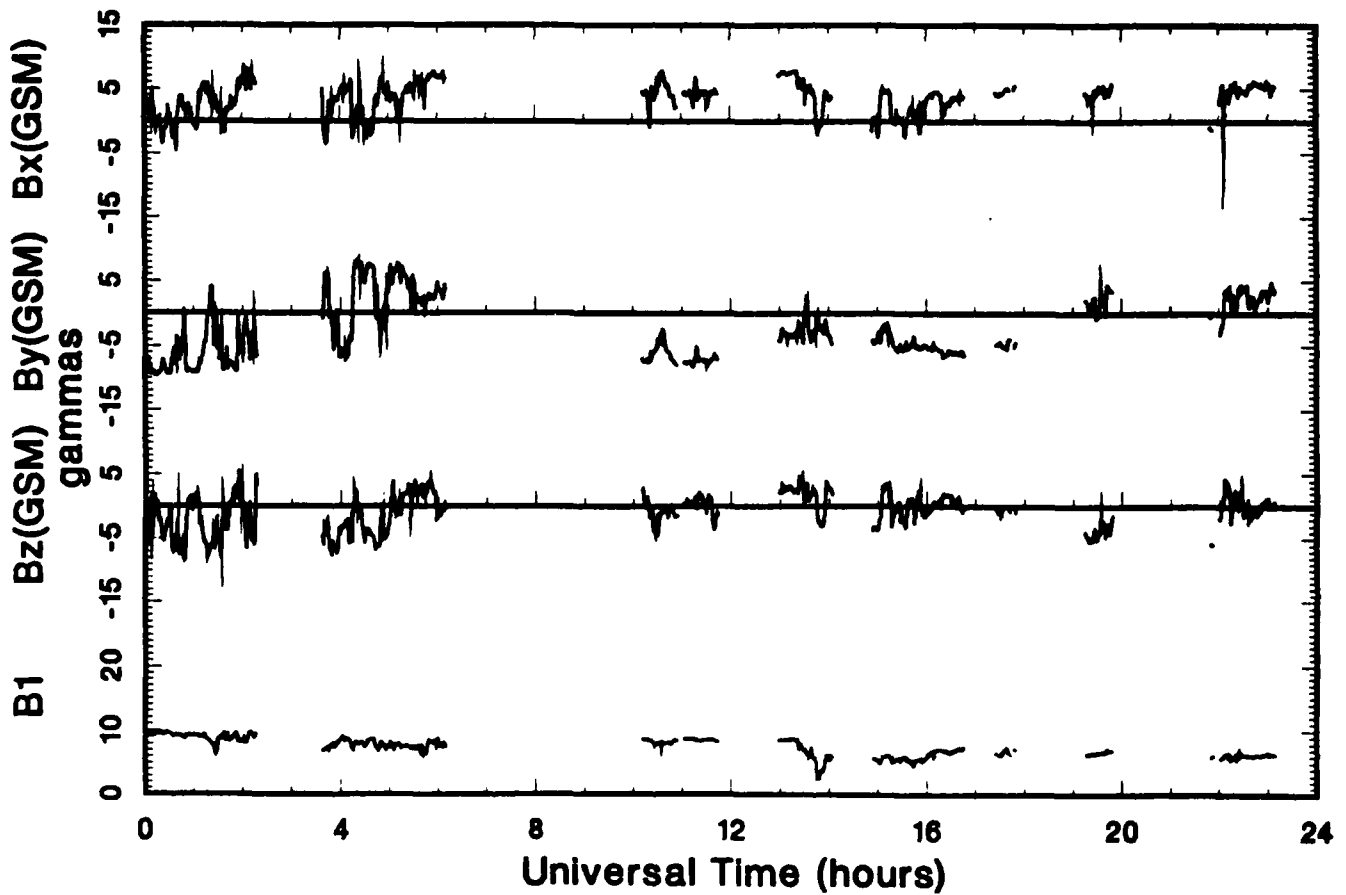


Figure 14: Interplanetary magnetic field measurements on 07 March 1984.

at the time of the DMSP satellite pass and shown in Figure 17.

These observations occur during an interval of IMF $B_y > 0$. The IMF measurements obtained by IMP-8 are shown in Figure 18. A summary of the observations superposed upon a schematic of the global convection pattern assumed for IMF $B_y > 0$ is shown in Figure 19.

MARCH 20, 1984: Pre Noon hours.

The prenoon observations on March 20, 1984 are very similar to those for March 16, 1984. The IMF observations are shown in Figure 6. Several DMSP passes have been examined, and all show current structures similar to those observed on March 16, 1984. DMSP passes occur at 10:28 UT, 12:08 UT and 13:50 UT. The 12:08 pass is measuring nearly the same meridian as the Sondrestrom radar. The DMSP data are shown in Figure 20 for the three passes. In Figure 21 we show as schematic representation of the DMSP observations together with the plasma convection measured by the Sondrestrom radar. The consistency of the field-aligned currents with the longitudinally separated measurements of the convection at 10:28 UT and 13:30 UT suggest that the triple current sheet structure observed in the pre-noon hours during IMF $B_y > 0$ extends longitudinally through a region of several hours of local time.

In contrast with the observations on March 7, 1984, the region 2 current is entirely associated with 1 KeV oval precipitation and the soft cusp precipitation occurs across the entire region 1 current and into the poleward cusp current sheet. The boundary between sunward convection and anti-sunward convection lies at the boundary between the region 1 and region 2 currents and is shown in the Sondrestrom convection measurements made at the time of the DMSP satellite pass and shown in Figure 17.

These observations occur during an interval of IMF $B_y > 0$. The IMF measurements obtained by IMP-8 are shown in Figure 18. A summary of the observations superposed upon a schematic of the global convection pattern assumed for IMF $B_y > 0$ is shown in Figure 19.

MARCH 7, 1984: Post Noon Hours

Some preliminary analysis has been completed of coordinated HILAT magnetometer data and Sondrestrom radar data during the post noon hours. These observations occurred during intervals of variable IMF B_z and $B_z \approx 0$ while $B_y < 0$ for both passes. The IMF observations are shown in Figure 14 and the HILAT magnetic observations are shown in Figure 22. The HILAT data show considerable structure in the field-aligned currents with multiple current sheets observed. The top panel of Figure 22 shows the HILAT pass beginning at 15:24 UT. There are 5 current sheets observed. The observations for the 17:04 pass (bottom panel) show considerably more structure, however, there are basically 3 major current sheets. Figure 23 shows the Sondrestrom convection

Observation Summary for
March 7, 1984

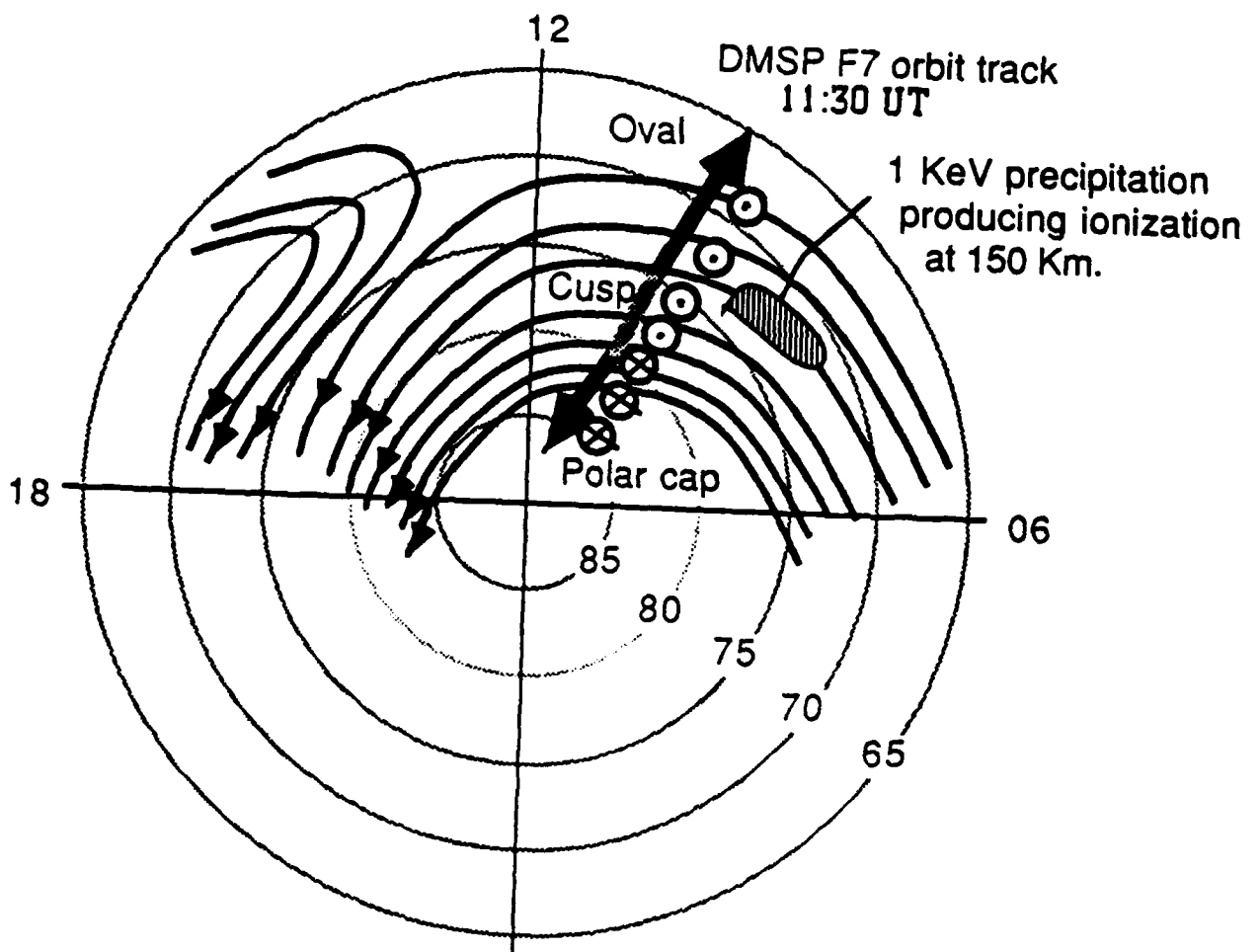


Figure 15: Schematic summary of March 7, 1984, 11:30 UT DMSF observations superimposed upon the large scale convection pattern assumed for IMF $B_y < 0$.

March 16, 1984
DMSP Magnetic Field

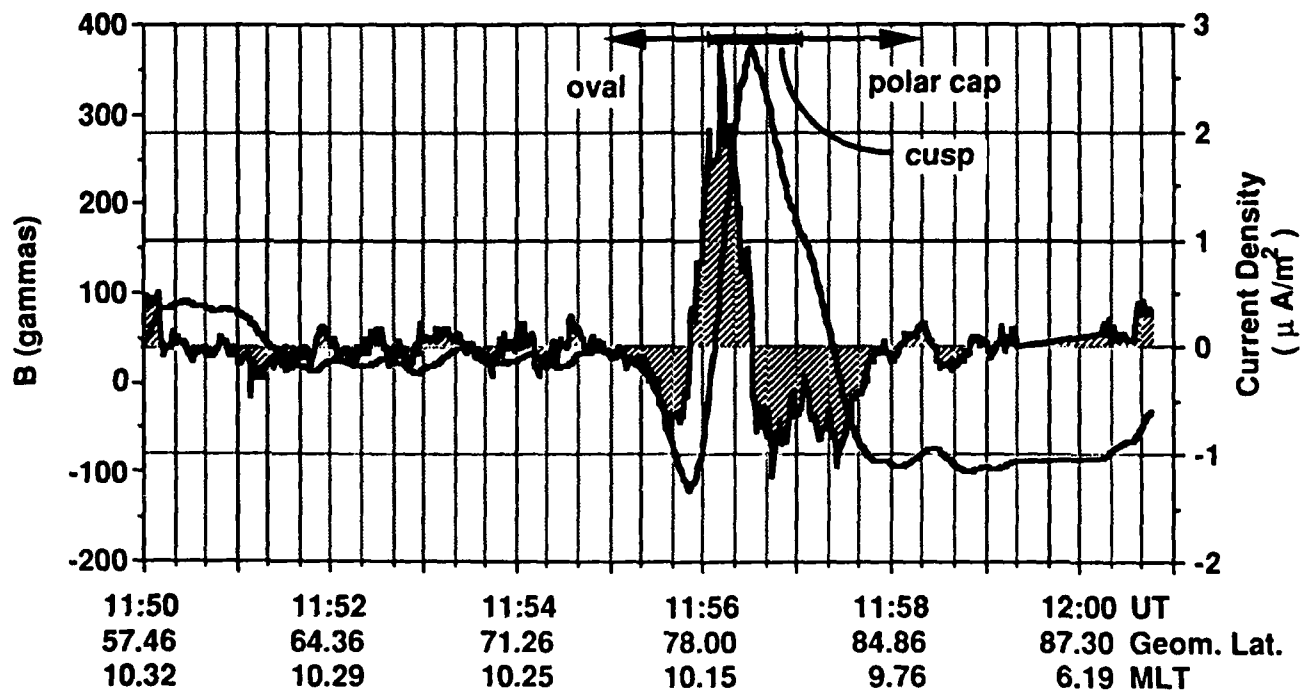


Figure 16: DMSP field and particle observations and computed field-aligned current density in the same format as Figure 11 for the satellite pass beginning at 11:50 UT on March 16, 1984.

SONDRESTROM ION VELOCITY

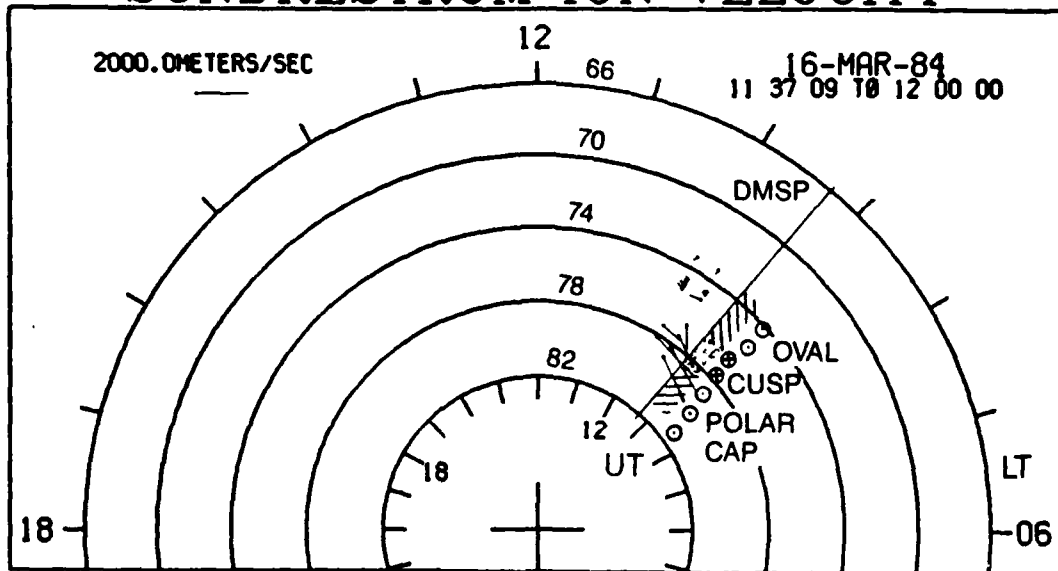


Figure 17: Measurements of ionospheric plasma convection obtained by the Sondre Stromfjord, Greenland radar during the period of the March 16, 1984, 11:50 UT DMSP satellite pass. The location of the DMSP track is indicated on the plot along with a schematic representation of the field-aligned current direction and plasma precipitation regions.

IMP-8 magnetic field
16-MAR-84 TO 17-MAR-84
00:00:00 00:00:00

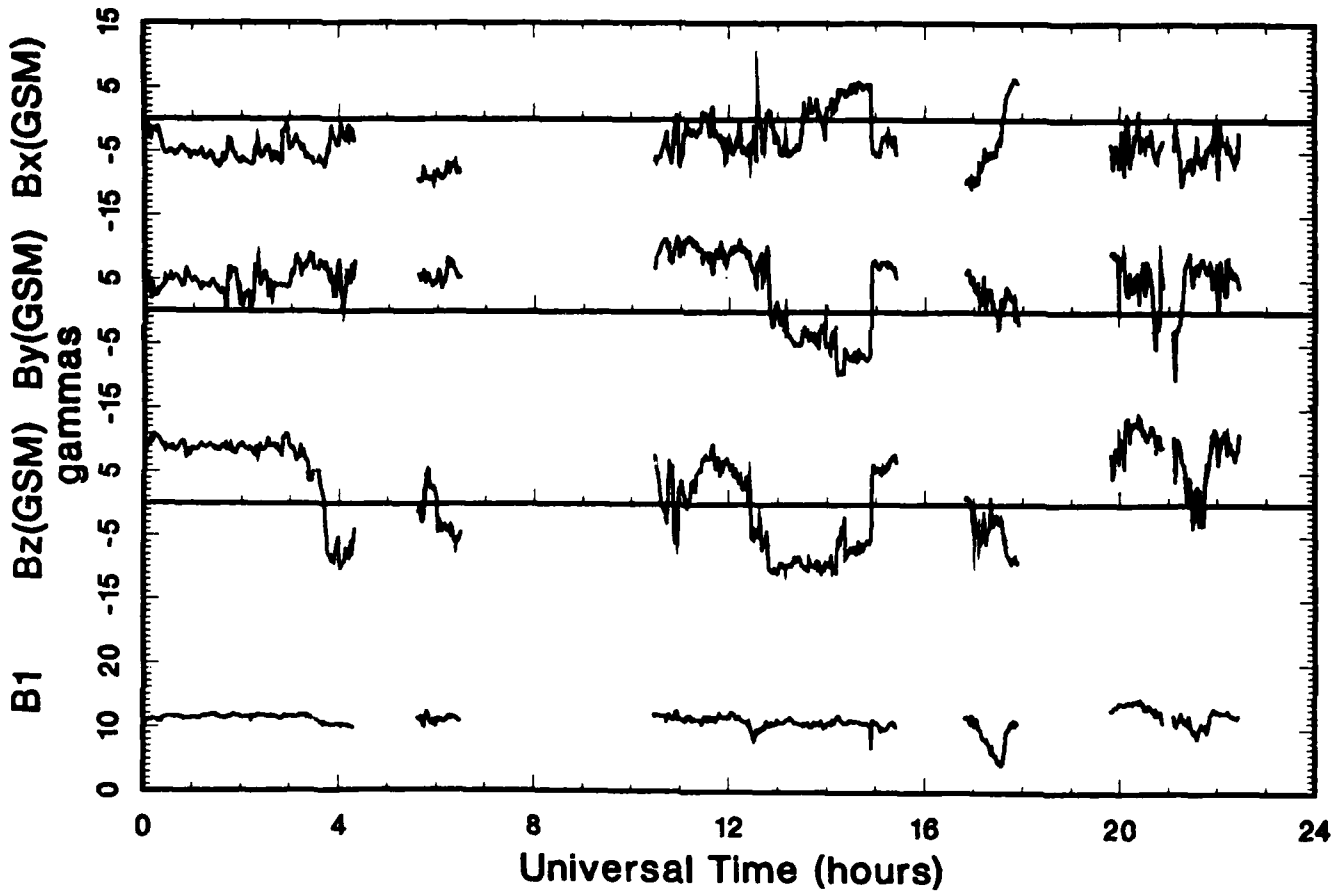


Figure 18: Interplanetary magnetic field measurements on 16 March 1984.

Observation Summary for
March 16, 1984

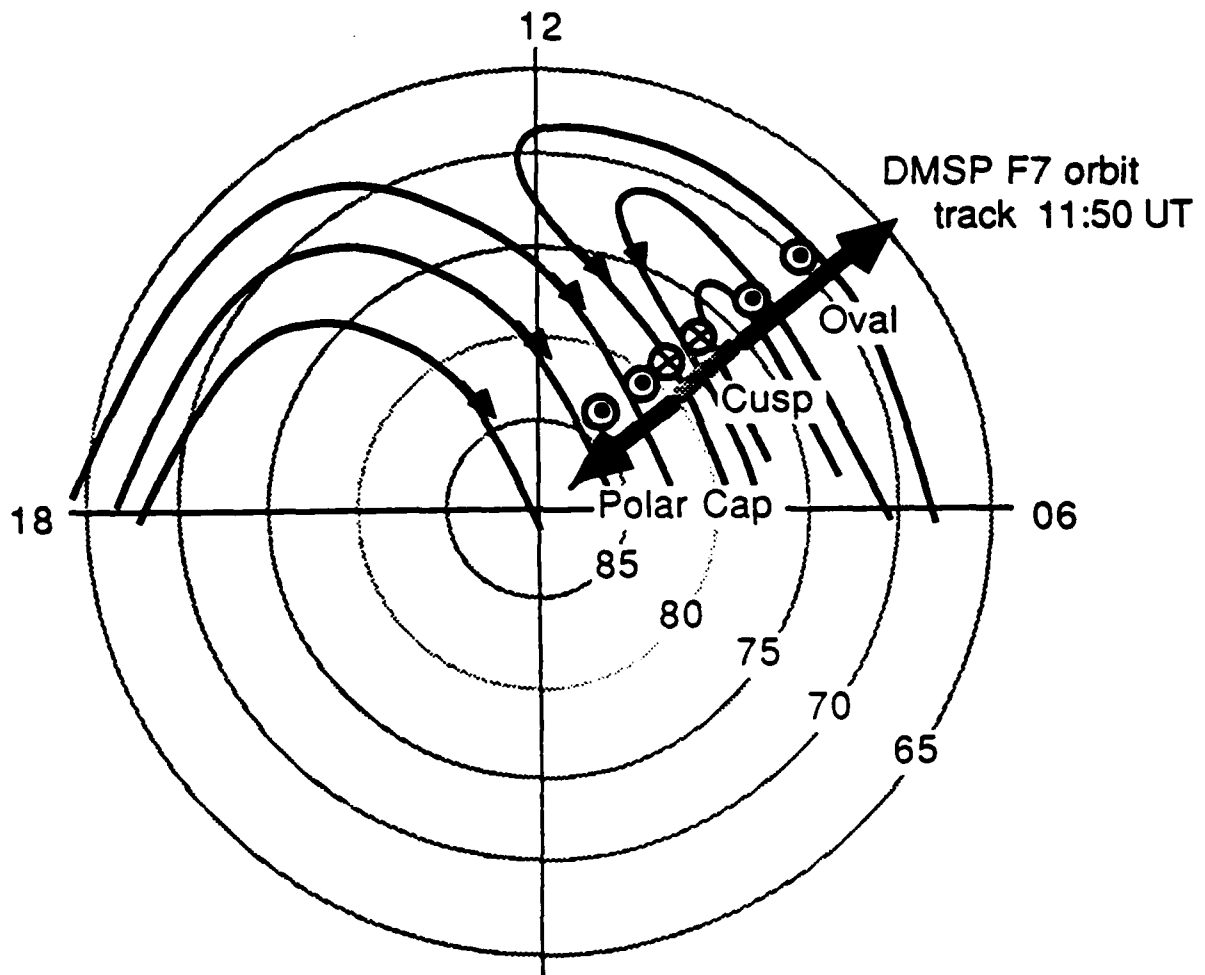


Figure 19: Schematic summary of March 16, 1984, 11:50 UT DMSP observations superimposed upon the large scale convection pattern assumed for IMF $B_y > 0$.

March 20, 1984
 DMSP Magnetic Field

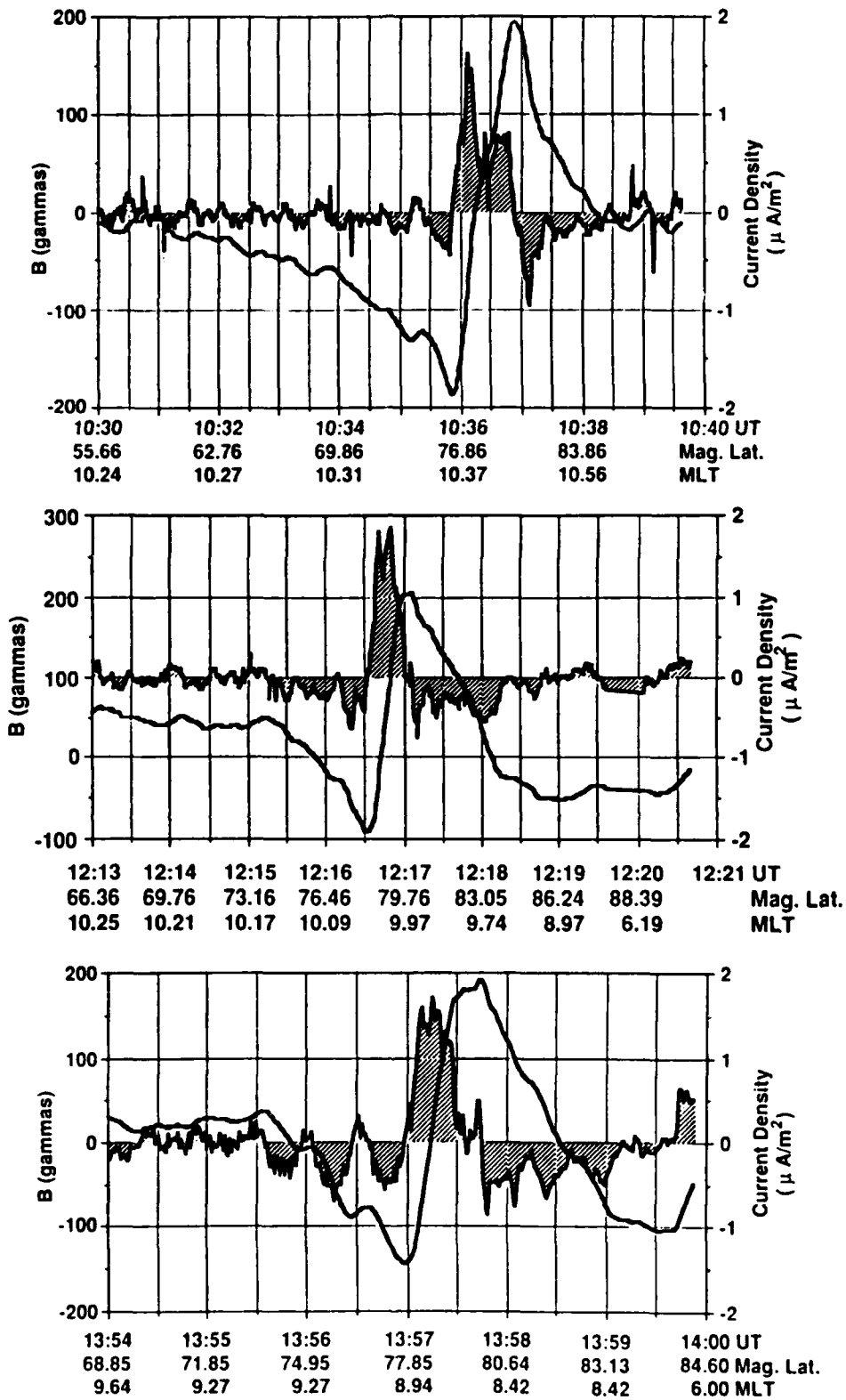


Figure 20: Magnetic field and computed field-aligned current density for three consecutive northern hemispheric passes of the DMSP satellite on March 20, 1984, 10:30 UT (top), 12:13 UT (middle) and 13:54 UT (bottom).

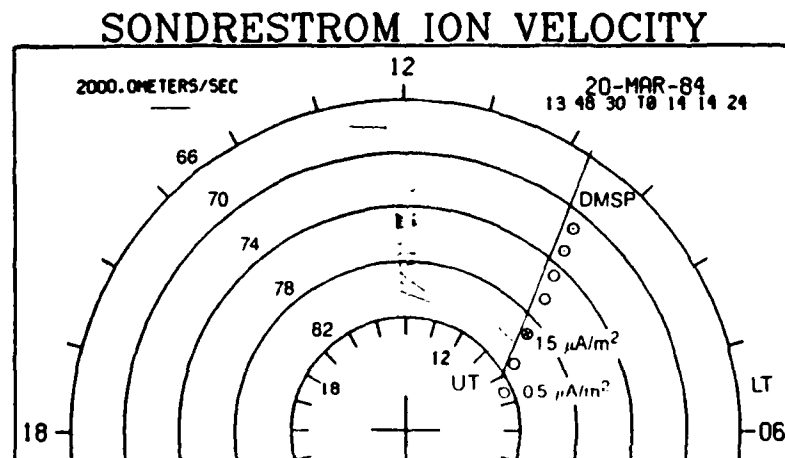
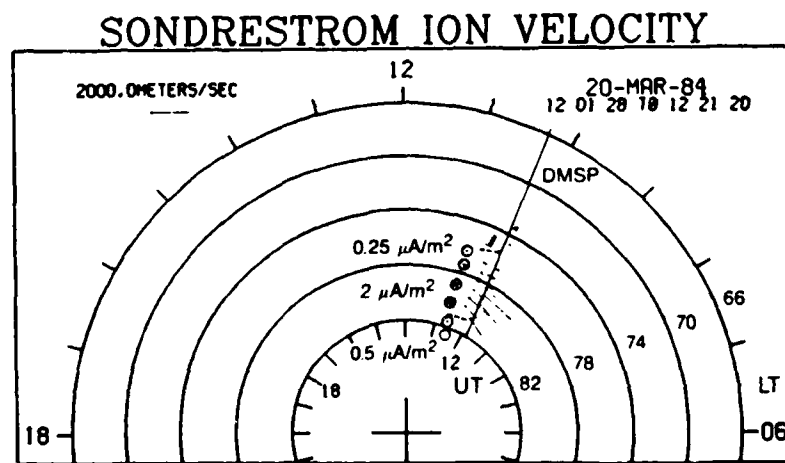
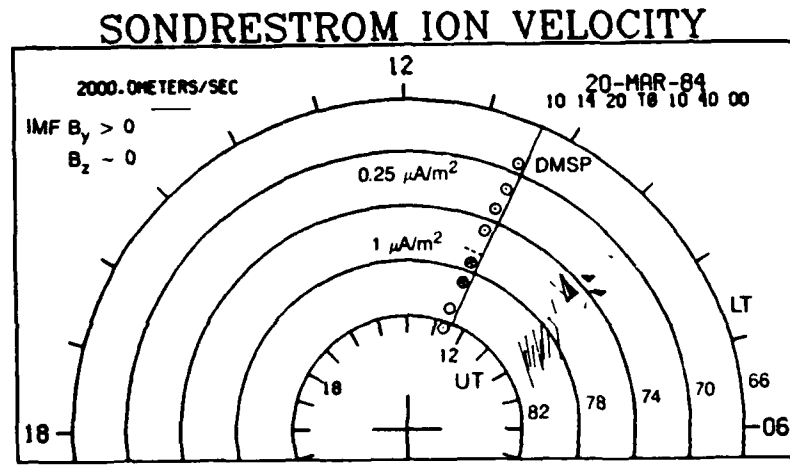


Figure 21: Ionospheric convection measured by the Sondrestrom radar during each of the DMSF satellite passes, 10:30 UT (a), 12:13 UT (b) and 13:54 UT (c), shown in Figure 20. Also shown is the track of the satellite pass and a schematic representation of the current regions.

March 7, 1984
HILAT Magnetic Field

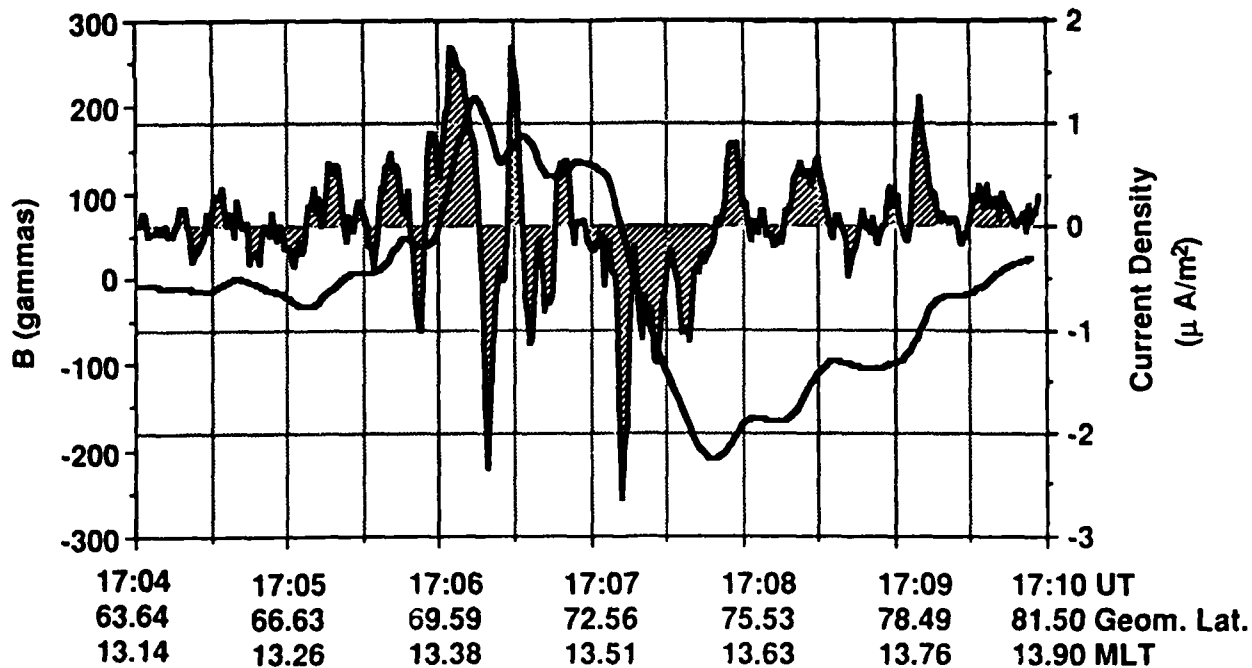
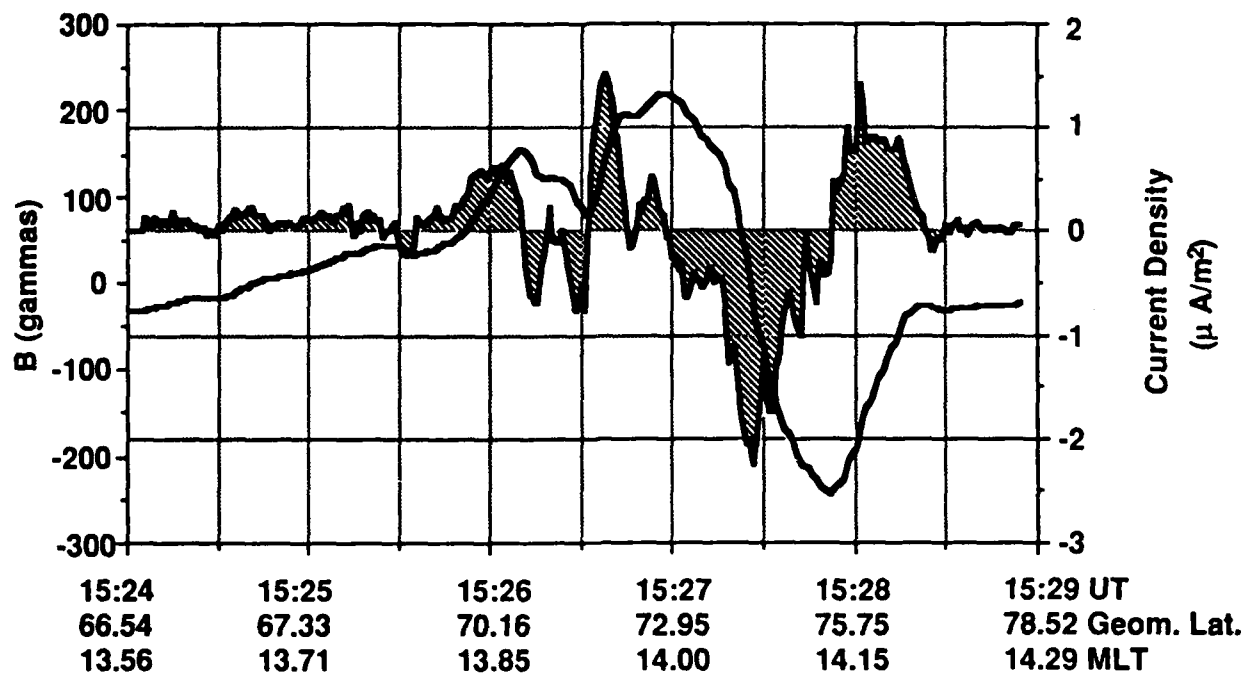
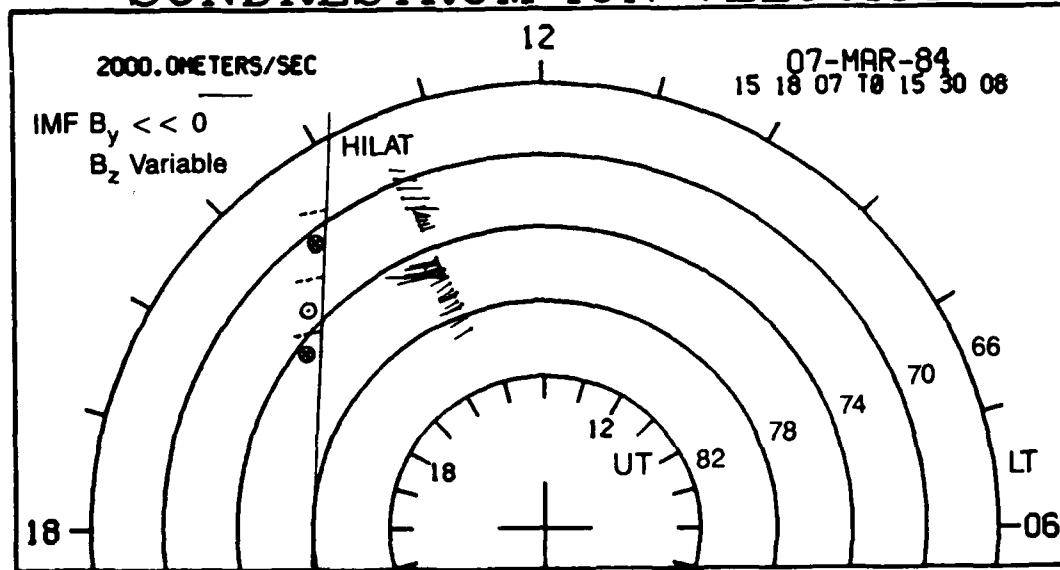


Figure 22: Magnetic field and computed field-aligned current density for two consecutive HILAT satellite passes on March 7, 1984 at 15:24 UT (top) and 17:04 UT (bottom). These passes are in the 13 - 14 local time sector. Current directed inward is positive, outward directed current is negative.

SONDRESTROM ION VELOCITY



SONDRESTROM ION VELOCITY

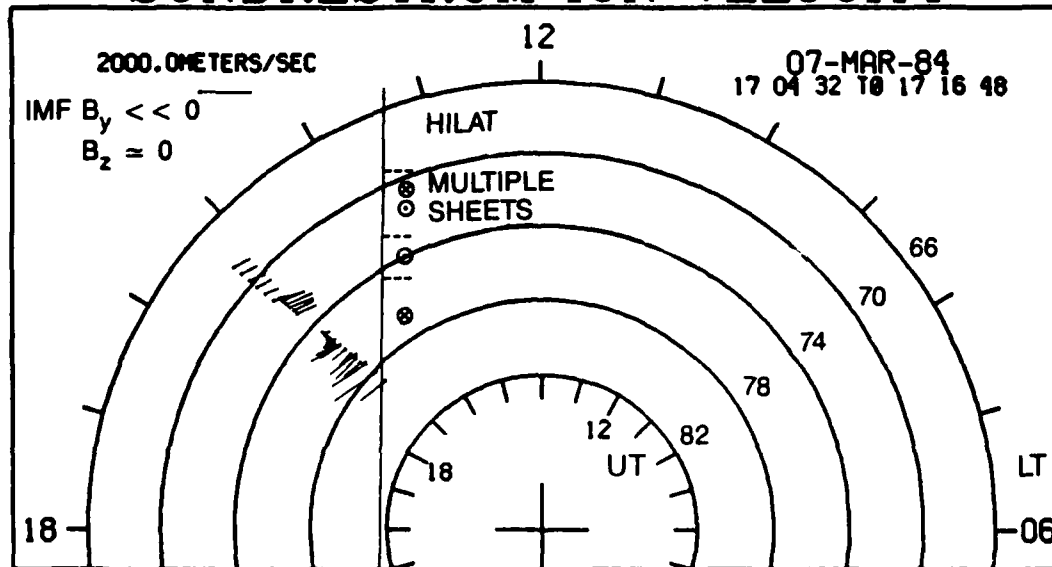


Figure 23: Ionospheric convection measured by the Sondrestrom radar during each of the HILAT satellite passes, 15:24 UT (top) and 17:04 UT (bottom) shown in Figure 22. Also shown is the track of the satellite pass and a schematic representation of the observed current regions.

March 16, 1984
HILAT Magnetic Field

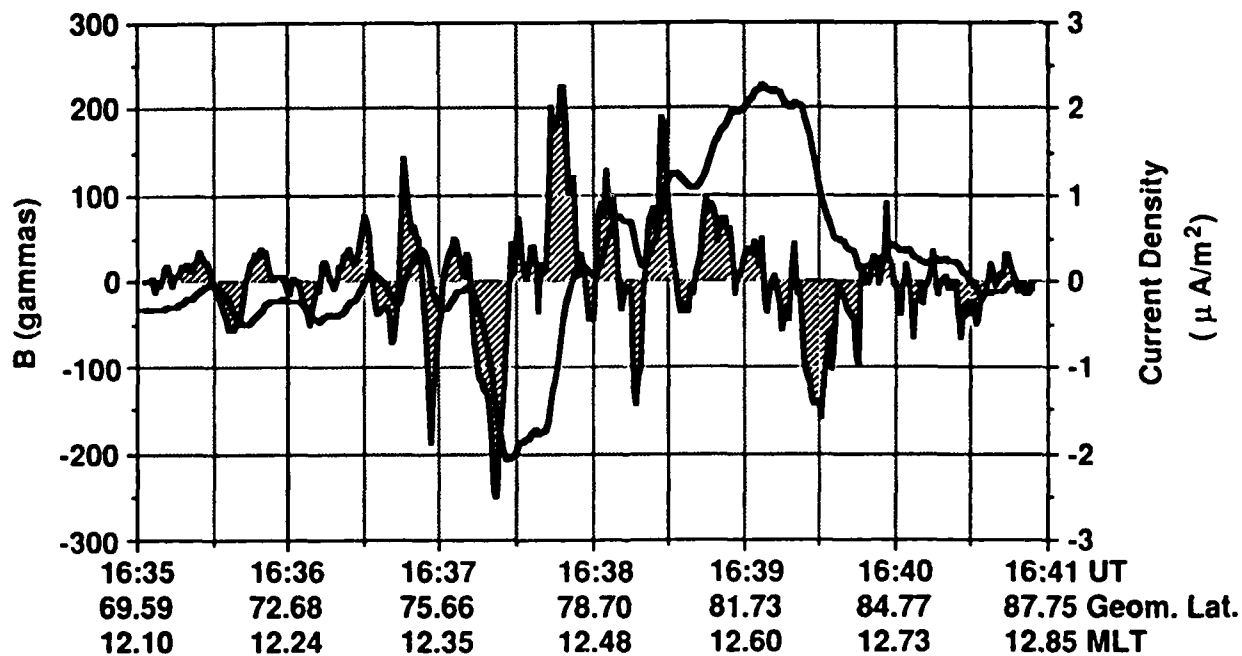
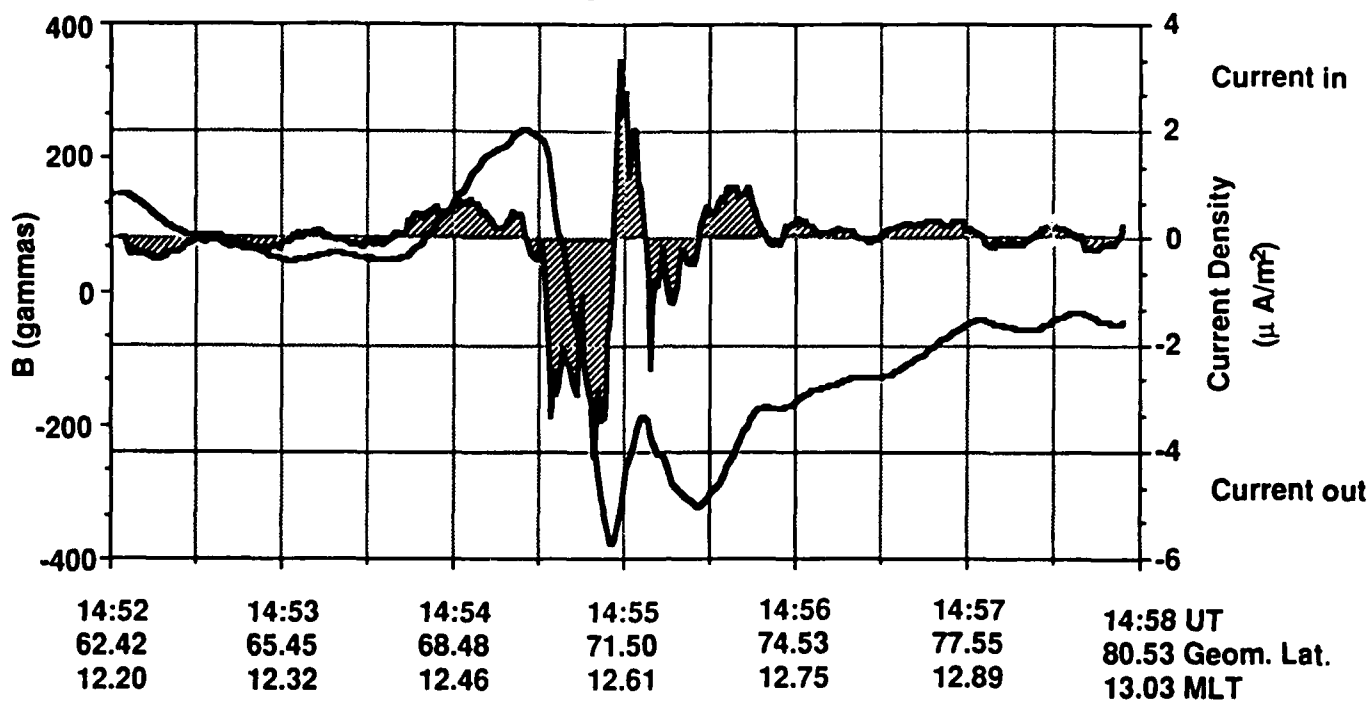
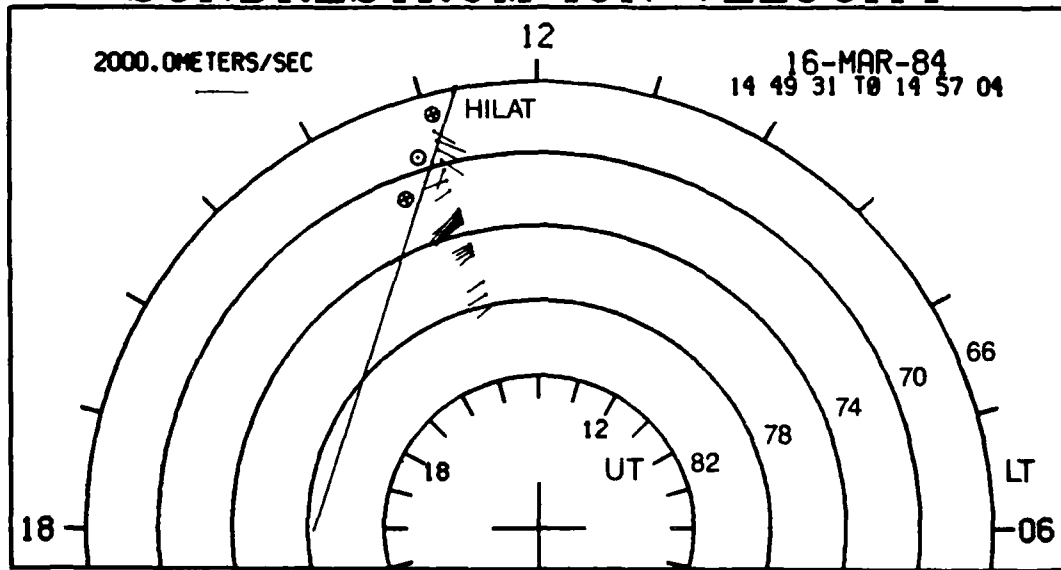


Figure 24: Magnetic field and computed field-aligned current density for two consecutive HILAT satellite passes on March 16, 1984 at 14:52 UT (top) and 16:35 UT (bottom). These passes are in the 12 - 14 local time sector. Current directed into the ionosphere is positive, outward current is negative

SONDRESTROM ION VELOCITY



SONDRESTROM ION VELOCITY

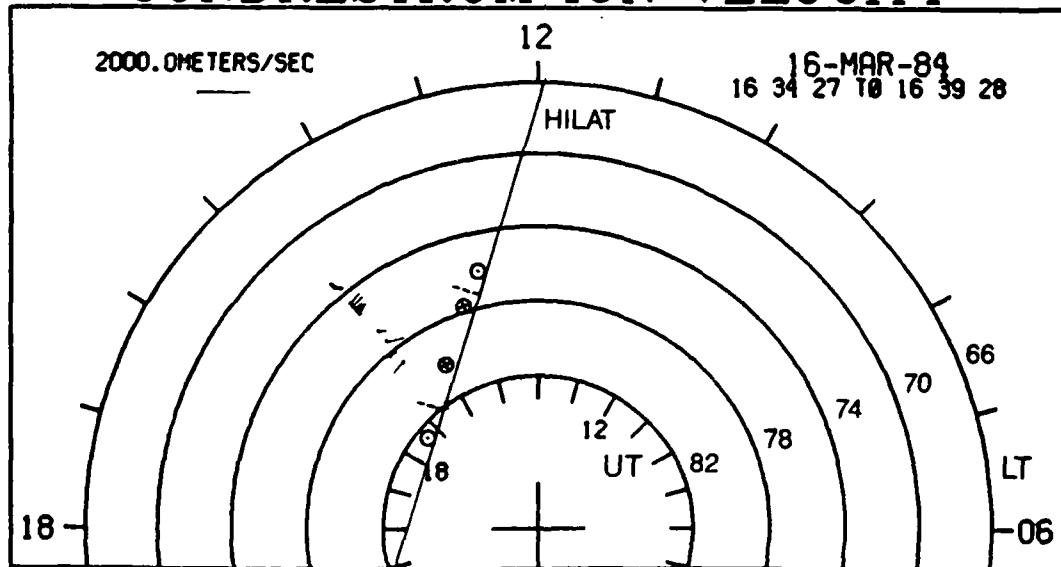


Figure 25: Ionospheric convection measured by the Sondrestrom radar during each of the HILAT satellite passes, 14:52 UT (top) and 16:35 UT (bottom) shown in Figure 24. Also shown is the track of the satellite pass and a schematic representation of the observed current regions.

observations for each of the HILAT satellite passes.

MARCH 16, 1984: Post Noon Hours

Preliminary analysis of the March 16, 1984 HILAT magnetic data and correlative Sondrestrom radar data have also been completed. The IMF observations on March 16 are shown in Figure 18. The HILAT magnetic data are shown in Figure 24. The HILAT pass beginning at 14:50 (top panel) occurs during an interval of IMF $B_y < 0$ and $B_z < 0$. The HILAT pass beginning at 16:30 UT (bottom panel) occurs during a data gap in the IMP-8 data, however, it seems possible to guess that during the gap $B_z > 0$ and $B_y > 0$. The 14:52 UT pass shows 5 current sheets while the 16:35 UT pass shows considerable structure and multiple current sheets, though possibly the sheets form a basic 3 sheet pattern.

SUMMARY

These sets of coordinated measurements provide a variety of conditions where explicit knowledge of the field-aligned current structure and ionospheric convection are known. In continuing investigations supported through other grants, we will incorporate these current configurations into our modeling effort to better understand the complex current distributions in the dayside cleft region, their relationship to high latitude ionospheric convection and their control by solar wind parameters. Figure 25 shows the Sondrestrom ionospheric convection measurements obtained during the HILAT pass intervals shown in Figure 24.

SMALL SCALE COUPLING PHENOMENA

Our investigations of small scale or localized solar wind-magnetosphere-ionosphere coupling has concentrated in three complimentary areas involving small scale field-aligned currents in the vicinity of the polar cleft. (1) Theoretical modeling of the ground magnetic signatures and ionospheric consequences of hypothetical flux transfer event current systems; (2) Analysis, in collaboration with Dr. Eigil Friis-Christensen, of magnetometer data from the Greenland chain and particularly the high time resolution data from the array of temporary stations operated around Sondrestrom during the summer of 1986; and (3) analysis of data from radar experiments which focus on rapid measurements of the ionospheric convection around the convection reversal boundary. Progress in these areas has been very good with a paper published describing our modeling techniques [McHenry and Clauer, 1987] and the publication of our discovery this summer of ionospheric traveling convection vortices (TCVs) in the Greenland magnetometer data [Friis-Christensen et al., 1988]. Both of these papers are attached to Appendix 1.

Our rapid measurements of the ionospheric convection near the reversal boundary have revealed that the boundary can be either steady or very dynamic. In the dynamic condition, it can move several hundred kilometers in a few minutes. Our initial efforts to understand the cause of these

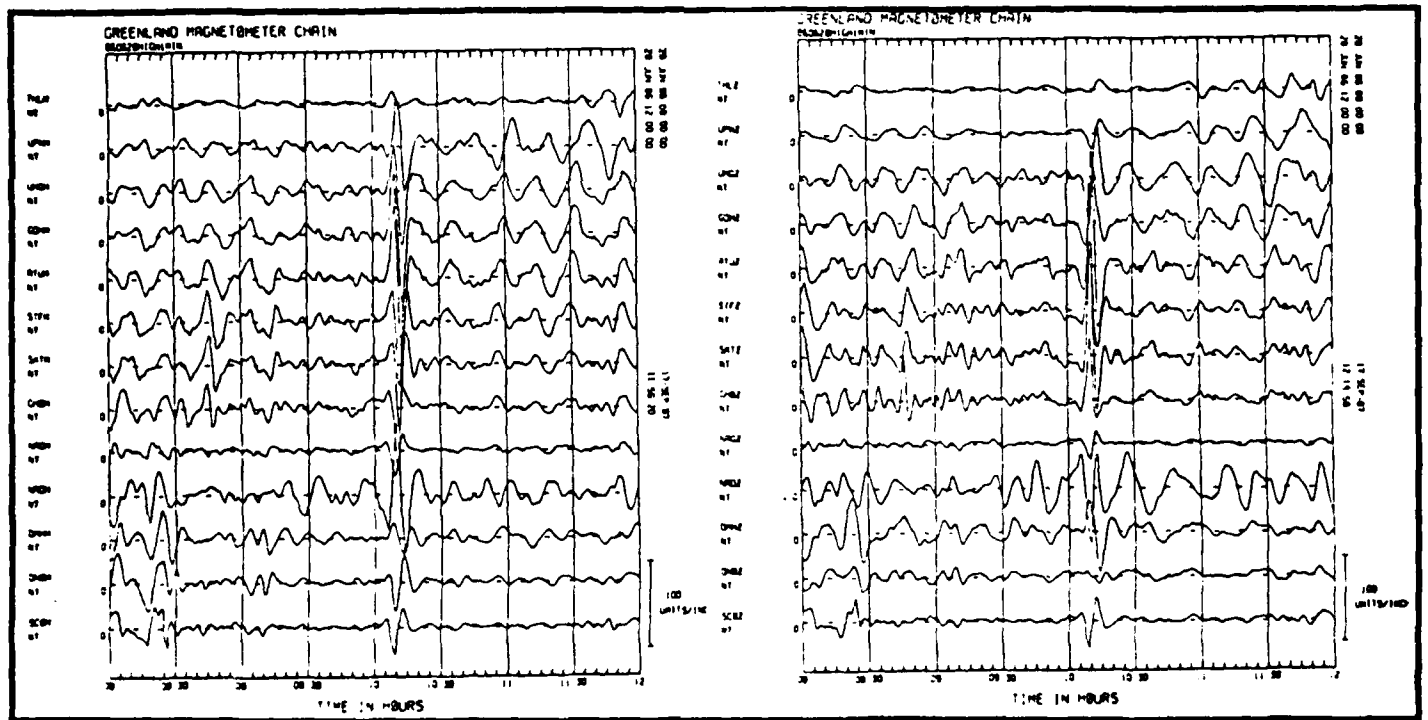


Figure 26: Data from the Greenland magnetometer chain showing the H perturbation in the left panel and the Z perturbation in the right panel. All of the stations are along the west coast except for the bottom 4 stations in each panel which are located on the east coast. The large single cycle pulsation at 10:10 UT is the TCV event under consideration.

several hundred kilometer movements of the boundary were inconclusive. However, we are now investigating the association of TCVs with the observed deflections of the boundary and there appears to be a relationship. The combined radar and ground magnetometer analysis promises to reveal new information about the dynamics of the convection reversal boundary.

Theoretical modeling efforts have concentrated on the ground magnetic signature to be expected from small scale field-aligned current systems as hypothesized for the so called flux transfer events (FTEs). FTEs are the basis for a popular theory to explain the observed transfer of magnetic flux from closed to open field lines through impulsive, localized magnetic reconnection [Russell and Elphic, 1979]. FTEs have been observed by satellites close to the magnetopause using a repeatable *in situ* magnetic perturbation caused by strong field-aligned currents. This magnetic signature is associated also with observations of plasma inside the flux tube having a mixture of magnetospheric and magnetosheath sources.

One of our goals has been to detect the signature of these events on the ionosphere. Because the plasma connecting the ionosphere and the area where FTEs have been detected obeys the "frozen in" MHD approximation, current densities and plasma velocities in the magnetosphere near the magnetopause and in the ionosphere should be very similar except for a scale factor depending upon the background magnetic field strength which is fairly well known.

Our theoretical effort has been to use the hypothesized field-aligned current structure of FTEs, assume that it is the same at the ionosphere except for the magnetic scale factor and solve for the electric field in the ionosphere. Because the dayside ionosphere is almost uniform, it is straight forward to solve for the ionospheric currents and then the magnetic field on the ground. This is presented in the paper by McHenry and Clauer [1987]. A copy of this paper showing the mathematical details and the resulting magnetic field strengths and patterns found for the FTE current systems is attached in Appendix 1. Simple estimates for the rate at which ground magnetometers would detect FTEs are also computed. Using FTE detection statistics at the magnetopause, we estimate the detection rate of FTEs at a ground station under the dayside convection reversal boundary to be between 12 and 60 minutes per sighting depending upon which model current system is considered.

We have also examined the ground induction effects caused by moving current systems. Results similar to the case for time varying currents fixed in location were found. At high ionospheric current speeds, the vertical magnetic field on the ground will diminish and the horizontal field will double. For translation speeds of convection vortices in the ionosphere of 10 km/sec and greater, induction effects are very strong. For speeds much below 10 km/sec, induction effects are weak. Thus, for the observed speeds which are between 1 and 4 km/sec, induction effects will be small and we neglect them. The large change in ground conductivity known as the 'coast effect' was also examined. Because the induction currents penetrate to depths of several tens of kilometers, i.e.

much more than the depth of the ocean, the large jump in surface conductivity between the sea and land should not effect geomagnetic observations of ionospheric currents moving less than 10 km/sec. This implies that vortex like disturbances in the ionosphere, which create a radial ground magnetic field, will still generate a radial pattern on the ground even near the sea coast where most of the Greenland high latitude observatories are located.

Guided by our modeling efforts and in collaboration with Dr. Eigil Friis-Christensen, we have focused our data analysis on a set of pulsation bursts observed in the Greenland magnetometer data. First results from this investigation showing the discovery of traveling convection vortices moving tailward near the ionospheric convection reversal boundary have been published by Friis-Christensen et al., [1988] attached in Appendix 1. Figure 26 shows such a pulsation recorded by the Greenland magnetometer chain with 1-minute data samples. During the summer of 1986, an array of magnetometer stations was operated around Sondre Stromfjord, Greenland collecting data at 20-second resolution. Figure 27 shows a series of plots from this array showing the horizontal magnetic perturbation vectors plotted at the geographic location of each station. The vectors appear to be pointing radially from a source which is at a different location in each frame, ie. moving across the array of stations. The source of this radial magnetic magnetic perturbation is thought to be a moving field-aligned current filament. These six frames of data represent only 2-minutes of the 20-second data. In Figure 28 we plot the entire event in a new format in a single plot.

If we assume that the magnetic perturbations which are observed by the stations result from a steady current system moving across the array of stations, we can equally well represent this as moving the array of stations across a fixed, steady current system. In Figure 28 we plot the horizontal perturbation vectors (which have been rotated by -90° to approximate the direction of the overhead convection) from the array and offset each set of measurements by a distance which corresponds to the velocity of the moving current structure. In this example, the motion of the current is 4 km/sec. This velocity can be judged fairly precisely since the array of stations contains one site located east of the meridional chain. The result is a twin vortex pattern which moves westward (tailward) over the stations. (The stations are located at about 10 Local Time). Numerous events or traveling convection vortices (TCVs) such as this have been identified in the data and are presently under investigation. At least two classes of TCVs have been identified. One class is associated with large single cycle pulsations such as shown in this example. Another class consists of large intervals (hours) of irregular pulsations which can be explained as series of oppositely directed field-aligned currents moving steadily across the array of stations.

Least squares fitting the modeled ground magnetic field of a single field-aligned current filament to Greenland magnetometer data, traveling vortices in the dayside ionospheric flow have been detected and tracked. They are observed during quiet periods for several hours at a time and move generally anti-sunward. Assuming each vortex to be the convection pattern produced by a small

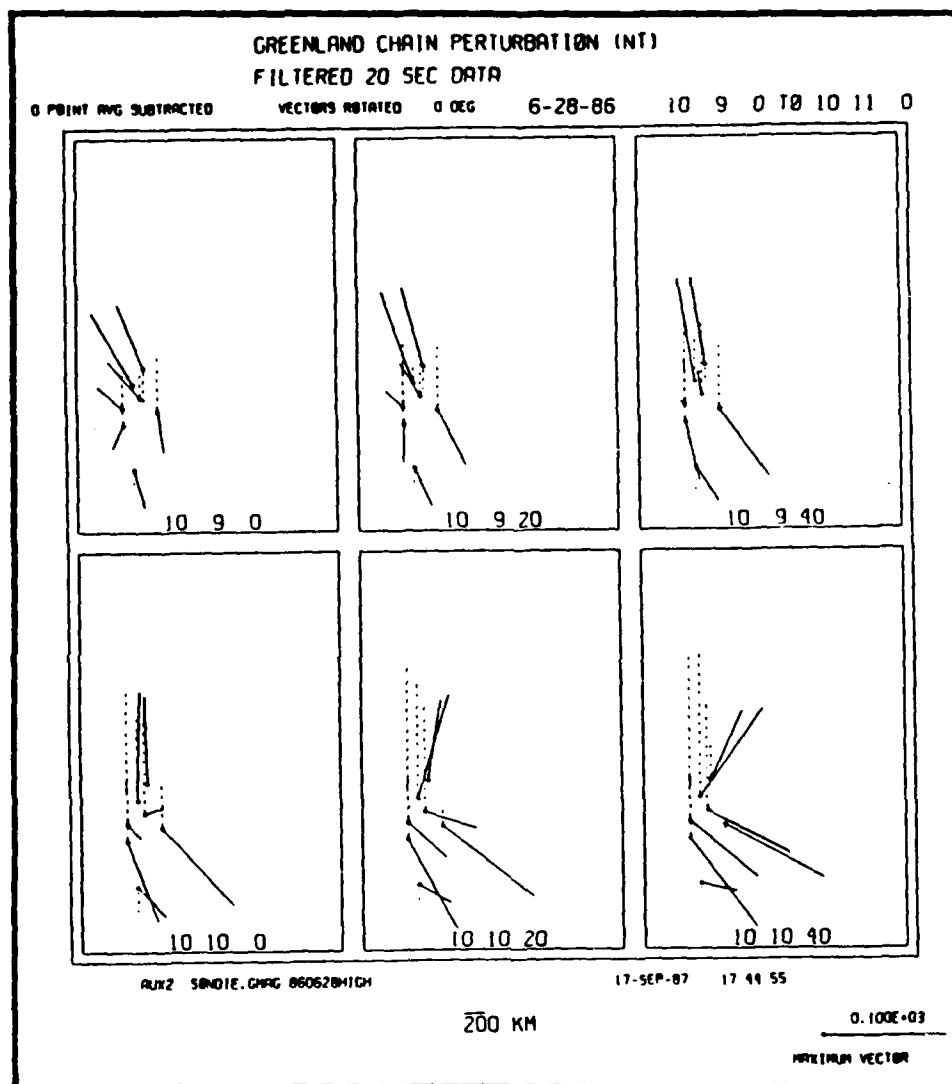


Figure 27: Magnetic perturbations are plotted in successive panels at the location of the corresponding station for the temporary array of observatories operated around Sondre Stromfjord, Greenland. This data is obtained at 20-second resolution so the time difference between each panel is 20 seconds. The total horizontal components of the magnetic perturbation are shown with a solid vector while the vertical component perturbations are shown with a vertical dashed line. At 10:08 UT, the disturbance approached the stations from the east causing a horizontal perturbation which points radially from a source position as well as a large vertical (dashed lines) perturbation. At 10:10 UT the disturbance is centered over the array of stations.

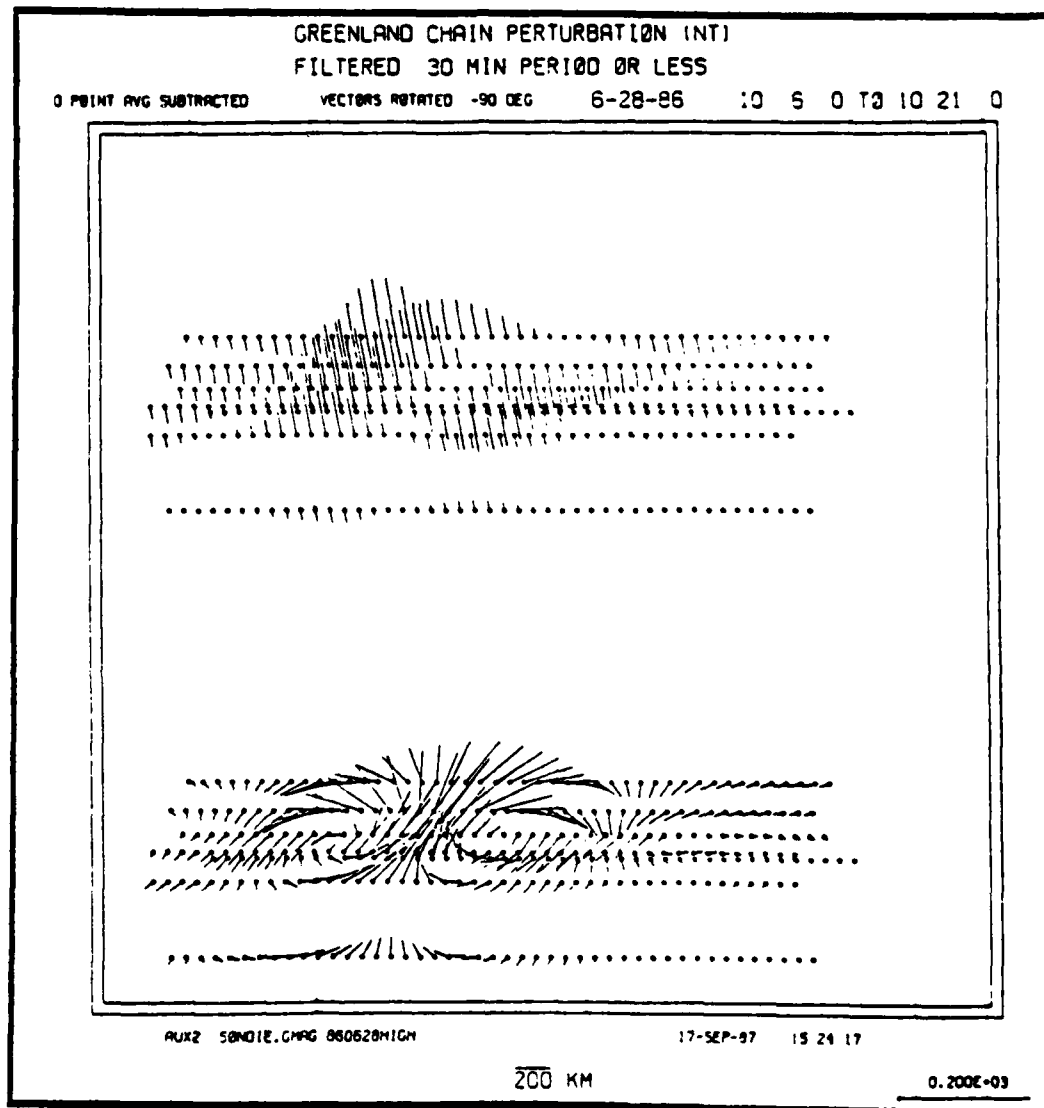


Figure 28: The magnetic perturbations in the vertical component (top) and horizontal component (bottom) from the array of 20-second stations for the interval 10:06 UT to 10:21 UT. The horizontal component has been rotated 90 degrees counter clockwise to show the equivalent ionospheric convection direction. We offset the station locations by 80 km for each set of 20 second data, corresponding to a velocity of about 4 km/sec. The resulting twin vortex pattern is indicative of a pair of oppositely directed field-aligned current filaments moving rapidly over the array of stations.

field aligned current moving across the ionosphere, the amount of field aligned current is found to be 10 to 50 kamps and they move at 1-3 km/sec across the ionosphere. During some periods, the vortices are aligned into 'trains' and the calculated field aligned current is seen to be steady for each vortex and neighboring vortices have currents of opposite sign. Other intervals have vortices which again move generally anti-sunward, have alternating field aligned current but the vortex trajectories and amount of field aligned current are irregular. These different situations indicate that there are different classes of small scale convection near the convection reversal. Simultaneous measurements using the Sondre Stromfjord Radar show the vortices are traveling along the convection reversal boundary. Because the vortices are conjugate to the magnetopause shear region and repeat in a regular fashion, we suggest that they probably results from the Kelvin-Helmholtz instability at the magnetopause. This is supported by a correlation between field aligned current strength and solar wind speed. Little correlation is found with IMF measurements.

Some time periods have been found where significant pulsations of the ground magnetic field exist but the data can not be fit with the modeled field of the simple vortex. Examining the cotemporal IMF in detail of these cases, we have found that the IMF has a high variance. It appears that these observed pulsations are directly related to the variance in the IMF. Most likely, the pulsations are caused by the large scale high latitude field aligned currents being modulated by the driving IMF. Since the magnetic field of the large scale currents is quite large, modulating them causes irregular pulsations that are larger than the ground magnetic field caused by any traveling vortices.

REFERENCES

- Araki, T., T. Kamei, and T. Iyemori, Polar cap vertical currents associated with northward interplanetary magnetic field, *Geophys. Res. Lett.*, 11, 23, 1984.
- Baker, D.N., T.A. Fritz, R.L. McPherron, D.H. Fairfield, Y. Kamide, and W. Baumjohann, Magnetotail energy storage and release during the CDAW 6 substorm analysis interval, *J. Geophys. Res.*, 90, 1205, 1985.
- Banks, P.M., T. Araki, C.R. Clauer, J.P. St. Maurice, and J.C. Foster, The interplanetary electric field, cleft currents, and plasma convection in the polar caps, *Planet. Space Sci.*, 32, 1551, 1984.
- Chiu, Y.T., N.U. Crooker, and D.J. Gorney, Model of oval and polar cap arc configurations, *J. Geophys. Res.*, 90, 5153, 1985.
- Clauer, C.R. and E. Friis-Christensen, High latitude dayside electric fields and currents during strong northward IMF: Observations and model simulation, *J. Geophys. Res.*, in press, 1988.
- Clauer, C.R. and P.M. Banks, relationship of the interplanetary electric field to the high-latitude ionospheric electric field and currents: Observations and model simulation, *J. Geophys. Res.*, 91, 6959, 1986.
- Clauer, C.R., P.M. Banks, A.Q. Smith, T.S. Jorgensen, E. Friis-Christensen, S. Vennerstrom, V.B. Wickwar, J. Kelly, and J. Doupnik, Observations of interplanetary magnetic field and of ionospheric plasma

- convection in the vicinity of the dayside polar cleft, *Geophys. Res. Lett.*, *11*, 891, 1984.
- Cowley, S.W.H., The causes of convection in the Earth's magnetosphere: A review of developments during the IMS, *Rev. Geophys.*, *20*, 531, 1982.
- Crooker, N.U., Dayside merging and cusp geometry, *J. Geophys. Res.*, *84*, 951, 1979.
- D'Angelo, N., Field-aligned currents and large scale magnetospheric electric fields, *Ann. Geophys.*, *36*, 31, 1980.
- Dungey, J.W., The structure of the ionosphere, or adventures in velocity space, in *Geophysics: The Earth's Environment*, (C. DeWitt, J. Hiebolt and A. Lebeau, editors), 526, Gordon and Breach, New York, 1963.
- Friis-Christensen, E. and J. Wilhelm, Polar cap currents for different directions of the interplanetary magnetic field in the Y-Z plane, *J. Geophys. Res.*, *80*, 1248, 1975.
- Friis-Christensen, E., M.A. McHenry, C.R. Clauer and S. Vennerstrom, Ionospheric traveling convection vortices observed near the polar cleft: A triggered response to sudden changes in the solar wind, *Geophys. Res. Lett.*, *15*, 253, 1988.
- Friis-Christensen, E., The effect of the IMF on convection patterns and equivalent currents in the polar cap and cusp, in *Magnetospheric Study 1979*, (Edited by Obayashi, T.), 290, Japanese IMS Committee, Tokyo, 1979.
- Friis-Christensen, E., Y. Kamide, A.D. Richmond, and S. Matsushita, Interplanetary magnetic field control of high-latitude electric fields and currents determined from Greenland magnetometer data, *J. Geophys. Res.*, *90*, 1325, 1985.
- Heikkila, W.J., Impulsive penetration and viscous interaction, *Proceedings of Magnetospheric Boundary Layer Conference*, Alpach, June 1979, ESA SP-148, 375, 1979.
- Heikkila, W.J., Transport of plasma across the magnetopause, *Solar Wind - Magnetosphere Coupling*, Y. Kamide and J.A. Slavin (Eds.), 337, Terra Scientific Publishing Co., Tokyo, 1986.
- Hill, T.W., Solar wind - magnetosphere coupling, in *Solar-Terrestrial Physics*, edited by R. L. Carovillano and J. L. Forbes, 261-302, D. Reidel, Dordrecht, 1983.
- Iijima, T. and Potemra, T.A., The amplitude distribution of field-aligned currents at northern high latitudes observed by Triad, *J. Geophys. Res.*, *81*, 2165, 1976.
- Iijima, T. and T. Shibaji, Global characteristics of northward IMF-associated (NBZ) field-aligned currents, *J. Geophys. Res.*, *92*, 2408, 1987.
- Iijima, T., T.A. Potemra, L.J. Zanetti, and P.F. Bythrow, Large-scale Birkeland currents in the dayside polar region during strongly northward IMF: A new Birkeland current system, *J. Geophys. Res.*, *89*, 7441, 1984.
- Lee, L.C. and J.G. Roederer, Solar wind energy transfer through the magnetopause of an open magnetosphere, *J. Geophys. Res.*, *87*, 1439, 1982.
- Lee, L.C., Magnetic flux transfer events at the Earth's magnetopause, in *Solar Wind - Magnetosphere Coupling*, Kamide Y. and Slavin, J. A. (editors), Terra Scientific Publishing Co., Tokyo, 1986.
- Lemaire, J., Impulsive penetration of filamentary plasma elements into the magnetospheres of the Earth and Jupiter, *Planet. Space Sci.*, *25*, 887, 1977
- Luhmann, J.G., R.J. Walker, C.T. Russell, N.U. Crooker, J.R. Spreiter, and S.S. Stahara, Patterns of potential magnetic merging sites on the dayside magnetopause, *J. Geophys. Res.*, *89*, 1739, 1984.
- Maezawa, K., Magnetospheric convection induced by the positive and negative Z components of the inter-

- planetary magnetic field: quantitative analysis using polar cap magnetic records, *J. Geophys. Res.*, *81*, 2289, 1976.
- McHenry, M.A. and C.R. Clauer, Modeled ground magnetic signatures of flux transfer events, *J. Geophys. Res.*, *92*, 11231, 1987.
- Paschmann, G., G. Haerendel, I. Papamastorakis, N. Sckopke, S.J. Bame, J.T. Gosling, and C.T. Russell, Plasma and magnetic field characteristics of magnetic flux transfer events, *J. Geophys. Res.*, *87*, 2159, 1982.
- Podgorny, I.M., E.M. Dubinin, and Y.N. Potanin, The magnetic field on the magnetospheric boundary from laboratory simulation data, *Geophys. Res. Lett.*, *4*, 207, 1978.
- Reiff, P.H., Sunward convection in both polar caps, *J. Geophys. Res.*, *87*, 5976, 1982.
- Reiff, P.H., and J.L. Burch, IMF B_y -dependent plasma flow and Birkeland currents in the dayside magnetosphere 2. A global model for northward and southward IMF., *J. Geophys. Res.*, *90*, 1595, 1985.
- Rich, F.J. and Y. Kamide, Convection electric fields and ionospheric currents derived from model field-aligned currents at high latitudes, *J. Geophys. Res.*, *88*, 271, 1983.
- Russell, C.T., and R.C. Elphic, ISEE observations of flux transfer events at the dayside magnetopause, *Geophys. Res. Lett.*, *6*, 33, 1979.
- Saunders, M.A., C.T. Russell, and N. Sckopke, Flux transfer events: Scale size and interior structure. *Geophys. Res. Lett.*, *11*, 131, 1984.
- Sergeev, V.A., and B.M. Kuznetsov, Quantitative dependence of the polar cap electric field on the IMF B_z component and solar wind velocity, *Planet. Space Sci.*, *29*, 205, 1981.
- Southwood, D.J., The ionospheric signature of flux transfer events, *J. Geophys. Res.*, *92*, 3207, 1987.
- Spence, H.E., M.G. Kivelson, and R.J. Walker, The dynamics of the nightside field-aligned currents and their linkage to the near-earth magnetotail, *International Union of Geodesy and Geophysics Abstracts V.2*, Vancouver, 1987.
- Wilhjelm, J., E. Friis-Christensen, and T.A. Potemra, The relationship between ionospheric and field-aligned currents in the dayside cusp, *J. Geophys. Res.*, *83*, 5586, 1978.
- Zanetti, L.J., T.A. Potemra, T. Iijima, W. Baumjohann, and P.F. Bythrow, Ionospheric and Birkeland current distributions for northward interplanetary magnetic field: Inferred polar convection, *J. Geophys. Res.*, *89*, 7453, 1984

Appendix 1

Published Papers Supported by AFGL Contract Number F19628-85-K-0001

1. Clauer, C.R., E. Friis-Christensen, High-Latitude Dayside Electric Fields and Currents During Strong Northward Interplanetary Magnetic Field: Observations and Model Simulation, *J. Geophys. Res.*, *93*, 2749, 1988.
2. Clauer, C.R. and P.M. Banks, Relationship of the Interplanetary Electric Field to the High-Latitude Ionospheric Electric Field and Currents: Observations and Model Simulation, *J. Geophys. Res.*, *91* 6959, 1986.
3. Clauer, C.R., The Technique of Linear Prediction Filters Applied to Studies of Solar Wind-Magnetosphere Coupling, *Solar Wind - Magnetosphere Coupling*, Kamide Y. and Slavin, J. A. (editors), Terra Scientific Publishing Co., Tokyo, 1986.
4. Friis-Christensen E., M.A. McHenry, C.R. Clauer, Ionospheric Traveling Convection Vortices Observed Near the Polar Cleft: A Triggered Response to Sudden Changes in the Solar Wind, *Geophys. Res. Lett.*, *15*, 253, 1988.
5. McHenry, M.A., and C.R. Clauer, Modeled Ground Magnetic Signatures of Flux Transfer Events, *J. Geophys. Res.*, *92* 11,231, 1987.
6. Robinson, R.M. C.R. Clauer, O. de La Beaujardiere, J.D. Kelly, and D.S. Evans, IMF B_y Control of Ionization and Electric Fields Measured by the Sondrestrom Radar, *Solar Wind - Magnetosphere Coupling*, Kamide Y. and Slavin, J. A. (editors), Terra Scientific Publishing Co., Tokyo, 1986.

High-Latitude Dayside Electric Fields and Currents During Strong Northward Interplanetary Magnetic Field: Observations and Model Simulation

C. ROBERT CLAUER

Space, Telecommunications and Radioscience Laboratory, Stanford Electronics Laboratories, Stanford University, Stanford, California

EIGIL FRIIS-CHRISTENSEN

Division of Geophysics, Danish Meteorological Institute, Copenhagen

On July 23, 1983, the Interplanetary Magnetic Field turned strongly northward, becoming about 22 nT for several hours. Using a combined data set of ionospheric convection measurements made by the Sondre Stromfjord incoherent scatter radar and convection inferred from Greenland magnetometer measurements, we observe the onset of the reconfiguration of the high-latitude ionospheric currents to occur about 3 min following the northward IMF encountering the magnetopause. The large-scale reconfiguration of currents, however, appears to evolve over a period of about 22 min. Using a computer model in which the distribution of field-aligned current in the polar cleft is directly determined by the strength and orientation of the interplanetary electric field, we are able to simulate the time-varying pattern of ionospheric convection, including the onset of high-latitude "reversed convection" cells observed to form during the interval of strong northward IMF. These observations and the simulation results indicate that the dayside polar cap electric field observed during strong northward IMF is produced by a direct electrical current coupling with the solar wind.

1. INTRODUCTION

It is well established that magnetospheric convection and the associated ionospheric plasma convection are strongly controlled by the strength and orientation of the interplanetary magnetic field (IMF) observed at the magnetopause [Heelis, 1984; Zanetti et al., 1984; Clauer et al., 1984; Reiff and Burch, 1985; Friis-Christensen et al., 1985; Clauer and Banks, 1986; and references therein]. A simple model to explain this observed control has been suggested by Banks et al. [1984]. In this model, the high-latitude ionospheric electric field is a consequence of direct electrical coupling between the interplanetary electric field and the high latitude ionosphere via field-aligned currents.

This model was adapted by Clauer and Banks [1986] to perform a series of electrostatic computations of the ionospheric electric field based upon measured IMF values obtained by the IMP 8 spacecraft. Using these computations, Clauer and Banks simulated the ion convection velocity which would be observed by the Sondre Stromfjord, Greenland, incoherent scatter radar under the conditions described by the model. The results of the simulations compared favorably, in general, with the ionospheric plasma convection measured by the radar.

The time intervals which were studied by Clauer and Banks [1986] consisted primarily of intervals having southward IMF and occasional brief intervals of northward IMF. The simulation of the northward IMF intervals did not agree well with the observations. Therefore, in this investigation we address more carefully the situation for both IMF B_z northward and southward. The current distributions used

by Clauer and Banks [1986] have been refined and are now more consistent with the field-aligned current systems which we hypothesize to connect the solar wind emf with the dayside high-latitude ionosphere.

The model follows a simple decomposition of the dayside high-latitude field-aligned currents into systems which are separately controlled by the IMF B_y and B_z components. These field-aligned current systems are referred to as the "field-aligned" DPY and DPZ current systems as they are associated with the ionospheric systems which have been originally labeled with these names [Friis-Christensen and Wilhelm, 1975]. Here, however, we modify slightly the definition of the DPZ disturbance. In the original definition, the DPZ disturbance included the entire two-cell current system also known as the DP2 system. We now limit the definition of the DPZ system to the more local two-cell pattern observed on the dayside at times when IMF $|B_z| \gg |B_y|$. This system corresponds to the cusp currents statistically described by Iijima and Potemra [1976] for IMF B_z southward and to the system observed by Araki et al. [1984] and termed NBZ currents by Iijima et al. [1984]. In our model, the field-aligned DPZ system is contained entirely on the dayside of the polar cap and does not extend into the nightside as described by Iijima et al. [1984], Zanetti et al. [1984], and Iijima and Shibaji [1987]. The DPY system is a single ionospheric system consisting of a Hall current flowing between a pair of oppositely directed field-aligned current sheets oriented longitudinally across and centered near the noon meridian, as observed by Wilhelm et al. [1978].

Refinements to the field-aligned DPY and DPZ current systems in our simulation now include latitudinal changes in the current systems when IMF B_z changes sign. The latitudinal changes in the currents agree better with observations and are more consistent with the theoretical notions regarding merging on lobe field lines poleward of the cleft for northward IMF and merging on field lines equatorward of

Copyright 1988 by the American Geophysical Union.

Paper number 7A9309.
0148-0227/88/007A-9309\$02.00

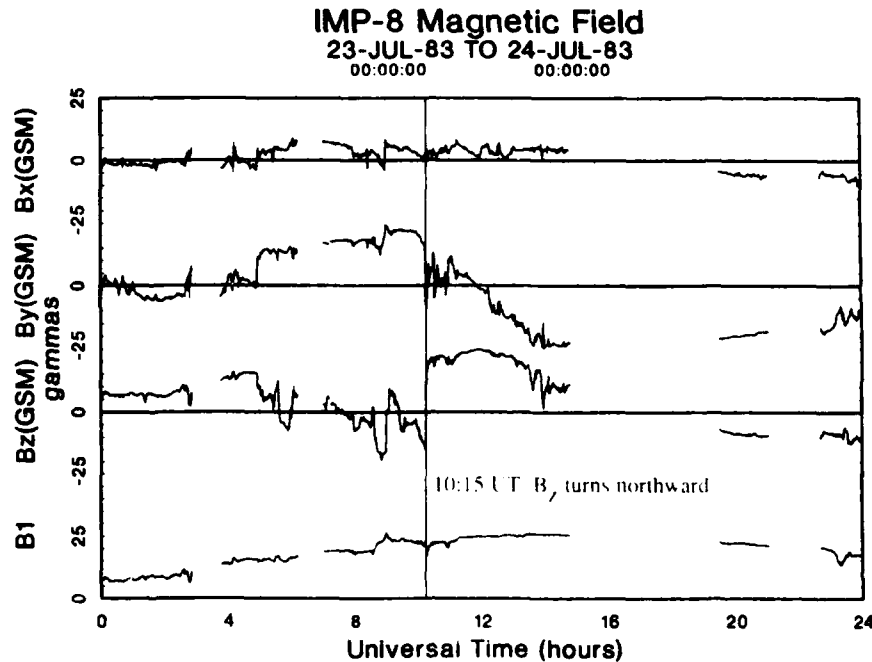


Fig. 1. Interplanetary magnetic field measurements in GSM coordinates during July 23, 1983.

the cleft for southward IMF [Dungey, 1963; Crooker, 1979; Reiff, 1982; Luhmann *et al.*, 1984; Chiu *et al.*, 1985 and references therein].

To examine the consequences of the new distributions of currents and to compare with observations, we are fortunate to have both radar convection observations and IMF measurements on July 23, 1983, during an interval when the IMF turns strongly northward for several hours. This day represents an extreme case and therefore is very interesting for investigation.

2. RESULTS

Observations

Figure 1 shows measurements of the interplanetary magnetic field in GSM coordinates obtained by the IMP 8 spacecraft located at $X_{gse} = 28 R_E$ and $Y_{gse} = -10 R_E$. The solar wind velocity is about 400 km/s and the proton number density is about $10/\text{cm}^2$. Assuming that the solar wind dynamic pressure is balanced by the magnetic pressure of the Earth's magnetic field, the distance from the center of the Earth to the subsolar magnetopause is about $7.5 R_E$. Using this information, we estimate that the transit time between IMP 8 and the magnetopause is about 7 to 9 min (see Clauer and Banks [1986] for a description of the estimation procedure).

The IMF was unusually large on July 23, 1983, having total field values of about 22 nT or larger for much of the day. At 1015 UT the field turns strongly northward with B_z becoming about 20 nT. It remains strongly northward for many hours. The B_y component of the field is much smaller than the strong B_z component from 1018 until about 1310 UT. The magnitude of B_y becomes larger than B_z at 1330 UT.

On July 23, 1983, the Sondre Stromfjord radar made iono-

spheric convection measurements in the invariant latitude range between 70° and 80° with about 25-min time resolution. In addition to the operations of the radar, the Danish Meteorological Institute Greenland magnetometer chain operates continuously and is roughly aligned along the Sondre Stromfjord magnetic meridian. In Figure 2 the convection observations obtained from both the Sondre Stromfjord radar and from Greenland magnetometer measurements are shown in a clock dial format. Local noon is at the top of the plot, and local time is shown around the outer circumference of the plot. UT is shown around the interior of the plot, and the radial dimension indicates invariant latitude. Velocity vectors are shown with a point at the measurement position and a line in the direction of the flow. The length of the line is proportional to the flow speed.

In general, the velocity vectors determined from the Sondre Stromfjord radar data lie below 79.5° . There are occasional vectors, however, above 80.0° obtained when significant signal is available in the most distant range gates. Details of the operating mode and data reduction are described by Clauer and Banks [1986]. In addition, we show three sets of velocity vectors at invariant latitudes 79.9° , 82.6° , and 85.5° which were inferred from the magnetic measurements of the three northernmost stations in the west Greenland magnetometer chain. The station names and coordinates are given in Table 1.

These equivalent velocity vectors were obtained by rotating the horizontal magnetic perturbation vector by 90° to give the equivalent current direction, then rotating another 180° to give the convection velocity direction. The magnetic measurements are not calibrated with the radar velocity measurements, so the magnitude of the vectors is only roughly proportional to the velocity. The direction indicated by the magnetically derived equivalent convection velocity vectors, however, is generally consistent with the

Table 1. Greenland Magnetic Observatories

Station	Symbol	Geographic North	Geographic East	Invariant Latitude	Declination
Thule	THL	77.48°	290.83°	85.5°	-73°
Kuvdlorssuaq	KUV	74.57°	302.82°	81.6°	-57°
Upernavik	UPN	72.78°	303.85°	79.9°	-54°

actual convection direction. Discrepancies, nevertheless, do occur in regions where there are conductivity gradients, and thus the equivalent velocity vectors near dawn and dusk may be rotated at some angle to the true convection. For example, this may explain the rotation of the magnetic vectors relative to the highest-latitude radar observations near dusk. During the northern hemisphere summer, the dayside high-latitude ionosphere has a fairly uniform conductivity except near the dayside terminator. The equivalent convection vectors should nevertheless respond in a consistent manner to changes in convection produced by changes in the external drivers of the convection.

Confining our attention to the radar data which lie below 79°, apart from a small variation in the latitudinal location of the convection reversal boundary between 1000 UT and 1030 UT we see no change in convection in response to the northward turning of IMF B_z at 1015 UT. From 0800 to 1300 UT, the convection reversal boundary is located between 71° and 75°. The antisunward convection observed at latitudes above this boundary is thought to be tailward convection on polar cap field lines. The low latitude of the convection reversal boundary indicates an expanded polar cap and is consistent with the several intervals of large southward IMF prior to 1015 UT. The convection is strong, being between 2 and 3 km/s. Note that the IMF B_y component is extremely large during this interval as well.

It is interesting that there is no apparent change in the

radar-measured convection at around 1015 UT when the IMF B_z turned northward. The radar measurements extend well into the polar cap antisunward convection. Extending the convection measurements further poleward by use of the magnetometer data does, however, show a change in convection at very high latitudes. Both KUV at $\Lambda = 81.6^\circ$ and THL at $\Lambda = 85.5^\circ$ observe a sunward rotation of the convection velocity. The sunward convection is restricted to very high latitudes. It is also noteworthy that the change in convection observed at KUV and THL follows the polarity change in B_z very directly.

Allowing an 8-min transit time from IMP 8 to the magnetopause, the polarity change would encounter the magnetopause at 1023 UT, and the ionospheric response observed in Figure 2 is seen at 1045. In Figure 3 we have plotted the δD component of the magnetic field at TLH, KUV and UPN using 1-min resolution magnetometer data. The quantity δD is the perturbation field declination angle measured relative to the average magnetic declination at each station. Examination of the 1-min magnetometer data shown in Figure 3 indicates that the field at THL and KUV begins a slow rotation at 1026 UT which continues through 1058 UT. Similar timing is seen at UPN. The plot shows that at THL and KUV the magnetic perturbation vector rotates from $\delta D = 30^\circ$ to $\delta D = 150^\circ$ between 1026 and 1058 UT. Thus, changes in the ionospheric currents associated with the northward turning of B_z begin about 3

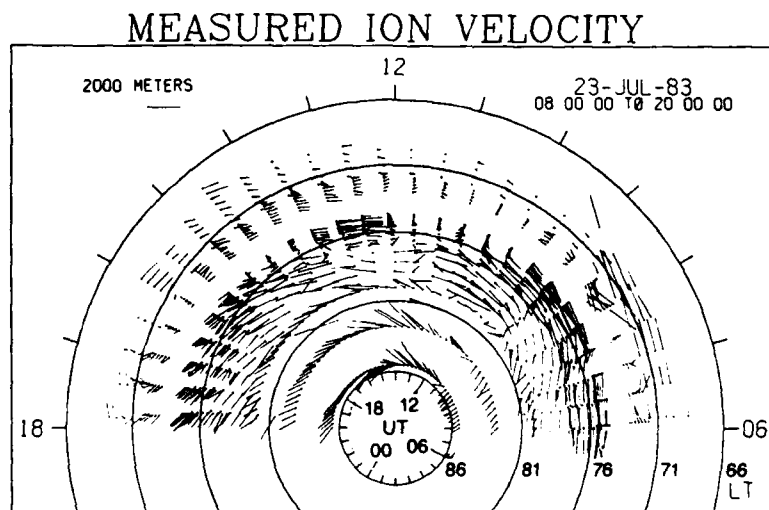


Fig. 2. Polar plot showing F region ion convection velocity vectors as a function of latitude and local time for July 23, 1983. Local time is indicated around the outer circumference of the plot, and universal time is indicated around the inner circumference. Local magnetic noon (1400 UT) is at the top of the plot. The three complete rows of highest-latitude vectors are convection velocities inferred from ground magnetometer data. The other vectors in the plot were obtained using the Sondre Stromfjord, Greenland, incoherent scatter radar.

Greenland Magnetometer Data

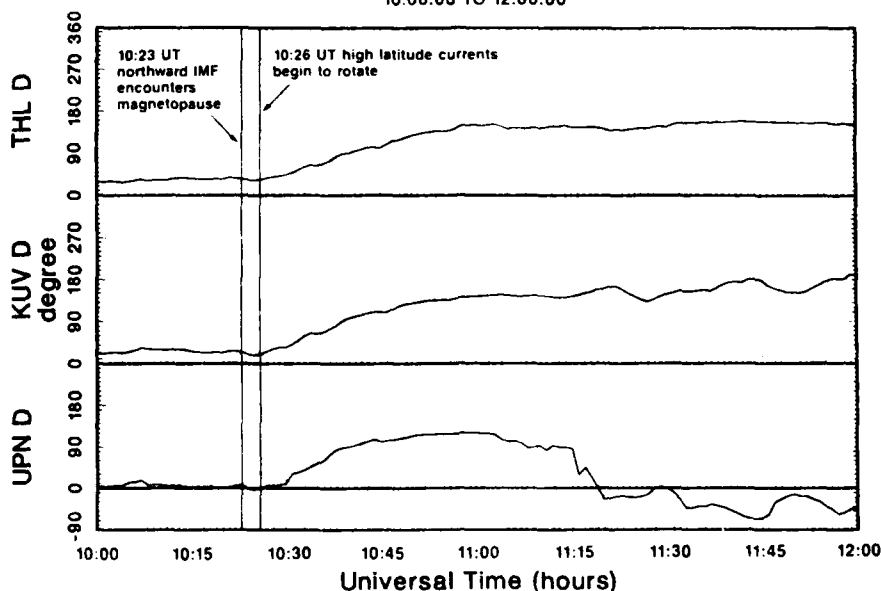
23-JUL-83
10:00:00 TO 12:00:00

Fig. 3. Horizontal magnetic field declination variations measured relative to the average declination at Thule (top), Kuvdlorsuaq (middle), and Upernavik (bottom). At 1023 UT the northward IMF is estimated to encounter the magnetopause, and at 1026 UT the field at THL and KUV begins a 120° rotation.

min following the estimated time that the northward field encounters the magnetopause. This delay time is comparable with the estimated propagation time for an Alfvén wave to travel from the dayside magnetopause to the ionosphere. We also notice that during the rotation of the field, there is a periodic variation in the field rotation with a period of about 6 min. Perhaps this is due to multiple reflections of the incident Alfvén wave which initiates the current reconfiguration. The large-scale reconfiguration of the currents appears to evolve over the 22 min during which the field rotation at THL and KUV takes place.

Model Simulation

Using the technique described by Clauer and Banks [1986] we have used a computer model to simulate the convection pattern observed on July 23, 1983. The model assumes that the distribution and strength of field-aligned currents in the dayside high-latitude regions are controlled by the direction and magnitude of the IMF. For a given conductivity distribution and field-aligned current distribution, the model computes the global ionospheric electrostatic potential distribution. Here we have adopted the realistic but simple conductivity model from Kamide and Matsushita [1979] with the additional inclusion of a conductivity enhancement in the auroral oval. From the computed electric potential, the $\mathbf{E} \times \mathbf{B}$ -region plasma drift can be determined. Thus, using the measurements of the IMF recorded by IMP 8 to determine the distribution and magnitude of the dayside high-latitude field-aligned currents, we compute the time-varying ionospheric electrostatic field and the associated plasma drift which would be measured by the Sondre Strofjord radar and high-latitude Greenland magnetometers.

We have now modified the distribution of current to better reflect our understanding of the dayside high-latitude currents and our ideas regarding the origins of these current systems. The distributions of current in our model have been guided by the following observational and theoretical considerations. We hypothesize that the region 1 currents map to the vicinity of the low-latitude boundary layer, and the region 2 currents map to the ring current region of the inner magnetosphere. Since the current is observed to be continuous in the observations of low-altitude polar satellites, we assume that the current is continuous throughout the region in the magnetosphere between the ring current and the low-latitude boundary layer. During periods of northward IMF, the region 1 and 2 currents diminish substantially in strength and are located at higher latitudes. Near local noon, where the low-latitude boundary layer is thin and the boundary layer flow is small, the primary contributions to the region 1 current system are the field-aligned *DPY* and *DPZ* currents which result from a direct electrical connection between the solar wind and the magnetosphere. We do not address how this electrical connection is accomplished but feel that it is consistent with the variety of magnetic merging models discussed in the literature. Also, since we are primarily concerned with dayside observations, these considerations may oversimplify the situation in the nightside magnetosphere.

In our model, we consider a set of independent dayside high-latitude field-aligned current systems each separately controlled by the IMF B_y and B_z components (or equivalently by the interplanetary electric field E_z and E_y components as discussed by Banks et al. [1984] and D'Angelo [1980]). In the model, the *DPY* ground magnetic disturbance is produced by the ionospheric Hall current flowing

Ionospheric Distribution of Field-Aligned Current

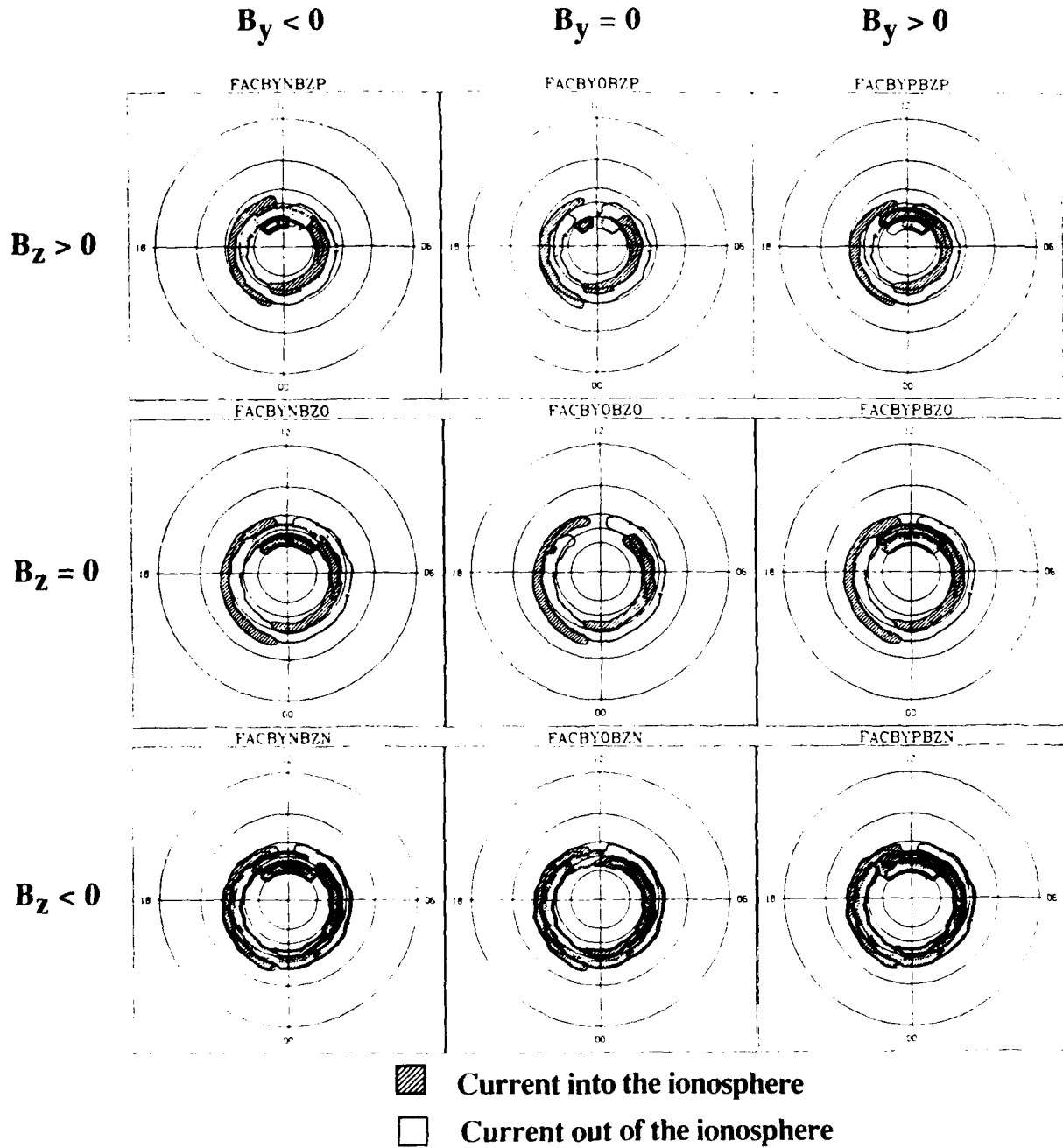


Fig. 4. Polar plot of the distribution of field-aligned current used in the computer model. The shaded region with solid contours indicates current into the ionosphere and the unshaded region with dashed contours indicates current out of the ionosphere in the northern hemisphere. The contour interval is at $0.5 \mu A/m^2$.

between a pair of oppositely directed field-aligned current sheets oriented longitudinally across and centered near the noon meridian as observed by *Wiltjelm et al.* [1978]. One of the current sheets is collocated with the region 1 currents, and the other current sheet is located poleward of the region 1 currents. During northward IMF, the *DPY*

currents are located at higher latitudes but maintain their relationship relative to the region 1 currents. The mapping of these currents to the magnetopause is that suggested by *Banks et al.* [1984] and shown schematically in their Figure 2. The poleward current sheet lies on field lines near the poleward boundary of the polar cleft, and the equatorward

Ionospheric Electric Potential Pattern

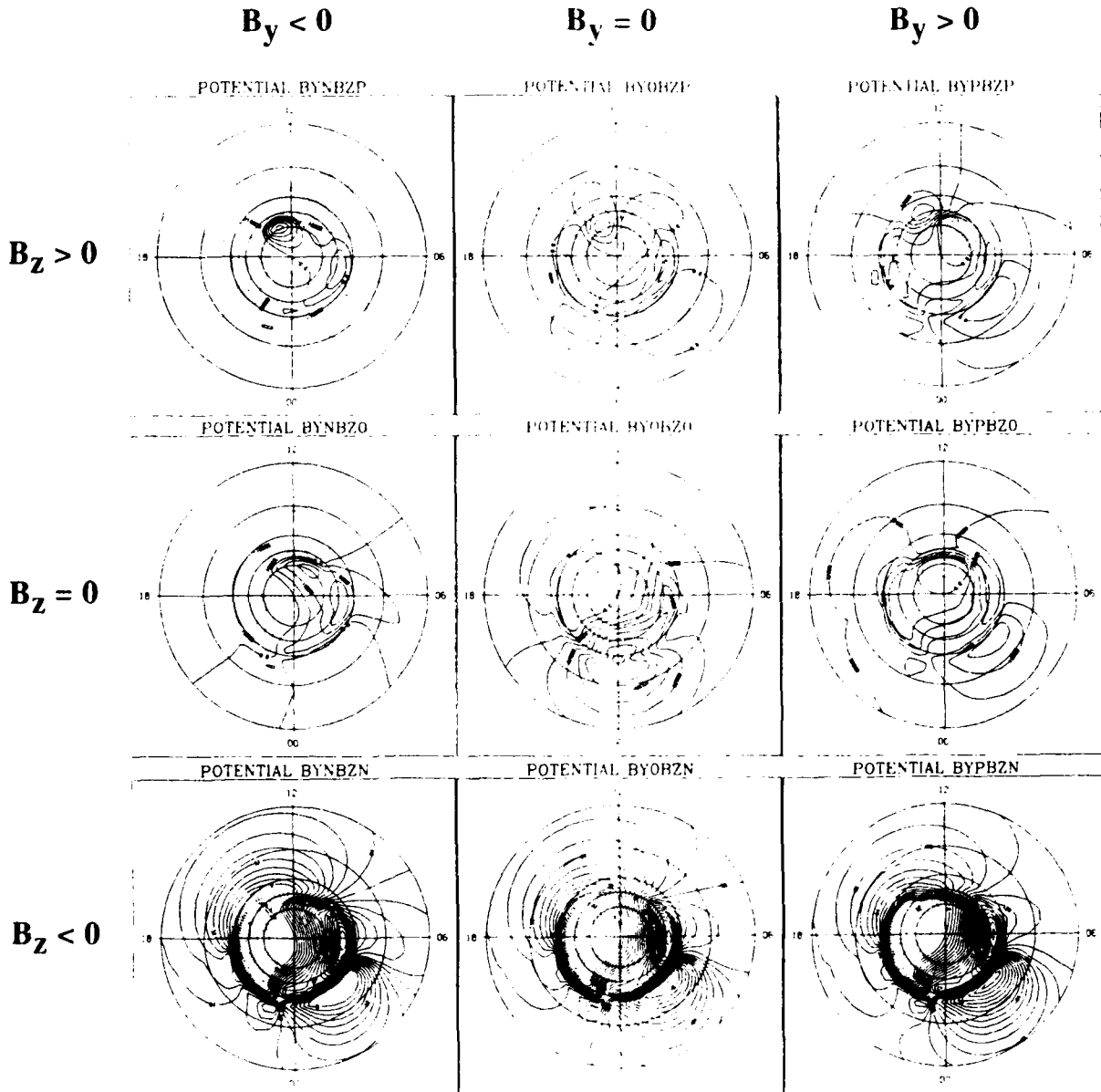


Fig. 5. Polar plot of the ionospheric potential distribution associated with each of the current distributions shown in Figure 4. The contour interval is 8 kV. The zero potential curve crosses the center of the polar cap; solid contours indicate positive values, and dashed contours indicate negative values.

sheet which partially forms the noon sector region 1 system lies near the equatorward boundary of the cleft. Associated with the IMF B_y component is an E_z interplanetary electric field which drives the DPY current sheets.

For southward IMF (negative B_z) the field-aligned DPZ current system is a current wedge with current flowing from the vicinity of the prenoon equatorial magnetopause into the ionosphere at the latitude of the region 1 current and out of the ionosphere in the postnoon region 1 current along field lines which extend to the vicinity of the postnoon equatorial magnetopause (also shown schematically in Banks *et al.*

[1984] Figure 2). During northward IMF the field-aligned DPZ system (or NBZ system as discussed by some researchers [e.g., Iyama *et al.*, 1984]) is a similar current wedge with opposite current direction polarity, but located on field lines near the poleward boundary of the polar cleft and thus collocated with the poleward sheet of the field-aligned DPY current system. Associated with the IMF B_z component is an E_y interplanetary electric field which drives the DPZ currents at the longitudinal ends of the cleft.

The nine plots in Figure 4 show the variability with respect to the IMF of the current distributions used in our

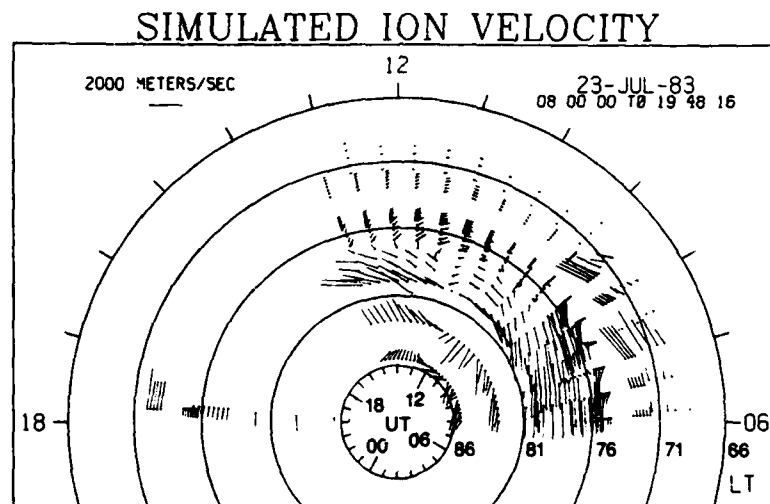


Fig. 6. Simulated *F* region ion convection velocity vectors for July 23, 1983, shown in the same format as Figure 2.

present model. The pattern in the center shows the baseline $B_x = B_y = 0$ configuration. The top row shows patterns for IMF $B_z > 8$ nT, and the bottom row shows patterns for IMF $B_z < -8$ nT. The right column shows patterns for IMF $B_y > 8$ nT, and the left column shows patterns for IMF $B_y < -8$ nT. For larger values of the field components, the currents remain saturated at these levels. The currents vary linearly in strength for IMF values between these saturation levels, and the positions change abruptly when the B_z component changes sign.

For positive B_z the total inward or outward region 1 current is about 0.9×10^6 A, and the total inward or outward region 2 current is about 0.7×10^6 A while for large negative B_z the total inward or outward region 1 current is about 5.5×10^6 A and the total inward or outward region 2 current is about 4.4×10^6 A. The total inward or outward field-aligned current in the *DPY* system is about 1.5×10^6 A for $B_z > 0$ and about $2. \times 10^6$ A for $B_z < 0$. The larger total *DPY* current for negative B_z is primarily a result of the larger spatial area of the currents spanning the same longitudinal range but at lower latitudes. The *DPY* current density is the same for positive or negative B_z with $1.9 \mu\text{A}/\text{m}^2$ in the poleward sheet and $2.4 \mu\text{A}/\text{m}^2$ in the equatorward sheet. The current density in the field-aligned *DPZ* currents is $1.7 \mu\text{A}/\text{m}^2$. The total inward or outward *DPZ* current is about $1. \times 10^6$ A for negative B_z and about 0.6×10^6 A for positive B_z .

In Figure 5 we show the corresponding electrical potential patterns for these nine current distributions. These potential patterns are derived using the modeling code described by Banks *et al.* [1984].

In order to simulate the convection pattern for July 23, 1983, we perform a series of steady state calculations using distributions of currents determined by the IMF measured using the IMP 8 satellite and corrected for propagation delay. A 20-min offset is used between the measurements at IMP 8 and the simulated velocity measurements. This offset is composed of the 8-min transit time from IMP 8 to the magnetopause and the 12-min delay for the large-scale currents to develop which was determined by Clauer *et al.*

[1984] and Clauer and Banks [1986]. From the computed electric field we calculate the ionospheric $\mathbf{E} \times \mathbf{B}$ drift velocity at the radar observation points and display them in a clock dial plot. The simulated convection pattern for July 23, 1983, is shown in Figure 6. The simulated velocity vectors are only determined over the interval where IMF measurements are available from IMP 8. As is apparent from Figure 1, there is a data gap from 1447 to 1929 UT.

Figure 6 can be directly compared with the measurements shown in Figure 2. The convection reversal boundary is located at about the same location in both figures. The simulated high-latitude vectors at the magnetometer measurement points at dawn and dusk are aligned more east-west than the measured vectors; however, this is likely due to skewing of the magnetometer vectors due to conductivity gradients and the associated field-aligned currents. The highest-latitude vectors measured by THL are well reproduced by the simulation. The rotation is seen at 1030 UT in both sets. The measurements at KUV, the next highest latitude vectors, are not as well simulated at 1030 UT but are fairly well modeled after 1200 UT. Thus the spatial arrangement of the high-latitude currents only approximates the actual distribution, but the agreement is quite reasonable and the time variations match well. Between 1400 and 1500 UT the magnitudes of the vectors equatorward of the convection reversal are smaller than observed. This has been a consistent feature in the simulations shown by Clauer and Banks [1986] and here also. In future work we will examine the conductivity measurements in this region to determine if that is the source of the disagreement.

The success of the model in simulating the high-latitude time-varying convection during a transition from strongly negative IMF B_z to strongly positive IMF B_z provides additional support for the suggestion of direct electrical coupling between the solar wind and high-latitude ionosphere during both IMF orientations. The poleward motion of the *DPY* and *DPZ* currents is consistent with motion of the coupling region from field lines below the cleft to lobe field lines above the cleft during periods of strongly northward B_z . In this instance, this occurs during an active interval having an ex-

panded polar cap. The result is the apparent development of "reversed" convection cells within the polar cap.

3. DISCUSSION AND CONCLUSIONS

Perhaps the most noteworthy observation presented within this paper is the rapid, almost immediate, response of the dayside high-latitude ionospheric currents to the northward IMF. We are fortunate that the location of the IMP 8 spacecraft yields little difference in travel time for orientations of the IMF discontinuity which lie between the Parker spiral angle and the plane orthogonal to the Earth-Sun line. The most likely orientation of the IMF discontinuity is assumed to lie within this range of angles.

Observing an ionospheric response within a few minutes of the time that the northward IMF is expected to encounter the magnetopause suggests very strongly that a direct electrical coupling between the solar wind and the dayside high-latitude ionosphere occurs during northward IMF. The rapid response is also somewhat in conflict with the notion that northward IMF corresponds to a "turning off" or "turning down" of the reconnection process and that it requires several hours for the ionospheric polar cap potential to respond [Wygant *et al.* (1983)]. This may be true when B_z becomes near 0 or slightly positive, but for large values of northward IMF, the polar cap electric field appears to respond rapidly. Following the initial response to the northward IMF, the currents are observed to evolve for about 22 min before achieving their final configuration.

To explain the apparent control of the observed high-latitude ionospheric electric field configuration we have used a simple model in which the dayside high-latitude field-aligned current distribution is controlled by the strength and orientation of the IMF. The dayside field-aligned currents are thought to connect to the solar wind at the tops and flanks of the magnetosphere. We speculate that they connect the ends of magnetic merging lines on the magnetopause to the high-latitude ionosphere. The *DPY* and *DPZ* systems are similar to that proposed by Banks *et al.* (1984). The *DPY* system is thought to be driven by the north-south component of the interplanetary electric field (IEF) shunted through the cleft ionosphere via sheets of field-aligned current while the *DPZ* system is driven by a similar shunting of the east-west IEF component through the ionosphere. The electric connection is made in the merging region poleward of the cleft for positive B_z and equatorward of the cleft for negative B_z .

We have simplified the behavior of these currents by fixing the longitudinal position of the currents and varying only the latitudinal position, strength, and polarity of the currents as determined by the time-varying IMF. Nevertheless, this simple representation of the currents controlled by the measured IMF reproduces the majority of features seen in the convection observations. Additional accuracy might be achieved with a more accurate conductivity model and with additional parameters to adjust the longitudinal positions of the cleft currents. We believe, however, that the simulation demonstrates that many of the complex features seen in the high-latitude convection are a reflection of where magnetospheric merging boundaries connect to the ionosphere. This appears to be true for both positive and negative IMF B_z .

In this simulation, we have chosen to treat the region 1 and region 2 currents in a simple manner, particularly

on the night hemisphere. They are continuous around the oval, having a distribution similar to the *Ijima and Potemra* [1976] distribution. The location and strength of the region 1 and 2 currents are constant for negative B_z . For $B_z = 0$ the region 1 and region 2 current strength is reduced and for $B_z > 0$ the currents move poleward. The location and strength are constant for $B_z \geq 0$ and there is a step change at $B_z = 0$. The continuous distribution of region 1 and 2 currents is a simplification based upon the early statistical analysis of satellite observations. Since our primary interest here concerns the dayside convection and its apparent direct control by the IMF, we feel justified in this simplification. Recent studies, however, suggest that the dayside and nightside region 1 and region 2 currents may be separated and may be produced by separate sources [Friis-Christensen *et al.*, 1985; Spence *et al.*, 1987]. Therefore, while we feel that our representation of the dayside high-latitude auroral zone and polar cap convection is explained by the model used in this paper, we make no such claim for the convection observed on the nightside hemisphere.

Finally, there has been some debate concerning the configuration of the large-scale convection pattern during intervals of northward IMF. Positive B_z convection models which contain three or four convection cells [e.g., Potemra *et al.*, 1984; Reiff and Burch, 1985; Banks *et al.*, 1984] as well as a model which achieves sunward polar cap convection through a distorted two-cell pattern [Heppner and Maynard, 1987] have been discussed.

To address this discussion, we have found that several factors influence the dayside high-latitude convection pattern: first, the relative strengths of the IMF B_y and B_z components, and second, the duration of the positive IMF B_z . As seen here, it required over 20 min for the high-latitude reversed convection to be established during an interval of very strong positive B_z . (This is in contrast to the more rapid reconfiguration of flow at lower latitudes, which undergo 180° reversals within about 12 min of the IMF polarity change encountering the magnetopause, in response to changes in the IMF B_y component [Clauer and Banks, 1986]). Also, we find that the region of reversed convection associated with northward IMF is confined to very high latitudes. In the case examined here, the convection reversal boundary, which one usually considers to be at or near the polar cap boundary, was located between 71° and 75° prior to the northward turning of the IMF. The reversal boundary appears to remain at those latitudes for some time following the northward turning of the IMF. Reversed convection, however, appears to be confined to invariant latitudes above 80°.

Some additional insight can perhaps be obtained from an examination of Figure 5. The top row of this figure shows model potential patterns for strong northward IMF. These potential patterns are congruent with the streamlines for the convection of ionospheric plasma. The center pattern, for IMF $B_y = 0$ shows a four-cell pattern. However, the combination of strong IMF positive B_z and strong positive or negative IMF B_y produces a pattern that more resembles the distorted 2-cell model. Thus, the appearance of a distorted two-cell system or a four-cell system during northward IMF may depend upon the relative strengths of the IMF components and the associated *DPY* and *DPZ* current systems. The effect of the *DPY* system is to distort or skew the conventional two-cell pattern on the dayside. The ef-

fect of the DPZ system is to add two additional convection cells which either enhance the conventional systems on the dayside, or are opposite to the conventional systems and produce either distortion or appear separately as reversed convection cells depending upon the relative strengths of the separate driving currents.

Unfortunately, our observations alone are not sufficient to resolve the controversy. To do so would require simultaneous observations at high-latitudes on the nightside to observe the closure of the convection cells. Observations of the northern very high-latitude convection pattern observed in the 0000 to 0600 LT sector during northward IMF and negative B_y conditions appear to be the crucial item to test the validity of the distorted two-cell pattern for strong northward IMF conditions.

Acknowledgments. The IMP 8 magnetic field data were kindly provided by Norm Ness, Ron Lepping and Joe King. The research has been supported by the National Science Foundation through grants ATM-8210562 and ATM-8503105 and by the Air Force Geophysics Laboratory through contract F19628-85-K-0001. NASA grant NAGW 235 supported the three-month visit by E.F.-C. to Stanford during the completion of this work. The authors are grateful to T. Araki for the use of the computer modeling code which was adapted to perform the simulations in this study. Values of the solar wind velocity and density measured by IMP 8 were obtained from the Solar-Geophysical Data Comprehensive Reports published by the National Geophysical Data Center. The Sondre Stromfjord, Greenland, radar is a national scientific research facility supported by the National Science Foundation in cooperation with the Danish Meteorological Institute and is operated by SRI International.

The Editor thanks C. E. Rasmussen and M. Sugiura for their assistance in evaluating this paper.

REFERENCES

- Araki, T., T. Kamei, and T. Iyemori, Polar cap vertical currents associated with northward interplanetary magnetic field, *Geophys. Res. Lett.*, **11**, 23, 1984.
- Banks, P. M., T. Araki, C. R. Clauer, J. P. St. Maurice, and J. C. Foster, The interplanetary electric field, cleft currents, and plasma convection in the polar caps, *Planet. Space Sci.*, **32**, 1551, 1984.
- Chiu, Y. T., N. U. Crooker, and D. J. Gorney, Model of oval and polar cap arc configurations, *J. Geophys. Res.*, **90**, 5153, 1985.
- Clauer, C. R., and P. M. Banks, Relationship of the interplanetary electric field to the high-latitude ionospheric electric field and currents: Observations and model simulation, *J. Geophys. Res.*, **91**, 6959, 1986.
- Clauer, C. R., P. M. Banks, A. Q. Smith, T. S. Jorgensen, E. Friis-Christensen, S. Vennerstrom, V. B. Wickwar, J. Kelly, and J. Doupnik, Observations of interplanetary magnetic field and of ionospheric plasma convection in the vicinity of the dayside polar cleft, *Geophys. Res. Lett.*, **11**, 891, 1984.
- Crooker, N. U., Dayside merging and cusp geometry, *J. Geophys. Res.*, **84**, 951, 1979.
- D'Angelo, N., Field-aligned currents and large scale magnetospheric electric fields, *Ann. Geophys.*, **36**, 31, 1980.
- Dungey, J. W., The structure of the ionosphere, or adventures in velocity space, in *Geophysics: The Earth's Environment*, edited by C. DeWitt, J. Hiebolt and A. Lebeau, pp. 526-537, Gordon and Breach, New York, 1963.
- Friis-Christensen, E., and J. Wilhjelm, Polar cap currents for different directions of the interplanetary magnetic field in the Y-Z plane, *J. Geophys. Res.*, **80**, 1248, 1975.
- Friis-Christensen, E., Y. Kamide, A. D. Richmond, and S. Matsushita, Interplanetary magnetic field control of high-latitude electric fields and currents determined from Greenland magnetometer data, *J. Geophys. Res.*, **90**, 1325, 1985.
- Heppner, J. P., and N. C. Maynard, Empirical high-latitude electric field models, *J. Geophys. Res.*, **92**, 4467, 1987.
- Heelis, R. A., The effects of interplanetary magnetic field orientation on dayside high-latitude ionospheric convection, *J. Geophys. Res.*, **89**, 2873, 1984.
- Iijima, T., and T. A. Potemra, The amplitude distribution of field-aligned currents at northern high latitudes observed by TRIAD, *J. Geophys. Res.*, **81**, 2165, 1976.
- Iijima, T., and T. Shibaji, Global characteristics of northward IMF-associated (NBZ) field-aligned currents, *J. Geophys. Res.*, **92**, 2408, 1987.
- Iijima, T., T. A. Potemra, L. J. Zanetti, and P. F. Bythrow, Large-scale Birkeland currents in the dayside polar region during strongly northward IMF: A new Birkeland current system, *J. Geophys. Res.*, **89**, 7441, 1984.
- Kamide, Y., and S. Matsushita, Simulation studies of ionospheric electric fields and currents in relation to field-aligned currents, 1, Quiet periods, *J. Geophys. Res.*, **84**, 4083, 1979.
- Luhmann, J. G., R. J. Walker, C. T. Russell, N. U. Crooker, J. R. Spreiter, and S. S. Stahara, Patterns of potential magnetic field merging sites on the dayside magnetopause, *J. Geophys. Res.*, **89**, 1739, 1984.
- Potemra, T. A., L. J. Zanetti, P. F. Bythrow, A. T. Y. Lui, and T. Iijima, B_y -dependent convection patterns during northward interplanetary magnetic field, *J. Geophys. Res.*, **89**, 9753, 1984.
- Reiff, P. H., Sunward convection in both polar caps, *J. Geophys. Res.*, **87**, 5976, 1982.
- Reiff, P. H., and J. L. Burch, IMF B_y -dependent plasma flow and Birkeland currents in the dayside magnetosphere, 2, A global model for northward and southward IMF, *J. Geophys. Res.*, **90**, 1595, 1985.
- Spence, H. E., M. G. Kivelson, and R. J. Walker, The dynamics of the nightside field-aligned currents and their linkage to the near-earth magnetotail, paper presented at 19th General Assembly, Int. Union of Geod. and Geophys. Vancouver, Aug. 1987.
- Wilhjelm, J., E. Friis-Christensen, and T. A. Potemra, The relationship between ionospheric and field-aligned currents in the dayside cusp, *J. Geophys. Res.*, **83**, 5586, 1978.
- Wygant, J. R., R. B. Torbert, and F. S. Mozer, Comparison of S3-3 polar cap potential drops with the interplanetary magnetic field and models of magnetopause reconnection, *J. Geophys. Res.*, **88**, 5727, 1983.
- Zanetti, L. J., T. A. Potemra, T. Iijima, W. Baumjohann, and P. F. Bythrow, Ionospheric and Birkeland current distributions for northward interplanetary magnetic field: Inferred polar convection, *J. Geophys. Res.*, **89**, 7453, 1984.

C. R. Clauer, STAR Laboratory, Stanford Electronics Laboratories, Stanford University, Stanford, CA 94805.

E. Friis-Christensen, Division of Geophysics, Danish Meteorological Institute, Lyngbyvej 100, DK-2100, Copenhagen, Denmark

(Received September 14, 1987;
revised November 16, 1987
accepted December 18, 1987.)

Relationship of the Interplanetary Electric Field to the High-Latitude Ionospheric Electric Field and Currents: Observations and Model Simulation

C. ROBERT CLAUER AND PETER M. BANKS

Space, Telecommunications and Radioscience Laboratory, Stanford Electronics Laboratories, Stanford University, Stanford, California

F-region ion convection in the vicinity of the dayside polar cleft is strongly controlled by the interplanetary magnetic field, suggesting a direct current-driven coupling between the solar wind and dayside, high-latitude ionosphere. This coupling has been explored through observations of high-latitude ion convection measured by the Sondre Stromfjord, Greenland incoherent scatter radar and subsequent computer simulations. The computer simulation calculates the ionospheric electric potential distribution for a given configuration of field-aligned currents and conductivity distribution. Using a simple model of the field-aligned currents linking the solar wind with the dayside, high-latitude ionosphere, we can explore the consequences of variations of the currents on ionospheric plasma convection. The direction and strength of the currents are set according to measurements in the upstream solar wind and the time varying ionospheric electric field and resulting plasma convection are simulated. Comparisons of the simulated plasma convection with the ion velocity measurements at Sondrestrom show very good agreement. Thus, a very simple model which provides a direct current-driven connection between the solar wind and the high-latitude ionosphere via field-aligned currents in the polar cleft is able to explain a large portion of the ionospheric electric field variations observed in the vicinity of the polar cleft.

1. INTRODUCTION

The regions in and around the dayside polar cleft offer an ideal location in which to investigate the electrodynamic coupling between the solar wind, magnetosphere, and ionosphere. Observations of current systems, electric fields, and plasmas within other regions of the auroral zone seem to involve many intervening interactions which obscure identification of the original processes at the magnetospheric boundary. The polar cleft, however, is known to contain solar wind plasma and the phenomena within it are expected to reveal a direct and detailed account of the interaction of the solar wind with the magnetosphere. Investigation of this region of the magnetosphere bears on the fundamental questions of whether the magnetosphere is open or closed, the electrical connectivity between the solar wind, magnetosphere and ionosphere, and how solar wind plasma enters the magnetosphere.

It is largely for this reason that the Chatanika incoherent scatter radar was moved to Sondre Stromfjord, Greenland [Banks and Evans, 1979]. Now located at an invariant latitude of 74°, the Sondre Stromfjord radar is able to make measurements of electrodynamic and plasma properties at the ionospheric end of the northern polar cleft on a routine basis. This report presents results from a series of measurements obtained from the Sondre Stromfjord radar together with correlative observations of the interplanetary magnetic field (IMF) and solar wind plasma obtained by the IMP-8 satellite. These experiments were designed primarily to examine the electrical connection between the solar wind, magnetosphere, and ionosphere.

It is well known that the high-latitude ionospheric con-

vection pattern, and therefore also the distribution of high-latitude electric fields and field-aligned currents, depends strongly on the orientation of the IMF [Heelis, 1984; Zanetti et al., 1984; Burch et al., 1985; Reiff and Burch, 1985; Friis-Christensen et al., 1985]. Ground based magnetic observations at high-latitudes provided the first indications that the interplanetary magnetic field was an important ordering parameter of high-latitude current systems [Svalgaard, 1973; Mansurov, 1969; Friis-Christensen et al., 1972]. High-latitude magnetic observations near local noon were found to be related to the B_y component of the IMF and were designated as "DPY" perturbations [Friis-Christensen and Wilhelm, 1975]. Satellite observations have shown the existence of field-aligned currents which could feed the DPY current system in the vicinity of the magnetospheric cleft [Iyama et al., 1978; McDiarmid et al., 1978]. Wilhelm et al. [1978] suggested that the DPY magnetic variation observed by ground observatories is the result of an ionospheric Hall current flowing between a pair of oppositely directed field-aligned current sheets.

The complexity of the total field-aligned current system, however, has made it difficult to determine the exact morphology of the currents and current sources in the cleft. This complexity, as seen from individual satellite passes, led McDiarmid et al. [1978] to describe the cleft as a "zone of confusion." Some hold that the DPY observations are merely the result of a redistribution of dayside auroral electrojets [Rostoker, 1980; McDiarmid et al., 1979], while others believe the DPY to be produced by a separate current which can vary independently with respect to the auroral electrojets [Friis-Christensen, 1981].

Satellite observations have established that distinct field-aligned currents exist poleward of the region 1 Birkeland currents in the cleft region between 0930 and 1430 MLT [Iyama and Potemra, 1976a, b; Iyama et al., 1978; Doyle et al., 1981]. It is known that the currents move spatially and they appear to vary in strength and polarity depending upon

Copyright 1986 by the American Geophysical Union.

Paper number 5A8321.
0148-0227/86/005A-8321\$05.00

The U.S. Government is authorized to reproduce and sell this report. Permission for further reproduction by others must be obtained from 6959 the copyright owner.

the B_y and B_z components of the IMF. The exact configuration of the currents in the cleft region, however, is not yet clearly determined. For example, *Bythrow et al.* [1982] suggest that the region 1 currents observed near local noon may have a source different from that of region 1 currents at other local times. Thus, region 1 currents near noon may be part of the cleft current system.

Rich and Kamide [1983] conducted computer modeling experiments to investigate the consequences of various patterns of field aligned current in the vicinity of the dayside cleft. They found that patterns of overlapping currents similar to those suggested by *McDiarmid et al.* [1978] and *Doyle et al.* [1981] better reproduced the known *DPY* ionospheric current behavior than patterns without overlapping current at noon such as the pattern suggested by *Ijima and Potemra* [1976b]. The overlapping current patterns were achieved through a reconfiguration of the region 1 and region 2 currents, whereas the nonoverlapping current configuration contained a separate cleft system in which the equatorward portion was continuous with the region 1 currents.

Vennerstrom et al. [1984] compared the latitudinal location of the *DPY* current system determined from the West Greenland meridian chain of magnetometers to the location of the convection reversal boundary and the maximum F -region electron temperature measured by the Sondrestrom radar. It was found that while the maximum of the F -region electron temperature roughly coincides with the convection velocity reversal boundary, the *DPY* current is always located more poleward. The auroral electrojets are observed to be equatorward of the convection reversal boundary. Thus, *Vennerstrom et al.* conclude that the *DPY* is indeed a current system separate from the auroral electrojets and that it is directly associated with the primary solar wind driven convection.

Models to explain the observed *DPY* variation have been proposed by several researchers [*D'Angelo*, 1980; *Primdahl and Spangselev*, 1981, 1983; *Barbosa*, 1979, 1983, 1984; *Banks et al.*, 1984]. In these models, the dayside cleft and polar cap contain currents which are directly related to the B_y component of the IMF. Some of the models also contain currents which are related to the B_z components of the IMF and produce *DPZ* variations which may also be related to the occasional occurrence of a narrow high-speed convection throat directed in the antisolar direction [*D'Angelo*, 1980; *Banks et al.*, 1984]. While the current configurations are similar in these models, they vary in terms of the generation mechanism. Figure 1, adapted from *D'Angelo* [1980] and *Banks et al.* [1984] schematically shows the configuration of IMF B_z (top) and B_y (bottom) associated field-aligned currents in the vicinity of the polar cleft. In the models proposed by *Barbosa* [1979], *D'Angelo* [1980] and by *Banks et al.* [1984], the currents in the polar cleft are driven by the interplanetary electric field apparent at the magnetopause as the magnetized solar wind plasma flows past the earth. While the exact nature of the electrical connection between the solar wind and magnetosphere is not addressed in detail in these models, it is shown that the models can reproduce most of the observed features in the vicinity of the cleft and that the magnitudes of the fields and currents are well within the realm of possibility. *Primdahl and Spangselev* [1981; 1983], and *Barbosa* [1983] consider a somewhat different approach for producing cleft currents. In this mechanism, rather than

a direct electrical connection with the solar wind E_z , the cleft currents (bottom of Figure 1) are part of the magnetopause shielding currents related to B_y variations in the IMF.

Due to the complexity of the observed field-aligned currents in the vicinity of the dayside polar cleft, it has not been possible to verify the configuration of currents sketched in Figure 1. Through computer simulation, however, one can explore the effects on ionospheric electric fields of different current distributions in the cleft [*Rich and Kamide*, 1983]. These can then, in turn, be compared with observations of convection obtained by high-latitude radars. In this paper, the model discussed by *Banks et al.* [1984] has been adapted to adjust the strength and direction of the *DPY* and *DPZ* field-aligned currents in the polar cleft based on IMF measurements obtained by the IMP - 8 satellite upstream in the solar wind. Then, through a series of steady state calculations, it is possible to simulate the temporally varying ionospheric convection expected during a particular interval based on this model. The simulated Sondrestrom radar convection observations can then be directly compared with the actual radar observations.

We note that while we use values of the IMF, our model presumes that the interplanetary electric field is the important driving parameter. Apart from the solar wind velocity, one should realize that IMF correlations are equivalent to correlations with the interplanetary electric field.

2. OBSERVATIONS

Measurement Procedure and Data Analysis

The radar data which have been analyzed were collected using pairs of stationary antenna positions on either side of the Sondrestrom magnetic meridian. The analysis uses line-of-sight ion velocities measured in the F -region. At F -region altitudes collisions are unimportant and the ion velocity is assumed to be purely the result of $\mathbf{E} \times \mathbf{B}$ drift. For each pair of positions the measured line-of-sight velocities are reduced to obtain the N-S and E-W components of the ion drift velocity as a function of latitude.

Reduction of the line-of-sight velocity measurements from the pairs of antenna positions to obtain a velocity vector orthogonal to the local magnetic field depends upon the assumption that the velocity is uniform over the spatial range of the measurements. If this assumption is not valid, that is if there is a gradient or a rotation in the ion flow from one measurement position to the second, the analysis procedure can over estimate the E-W component of velocity and underestimate the N-S component of velocity.

Assuming a vertical magnetic field for simplicity of illustration, the radar-deduced ion velocity is derived from the pair of measurements in the following manner: Let \mathbf{l}_1 and \mathbf{l}_2 be unit vectors in the antenna azimuth pointing direction for the two radar positions. Let \mathbf{V} be the velocity which is uniform over the two measurement points P_1 and P_2 . The magnitudes of the measured line-of-sight velocities a_1 and a_2 at the respective points are given by,

$$a_1 = \mathbf{l}_1 \cdot \mathbf{V}$$

and

$$a_2 = \mathbf{l}_2 \cdot \mathbf{V}$$

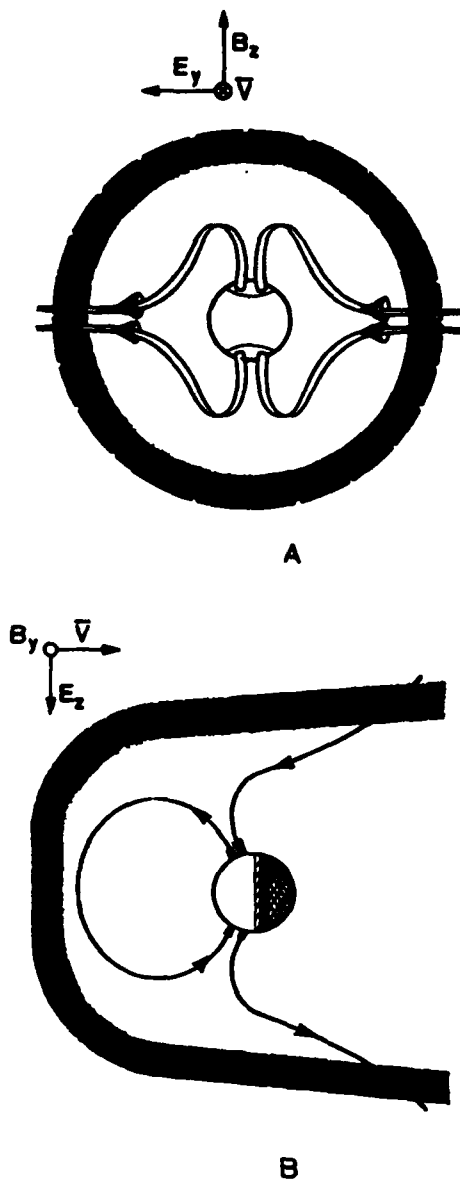


Fig. 1. A general view of the way cleft currents driven by the interplanetary electric field connect across the magnetosphere. In Figure 1 a, line currents arising from E_y connect from the flanks of the magnetosphere to two discrete zones on either side of local magnetic noon. The direction of the current is determined by the sign of B_z and the case for $B_z > 0$ is shown. In figure 1b currents arising from E_z connect to each cleft through sheet currents centered at local magnetic noon. Completion of the current path through the opposite hemisphere is accomplished by means of a sheet current along closed field lines lying at or near the magnetopause. The direction of currents shown here corresponds to $B_y < 0$. Oppositely directed current would result for $B_y > 0$. After Banks *et al.* [1984].

So,

$$\begin{bmatrix} l_{1E} & l_{1N} \\ l_{2E} & l_{2N} \end{bmatrix} \begin{bmatrix} V_E \\ V_N \end{bmatrix} = \begin{bmatrix} a_1 \\ a_2 \end{bmatrix}$$

where the subscripts E and N refer to eastward and northward components respectively.

The solutions to this equation are given by

$$V_E = \frac{l_{2N}a_1 - l_{1N}a_2}{l_{1E}l_{2N} - l_{1N}l_{2E}}$$

$$V_N = \frac{l_{1E}a_2 - l_{2E}a_1}{l_{1E}l_{2N} - l_{1N}l_{2E}}$$

We have examined the velocity computations using a qualitative method to estimate the validity of the assumption that the velocity be uniform over the spatial dimensions of the measurement points. This was done by conducting an experiment using four beam positions at 30° elevation in the northward direction. The azimuths of the positions were -26° , -13° , $+13^\circ$, and $+26^\circ$ measured from magnetic north. Velocities were computed separately using the inner pair and the outer pair of positions. This experiment was run on April 25 and April 27, 1983 during period of moderate geomagnetic activity ($kp \approx 3-4$).

Before presenting the results of these experiments, however, it is useful to consider the effects of a nonuniformity in the flow. Suppose that the velocity at the westward measurement point is 400 m/s to the east and the velocity at the eastward measurement point is 400 m/s to the north. Such a situation would result from a 90° rotation in the flow between the measurement points. For the inner pair of positions, $l_N = 0.9744$ and $l_E = 0.2250$ which lead to $a_1 = 389.76$ m/s and $a_2 = -90.0$ m/s. Then,

$$V_E = \frac{389.76 + 90.0}{2(0.2250)} = 1066.1 \text{ m/s}$$

$$V_N = \frac{389.76 - 90.0}{2(0.9744)} = 153.8 \text{ m/s}$$

Similarly, for the outer positions one obtains $V_E = 609$ m/s and $V_N = 102$ m/s. Thus, the eastward velocity is greatly overestimated and both the inner and outer pair of points give essentially an eastward velocity but of different magnitudes.

Suppose, for a second example, that the velocity at the westward measurement point is 300 m/sec to the north and at the eastward measurement point is 600 m/s northward. Thus, there is a gradient in the flow. Using the inner points yields $V_E = 649.5$ m/s and $V_N = 501.3$ m/s and using the outer points yields $V_E = 307$ m/s and $V_N = 450$ m/s. Again a substantial eastward velocity is introduced into the result.

Plates 1a and 1b show the results of the experiments which were performed on April 25 and April 27. The F -region ion velocities orthogonal to \mathbf{B} are plotted as a function of invariant latitude and universal time (shown around the inner circumference of the plot). Local time is shown around the outer circumference of the plot with magnetic local noon at the top of the plot. The black vectors were obtained using the interior antenna positions while the red vectors were obtained using the outer antenna positions. The sets of vectors obtained from the inner and outer pairs of measurement positions have been superposed for comparison. For the most part, the agreement is very good. However, there are occasional times when there is considerable disagreement between the velocities obtained using the two pairs of points, thus indicating that occasionally the assumption of uniform velocity breaks down. It is not clear whether this is the result of a spatial difference in the velocities or the result of a temporal change.

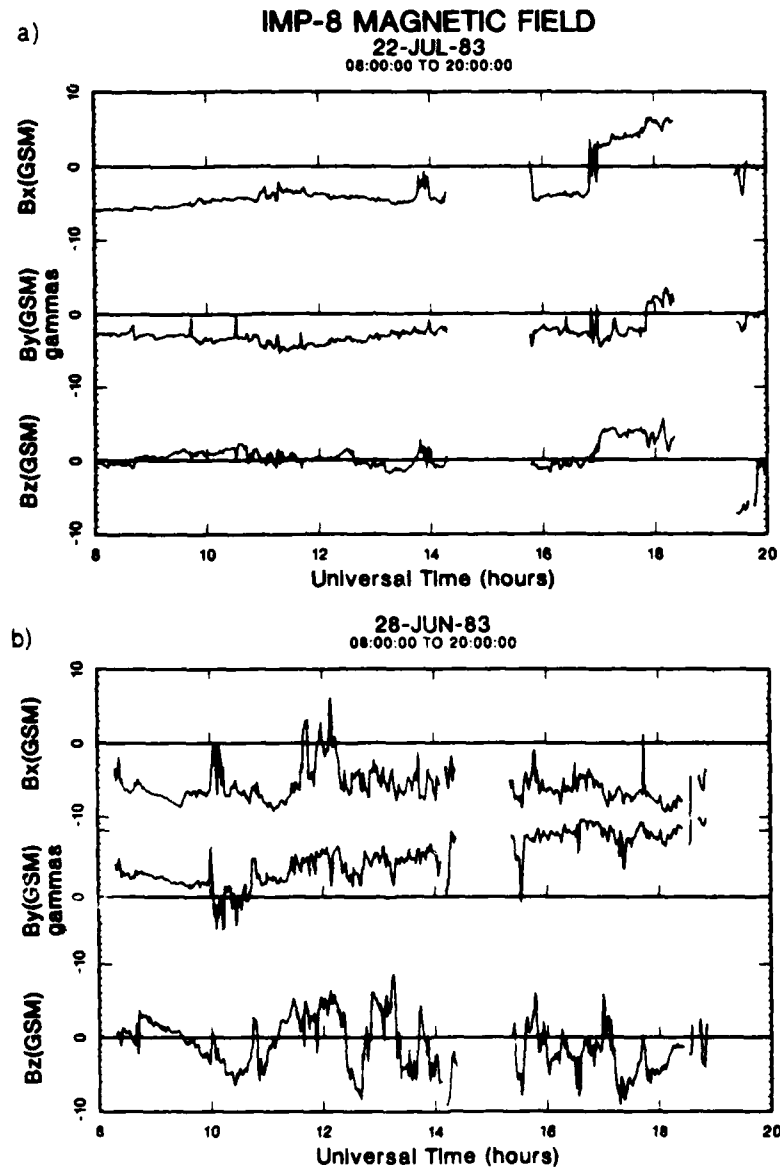


Fig. 2. Interplanetary magnetic field observations shown in GSM coordinates for (a) July 22, 1983 and (b) June 28, 1983.

Nevertheless, the good general agreement between the black and red velocity vectors indicates that the multiposition method of determining the vector ion velocity is accurate. There are occasional small-scale features in the real ion velocity which cause errors in the velocity determination. However, the points which we shall discuss in this paper should be unaltered by the uncertainties in the computed velocities.

During the course of our experiments we used several variations of the positions and dwell times. These changes affected the cycle time of the observations, the latitudinal range covered and the uncertainty in the line-of-sight velocity measurements. Additional details of the radar capabilities and analysis techniques can be found in Wickwar *et al.* [1984].

Correlative observations of the solar wind speed, density and magnetic field are provided by the IMP - 8 spacecraft.

These data together with the observations of high-latitude ion convection obtained using the Sondrestrom radar are studied to determine the solar wind control of high-latitude dayside currents and fields. The analysis presented here extends the preliminary results reported by Clauer *et al.* [1984] and Jorgensen *et al.* [1984].

Data Presentation

It is well known that variations in the Y component of the IMF are associated with changes in the high-latitude ionospheric convection pattern [Heelis, 1984]. This is particularly true in the dayside polar cleft region. Plates 2a and 2b show observations of F -region ion velocities obtained using the Sondrestrom radar. Correlative measurements of the IMF obtained from the IMP - 8 satellite are shown in figures 2a and 2b. On July 22, 1983, shown in Plate 2a, the IMF B_y component was negative for most of the observing interval.

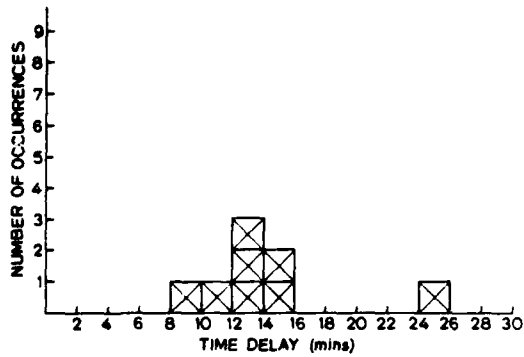


Fig. 3. Histogram showing time delay from when a change in sign of IMF B_y encounters the magnetopause to the time when a change in polarity of the east - west F - region ion drift is observed in the vicinity of the cleft.

while on June 28, 1983, shown in Plate 2b. the B_y component was primarily positive. The difference in the sign of B_y appears to control the direction of the dayside high-latitude convection with $B_y > 0$ associated with westward convec-

tion and $B_y < 0$ associated with eastward convection. The magnitudes of the B_y and B_z components are also different on these days and this is associated with the differences in magnitude of the ion velocities and the latitudinal location of the convection reversal boundary on these two days.

The basic behavior of the high-latitude currents has previously been described based on magnetometer observations [Friis-Christensen, 1981; Rostoker, 1980]. The electric field observations (orthogonal to the ion velocity measurements) confirm the hypothesis that the DPY current system is a Hall current [Friis-Christensen, 1986].

Clauer et al. [1984] showed that the dayside high-latitude ionospheric electric field responds very directly to changes in the IMF B_y component. Polarity changes in the east-west ion convection were measured to occur within about 10 or 15 minutes of the time that an IMF B_y polarity change was estimated to encounter the magnetopause. Figure 3 shows a histogram which displays the delay times obtained for all of the clear correlated polarity changes found in our data base. This data base contains 264 hours of radar observations in the vicinity of the polar cleft during 1983 and 1984. For events to be included, we have required that the IMF

FIELD ALIGNED CURRENT

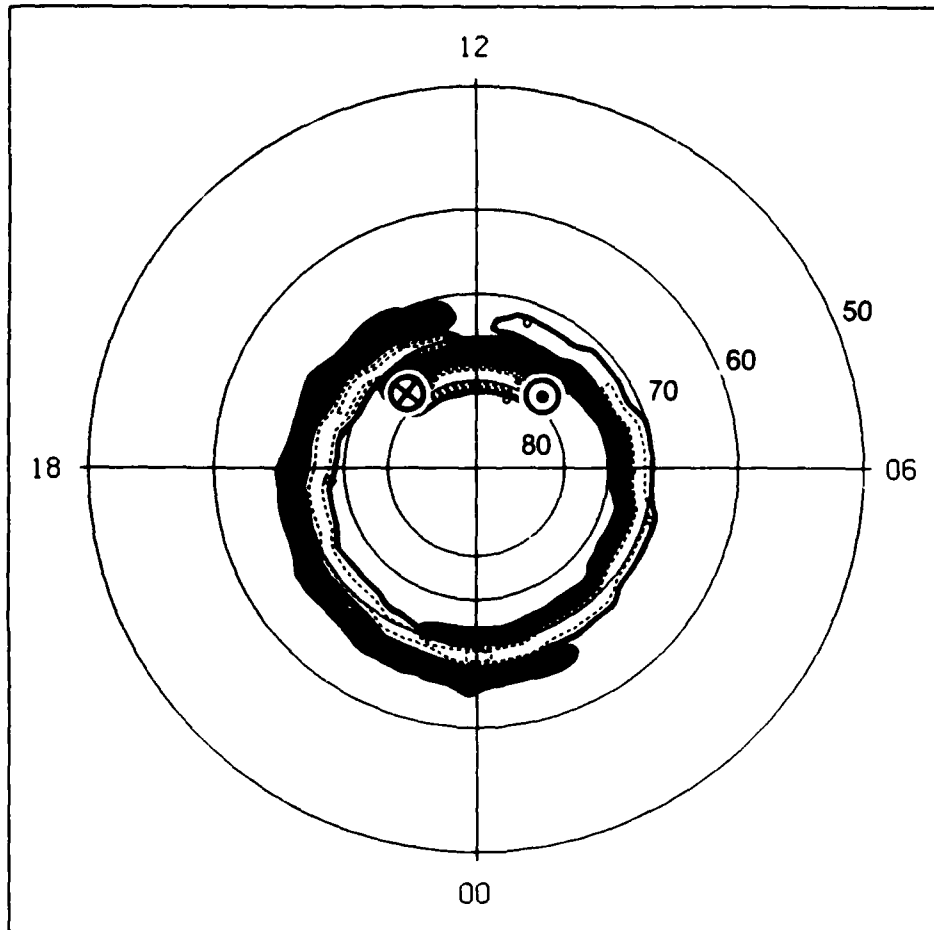


Fig. 4. Polar plot of the distribution of field-aligned current used in the computer model. Three regions of current are shown: (1) the region 1 and region 2 currents around the auroral oval with inward current denoted by shading (2) the DPY sheet currents centered at local magnetic noon and lying poleward of the region 1 currents, and (3) the DPZ line currents at the longitudinal ends of the DPY currents. The polarities of the currents in this illustration correspond to the case of IMF $B_y > 0$ and $B_z > 0$.

change in B_y measured by IMP - 8 in the upstream solar wind have a constant polarity for 20 minutes on both sides of the sign change. We have then estimated the delay time between the satellite and the magnetopause. This is done by first computing the subsolar magnetopause standoff distance based on a balance between the solar wind dynamic pressure and magnetospheric magnetic pressure. The transit time between IMP - 8 and the magnetopause is computed using the measured solar wind velocity. An additional delay of four minutes is added to account for the magnetosheath transit time based on the gasdynamic model calculations of Spreiter and Stahara [1980]. Two calculations are made: (1) assuming that the plane of the IMF B_y polarity change lies orthogonal to the earth-sun line, and (2) assuming that it lies along the Parker spiral angle. This gives two estimates of the delay time between the satellite and the magnetopause which can be quite similar or quite different depending on the position of the satellite. For the purpose of the plot, we have taken the average of the computed times. The time delay for the high-latitude ionospheric convection to change polarity is then measured relative to the estimated time that the B_y sign change encounters the magnetopause.

While we have 264 hours of observation time at Sondre Stromfjord, the relatively few observations shown in the histogram reflects the inconsistent tracking of the IMP - 8 satellite together with our selection criterion.

The peak of the distribution shown in Figure 3 is at a delay time of about 14 minutes. If the change in current to the ionosphere from the magnetopause is carried by a transverse Alfvén wave, this suggests that several bounces of the wave probably occur since the Alfvén transit time is on the order of 2 minutes or less. This may be reasonable since the dayside ionosphere would be a good reflector of the wave.

Model Simulation

As mentioned in the introduction, the model presented by Banks *et al.* [1984] has been adapted to perform a series of computations of the ionospheric electric field based on measurements of the IMF obtained by the IMP - 8 spacecraft. Using these computations, we may simulate the ion convection velocity which would be observed by the Sondrestrom radar under the conditions described by the model.

In Figure 4 we show a polar projection of the distribution of currents which is input to the model. The current distribution includes the region 1 and region 2 currents using the approximate statistical distribution and spatial arrangement from Iijima and Potemra [1976a] and the suggested DPY and DPZ field-aligned currents in the polar cleft from Banks *et al.* [1984]. This figure shows the current flow for the case when $B_z > 0$ and $B_y > 0$. When $B_z = B_y = 0$ no cleft currents would flow and for $B_z < 0$ and $B_y < 0$ the polarities of the cleft currents would reverse. In all of the simulations presented here, the total region 1 inward and outward currents are each 1.7×10^6 A and the total region 2 inward and outward currents are each 1.5×10^6 A. The simulations use the conductivity model from Kamide and Matsushita [1979] with a conductivity enhancement in the auroral oval. The peak potential difference across the polar cap resulting from the region 1 and region 2 currents alone is 128 kV. The region 1 and 2 currents are constant in location and strength in all of our simulations. The only variations are in the direction and strength of the DPY and DPZ currents in the cleft. The direction of the DPY currents depends

upon the sign of the IMF B_y component. The magnitude of the current varies linearly between 1.06×10^6 A and 0 A for $|B_y| = 8$ nT and 0 nT respectively. The currents saturate at 1.06×10^6 A for larger absolute values of B_y . Similarly, the direction of the DPZ currents depends upon the sign of the IMF B_z component. The magnitude of the DPZ current varies linearly between 3.26×10^5 A and 0 A for $|B_z| = 8$ nT and 0 nT respectively. The currents saturate at 3.26×10^5 A for larger absolute values of B_z . The location of the cleft currents remains constant in the model simulations.

For each measurement time at Sondrestrom, we take the measured IMF at IMP - 8 using the appropriate delay time determined from the actual solar wind conditions during the event. Based on these IMF values, we adjust the strength and direction of the DPY and DPZ currents and compute the hemispheric electric field distribution. Using the computed model electric field, the $\mathbf{E} \times \mathbf{B}$ drift at the radar measurement point is determined and the simulated vector velocity is plotted.

Plate 3a and 3b shows the measured and simulated convection velocities for April 25, 1983, respectively, while Figure 5 shows the IMF observations for this same interval. The IMF measurements show a gap between 1113 and 1207 UT. However, from the Greenland meridian chain of magnetometers, one can infer that the B_y was negative for most of that interval. For the model simulations, therefore, we have used the values of the IMF measured at 1207 UT throughout the data gap.

In comparing Plate 3a with 3b, the overall agreement must be said to be very good. Some of the vectors at lower latitudes on the evening-side do not match well and the location of the cleft currents in the model appears to be at too low a latitude, indicated by the poleward velocities of the most northern vectors in the simulation.

The most important feature in Plate 3a is the interval between 1230 UT and 1400 UT where the high-latitude flow direction changed by about 180 degrees compared with the flows on either side of this interval. Clauer *et al.* [1984] suggested that these two changes in ion flow direction were directly related to changes in the polarity of the IMF B_y component at 1215 UT and 1343 UT respectively. This suggestion appears to be, for the most part, verified by the results of the simulation shown in Plate 3b. The reversal in the east - west ion velocities is observed between 1230 UT and 1400 UT. There is, however, a set of poleward velocities at 1300 UT which appear to be associated with the southward fluctuation of the IMF at 1249 to 1300 UT. Such poleward velocities were not observed in the actual measurements. Perhaps the sampling frequency was too slow, thus causing us to miss sampling the poleward flow, or perhaps the 10-minute southward fluctuation was of insufficient duration to establish the large-scale cleft current system which links the solar wind with the ionosphere. The magnetosphere has been modeled as a low-pass filter which only couples variations of the solar wind electric field with frequencies less than 10^{-4} Hz to auroral current systems [Clauer *et al.*, 1981, 1983]. Perhaps the cleft currents also respond only to variations in the IMF below some critical frequency.

Plate 4a and 4b show another example of observations and model simulation. March 16, 1984 is a particularly interesting day because of the extended region of poleward flow from 1300 UT through 1445 UT. This region of strong poleward flow is associated with a large southward IMF shown

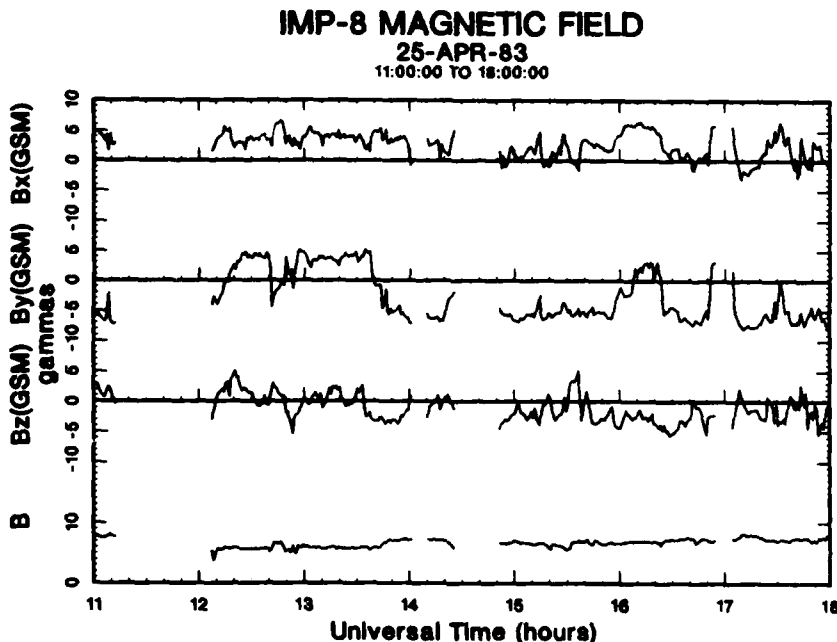


Fig. 5. Interplanetary magnetic field on April 25, 1983, in GSM coordinated measured by the IMP - 8 satellite. The traces, from the top, show the B_x , B_y , B_z components, and the total field.

in Plate 6. In this and the following simulation, simulated convection velocities are not computed during times when IMP - 8 measurements are not available. We find that the simulation reproduces the observed poleward flow very well, thus suggesting that DPZ currents similar to those of the model flow during southward B_z conditions. Further comparison of Plate 4a with 4b also reveals very good agreement.

One region of disagreement appears at about $\Lambda < 75^\circ$ near local noon. This may suggest some different configuration of the dayside auroral electrojets and the region 1 and region 2 currents at this time.

A final example is shown in Plates 5a and 5b with the IMF observations shown in Figure 7. July 24, 1983 showed more complex temporal variations than the previous exam-

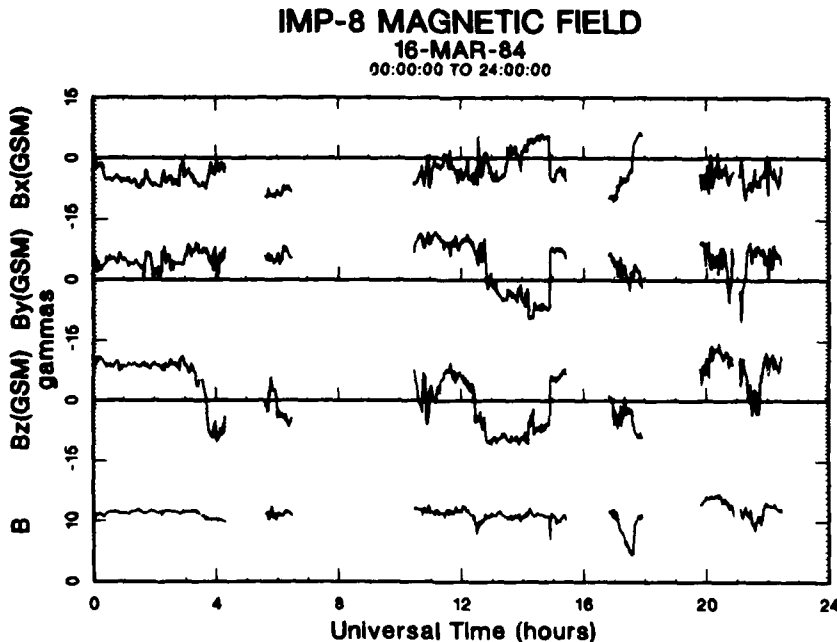


Fig. 6. Interplanetary magnetic field on March 16, 1984.

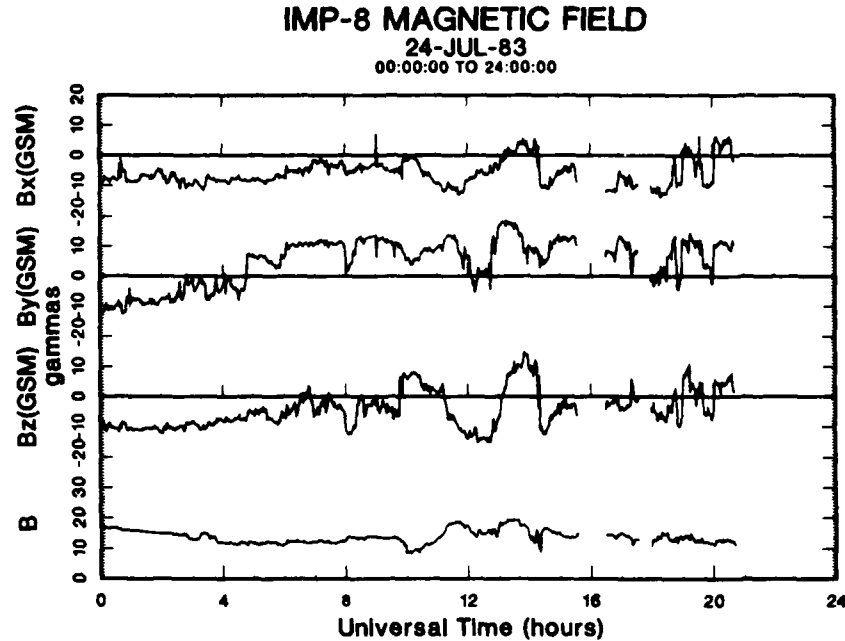


Fig. 7. Interplanetary magnetic field on July 24, 1983.

ples and is a very interesting case to attempt to simulate with our simple model. The results are very interesting. From 1230 UT to 1330 UT a region of strong poleward flow is observed in the ion convection. This is associated with a strong southward IMF as were the observations in the previous example. However, when one examines the timing of the southward variation and the onset of poleward ion flow, a problem appears to arise. B_z turns southward at 11:15 UT and the expected delay time between the satellite and magnetopause is between 8 and 12 minutes. Thus, the time delay from when the southward fluctuation encounters the magnetopause and the onset of poleward flow is over 50 minutes and is inconsistent with the histogram shown in Figure 5. Further examination of the IMF variations indicates that B_x was large and positive at the time B_z turned southward. B_y became nearly 0 at about 1300. This suggests the possibility that the relative magnitudes of B_y and B_z may be important in determining the ionospheric effects of the DPY and DPZ currents. Alternatively, perhaps the effects of the DPZ current were not observed around 1140 UT because of a shift in the spatial distribution of the DPZ currents.

It is very interesting to see that the simulation of ion velocity measurements agrees very well with the observations. The interval of poleward flow between 1230 and 1330 UT is reproduced. We note that the simulation only varies the strength of the cleft currents keeping the location constant. Therefore, the results of the simulation indicate that adjusting the relative strengths of the DPY and DPZ currents is sufficient to explain the observations. Following 1330 UT, the simulation and measured velocities do not agree. This region of disagreement appears to occur during an interval of northward IMF. This suggests that it is not sufficient to simply reverse the polarity of the DPZ current during intervals of strongly northward IMF. Other regions of disagreement occur at lower latitudes, particularly on the afternoonside and at local noon. Otherwise, we find generally good agree-

ment between the results of the simulation and the observed ionospheric convection on July 24, 1984.

3. DISCUSSION AND CONCLUSIONS

This report has described experimental observations of high-latitude ion convection using the Sondre Stromfjord, Greenland, incoherent scatter radar. The technique for measuring F -region ion velocities at high time resolution over a large range of latitudes has been described and experiments have indicated that the technique provides reliable measurements of the ion velocity orthogonal to the local magnetic field under most circumstances. Small-scale spatial variations, however, will tend to cause errors in the computed velocity vector, and such variations probably occur at some times. Nevertheless, our results indicate that the pattern of convection obtained from our measurements is, in general, accurate.

Correlative observations of solar wind plasma parameters and IMF from the IMP - 8 satellite have also been studied. These data indicate that the dayside high-latitude ionospheric electric field, which drives the observed F -region plasma convection, responds within about 14 minutes to IMF variations at the magnetopause. There is also indication that IMF fluctuations of 10 minutes or less do not produce changes in the ionospheric electric field configuration.

Finally, we have found that the use of a very simple model of the polar cleft currents driven by solar wind electric fields is able to explain much of the temporal variations in the ionospheric plasma convection pattern observed using the Sondrestrom radar. In addition we find several areas of disagreement which will require refinement of the simple model. For example, observations during intervals of northward IMF are not consistent with the simulations. Also, occasionally the convection equatorward of the cleft currents

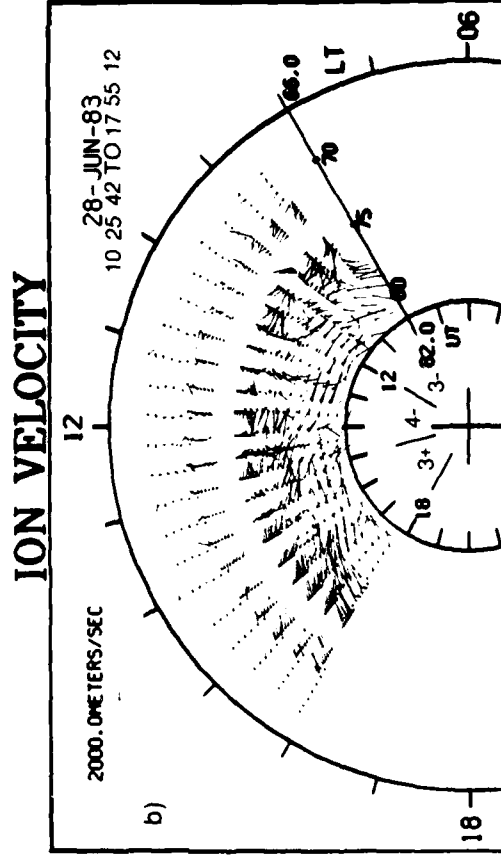
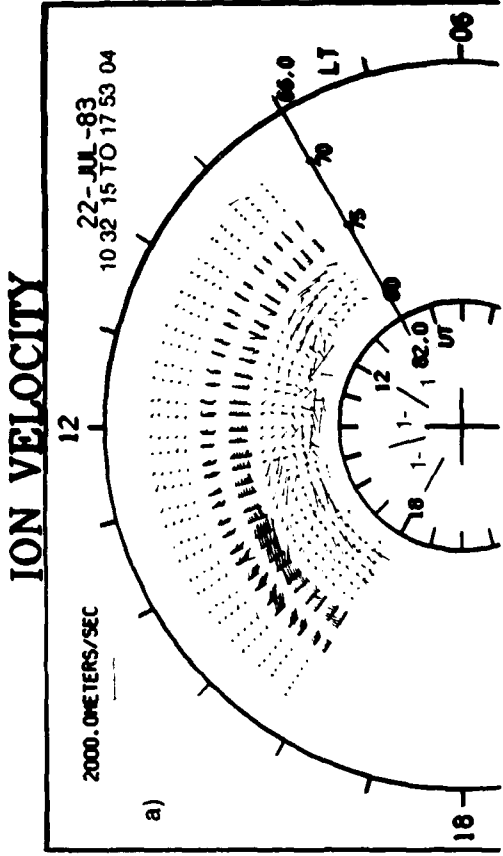


Plate 2. *F*-region ion convection velocity measured on July 22, 1983 (top), during an interval of IMF $B_y < 0$ and June 28, 1983 (bottom), during an interval of IMF $B_y > 0$. The format is similar to Plate 1; however velocities with a westward component are shown by red vectors and velocities with an eastward component are shown by black vectors.

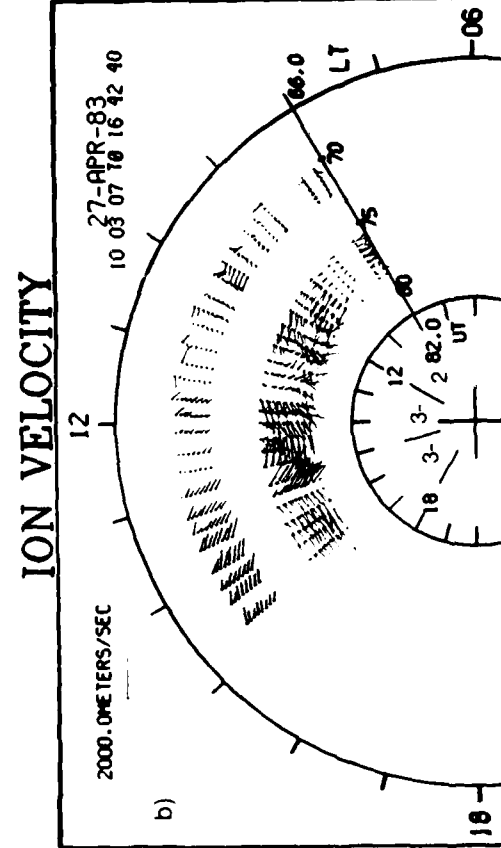
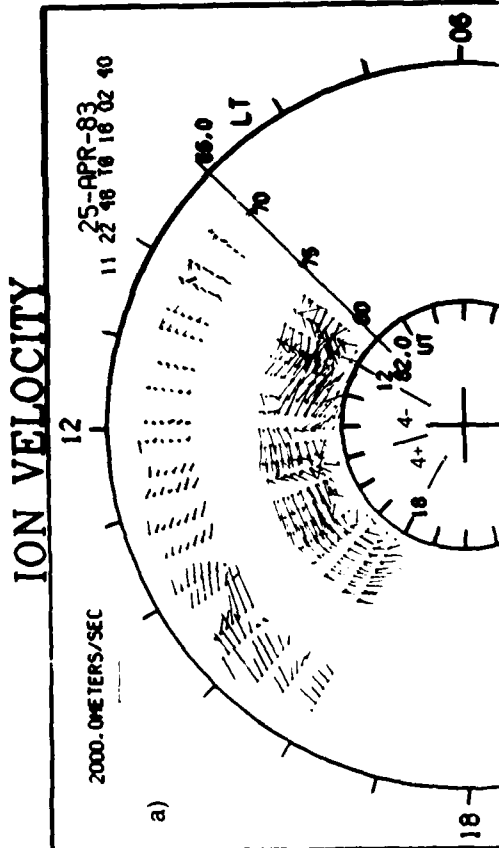


Plate 1. Polar plots showing *F*-region ion convection velocity vectors as a function of invariant latitude and local time for April 25, 1983 (top) and April 27, 1983 (bottom). Local time is indicated around the outer circumference of each plot and universal time is indicated around the inner circumference. Local magnetic noon is at the top of each plot. K_p values are shown around the inner circumference of each plot. Black vectors indicate velocities determined from two beam positions separated by 26° and red vectors indicate velocities determined from two beam positions separated by 52° .

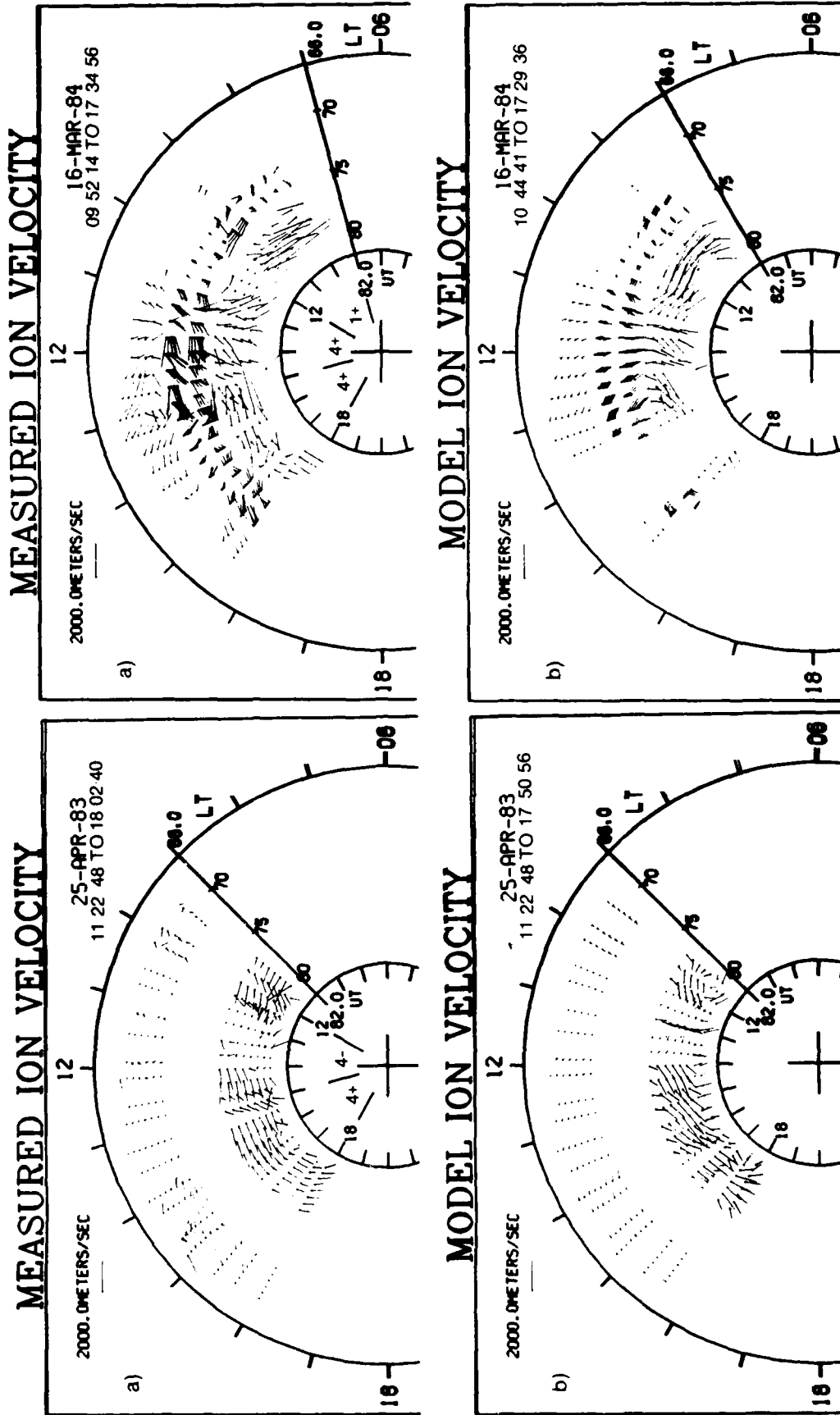


Plate 4. Measured (top) and simulated (bottom) F - region ion convection velocity for March 16, 1983, shown with the same format as Plate 2.

Plate 3. Measured (top) and simulated (bottom) F - region ion convection velocity for April 25, 1983, shown with the same format as Plate 2.

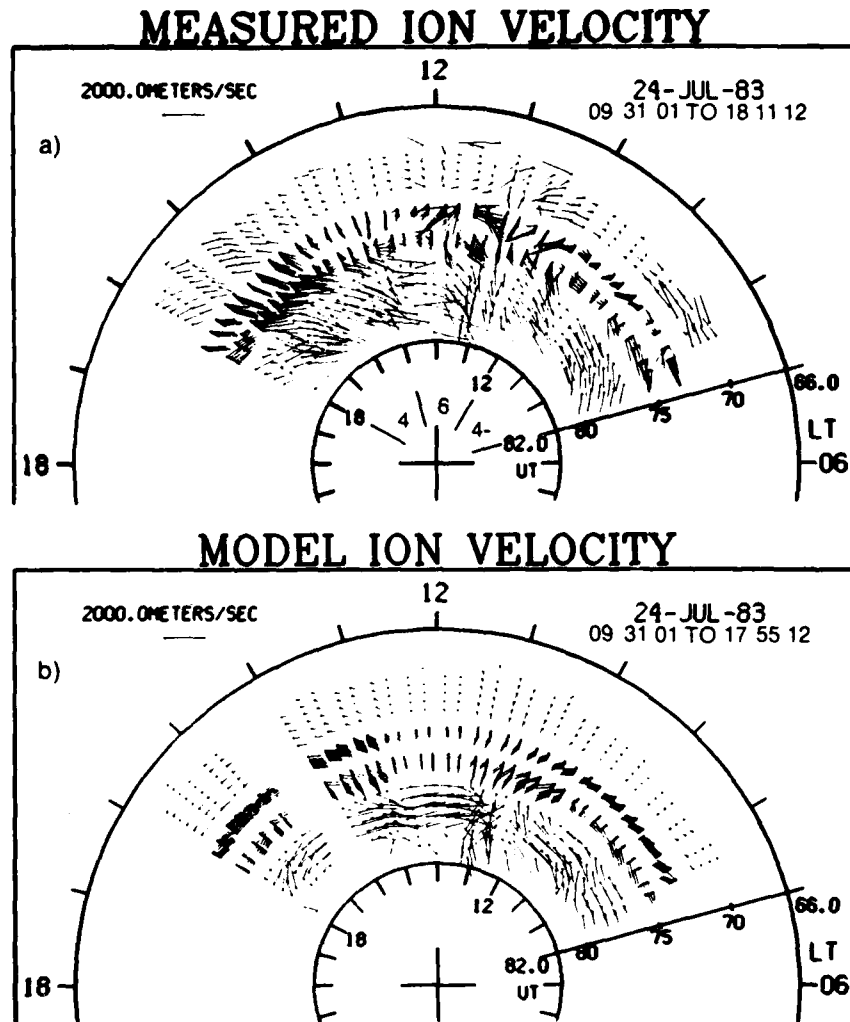


Plate 5. Measured (top) and simulated (bottom) *F*-region ion convection velocity for July 24, 1983, shown with the same format as Plate 2.

in the model is inconsistent with observations, particularly near local noon. This suggests that the region 1 and region 2 currents near noon may not be modeled properly.

When beginning these simulations, it was expected that the model would be an oversimplification of the actual current systems in the cleft. For example, we do not move the currents in local time in response to IMF B_y variations as suggested by the observations of Doyle *et al.* [1981] and the antiparallel merging model [Crooker, 1979; Luhmann *et al.*, 1984]. In addition, the currents in our simulation do not move in latitude as one would expect if the polar cap grows or shrinks in response to IMF B_z variations. We have made the DPY current system separate and above the region 1 and region 2 currents. However, as suggested by Bythrow *et al.* [1982], the equatorward portion should perhaps overlap the region 1 currents. Finally, perhaps a different configuration of currents during northward IMF such as the NBZ currents suggested by Iijima *et al.* [1984] is required.

Some of these modifications may correct some of the inconsistencies noted above. Nevertheless, it is quite remarkable that the simulations reproduce the observations as well as they do. This seems to indicate that the structure of the currents in the polar cleft is indeed rather similar to that of the model. It also argues strongly that the currents are indeed directly driven by the solar wind.

Acknowledgments. The IMP - 8 magnetic field data were kindly provided by Norm Ness, Ron Lepping and Joe King. The research has been supported by the National Science Foundation through grants ATM-8210562 and ATM-8503105 and by the Air Force Geophysics Laboratory through contract F19628-85-K-0001. Additional partial support was also provided by NASA grant NAGW 235. The authors are grateful to T. Araki for the use of the computer modeling code which was adapted to perform the simulations in this study. Values of the solar wind velocity and density measured by IMP - 8 were obtained from the Solar-Geophysical Data Comprehensive Reports published by the National Geophysical Data Center.

The Editor thanks W. J. Burke and E. Friis-Christensen for their assistance in evaluating this paper.

REFERENCES

- Banks, P. M., and J. V. Evans. *An Initial Feasibility Study to Establish a Very High Latitude Incoherent Scatter Radar*. Utah State University, Logan, 1979.
- Banks, P. M., T. Araki, C. R. Clauer, J. P. St. Maurice, and J. C. Foster. The interplanetary electric field, cleft currents, and plasma convection in the polar caps. *Planet. Space Sci.*, **32**, 1551, 1984.
- Barbosa, D. D., High-latitude field-aligned current sources and induced electric fields. *J. Geophys. Res.*, **84**, 5175, 1979.
- Barbosa, D. D., Dynamics of field-aligned current sources at Earth and Jupiter, in *Magnetospheric Currents*, *Geophys. Monogr., Ser.*, vol. 28, edited by T. A. Potemra, pp. 350-357. AGU, Washington, D.C., 1983.
- Barbosa, D. D., Fourier analysis of polar cap electric field and current distributions. *J. Geophys. Res.*, **89**, 867, 1984.
- Burch, J. L., P. H. Reiff, J. D. Menietti, R. A. Heelis, W. B. Hanson, S. D. Shawhan, E. G. Shelley, M. Sugura, D. R. Weimer, and J. D. Winningham. IMF B_y -dependent plasma flow and Birkeland currents in the dayside magnetosphere. 1. Dynamics Explorer observations. *J. Geophys. Res.*, **90**, 1577, 1985.
- Bythrow, P. E., T. A. Potemra, and R. A. Hoffman. Observations of field aligned currents, particles and plasma drift in the polar cusps near solstice. *J. Geophys. Res.*, **87**, 5131, 1982.
- Clauer, C. R., R. L. McPherron, C. Searls, and M. G. Kivelson. Solar wind control of auroral zone geomagnetic activity. *Geophys. Res. Lett.*, **8**, 915, 1981.
- Clauer, C. R., R. L. McPherron, and C. Searls. Solar wind control of the low-latitude asymmetric magnetic disturbance field. *J. Geophys. Res.*, **88**, 2123, 1983.
- Clauer, C. R., P. M. Banks, A. Q. Smith, T. S. Jorgensen, E. Friis-Christensen, S. Vennerstrom, V. B. Wickwar, J. Kelly, and J. Doupanik. Observations of interplanetary magnetic field and of ionospheric plasma convection in the vicinity of the dayside polar cleft. *Geophys. Res. Lett.*, **11**, 891, 1984.
- Crooker, N. U., Dayside merging and cusp geometry. *J. Geophys. Res.*, **84**, 951, 1979.
- D'Angelo, N., Field-aligned currents and large scale magnetospheric electric fields. *Ann. Geophys.*, **36**, 31, 1980.
- Doyle, M. A., F. J. Rich, W. J. Burke, and M. Smiddy. Field-aligned currents and electric fields observed in the region of the dayside cusp. *J. Geophys. Res.*, **86**, 5656, 1981.
- Friis-Christensen, E., High-latitude ionospheric currents, in *Exploration of the Polar Upper Atmosphere*, edited by C. S. Deehr and J. A. Holtet, D. Reidel, Hingham, Mass., 1981.
- Friis-Christensen, E., Solar wind control of the polar cusp, in *Proceedings of the Chapman Conference on Solar Wind-Magnetosphere Coupling*, edited by Y. Kamide, and J. A. Slavin, D. Reidel, in press, Hingham, Mass., 1986.
- Friis-Christensen, E., K. Lassen, J. Wilhelm, J. M. Wilcox, W. Gonzalez, and D. S. Colburn. Critical component of the interplanetary magnetic field responsible for large geomagnetic effects in the polar cap. *J. Geophys. Res.*, **77**, 3371, 1972.
- Friis-Christensen, E., and J. Wilhelm. Polar cap currents for different directions of the interplanetary magnetic field in the Y - Z plane. *J. Geophys. Res.*, **80**, 1248, 1975.
- Friis-Christensen, E., Y. Kamide, A. D. Richmond, and S. Matsushita. Interplanetary magnetic field control of high-latitude electric fields and currents determined from Greenland magnetometer data. *J. Geophys. Res.*, **90**, 1325, 1985.
- Heelis, R. A., The effects of interplanetary magnetic field orientation on dayside high-latitude ionospheric convection. *J. Geophys. Res.*, **89**, 2873, 1984.
- Iijima, T., and T. A. Potemra. The amplitude distribution of field-aligned currents at northern high-latitudes observed by TRIAD. *J. Geophys. Res.*, **81**, 2165, 1976a.
- Iijima, T., and T. A. Potemra. Field-aligned currents in the dayside cusp observed by TRIAD. *J. Geophys. Res.*, **81**, 5971, 1976b.
- Iijima, T., R. Fujii, T. A. Potemra, and N. A. Saffekos. Field-aligned currents in the south polar cusp and their relationship to the interplanetary magnetic field. *J. Geophys. Res.*, **83**, 5595, 1978.
- Iijima, T., T. A. Potemra, L. J. Zanetti, and P. F. Bythrow. Large-scale Birkeland currents in the dayside polar region during strongly northward IMF: A new Birkeland current system. *J. Geophys. Res.*, **89**, 7441, 1984.
- Jorgensen, T. S., E. Friis-Christensen, V. B. Wickwar, J. D. Kelly, C. R. Clauer, and P. M. Banks. On the reversal from "sunward" to "antisunward" plasma convection in the dayside high-latitude ionosphere. *Geophys. Res. Lett.*, **11**, 887, 1984.
- Kamide, Y., and S. Matsushita. Simulation studies of ionospheric electric fields and currents in relation to field-aligned currents. 1. Quiet periods. *J. Geophys. Res.*, **84**, 4083, 1979.
- Luhmann, J. G., R. J. Walker, C. T. Russell, N. U. Crooker, J. R. Spreiter, and S. S. Stahara. Patterns of potential magnetic field merging sites on the dayside magnetopause. *J. Geophys. Res.*, **89**, 1739, 1984.
- Mansurov, S. M., New evidence of a relationship between magnetic fields in space and on earth. *Geomagn. Aeron., Engl. Transl.*, **9**, 622, 1969.
- McDiarmid, J. B., J. R. Burrows, and M. D. Wilson. Magnetic field perturbations in the dayside cleft and their relationship to the IMF. *J. Geophys. Res.*, **83**, 5753, 1978.
- McDiarmid, J. B., J. R. Burrows, and M. D. Wilson. Large-scale magnetic field perturbations and particle measurements at 1400 km on the dayside. *J. Geophys. Res.*, **84**, 1431, 1979.
- Prindahl, F., and F. Spangnsley. Cusp region and auroral zone field aligned currents. *Ann. Geophys.*, **37**, 529, 1981.
- Prindahl, F., and F. Spangnsley. Does IMF B_y induce the cusp field aligned currents?. *Planet. Space Sci.*, **31**, 363, 1983.
- Reiff, P. H., and J. L. Burch. IMF B_y -dependent plasma flow and Birkeland currents in the dayside magnetosphere. 2. A global

- model for northward and southward IMF. *J. Geophys. Res.*, **90**, 1595, 1985.
- Rich, F. J., and Y. Kamide. Convection electric fields and ionospheric currents derived from model field-aligned currents at high-latitudes. *J. Geophys. Res.*, **88**, 271, 1983.
- Rostoker, G., Magnetospheric and ionospheric currents in the polar cusp and their dependence on the B_y component of the interplanetary magnetic field. *J. Geophys. Res.*, **85**, 4167, 1980.
- Spreiter, J. R., S. S. Stahara. A new predictive model for determining solar wind-terrestrial planet interactions. *J. Geophys. Res.*, **85**, 6769, 1980.
- Svalgaard, L., Polar cap magnetic variations and their relationship with the interplanetary magnetic sector structure. *J. Geophys. Res.*, **78**, 2064, 1973.
- Vennerstrom, S., E. Friis-Christensen, T. S. Jorgensen, O. Rasmussen, C. R. Clauer, and V. B. Wickwar. Ionospheric currents and F -region plasma boundaries near the dayside cusp. *Geophys. Res. Lett.*, **11**, 903, 1984.
- Wickwar, V. B., J. D. Kelly, O. de la Beaujardiere, C. A. Leger, F. Steenstrup, and C. H. Dawson. Sondrestrom overview. *Geophys. Res. Lett.*, **11**, 883, 1984.
- Wilhelm, J., E. Friis-Christensen, and T. A. Potemra. The relationship between ionospheric and field-aligned currents in the dayside cusp. *J. Geophys. Res.*, **83**, 5586, 1978.
- Zanetti, L. J., T. A. Potemra, T. Iijima, W. Baumjohann, and P. F. Bythrow. Ionospheric and Birkeland current distributions for northward interplanetary magnetic field: Inferred polar convection. *J. Geophys. Res.*, **89**, 7453, 1984.

P. M. Banks and C. R. Clauer, STAR Laboratory, Stanford Electronics Laboratories, Stanford University, Stanford, CA 94805.

(Received November 25, 1985;
revised January 22, 1986;
accepted January 27, 1986.)

The U.S. Government is authorized to reproduce and sell this report. Permission for further reproduction by others must be obtained from the copyright owner.

Solar Wind-Magnetosphere Coupling, edited by Y. Kamide and J. A. Slavin, 39-57.
Copyright © 1986 by Terra Scientific Publishing Company (TERRAPUB), Tokyo.

The Technique of Linear Prediction Filters Applied to Studies of Solar Wind-Magnetosphere Coupling

C. Robert CLAUER

*Space, Telecommunications and Radioscience Laboratory, Stanford Electronics Laboratories
Stanford University, Stanford, California 94305, U.S.A.*

Linear prediction filtering is a powerful empirical technique suitable for the study of stimulus-response behavior. The technique enables one to determine the most general linear relationship between multiple time-varying quantities, assuming that the physical systems relating the quantities are linear and time invariant. Several researchers have applied linear prediction analysis to investigate solar wind-magnetosphere interactions. This short review describes the method of linear prediction analysis, its application to solar wind-magnetosphere coupling studies both in terms of the assumptions and in terms of physical processes, and the results of investigations which have used this technique.

1. Introduction

A great deal of scientific effort has been invested over the past several decades to understand the causes of geomagnetic activity. It is now known that the sun through its expanding outer atmosphere, the solar wind, is the primary source of the energy which produces geomagnetic disturbances. These disturbances recorded at our geomagnetic observatories result from electrical currents which flow around the earth in space, through the ionosphere and within the conducting earth. The magnetic effects produced by these currents are characterized by various simple measures called geomagnetic indices (ROSTOKER, 1972; MAYAUD, 1980; KAMIDE and AKASOFU, 1983). Careful understanding of the methods used to create indices and the consequent limitations of the indices is required when making a physical interpretation based on their use. The benefit of the indices, however, is to synthesize a variety of complex geomagnetic disturbance measurements into a simple time series. Because of this simplification, geomagnetic indices have been used extensively in studies of magnetospheric behavior. Our understanding of the solar wind's control over geomagnetic activity has been largely acquired through studies based on correlations between solar wind quantities and geomagnetic indices. These correlations have formed the framework within which theories of solar wind-magnetosphere coupling have been developed.

Most correlative studies have used regression, superposed epoch, or cross correlation techniques to establish relationships between the solar wind and geomagnetic activity and a discussion of these techniques is given by BAKER (1986) in this volume. Recently another very powerful technique, that of linear prediction filtering, has been introduced to the field of magnetospheric physics (IYEMORI *et al.*, 1979; IYEMORI and MAEDA, 1980). This technique allows one to empirically

determine the most general linear relationship between a solar wind input function and a geomagnetic disturbance output function taking into account time delays and frequency response. Such a functional relationship provides a more detailed set of constraints for models which must account for the physical mechanisms associated with the coupling of solar wind energy to magnetospheric current systems.

The technique of linear prediction filtering is based on least squares criteria and leads to filters (functions which transform the input into the output) which are linear. The method is particularly noteworthy because of the quality of the results obtained and the simplicity of the concepts involved. The theory on which linear prediction analysis is based was originally developed by the mathematician Norbert Wiener and is put forth in his book on linear least squares prediction and signal enhancement (WIENER, 1942). The technique is now commonly referred to as Wiener Filtering. While the original work by Wiener was formulated in terms of continuous time series, the important adaptation to discrete time series was developed by LEVINSON (1942) and appears as an appendix to Wiener's book. Perhaps one of the most useful books to deal with the application of Wiener filtering to geophysical problems is by ROBINSON (1967). This book provides a clear description of the technique plus Fortran computer code for the subroutines required to perform the analysis. The more recent book by ROBINSON and TREITEL (1980) also provides a good reference. In the following sections of this review, I will provide a mathematical introduction to the technique followed by a review of the applications which have used Wiener filtering in studies of solar wind-magnetosphere coupling.

2. Principles of Digital Wiener Filtering

The basic model for the filtering process considered here consists of a system having an input signal, a desired or measured output signal and a computed output signal. This is shown schematically in Fig. 1 where $I(t)$ is the input time series, $O(t)$ is the desired output time series and $\hat{O}(t)$ is the computed output. The input and the computed output are related by a filter f which must be determined from the input and the desired output time series. A basic assumption of the analysis is that the physical systems characterized by $I(t)$ and $O(t)$ can be related by a linear time invariant filter f . This can be described mathematically by the equation

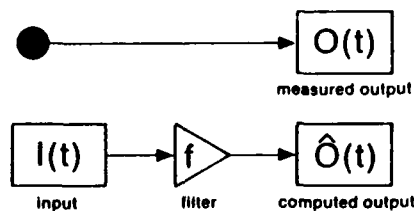


Fig. 1. The Wiener Filter model.

$$\alpha(t) = \int_{-\infty}^{+\infty} f(\tau)I(t - \tau)d\tau. \tag{1}$$

For the case of discrete time series data, Equation (1) may be written as

$$O_t = \sum_{\tau=-\infty}^{\infty} f_{\tau}I_{t-\tau} = \sum_{\tau=-\infty}^{-1} f_{\tau}I_{t-\tau} + \sum_{\tau=0}^{\infty} f_{\tau}I_{t-\tau}. \tag{2}$$

Here f_{τ} is the prediction filter or impulse response function, t denotes time and τ denotes time lag. Note that Equation (2) can be broken into two summations, one with $\tau < 0$ and the second with $\tau \geq 0$. Negative values of τ indicate times in the future. Thus, applying limits to the summation can force assumptions about causality. If $\tau \geq 0$, the filter will be purely causal and the output will strictly follow the input.

Given finite and noisy measurements of I_t and O_t our task is to solve for the predictive filter f . To do this, we must assume that both the input and output time series are stationary. That is, their statistical properties do not change in time. We also must assume that errors in the two time series I_t and O_t are random and uncorrelated. And finally we must assume that they are related by a linear operator as in Eq. (2). If these assumptions are not met this procedure will still produce the best linear filter which transforms the input into the output. This filter, however, will be based on the finite set of data utilized in the analysis and may not be generally valid for other subsets of the infinite data domain from which the data was sampled.

The determination of the filter coefficients ($f_0, f_1, f_2, \dots, f_m$) is based on the least-squares criterion: one minimizes the power existing in the difference time series obtained by subtracting the actual or measured output O_t from the computed output \hat{O}_t . This will be illustrated through the example of a single channel filter.

2.1. *Single channel filter*

The single channel filter has one input and one output. In this example let

- X_t =input,
- Y_t =desired output,
- \hat{Y}_t =computed output.

Assuming a causal relationship, the convolution Equation (2) will become

$$\hat{Y}_t = f_0X_t + f_1X_{t-1} + \dots + f_mX_{t-m} = \sum_{\tau=0}^m f_{\tau}X_{t-\tau}. \tag{3}$$

The error at point t is given by the difference between the measured output and the computed output. This is expressed by e_t in the following equation

$$e_t = Y_t - \hat{Y}_t = Y_t - \sum_{\tau=0}^m f_{\tau}X_{t-\tau}. \tag{4}$$

The mean-square-error or error power is then given by

$$\begin{aligned}
 I &= E\{e_i^2\} \\
 &= E\{[Y_i - (f_0 X_i + f_1 X_{i-1} + \dots + f_m X_{i-m})]^2\}
 \end{aligned} \tag{5}$$

where E is the Ensemble Average operator. This quantity is minimized by setting its partial derivatives with respect to the filter coefficients f_i equal to zero. That is $\partial I / \partial f_i = 0$. Doing this produces the set of equations called the normal equations

$$\begin{aligned}
 \frac{\partial I}{\partial f_0} &= E\{[Y_i - (f_0 X_i + f_1 X_{i-1} + \dots + f_m X_{i-m})]X_i\} = 0 \\
 \frac{\partial I}{\partial f_1} &= E\{[Y_i - (f_0 X_i + f_1 X_{i-1} + \dots + f_m X_{i-m})]X_{i-1}\} = 0 \\
 &\vdots \\
 \frac{\partial I}{\partial f_m} &= E\{[Y_i - (f_0 X_i + f_1 X_{i-1} + \dots + f_m X_{i-m})]X_{i-m}\} = 0.
 \end{aligned} \tag{6}$$

where both sides of the equations have been divided through by -2.

These equations can be written in terms of the autocorrelation coefficients $R_{ij} = E\{X_{i-i}X_{i-j}\}$ and the cross correlation coefficients $G_i = E\{Y_i X_{i-i}\}$ becoming

$$\begin{aligned}
 f_0 R_{00} + f_1 R_{10} + f_2 R_{20} + \dots + f_m R_{m0} &= G_0 \\
 f_0 R_{01} + f_1 R_{11} + f_2 R_{21} + \dots + f_m R_{m1} &= G_1 \\
 &\vdots \\
 f_0 R_{0m} + f_1 R_{1m} + f_2 R_{2m} + \dots + f_m R_{mm} &= G_m.
 \end{aligned} \tag{7}$$

Given the covariances R_{ij} and g_i we can solve these $m+1$ equations for the $m+1$ unknown filter coefficients f_i .

Since $R_{ij} = R_{ji}$ we can simplify the notation by letting R_τ equal the autocorrelation coefficient at lag τ . The normal equations form a set of $m+1$ linear simultaneous equations which can be written in matrix form as

$$\begin{pmatrix} R_0 & R_1 & R_2 & \dots & R_m \\ R_1 & R_0 & R_1 & \dots & R_{m-1} \\ \vdots & \vdots & \vdots & \ddots & \vdots \\ R_m & R_{m-1} & R_{m-2} & \dots & R_0 \end{pmatrix} \begin{pmatrix} f_0 \\ f_1 \\ f_2 \\ \vdots \\ f_m \end{pmatrix} = \begin{pmatrix} G_0 \\ G_1 \\ G_2 \\ \vdots \\ G_m \end{pmatrix} \tag{8}$$

These equations could be solved by normal techniques, however, because of the symmetries in the matrices a much more efficient method is possible. The matrix R has the special form of a Töplitz matrix (i.e., a matrix with equal submatrices on any diagonal). Thus the matrix involves only $m+1$ distinct elements namely $R_0, R_1, R_2, \dots, R_m$. An efficient computational solution to these equations is the Töplitz recursive

method. This method is essentially the same as the Levinson algorithm (LEVINSON, 1949). A description of the recursion will not be given here but can be found in ROBINSON, (1967) and ROBINSON and TREITEL, (1980). Using the recursion technique, one usually computes filters of successively increasing length. The value of the minimum mean-square-error I_{min} decreases with each recursion. The recursion from n to $n+1$ may be stopped whenever a certain preset criterion is met. For example:

1. The filter reaches a maximum preset length.
2. The normalized mean-square-error reaches some minimum preset value.
3. The normalized mean-square-error sequence levels out and shows little likelihood of further appreciable decrease.

When the analysis is completed, we have a computed filter which transforms the input into the output time series. In addition, we have a measure of the filter's efficiency at converting the input to the output. This efficiency measure is based on the power in the residual or error time series and is given by the value of $I = I_{min}$ from Eq. (5).

2.2. Multichannel filters

Many systems have multiple inputs and outputs. Such systems are called multichannel systems. A multichannel system involves many time series which are related. The theory of multichannel filters is conceptually the same as the theory of the single channel filter and mathematically it represents only an extension from ordinary scalar algebra to matrix algebra. That is, multichannel theory can be obtained from single channel theory by the appropriate substitution of matrices for scalars. If the system has the same number of input and output channels, the equation will contain square matrices and vectors. If the number of input channels and output channels is different, then the matrices will be rectangular.

For example, consider a system having two input channels and two output channels where

$$X_t = \begin{pmatrix} X_{1t} \\ X_{2t} \end{pmatrix} = \text{input,}$$

and

$$Y_t = \begin{pmatrix} Y_{1t} \\ Y_{2t} \end{pmatrix} = \text{output.}$$

The basic convolution formula is:

$$Y_t = f_0 X_t + f_1 X_{t-1} + \dots + f_m X_{t-m} \tag{9}$$

where t is again an integer denoting discrete time. Y and X are 2×1 column vectors and the coefficients f_s are given by 2×2 matrices. Expanding Equation (9) yields,

$$\begin{aligned}
\begin{pmatrix} Y_{1t} \\ Y_{2t} \end{pmatrix} &= \begin{pmatrix} f_{11}(0) & f_{12}(0) \\ f_{21}(0) & f_{22}(0) \end{pmatrix} \begin{pmatrix} X_{1,t} \\ X_{2,t} \end{pmatrix} \\
&+ \begin{pmatrix} f_{11}(1) & f_{12}(1) \\ f_{21}(1) & f_{22}(1) \end{pmatrix} \begin{pmatrix} X_{1,t-1} \\ X_{2,t-1} \end{pmatrix} \\
&+ \quad \vdots \\
&+ \begin{pmatrix} f_{11}(m) & f_{12}(m) \\ f_{21}(m) & f_{22}(m) \end{pmatrix} \begin{pmatrix} X_{1,t-m} \\ X_{2,t-m} \end{pmatrix}.
\end{aligned} \tag{10}$$

In general, given N input channels and M output channels, one has:

$$\begin{aligned}
X_t \equiv X(t) &= \begin{pmatrix} X_1(t) \\ X_2(t) \\ \vdots \\ X_M(t) \end{pmatrix} = \text{Input,} \\
Y_t \equiv Y(t) &= \begin{pmatrix} Y_1(t) \\ Y_2(t) \\ \vdots \\ Y_M(t) \end{pmatrix} = \text{Desired Output,} \\
\hat{Y}_t \equiv \hat{Y}(t) &= \begin{pmatrix} \hat{Y}_1(t) \\ \hat{Y}_2(t) \\ \vdots \\ \hat{Y}_M(t) \end{pmatrix} = \text{Computed Output,}
\end{aligned}$$

and a set of $M \times N$ matrix valued filter coefficients

$$f \equiv f(s) = \begin{pmatrix} f_{11}(s) & f_{12}(s) & \dots & f_{1M}(s) \\ f_{21}(s) & f_{22}(s) & \dots & f_{2M}(s) \\ \vdots & \vdots & \ddots & \vdots \\ f_{M1}(s) & f_{M2}(s) & \dots & f_{MM}(s) \end{pmatrix}.$$

The error e_t between the desired output and the actual output is then a $M \times 1$ vector valued time series

$$e_t = \hat{Y}_t - Y_t = \begin{pmatrix} \hat{Y}_1(t) - Y_1(t) \\ \hat{Y}_2(t) - Y_2(t) \\ \vdots \\ \hat{Y}_M(t) - Y_M(t) \end{pmatrix} \equiv \begin{pmatrix} e_1(t) \\ e_2(t) \\ \vdots \\ e_M(t) \end{pmatrix}. \tag{11}$$

The mean-square-error matrix is defined as

$$E\{e_i e_i^T\} = \begin{pmatrix} E\{e_1^2(t)\} & E\{e_1(t)e_2(t)\} & \dots & E\{e_1(t)e_M(t)\} \\ & \dots & & \\ E\{e_M(t)e_1(t)\} & E\{e_M(t)e_2(t)\} & \dots & E\{e_M^2(t)\} \end{pmatrix} \quad (12)$$

The mean-square-error or error power is given by the trace of the mean-square-error matrix which is defined to be the sum of the diagonal terms,

$$I = \text{tr}E\{e_i e_i^T\} = \sum_{i=1}^m E\{e_i^2(t)\} \quad (13)$$

Again setting the partial derivative of I with respect to each filter coefficient equal to zero produces a set of normal equations given by:

$$\begin{aligned} f_0 \phi_{xx}(0) + f_1 \phi_{xx}(-1) + \dots + f_m \phi_{xx}(-m) &= \phi_{yx}(0) \\ f_0 \phi_{xx}(1) + f_1 \phi_{xx}(0) + \dots + f_m \phi_{xx}(1-m) &= \phi_{yx}(1) \\ &\vdots \\ f_0 \phi_{xx}(m) + f_1 \phi_{xx}(m-1) + \dots + f_m \phi_{xx}(0) &= \phi_{yx}(m) \end{aligned} \quad (14)$$

where $\phi_{xx}(\tau)$ are the autocorrelation of the input X at lag τ and $\phi_{yx}(\tau)$ are the cross correlation of the desired output Y with the input X . This set of linear simultaneous equations can also be solved by the Töplitz recursion method discussed above. The reader is directed to texts by Robinson for further information about the calculation of the multichannel autocorrelation and cross correlation coefficients and the Töplitz recursive solution.

3. Application to Studies of Solar Wind-Magnetosphere Coupling

Wiener filtering has been applied to the problem of solar wind-magnetosphere coupling using various parameters measured in the solar wind and indices of geomagnetic activity. In these studies, solar wind parameters represent the input and geomagnetic activity the output. The computed filters or impulse response functions characterize the processes which link solar wind energy to the currents monitored by the various geomagnetic indices used in the analyses.

The technique of Wiener filtering was introduced to the solar wind-magnetosphere coupling problem by IYEMORI *et al.* (1979). In this study the authors used 300 days of hourly average data from 1967 through 1969. Filters relating the solar wind quantities $V B_z$ and B_z to auroral magnetic indices AL , AU , AE and to the low-latitude ring current magnetic index D_{st} were computed. The D_{st} filter develops in 1 hour and decays with a time constant of about 8 hours which is consistent with the previous empirical model developed by BURTON *et al.* (1975). The AE and AL filters are a narrow pulse peaking at 1 hour lag. The AU filter is a broader peak at 1 hour lag. Since the AU filter is significantly different than the AL filter in shape, IYEMORI *et al.*, suggest that the generation for the currents monitored by AU may be different than those for AL or else the generation may be complex, consisting of multiple

mechanisms. The prediction efficiency was fairly high for all of the predictions.

The Wiener Filtering technique was extended to studies of high time resolution data by a number of subsequent researchers (CLAUER *et al.*, 1981, 1983; MCPHERRON *et al.*, 1984; BARGATZE *et al.*, 1985; and AKASOFU *et al.*, 1985). Figure 2 from CLAUER *et al.* (1981) shows high time resolution Wiener filters which relate 3 forms of the solar wind input function to the *AL* index. The three input functions have a $\sqrt{B^2 \sin^4(\theta/2)}$, $\sqrt{B_z}$, an $\sqrt{B_z}$ dependence respectively where

$$\theta = \begin{cases} \tan^{-1} \frac{|B_z|}{|B_r|}, & \text{for } B_z > 0; \\ 180^\circ - \tan^{-1} \frac{|B_z|}{|B_r|}, & \text{for } B_z < 0. \end{cases}$$

and

$$B_r = \begin{cases} 0, & \text{for } B_z \geq 0 \\ -B_z, & \text{for } B_z < 0. \end{cases}$$

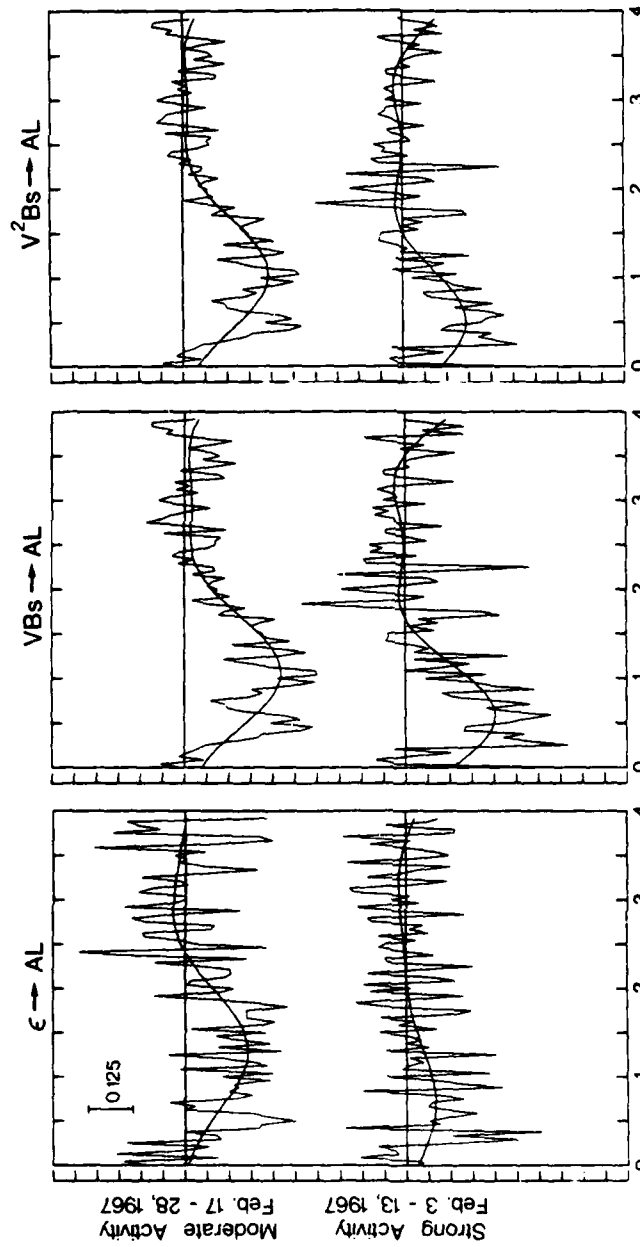
Two time intervals were analyzed. The filters at the top of Fig. 2 were created from an interval of moderate level geomagnetic activity while the bottom panel filters were created from an interval of strong activity. The horizontal axis of the plots is time lag. A smooth curve is drawn through the filters and is shown only as an aid to the reader. The filters are very spiky. This is due to uncertainties which result from correlations based on a small number of active periods in the 10 and 12 day intervals used in the analysis. Less noisy filters result from analysis on long intervals which include many repeated correlated variations between the input and output time series. For example, compare the $\sqrt{B_z} \rightarrow AL$ filters in Fig. 2 with the $\sqrt{B_z} \rightarrow AL$ filter shown in Fig. 5 which was created using 56 days of data.

The dominant feature of the filters in Fig. 2 is a delayed negative pulse indicative of a low pass filter with a time delay. It is interesting to see that the filters for the strong activity and moderate activity intervals show different time delays suggesting some form of nonlinearity in the $\sqrt{B_z} \rightarrow AL$ relationship.

The variation in the $\sqrt{B_z} \rightarrow AL$ impulse response as a function of geomagnetic activity level has been examined in greater detail by BARGATZE *et al.* (1985). The data set examined contains 73 days of 2.5 minute resolution data. An activity level based on the *AL* index was assigned to each of the 34 intervals comprising the data set. These intervals were sorted by activity level to produce a time series of increasing level of geomagnetic activity. A set of running filters was determined over the entire data set by first using 5 consecutive intervals to compute a Wiener filter and then stepping ahead one interval at a time. Figure 3 shows the set of 30 $\sqrt{B_z} \rightarrow AL$ filters thus obtained with the weak activity filters at the bottom ranging to the strong activity filters at the top.

Two peaks can be identified in these filters, the first at 20 minutes lag and the second at 60 minutes lag. The relative importance of the peaks varies as a function of activity level, with the second peak dominant at middle activity levels, the first peak

IMPULSE RESPONSE OF THE MAGNETOSPHERE
SOLAR WIND POWER TO AL INDEX



TIME (HOURS)

Fig. 2. Linear prediction filters relating various proposed solar wind power input parameters to the AL index during two intervals of moderate and severe geomagnetic activity. Time lag is plotted along the horizontal axis and the filter value is plotted along the vertical axis (CLAUER *et al.*, 1981).

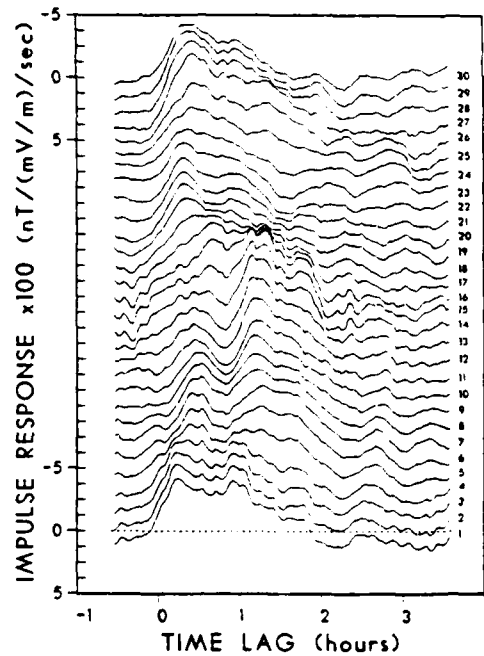


Fig. 3. Stack plot of Wiener Filters for varying levels of geomagnetic activity ranging from quiet at the bottom to severe at the top (BARGATZE *et al.*, 1985).

dominant at strong activity levels and both peaks about equal at weak activity levels.

It is suggested that the two peaks correspond to separate response modes of the magnetosphere and that the relative dominance of these modes varies with the level of activity. The physical interpretation given to the two peaks regards the first peak as corresponding to auroral activity which is directly driven by the solar wind-magnetospheric dynamo while the second peak corresponds to auroral activity which results from the release of stored energy from the magnetotail.

While auroral currents have obtained the greatest attention in linear prediction investigations, four studies have presented analysis which relate solar wind parameters to the ring current index D_{st} : IYEMORI *et al.* (1979); IYEMORI and MAEDA (1980); MCPHERRON *et al.* (1984); and indirectly AKASOFU *et al.* (1985). The results of these studies indicate that D_{st} is the best determined geomagnetic index using solar wind information alone. Using 5-minute data and a multi-channel filter with solar wind dynamic pressure and electric field inputs, MCPHERRON *et al.*, (1984) reproduced 70% of the variance in the D_{st} index.

Most of the studies using linear prediction filtering have concluded that only a portion of the output index is predictable from solar wind information alone IYEMORI *et al.*, 1979, 1980; CLAUER *et al.*, 1981, 1983; MCPHERRON *et al.*, 1984; and BARGATZE *et al.*, 1985). This is illustrated for the AL index in Fig. 4 which shows a

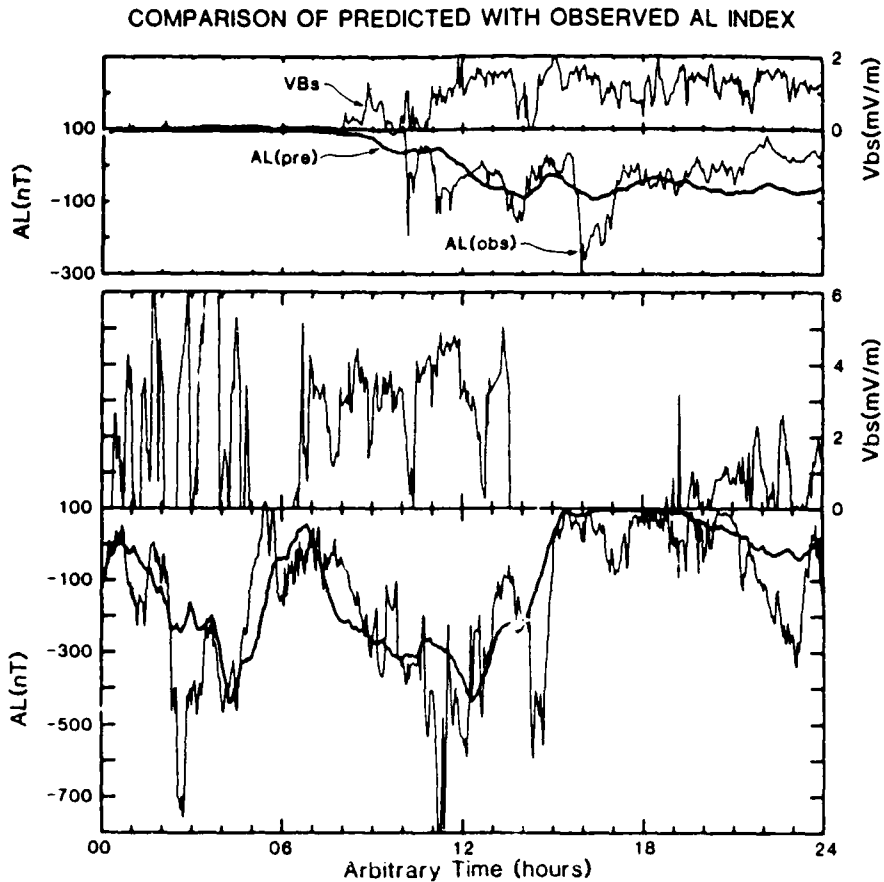


Fig. 4. Comparison of predicted and observed AL index for periods of moderate (top) and strong (bottom) geomagnetic activity. Each frame shows a plot of the solar wind input function V_B at the top with the predicted (dark line) and observed (light line) AL index underneath, (figure courtesy of R. L. McPherron).

comparison between the measured AL index and the computed AL index. The top panel shows an interval of moderate level activity and the bottom panel shows an interval of strong activity. In each case the computed AL looks like a smoothed or low-pass filtered version of the observed index. It is suggested that unpredicted portions of the index can be attributed to noise in the measurements of the proper input parameters and in the indices which characterize the magnetospheric current systems, and also to real variations in the currents which are not consistently related to the solar wind driving function. That is, currents which are controlled by internal magnetospheric processes. There are several examples of large, sudden, negative excursions of the AL index which are not predicted and which are thought to result

from intensifications of the westward electrojet caused by substorm expansions initiated within the magnetotail by internal processes.

The analysis presented by CLAUER *et al.* (1983) provides a fairly strong case for this point of view. Fifty-six days of 10-minute resolution data were used in the analysis. Figure 5 shows the filters computed in that study. Note that both future and past time lags were used in this analysis. The solar wind input function used in the analysis was VB_s , and the magnetic indices examined were the auroral AL index and the low-latitude $ASYM$ index defined to be the difference between the dawn and dusk perturbations in the X component of the geomagnetic field. $ASYM$ is thus an index of the partial ring current magnetic perturbation.

The $VB_s \rightarrow ASYM$ and $VB_s \rightarrow AL$ filters in Fig. 5 are essentially zero prior to 0 time lag, thus they are purely causal. Both are delayed pulses and are essentially low

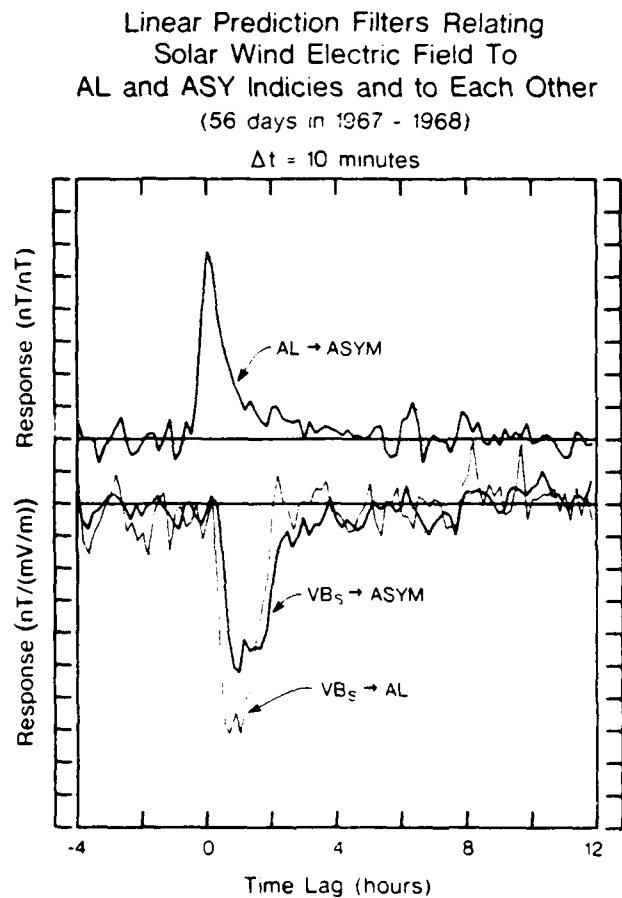


Fig. 5. Three Wiener Filters, $AL \rightarrow ASYM$, $VB_s \rightarrow ASYM$, and $VB_s \rightarrow AL$, plotted together for comparison (CLAUER, *et al.*, 1983).

pass filters with a time delay. The $AL \rightarrow ASYM$ filter is also shown in Fig. 5. This filter was created to test the notion that the partial ring current is the result of individual substorm expansions injecting bursts of energetic ions into the ring current region. These ions would drift westward to produce a partial ring current (BOGUNIT and MOZER, 1973). We find, however, that the filter is nonzero at negative lags indicating that development of $ASYM$ precedes AL . This feature of the Wiener filter is consistent with the analysis of several individual events which showed the development of the partial ring current preceding the substorm expansion onset determined from both the AL index and the midlatitude positive bay signature (CLAUER and MCPHERRON, 1980).

The measures of the prediction efficiency provide some interesting information. About 45% of the variance of the $ASYM$ index is predictable from VB_s , while 56% is predictable from AL . Also, 41% of the variance of AL is predictable using VB_s . This suggests that the AL index contains information that is correlated with $ASYM$ but is unrelated to the solar wind. CLAUER *et al.* (1983) hypothesize that both AL and $ASYM$ are produced by two uncorrelated processes, one which directly involves the solar wind and another which is due to internal magnetospheric processes.

Additional analysis was performed on the error (or residual) time series. It was reasoned that the solar wind related portion of the signal is absent in the residual time series. There should, however, still remain the signal due to internal magnetospheric processes which are not directly determined by the solar wind input alone. To see if the error time series for AL and $ASYM$ both contained this internal magnetospheric signal, a filter relating the prediction residual of AL to the prediction residual of $ASYM$ was computed. It was found that 24% of the variance of the $ASYM$ residual was related to the AL residual.

Figure 6 shows a schematic model of the hypothesized system. The solar wind input VB_s is transformed to the output AL , by filter g_1 . A second component AL_i is assumed to be produced by the internal magnetospheric process through filter g_i , and is added to AL_s to produce AL . The AL index in turn is transformed by filter g_2 into the $ASYM$ index. Therefore, in this model the solar wind input VB_s is related to $ASYM$ by a cascade of two filters g_1 and g_2 . Provided that both systems are linear, the cascade can be represented by a single filter g_0 which is the convolution of g_1 and g_2 . Thus,

$$g_{0,m} = \sum_{n=0}^N g_{1,n} g_{2,(m-n)}$$

Figure 5 shows the empirically determined filters g_0 and g_2 . The output of filter g_1 , AL_s , is not directly observed. By hypothesis, however, AL_s is uncorrelated with the solar wind so that g_1 is the filter determined from VB_s and AL . As a check of this hypothesis the $VB_s \rightarrow AL$ filter was convolved with the $AL \rightarrow ASYM$ filter for comparison with the $VB_s \rightarrow ASYM$ filter. The comparison is shown in fig. 7. A dashed line shows the empirical $VB_s \rightarrow ASYM$ filter and a solid line shows the filter produced by the convolution. The agreement between the two curves is quite good, thus supporting the hypothesis that AL is composed of both a solar wind driven

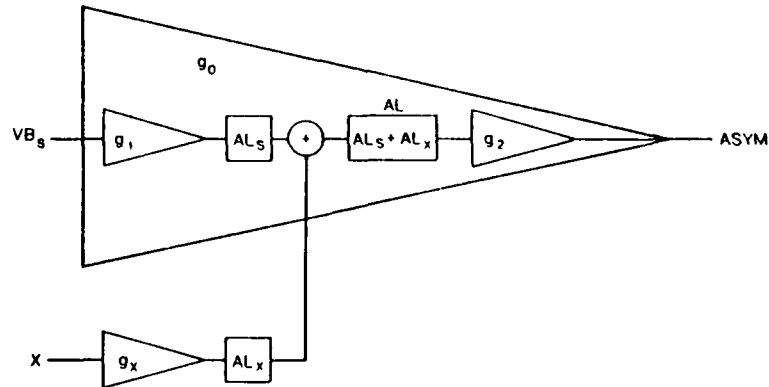
A POSSIBLE LINEAR SYSTEM RELATING VB_S , AL , $ASYM$ 

Fig. 6. Schematic diagram of a model in which the solar wind input function VB is transformed into the $ASYM$ index by filter g_0 . The AL index is transformed into $ASYM$ by filter g_2 . The AL index, however, is composed of two components. One component AL is related to the solar wind VB through filter g_1 while the other component AL_x is related to another process X by filter g_x . AL is the sum of these two signals (CLAUSER *et al.*, 1983).

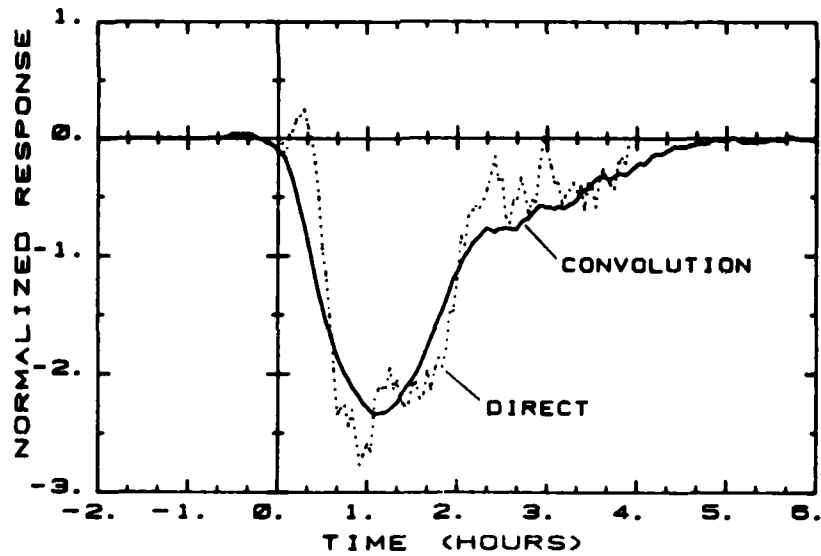
COMPARISON OF VBS TO $ASYM$ FILTERS

Fig. 7. Comparison of the $VB_S - ASYM$ filter (g_0 in Fig. 5) with the convolution of the $VB_S - AL$ and $AL - ASYM$ filters (g_1 and g_2 in Fig. 5) (CLAUSER *et al.*, 1983).

component and another component uncorrelated with the solar wind.

A somewhat different conclusion, however, was reached by AKASOFU *et al.* (1985) in an analysis which computed Wiener filters relating the ϵ parameter with the so-called total magnetospheric energy dissipation rate parameter, U_T . This investigation used 5-minute resolution data during magnetic storm intervals. The solar wind input parameter $\epsilon \propto V B^2 \sin^4(\theta/2)$ was measured by the ISEE-3 satellite located 240 R_e upstream from the subsolar magnetopause. The output parameter U_T is given by:

$$U_T(\text{erg/sec}) = 4 \cdot 10^{20} \left(\frac{\partial \overline{D_{st}}}{\partial t} + \frac{\overline{D_{st}}}{\tau_R} \right) + 3 \cdot 10^{15} AE$$

where $\overline{D_{st}}$ is a solar wind pressure adjusted D_{st} index and τ_R denotes a ring current decay time scale.

Figure 8 show plots from 3 of the 6 storms. Each column of plots shows data from one storm. The top panel shows the input ϵ parameter, the next panel shows the

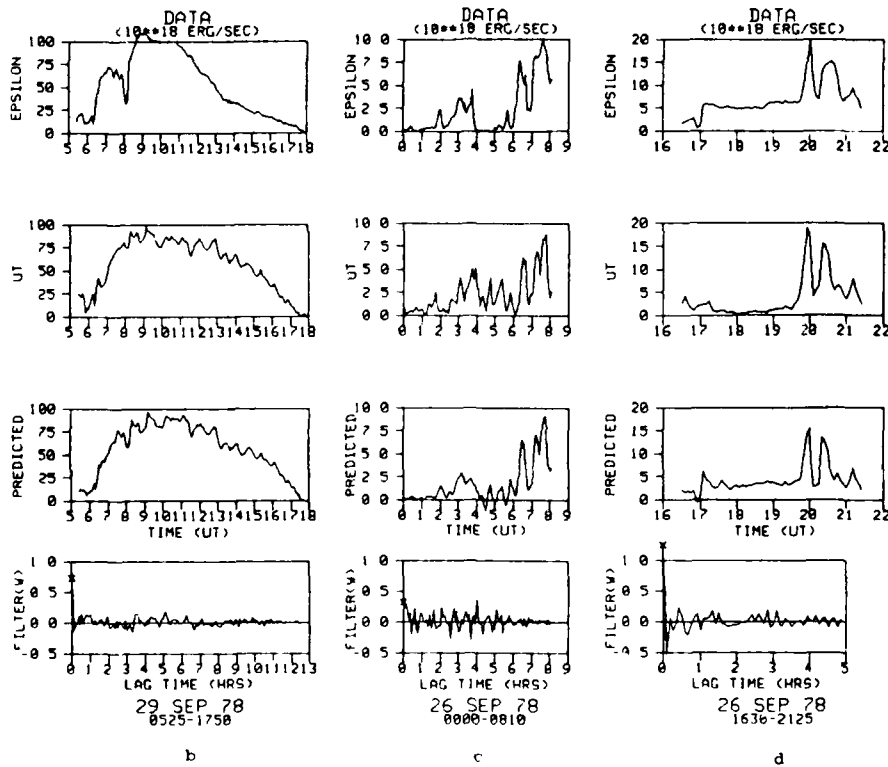


Fig. 8. Examples of linear prediction analysis for 3 geomagnetic storms on September 29, 1978. From the top are shown the input parameter ϵ , the output function U_T , the prediction of U_T , and the prediction filter (AKASOFU *et al.*, 1985)

output U_T parameter, the next panel shows the predicted \hat{U}_T parameter and the bottom panel shows the computed Wiener filter. Figure 9 shows a superposition of all six of the computed Wiener filters.

The authors note that for the 3 largest storms studied the predicted \hat{U}_T is a good fit to the measured U_T while the smaller 3 storms were not well fit. The filters shown in Figs. 8 and 9 are essentially δ functions at $t=0$. These results, the zero time lag and the good prediction, are interpreted to indicate that for periods of strong activity magnetospheric energy dissipation is directly driven with little or no time lag.

The zero time lag in the Akasofu *et al.* filters, however, is troubling and seems physically implausible, particularly when the uncertainty of the transit time between ISEE-3 and the magnetopause is greater than the accuracy of the 5-minute data resolution (RUSSELL *et al.*, 1980). Further, spikes at the ends of filters are often characteristic of errors in removing the mean or trends from time series. Alternatively, it is likely that the methods used to compute U_T are cause of this artifact. The

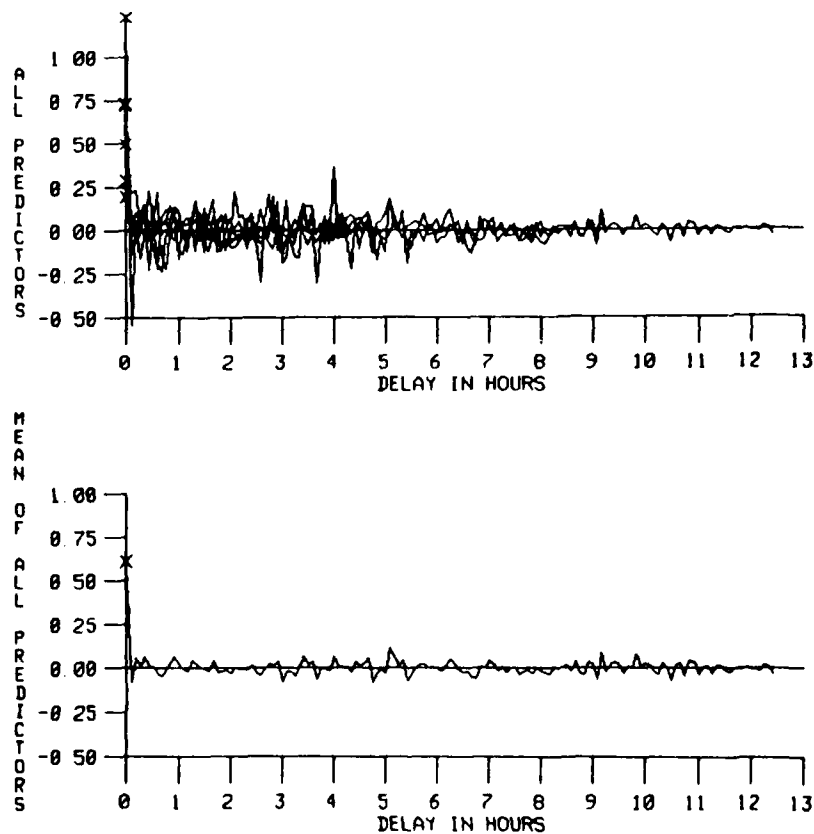


Fig. 9. Superposition (top) and average (bottom) of 6 impulse response functions computed for 6 geomagnetic storms (AKASOFU *et al.*, 1985).

derivation of U_T is based on several solar wind parameters. The value of D_{st} is adjusted for the solar wind pressure and the ring current decay "constant" τ_R is a function of the input function ϵ . The output parameter therefore contains terms from the measured input thereby confusing the correlation and producing a zero-lag artifact. One must also note that the application of Wiener filtering to single event studies may be inappropriate. The spikey character of the filters obtained is an indication of this. The ability to compute physically meaningful filters relies on the least squares aspects of the analysis and requires many correlated variations in the input and output time series.

The pressure effect could more properly be taken care of by using a multichannel analysis which inputs both solar wind dynamic pressure and ϵ to an output composed only of geomagnetic measurements. To do this, τ_R must be obtained independently from the input time series ϵ . For example, FELDSTEIN *et al.* (1984) estimate values for τ_R based on the magnitude of D_{st} . Such a multichannel technique would also provide a better method of determining the transit time from ISEE-3 to the magnetopause since the $\rho V^2 - D_{st}$ filter was shown to be a narrow pulse at a delay time consistent with the expected propagation time between the satellite and magnetopause (MCPHERRON *et al.*, 1984).

4. Summary and Conclusions

The technique of linear prediction filtering has provided another powerful statistical tool for the data analyst to use in an attempt to resolve some of the complex relationships which exist between various geomagnetic current systems and solar wind input energy. It appears clear from all of the Wiener filtering studies cited above that a substantial portion of the geomagnetic disturbances observed on the earth can be directly related to solar wind measures by linear impulse response functions. This suggests that the responsible current systems are very directly coupled to (or driven by) the solar wind-magnetosphere MHD dynamo. In addition, however, there appears to be a substantial portion of the *AL* index which results from currents not strictly determined by the solar wind input.

Investigations have used Wiener analysis to compute the linear prediction filters which relate solar wind input parameters, primarily ϵ and VB_s , with the current systems manifested in *AL*, *AU*, D_{st} , and *ASYM*. In general, these filters have low pass characteristics with linear phase and time delays. The different filters, however, quantitatively show that different indices respond differently to the solar wind electric field and hence, that different physical processes produce the electric currents which influence each index. It also seems clear that the assumptions of linear and time invariant relationships between the input and output are only approximately valid.

The D_{st} index appears to be the most predictable. Solar wind inputs can reproduce over 70% of the variance in the D_{st} index (IYEMORI *et al.*, 1979; MCPHERRON *et al.*, 1984). The *AL* and *ASYM* indices can be predicted relatively well with about 40% of the variance of each predicted by the solar wind electric field or ϵ . This seems impressive in view of the errors present in the measurements of both the input and output time series. The *AU* index is only poorly predicted and this is a major

concern to this author. This may indicate either a major misunderstanding of the sources controlling the eastward electrojet or serious problems with the interpretation that AU in fact characterizes the eastward electrojet.

The low pass characteristics of the $VB \rightarrow AL$ filters indicate that the magnetosphere attenuates solar wind electric field frequencies above 10^4 hertz in the generation of the current systems linked with the westward auroral electrojet. Also, careful examination of the residual or error time series suggests that there are variations in the output indices which are produced by processes not directly related to the solar wind input function. It has been suggested, for example, that these separate sources of current in the westward electrojet are controlled by processes in the magnetotail which are associated with the release of stored energy.

The results of these analyses provide an empirical description of the solar wind-magnetospheric system. This, in turn, provides insight to the physical processes which operate in the system. Most of the studies reported above have utilized Wiener filtering in this way. The technique, however, may eventually be employed in the more pragmatic way of providing the ability to forecast short term geomagnetic activity if the proper inputs were provided sufficiently far upstream in the solar wind. A satellite at the Lagrangian point $240 R_s$ upstream, for example, might provide such short term input. If proper filters could be produced to relate observations at this location with geomagnetic activity indices, predictions could easily be computed. Based on present results, it seems reasonable to expect that such filters could be obtained and reasonably accurate predictions could be produced. Such predictions could have great benefit to a variety of commercial and scientific activities which are influenced by the level of geomagnetic disturbance.

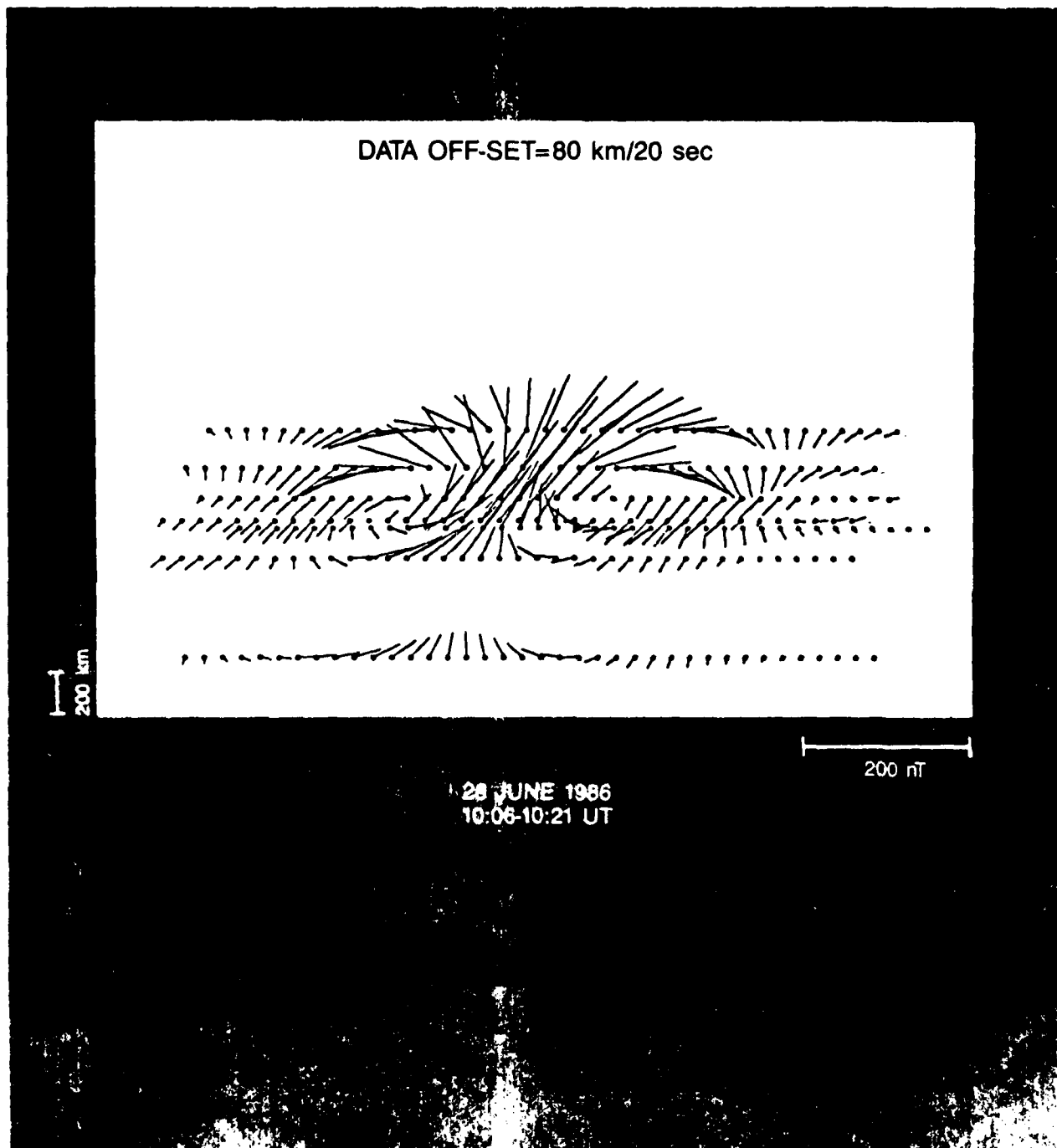
The preparation of this review was supported by NASA under grant NAGW-235, by the National Science Foundation under grant ATM-8210562, and by the Air Force Geophysics Laboratory under Contract F19628-85-K-0001. I am indebted to Dr. R. L. McPherron for many challenging and helpful discussions and to Dr. McPherron, Mr. Lee Bargarze, and Dr. S.-I. Akasofu for assistance in obtaining figures for this paper. I very much appreciate the critical reading of an earlier version of this manuscript and helpful suggestions by Dr. R. D. Zwickl and Dr. D. N. Baker.

REFERENCES

- AKASOFU, S.-I., C. OLMSTED, E. J. SMITH, B. TSUKUTANI, R. OKIDA, and D. N. BAKER. Solar wind variations and geomagnetic storms: A study of individual storms based on high time resolution ISEE 3 data, *J. Geophys. Res.*, **90**, 325, 1985.
- BAKER, D. N., Statistical analyses in the study of solar wind-magnetosphere coupling, this volume, 1986.
- BARGATZE, L. F., D. N. BAKER, R. L. MCPHERRON, and F. W. HUNTS, Magnetospheric response for many levels of geomagnetic activity, *J. Geophys. Res.*, **90**, 6387, 1985.
- BOGOTT, R. K. and F. S. MOZER. ATS 5 observations of energetic proton injection, *J. Geophys. Res.*, **78**, 8113, 1973.
- BURTON, R. K., R. L. MCPHERRON, and C. T. RUSSELL. An empirical relationship between interplanetary conditions and D_s , *J. Geophys. Res.*, **80**, 4204, 1975.
- CLAUER, C. R. and R. L. MCPHERRON. The relative importance of the interplanetary electric field and magnetospheric substorms on partial ring current development, *J. Geophys. Res.*, **85**, 6747, 1980.
- CLAUER, C. R., R. L. MCPHERRON, C. SEARIS, and M. G. KIVELSON. Solar wind control of auroral zone

- geomagnetic activity, *Geophys. Res. Lett.*, **8**, 915, 1981.
- CLAUER, C. R., R. L. MCPHERRON, and C. SFARIS, Solar wind control of the low-latitude asymmetric magnetic disturbance field, *J. Geophys. Res.*, **88**, 2123, 1983.
- FELDSTEIN, Y. I., V. YU. PISARSKY, N. M. RUDNEVA, and A. GRAFE, Ring current simulation in connection with interplanetary space conditions, *Planet. Space Sci.*, **32**, 975, 1984.
- IYEMORI, T., H. MAEDA, and T. KAMEI, Impulse response of geomagnetic indices to interplanetary magnetic fields, *J. Geomag. Geoelectr.*, **31**, 1, 1979.
- IYEMORI, T. and H. MAEDA, Prediction of geomagnetic activities from solar wind parameters based on the linear prediction theory, in *Solar-Terrestrial Predictions Proceedings, Vol. 4, A-1*, U.S. Dept. of Commerce, Boulder, CO, 1980.
- KAMIDE, Y. and S.-I. AKASOFU, Notes on the auroral electrojet indices, *Rev. Geophys. Space Phys.*, **21**, 1647, 1983.
- LEVINSON, N., The Wiener RMS (root mean square) error criterion in filter design and prediction, Appendix B in N. Wiener's book, 1949.
- MAYAUD, P. N., *Derivation, Meaning and Use of Geomagnetic Indices*, Geophys. Monogr. 22, AGU, Washington, D.C., 1980.
- MCPHERRON, R. L., R. A. FAY, C. R. GARRITY, L. F. BARGATZE, D. N. BAKER, C. R. CLAUER, and C. SFARIS, "Coupling of the solar wind to measures of magnetic activity," in *Achievements of the International Magnetospheric Study (IMS), Proceedings of an International Symposium, Graz, Austria 26-28 June*, pp. 161, ESA SP-217, European Space Agency, Paris, 1984.
- ROBINSON, E. A., *Multichannel Time Series Analysis with Digital Computer Programs*, Holden-Day, San Francisco, 1967.
- ROBINSON, E. A. and Sven TREITEL, *Geophysical Signal Analysis*, Prentice-Hall, Englewood Cliffs, 1980.
- ROSTOKER, G., Geomagnetic indices, *Rev. Geophys. Space Phys.*, **10**, 935, 1972.
- RUSSELL, C. T., G. L. SISCOF, and E. J. SMITH, Comparison of ISEE-1 and -3 interplanetary magnetic field observations, *Geophys. Res. Lett.*, **7**, 381, 1980.
- WIENER, N., *Extrapolation, Interpolation, and Smoothing of Stationary Time Series with Engineering Applications*, M.I.T. Press, Cambridge, Mass. 1942.

Geophysical Research Letters



MARCH
1988

Volume 15
Number 3

IONOSPHERIC TRAVELING CONVECTION VORTICES OBSERVED NEAR THE POLAR CLEFT: A TRIGGERED RESPONSE TO SUDDEN CHANGES IN THE SOLAR WIND

E. Friis-Christensen¹, M. A. McHenry², C. R. Clauer², S. Vennerstrøm¹

Abstract. Analysis of 20-second resolution magnetometer data from an array of temporary stations operated around Søndre Strømfjord, Greenland during the summer of 1986 shows the signatures of localized ionospheric traveling convection vortices. An example of an isolated event of this kind observed near 08 local time is presented in detail. This event consists of a twin vortex pattern of convection consistent with the presence of two field-aligned current filaments separated by about 600 km in the east-west direction. This system of currents is observed to move westward (tailward) past the array of stations at about 4 km/sec. The event is associated with relative quiet time ionospheric convection and occurs during an interval of northward IMF. It is, however, associated with a large fluctuation in both the Z and Y components of the IMF and with a large sudden decrease in the solar wind number density. The propagation of the system is inconsistent with existing models of FTE current systems, but nevertheless appears to be related to a readjustment of the magnetopause boundary to a sudden change in the solar wind dynamic pressure and/or to a change in reconnection brought about by a sudden reorientation of the IMF.

Introduction

The immediate response of the large scale polar magnetospheric plasma convection to changes in the solar wind electric field apparent at the dayside magnetopause is well established through a number of studies [Clauer et al., 1984; Rishbeth et al., 1985; Friis-Christensen, 1986; Clauer and Banks, 1986; Clauer and Friis-Christensen, 1988]. The most direct response to changes in the solar wind is seen at high latitudes around magnetic local noon in the vicinity of the polar cleft. This region is generally thought to be near the ionospheric projection of the boundary between open and closed magnetic field lines.

This is also a region where irregular magnetic pulsations often occur. The intensity of these pulsations, called ipcl-type pulsations (irregular pulsations, continuous, long) increases with increasing negative values of IMF B_z [Bolshakova et al., 1975], and the latitude of maximum ipcl-pulsations is close to the equatorward boundary of the cusp statistically defined by means of particle data [Kleymenova et al., 1982].

Kleymenova et al. [1985] divided the ipcl-pulsations into two classes: "noise pulsations" (np) within the 3-8 minute period range and "long period" pulsations (lp) with a quasi-period from 15-20 minutes. It was proposed that the lp-pulsations occur on open field lines because of their intimate relationship to IMF variations, while the np-pulsations were proposed to be generated in the boundary layer on closed field-lines. It was found that np-pulsations occur for both IMF $B_z < 0$ and $B_z > 0$ and that the maximum occurrence is in the prenoon sector (0600 to 1100 MLT). When $B_z < 0$ the magnitude of the pulsations is larger and the presence of np-pulsations is often accompanied by the occurrence of Pc5 pulsations at lower latitudes.

¹Division of Geophysics, Danish Meteorological Institute, Copenhagen

²STAR Laboratory, Stanford University, Stanford, California

The latitude of occurrence, relationship to IMF B_z , and temporal duration of ipcl pulsations seem consistent with the properties of pulsations which are expected to be produced by sporadic reconnection near the subsolar point of the magnetopause. Thus, Bolshakova and Troitskaya [1982] suggest that ipcl pulsations may be related to "pulsed reconnection" or flux transfer events (FTE's) described by Russell and Elphic [1979].

Two different models of FTE field-aligned current systems have been proposed. The first by Saunders et al. [1984] and Lee [1986] consists of a central core of field-aligned current which spreads radially in the ionosphere and closes through a local or distant sheath of field-aligned current. The second system which consists of two oppositely directed field-aligned currents on the flanks of the FTE flux tube producing flux tube motion perpendicular to a line connecting the vortex centers, was proposed by Southwood [1985: 1986].

Considerable effort has been made to uniquely relate ionospheric signatures to the existence of FTEs. Goertz et al. [1985] associated STARE ionospheric radar observations of localized regions of poleward ionospheric flow with the existence of an ionospheric signature of FTE's. Lanzerotti et al. [1986] used magnetometer observations from a station near the southern cusp (South Pole) to support the idea of the existence of a localized Hall current system consistent with the FTE signature of a Saunders et al. - Lee system [Saunders et al., 1984; Lee, 1986]. Results from a theoretical study of FTE current systems indicate that a closely spaced array of high time resolution magnetometer observations is needed in order to adequately resolve the question of the existence of ionospheric FTE signatures [McHenry and Clauer, 1987].

The purpose of this paper is to report on the first results of an experiment conducted to investigate, in detail, the irregular pulsations measured by ground-based magnetometers in the vicinity of the dayside cleft. In particular, we report on the observation of traveling small scale two-cell ionospheric current systems. These systems, which seem to explain a number of the observed irregular pulsations and/or spike-like variations in the ground based magnetic records, are the ionospheric manifestations of a pair of oppositely directed field-aligned currents moving rapidly near the convection reversal boundary. These events, however, do not appear to be consistent with existing models of the ionospheric signatures of FTEs.

Observations

To obtain high temporal and spatial resolution observations of the polar cleft ionosphere the Greenland Magnetometer Array was supplemented with additional temporary stations near Søndre Strømfjord. During the summer of 1986 a total of 8 stations within the invariant latitude range from 68° to 76° were operated with a time resolution of 20-seconds.

A map showing the magnetometer stations in Greenland used in this study is shown in Figure 1. The stations to the south of and including GDH recorded 20-second magnetic field measurements. While primarily a latitudinal array, some east-west separation exists, in particular between the SKT and DYB stations.

Figure 2 shows a stacked plot of H-component magnetograms for 0700 to 1300 UT on June 28, 1986. Around 1000 to 1020 UT (4 hours prior to magnetic local noon) a spike-like disturbance is seen at nearly all the stations, with a maximum peak to peak disturbance of approximately 200 nT near the

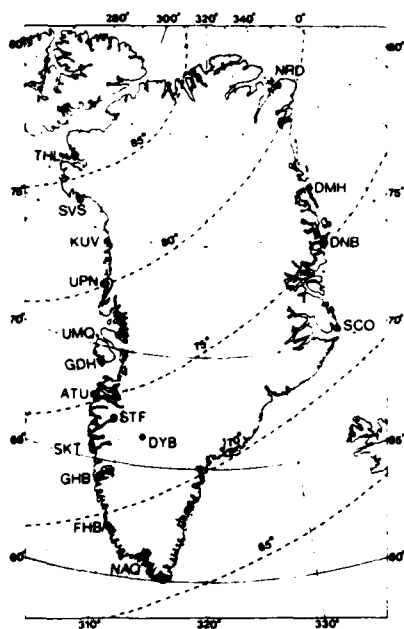


Figure 1. Map of Greenland showing the magnetometer stations used in this study. Godhavn (GDH) and all stations on the west coast to the south of GDH were equipped to record 20-second resolution magnetic field measurements. The broken lines indicate invariant latitude circles.

station ATU at 75.3° invariant latitude. In Figure 3 the same event is shown in all three components with higher time resolution using the 20-second data. From this figure it is evident that the current system responsible for the variations is small scale or localized in character (large gradients in the H- and Z-components) and that there seems to be a phase shift be-

GREENLAND CHAIN 1 MIN MAGNETIC FIELD—H COMPONENT

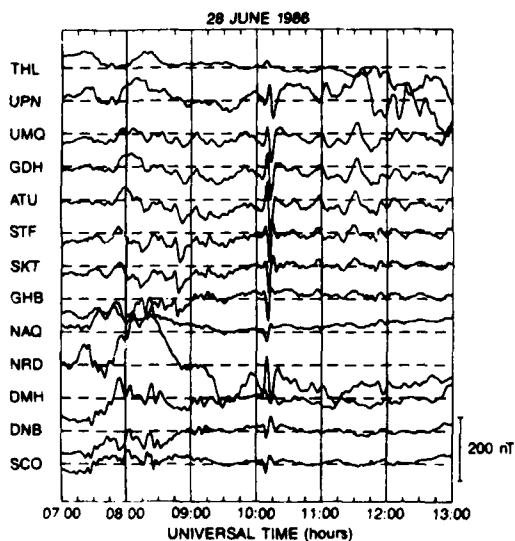
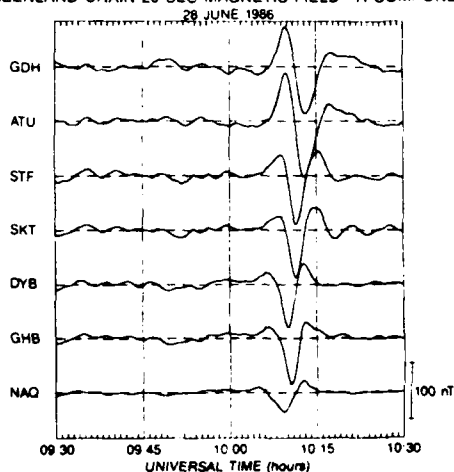
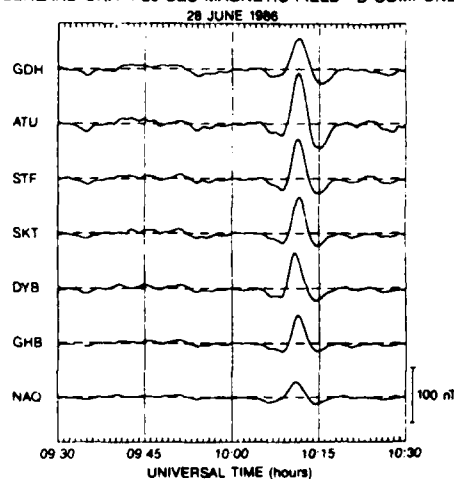


Figure 2. Stacked plot of H-component magnetograms from the Greenland chain of magnetometers for 0700 to 1300 UT on June 28, 1986. The location of the stations are shown in Figure 1. Magnetic local noon occurs at 1400 UT.

GREENLAND CHAIN 20 SEC MAGNETIC FIELD—H COMPONENT



GREENLAND CHAIN 20 SEC MAGNETIC FIELD—D COMPONENT



GREENLAND CHAIN 20 SEC MAGNETIC FIELD—Z COMPONENT

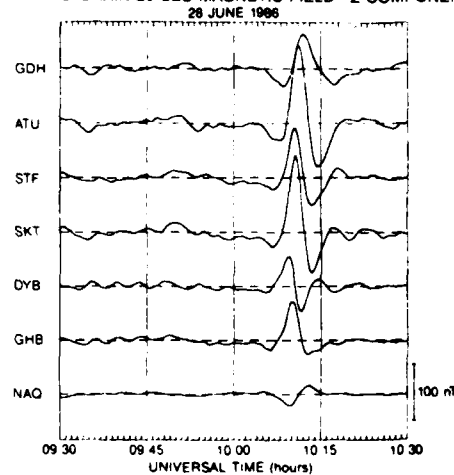


Figure 3. Stacked plot of 20 second resolution magnetograms from the Greenland chain for 0930 to 1030 UT on June 28, 1986. The data have been filtered using a high-pass filter (corner frequency corresponding to a period of 30 minutes). The H-component (northward) is shown on the top panel, D (eastward) in the middle, and the Z-component (downward) is given in the bottom panel.

tween SKT and DYB. This latter point indicates a westward (anti-sunward) movement of about 3 to 5 km/sec of the current system which is producing the pulsations.

Assuming that the perturbations are caused by a moving current structure which changes very little in time, we are able to use the meridian chain of magnetometers to "scan" the pattern as it moves across the line of stations. The velocity of the current structure is estimated from the phase shift between SKT and DYB. Using an estimated velocity of 4 km/sec we have plotted in Figure 4 the total horizontal magnetic perturbation vectors in a coordinate system moving with the current pattern. For simplicity the perturbation vectors have been rotated by 90° counterclockwise to be consistent with the convection direction. That is, we assume the magnetic signature to result from ionospheric Hall currents. Since the event occurred in the dayside oval at midsummer the ionospheric Hall conductivity is probably sufficiently large and uniform to support this assumption.

The observed convection pattern consists of a twin-vortex moving westward (tailward) roughly along a line connecting the centers of the two vortices. The consonance of the pattern derived from the distribution of measurements in space and time confirms the velocity determination and the stability of the pattern during its passage across the magnetometer array.

McHenry and Clauer [1987] calculated the distribution of currents and fields corresponding to a single filament of current impressed on the ionosphere. Two field aligned currents of nearly equal magnitude and opposite sense would generate a distribution of magnetic fields below the ionosphere close to the observed distribution. The observed pattern, however, seems to be distorted so that the derived convection directions are not exactly perpendicular to the line connecting the vortex-centers as would be expected. McHenry and Clauer ignore both ground-induction and conductivity gradients. It is not yet known if these effects are the cause of the distortion of the observed perturbation pattern or if the distortion is due to a more complex distribution of the field-aligned currents.

In Figure 5 solar wind data measured by IMP-8 are shown. B_z is positive during the event and the solar wind velocity is around 450 km/sec. A sudden drop in the plasma density from 11 per cc to 6 per cc occurs at 0955. Considering the propagation time between IMP-8 and the magnetopause (about 10 minutes) fluctuations in the sign of B_y , a large sudden change in the value of the positive B_z and the sudden drop in plasma density are proximate to the observed vortex event.

While we show here detailed observations for one event, we have examined 15 cases. Analysis has concentrated on rela-

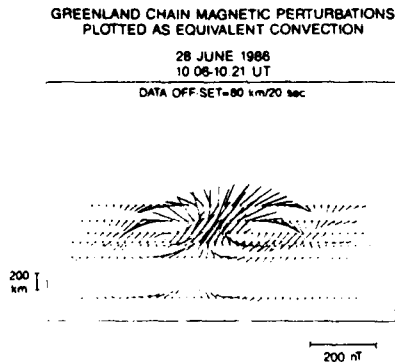


Figure 4. Total horizontal magnetic perturbation vectors corresponding to the variations in Figure 3 have been rotated by 90° counterclockwise and plotted every 20 seconds during the interval from 10:06:00 to 10:18:40 UT. For each time the position of the vectors have been off-set to the right by a distance corresponding to 80 km to account for an assumed 4 km/sec westward motion (to the left) of the pattern.

IMP-8 PLASMA AND FIELD MEASUREMENTS

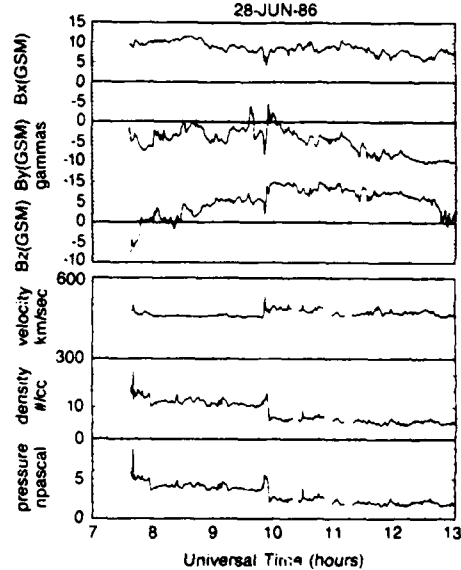


Figure 5. Solar wind data measured by IMP-8. From top to bottom is shown the interplanetary magnetic field components in GSM coordinates B_x , B_y , and B_z , the solar wind velocity, and the number density. The bottom trace shows the derived solar wind dynamic pressure plotted in units of nanopascals.

tively quiet intervals having isolated spike-like pulsations, since during disturbed or even moderately disturbed conditions the pulsations are difficult to extract from the background field. Events were chosen according to this criterion as well as according to the magnitude of the perturbation. A high-pass filter (30 minutes cut-off) was applied to the data to extract the events from the background field.

The pulsations are not always associated with a twin vortex pattern. Our study has shown that the events can be sorted into different categories corresponding to the following types: 1) isolated twin vortices, 2) single vortices, and 3) multiple vortices. Some of the pulsations could not be identified in a consistent way as any of the mentioned types. We are presently conducting a more comprehensive analysis of the different types of events.

Discussion

Irregular pulsations are a common phenomenon in ground-based magnetometer data measured near the polar cleft. The irregularity, however, makes them difficult to extract from the usually noisy background field. During intervals with a relatively quiet background field it is possible to extract a relatively unique current pattern which produces the observed perturbations. Because of the scale size of the phenomena, a relatively dense array of stations near the polar cleft is necessary to resolve the current structures and their motion.

To put this event into a more global context, we find that it is associated with a small, world wide SI (sudden impulse) related to the solar wind dynamic pressure change. Stations on the east coast of Greenland located near local magnetic noon exhibit large variations. It is, however, not possible to identify a signature corresponding to the twin vortex pattern observed on the west coast. Stations in the afternoon sector at high latitudes which we examined show only a small SI variation. This suggests to us that the observed traveling vortex current system is a result of a generation near local noon with subsequent westward motion.

The twin vortex observation which we describe is similar to events observed in the auroral zone [Hönisch and Glassmeier, 1986; Glassmeier (private communication) 1987]. Using the Scandinavian Magnetometer Array, their events had amplitudes of order 40 nT, but only viewed a portion of the 2-cell system well below the vortex centers. They also found westward (tailward) motion at about 4 km/sec.

The magnetic signature of the event presented here is similar to those previously reported by Lanzerotti et al. [1986; 1987]. Our modeled current system to explain these variations, however, is quite different. Having only one station Lanzerotti et al. [1986] modeled the current structure as a Saunders-Lee type of distribution moving poleward. Using a meridional chain of stations it is possible, even without detailed modeling, to test the assumption of a poleward movement, and with the additional east-west distribution of stations it is possible to estimate the east-west movement of the currents. The event presented here, and several others which have been examined, show a predominant east-west movement of the currents.

The two pre-noon events (June 03, 1982 and October 16, 1985) discussed by Lanzerotti et al. [1986; 1987] are very similar to the event discussed in the present paper. We have examined the available Greenland magnetic data and found them to be consistent in all components with a westward moving twin-vortex. The data are not consistent with a poleward moving single vortex. Although Lanzerotti et al. [1986; 1987] modeled the events with a poleward moving Hall current pattern they did in fact, for the October 16, 1985 event find a westward 5 km/sec motion in the pattern when comparing the magnetic signatures at Søndre Strømfjord and Frobisher Bay. Using conjugate data from the northern and southern hemisphere Lanzerotti et al. [1987] suggested that the October 16, 1985 event occurred on closed field lines and might be associated with the convection of an elongated plasma cloud in the boundary layer.

The study of the June 28, 1986 event and a reexamination of the previously reported events suggested to be the ionospheric signatures of FTE's, leads to the conclusion that none of the examined events corresponds to either of the two proposed models of FTE's, the Saunders-Lee type of a single poleward moving Hall current vortex, or the Southwood type of a twin-vortex. Although the event presented here is consistent with a twin-vortex pattern of plasma convection, its direction of movement is perpendicular to the motion predicted by the model. The high velocities (3-6 km/sec) and a direction of motion, parallel to the electric field impressed on the ionosphere by the two oppositely directed field-aligned currents means that the event does not correspond to a net transport of plasma from closed to open field-lines, since this would require an electric field perpendicular to the direction of motion to create the necessary $\mathbf{J} \times \mathbf{B}$ force. The event seems more probably to correspond to a motion of a structure in the magnetopause boundary possibly created by either a sudden change in the solar wind density and/or by a sudden change in the reconnection regions, caused by an abrupt change in the IMF orientation. Such a readjustment might propagate downstream associated with field-aligned currents mapping down to the ionosphere as observed with the chain of magnetometers.

Acknowledgements. Support for this research at Stanford University has been provided by National Science Foundation grant ATM-8503105 and by Air Force Geophysics Laboratory contract F19628-85-K-0001. M. A. M. was partially supported by the NASA Student Researchers Program through grant NGI 50016. Partial support for E. F.-C. to visit Stanford was provided by NASA grant NAGW 235. The authors would like to thank Drs. R. Lepping and J. King for the IMP-8 magnetic field data, and the solar wind group at MIT, supported in part by NASA Goddard under grant NAG5-584, for the IMP-8 solar wind plasma data. E. F.-C. would like to thank Dr. K.-H. Glassmeier for useful discussions and suggestions.

REFERENCES

- Bolshakova, O. V., V. A. Troitskaya and V. P. Hessler: Determination of the position of the polar boundary of the day side cusp from the intensity of high-latitude pulsations. *Geomagnetism and Aeronomy*, 15, 569, 1975.
- Bolshakova, O. V. and V. A. Troitskaya: Pulsed reconnection as a possible source of icpl type pulsations. *Geomagnetism and Aeronomy*, 22, 723, 1982.
- Clauer, C. R. et al.: Observations of interplanetary magnetic field and of ionospheric plasma convection in the vicinity of the dayside polar cleft. *Geophys. Res. Lett.*, 11, 891, 1984.
- Clauer, C. R., and P. M. Banks, Relationship of the interplanetary electric field to the high-latitude ionospheric electric field and currents: Observations and model simulation, *J. Geophys. Res.*, 91, 6959, 1986.
- Clauer C. R. and E. Friis-Christensen, High latitude dayside electric fields and currents during strong northward IMF: Observations and model simulation. *J. Geophys. Res.*, in press, 1988
- Friis-Christensen, E., Solar wind control of the polar cusp, in *Solar Wind - Magnetosphere Coupling*, Y. Kamide and J. A. Slavin, Editors, Terra, Tokyo, 1986.
- Goertz, C. K., et al., Observations of a possible ground signature of flux transfer events, *J. Geophys. Res.*, 90, 4069, 1985.
- Hönisch, M. and K. H. Glassmeier, Isolated transient magnetic variations in the auroral zone. *EOS, Trans. Amer. Geophys. Union*, 67, 1163, 1986.
- Kleyменова, N.G., O.V. Bolshakova, V.A. Troitskaya, and E. Friis-Christensen: Long period geomagnetic fluctuations and the polar chorus at latitudes corresponding to the daytime polar cusp. *Geomagnetism and Aeronomy*, 22, 580, 1982.
- Kleyменова, N.G., O.V. Bolshakova, V.A. Troitskaya, and E. Friis-Christensen: Two forms of long-period geomagnetic pulsations near the equatorial border of the dayside polar cusp. *Geomagnetism and Aeronomy*, 25, 139, 1985.
- Lanzerotti, J.L. et al., Possible evidence of flux transfer events in the polar ionosphere. *Geophys. Res. Lett.*, 13, 1089, 1986.
- Lanzerotti, J.L. et al., Ionosphere and ground-based response to field-aligned currents near the magnetospheric cusp regions. *J. Geophys. Res.*, 92, 7739, 1987.
- Lee L. C., Magnetic flux transfer at the Earth's magnetopause, in *Solar Wind - Magnetosphere Coupling*, Y. Kamide and J. A. Slavin, Editors, Terra, Tokyo, 1986.
- McHenry, Mark A., and C. Robert Clauer, Modeled ground magnetic signatures of flux transfer events. *J. Geophys. Res.*, 92, 11231, 1987.
- Risbeth, H. et al., Ionospheric response to changes in the interplanetary magnetic field observed by EISCAT and AMPTE-UKS. *Nature*, 318, 451, 1985.
- Russell, C. T. and R. C. Elphic, ISEE observations of flux transfer events at the dayside magnetopause. *Geophys. Res. Lett.*, 6, 33, 1979.
- Saunders, M. A., C. T. Russell, and N. Scokpe, Flux transfer events: Scale size and interior structure. *Geophys. Res. Lett.*, 11, 131, 1984.
- Southwood, D. J., Theoretical aspects of ionospheric - magnetosphere - solar wind coupling. *Adv. Space Res.*, 5, 7, 1985.
- Southwood, D. J., The ionospheric signature of flux transfer events. *J. Geophys. Res.*, 92, 3207, 1987.
- E. Friis-Christensen and S. Vennerstrøm, Danish Meteorological Institute, Div. of Geophysics, Lyngbyvej 100, DK-2100 Copenhagen, Denmark.
- M. A. McHenry and C. R. Clauer, STAR Laboratory, Stanford University, Stanford, CA 94305.

(December 14, 1987;
January 21, 1988;
January 25, 1988.)

Modeled Ground Magnetic Signatures of Flux Transfer Events

MARK A. MCHENRY AND C. ROBERT CLAUER

STAR Laboratory, Stanford University, Stanford, California

The magnetic field on the ground due to a small (≤ 200 km scale size) localized field-aligned current system interacting with the ionosphere is calculated in terms of an integral over the ionospheric distribution of field-aligned current. Two different candidate current systems for flux transfer events (FTEs) are examined. The first system has current flowing down the center of a cylindrical flux tube with a return current uniformly distributed along the outside edge. The second system has upward current on one half of the perimeter of a cylindrical flux tube with downward current on the opposite half. The peak magnetic field on the ground is found to differ by a factor of 2 between the two systems, and the magnetic perturbations are in different directions depending on the observer's position. Assuming the current system moves in a constant linear poleward direction, we predict the ground magnetic field versus time which would be measured by a ground observatory. Using FTE detection statistics at the magnetopause, we estimate the detection rate of FTEs at a ground station under the dayside convection reversal to be between 12 and 60 min per sighting depending on which FTE current system is considered.

1. INTRODUCTION

The transfer of energy from solar plasma to the Earth's magnetospheric plasma is a topic which has received many years of study but which still holds many mysteries. While several mechanisms have been proposed to account for the transport of momentum across the magnetopause from the solar wind to the magnetosphere, magnetic reconnection [Dungey, 1961] has been considered one of the principal electrodynamic mechanisms to produce this momentum exchange. Observations from the ISEE spacecraft have recently suggested that this process may occur in both a quasi-steady form [Paschmann et al., 1979] and also in a more impulsive and sporadic form termed flux transfer events (FTE) [Russell and Elphic, 1978; Sonnerup et al., 1981]. At times the occurrence rate of FTEs appears to be sufficient to account for a major portion of the momentum transfer across the magnetopause [Cowley, 1982; Goertz et al., 1985].

The magnetic structures associated with FTEs observed at the magnetopause are approximately $1 R_E$ in cross section and also contain a unique twisting magnetic field indicating the presence of significant field-aligned currents. Satellite particle detectors also have found that inside the FTE, the plasma is a mixture of magnetospheric and magnetosheath plasma [Russell and Elphic, 1979]. This plus the observation that FTEs occur primarily when the interplanetary magnetic field (IMF) is largely opposite to the Earth's magnetic field [Rijnbeek et al., 1984; Berchem and Russell, 1984] suggests that FTEs are the result of localized reconnection between interplanetary and magnetospheric magnetic fields at the dayside magnetopause.

Because of the potentially important role of FTEs in coupling energy to the magnetosphere from the solar wind, the study of FTEs has received recent attention both experimentally and theoretically (see the recent review by Cowley [1982]). Among the areas to receive considerable interest recently is a search for the signatures of FTEs in the iono-

sphere [Goertz et al., 1985; Todd et al., 1986; Lanzerotti et al., 1986]. Such independent observations, if consistent with the interpretation of FTEs at the magnetopause, would also provide considerable strength to the arguments supporting the FTE interpretation, and would also provide another abundant source of observational information regarding dayside magnetopause reconnection.

If the interpretation of the FTE observations at the magnetopause is correct, one would expect that the stress applied to the reconnected flux tube as it is pulled tailward must be transmitted to the ionosphere. This must be accomplished by closing field-aligned currents, associated with the moving flux tube, through the ionosphere. The ionospheric signature which might be expected from a FTE will depend upon the distribution of current associated with the moving flux tube.

There are two proposed FTE current distributions which have been qualitatively discussed. The first consists of a central core of field-aligned current which spreads radially in the ionosphere. The current closes with field-aligned return currents in a diffuse shell around the central core current or through distant return currents [Saunders et al., 1984; Lee, 1986]. One should note the symmetry of this system, which is shown schematically in Figure 1a. A second system which is asymmetric has been suggested by Southwood [1985, 1987]. This system consists as a first approximation of two oppositely directed field-aligned currents on opposing edges of the FTE flux tube. A refined version distributes the currents over the circumference of the flux tube. This is shown schematically in Figure 1b.

In this paper we examine the magnetic effects of these two postulated FTE current systems. This is accomplished by first obtaining the Green's function solution for a single field-aligned current filament. The solution for a distributed FTE current system is then obtained by numerically summing the single-filament solutions. We compute the ground magnetic perturbation of each FTE system and then, assuming a 1 km/s poleward velocity, determine the expected time-varying field which would be measured by a ground observatory located 100 km from the ground track of the moving current system.

Copyright 1987 by the American Geophysical Union.

Paper number 7A8970.
0148-0227/87/007A-8970\$02.00

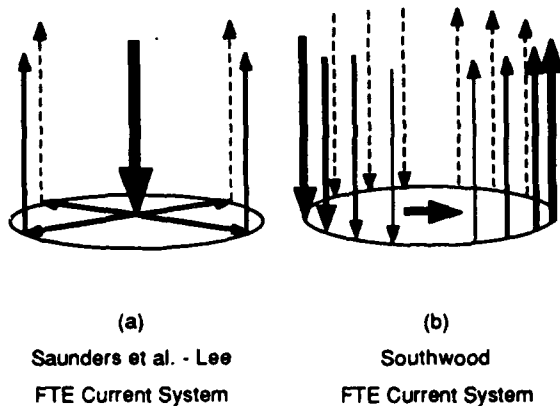


Fig. 1 (a) Postulated [Saunders et al., 1984; Lee, 1986] symmetric FTE current system composed of a central core with return current around the outside edge. (b) Postulated [Southwood, 1985, 1987] asymmetric FTE current system composed of current flowing along the outside edge. The direction of the current reverses along the perimeter.

2. CALCULATION OF THE GROUND MAGNETIC FIELD OF A SMALL-SCALE FIELD-ALIGNED CURRENT SYSTEM

Formulation of Problem

Our goal in this section is to find the magnetic field on the ground created when a small (200-km scale size) current system is impressed on the ionosphere. Because of the small size of the current system and because the fields drop off quickly with distance, we can assume the ionosphere is flat and parallel to the Earth's surface. Similarly, we assume the Earth's magnetic field lines are straight but uniformly tilted in a local north/south plane. We also use the assumptions commonly used to find the effect of larger-scale current systems [Kamide and Matsushita, 1979]: the ionosphere is represented by a two-dimensional layer with height-integrated Hall and Pedersen conductivities, and only steady state solutions are considered.

We also assume the height-integrated conductivity is uniform in a region around the small-scale current system. Radar measurements around the dayside convection reversal boundary where FTEs are likely to occur [Robinson et al., 1984] have been used to determine the height-integrated conductivity and found this to be a good approximation. When nonuniformity does exist, one can expect the magnetic field on the ground to be higher than otherwise calculated because of the loss of symmetry in the driven ionospheric currents.

The final approximation is to ignore any ground induction effects. Typically, they are modeled by placing a perfectly conducting layer approximately 200 km below the Earth's surface [Kisabeth and Rostoker, 1977]. Image currents are then placed below the perfectly conducting layer at the same distance as the true currents are above the layer. It will be shown later that the magnetic field from our small-scale current patterns decreases rapidly with distance, so observers on the Earth's surface (on the order of 500 km away from the image sources) will to first order not see the induction effects.

We start with a coordinate system where the ionosphere is in the $X - Y$ plane and Z points downward. A simple

application of Ohm's law and current continuity [Kamide and Matsushita, 1979] gives

$$\nabla \cdot (\Sigma \cdot \nabla \Phi) = j_{\parallel}(\mathbf{r}) \sin \chi \quad (1)$$

where the derivatives are in the $X - Y$ plane, Σ is the height-integrated conductivity tensor, Φ is the electric potential, $j_{\parallel}(\mathbf{r})$ is the field-aligned current density toward the Earth and χ is the angle of Earth's magnetic field line in the $X - Z$ plane with 90° being vertical. It can easily be shown [Ratcliffe, 1972] that Σ has antisymmetric off-diagonal elements even when the field lines are not vertical. This with the assumption of uniform conductivities gives

$$\nabla^2 \Phi = j_{\parallel}(\mathbf{r}) \sin \chi / \Sigma_p \quad (2)$$

where Σ_p is the height-integrated Pedersen conductivity. To have a solution which has no currents far away from the source, we require

$$\frac{\partial \Phi}{\partial r} \rightarrow 0 \quad \text{as} \quad r \rightarrow \infty \quad (3)$$

Green's Function Solution

A straight-forward application of Green's functions [Morse and Feshbach, 1953] gives the potential as an integral over the source field-aligned currents in a manner similar to the familiar solution of Poisson's equation for a two-dimensional distribution of charge.

$$\Phi(\mathbf{r}_0) = -\frac{\sin \chi}{2\pi \Sigma_p} \int \int \ln r j_{\parallel}(\mathbf{r}) dA \quad (4)$$

Here \mathbf{r}_0 is some point in the ionosphere, r is the distance from \mathbf{r}_0 to the source point (where the field-aligned current intersects the ionosphere), and A is the area containing the source points. The electric field is

$$\mathbf{E}(\mathbf{r}_0) = -\nabla \Phi = \frac{\sin \chi}{2\pi \Sigma_p} \int \int \frac{\mathbf{r}}{r^2} j_{\parallel}(\mathbf{r}) dA \quad (5)$$

and the height-integrated current density \mathbf{i} is

$$\mathbf{i}(\mathbf{r}_0) = \Sigma \cdot \mathbf{E}(\mathbf{r}_0) = \frac{\sin \chi}{2\pi \Sigma_p} \int \int \Sigma \cdot \frac{\mathbf{r}}{r^2} j_{\parallel}(\mathbf{r}) dA \quad (6)$$

If we temporarily put the origin at a source point, we find

$$\Sigma \cdot \frac{\mathbf{r}}{r} = \Sigma_p \hat{\mathbf{r}} - \Sigma_h \hat{\phi} \quad (7)$$

where Σ_h is the height-integrated Hall conductivity and $\hat{\mathbf{r}}$ and $\hat{\phi}$ are unit vectors which change during the integration. Using this expression in the above current expression $\mathbf{i}(\mathbf{r}_0)$,

$$\mathbf{i}(\mathbf{r}_0) = \Sigma \cdot \mathbf{E}(\mathbf{r}_0) = \frac{\sin \chi}{2\pi \Sigma_p} \int \int (\Sigma_p \hat{\mathbf{r}} - \Sigma_h \hat{\phi}) \frac{j_{\parallel}(\mathbf{r})}{r} dA \quad (8)$$

we see the familiar Pedersen and Hall currents. To get the magnetic field of currents in the ionosphere, we use the Biot-Savart law

$$\mathbf{B}(\mathbf{r}') = \frac{\mu_0}{4\pi} \int \int \mathbf{i}(\mathbf{r}_0) \times \frac{\hat{\mathbf{a}}}{R^2} dA' \quad (9)$$

where \mathbf{r}' is the location of the observer, $\hat{\mathbf{a}}$ is a unit vector from the observer on the ground to the integration point at the ionosphere, R is the distance from the observer to the integration point at the ionosphere, and the area of integration A' is the entire ionosphere. The field-aligned current which acts as the point source in the above equations is a

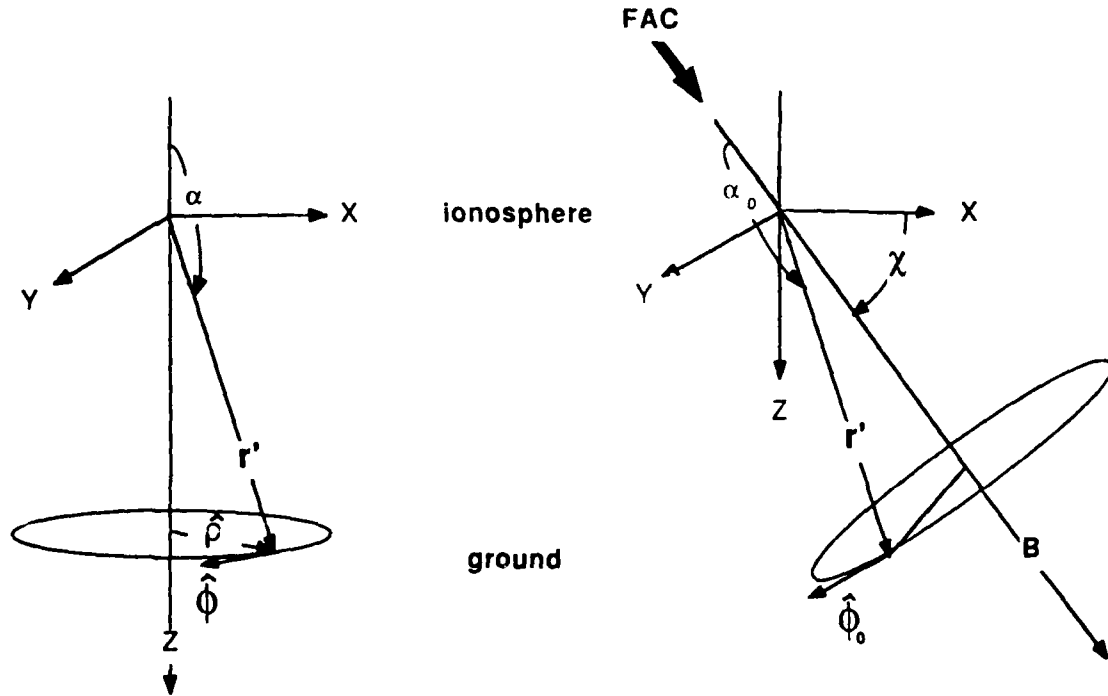


Fig. 2. Unit vectors and angles used in calculations. X is northward, Y is eastward and Z is down. The background magnetic field is in the $X-Z$ plane. The axes have been repeated for clarity and have their origins at the point where the field-aligned current intersects the ionosphere.

semi-infinite line current, and using Biot-Savart, its contribution can be found. After integrating, we find

$$\mathbf{B} = \mathbf{B}_{\text{FAC}} + \mathbf{B}_{\text{Pedersen}} + \mathbf{B}_{\text{Hall}} \quad (10)$$

with

$$\mathbf{B}_{\text{FAC}} = -\frac{\mu_0}{4\pi} \iint \frac{(1 + \cos \alpha_0)}{r' \sin \alpha_0} j_{\parallel}(\mathbf{r}) \hat{\phi}_0 dA \quad (11)$$

$$\mathbf{B}_{\text{Pedersen}} = \frac{\mu_0}{4\pi} \iint \frac{(1 + \cos \alpha)}{r' \sin \alpha} j_{\parallel}(\mathbf{r}) \hat{\phi} dA \quad (12)$$

$$\mathbf{B}_{\text{Hall}} = -\frac{\Sigma_h \mu_0}{\Sigma_p 4\pi} \iint \left(\frac{1 + \cos \alpha}{\sin \alpha} \hat{\rho} + \hat{\mathbf{z}} \right) \frac{j_{\parallel}(\mathbf{r})}{r'} dA \quad (13)$$

where α_0 is the angle between a line connecting the observer with the source point and the background magnetic field line (greater than 90° if the observer is below the ionosphere). α is the vertical angle of the line connecting the source and observer, and r' is the distance from the source point to the observer. The azimuthal unit vector $\hat{\phi}_0$ is about the field-aligned current, while $\hat{\phi}$ is about the vertical line passing through the point where the field-aligned current intersects the ionosphere. The unit vector $\hat{\rho}$ is along the horizontal projection of r' pointing from the source to the observer. The magnetic field is in the $X-Z$ plane and tilted χ from the X axis. In Figure 2, a repeated set of axes shows these coordinates and unit vectors. The integration is to be carried out over the area where field-aligned currents intersect the ionosphere. Note that if the field is vertical ($\chi = \pi/2$),

the angles α and α_0 are the same and the magnetic fields of the field-aligned current cancels that of the Pedersen current, leaving only the field due to the Hall currents. This demonstrates what has become known as Fukushima's theorem [Fukushima, 1969]. Consequently, if we assume the Hall and Pedersen conductivities are comparable and the magnetic field lines are nearly vertical, we can neglect contributions to the magnetic field from the combined effect of field-aligned currents and Pedersen currents.

Discussion of Assumptions

A critical assumption which would probably receive little debate is that field-aligned currents on closed field lines must interact with the lower ionosphere where significant cross B conductivity exists. However, in recent experiments, Stenzel and Urrutia [1986] have found that when the electric field across B is large, instabilities occur which lead to unexpected currents across B . This might occur in the F region with FTE current systems. If this is the case, the currents will not come as close to the surface of the Earth, and hence the ground magnetometer signature would be greatly reduced. In this paper, we will neglect this possibility and assume field-aligned currents close in the E region.

Another assumption was the use of a quasi-static solution. If the induction electric field created by the time-varying magnetic field is large compared to the impressed electric field in the ionosphere, perhaps a different pattern of currents will exist in the ionosphere. To estimate these induction electric fields, we use Faraday's law, a scale size of

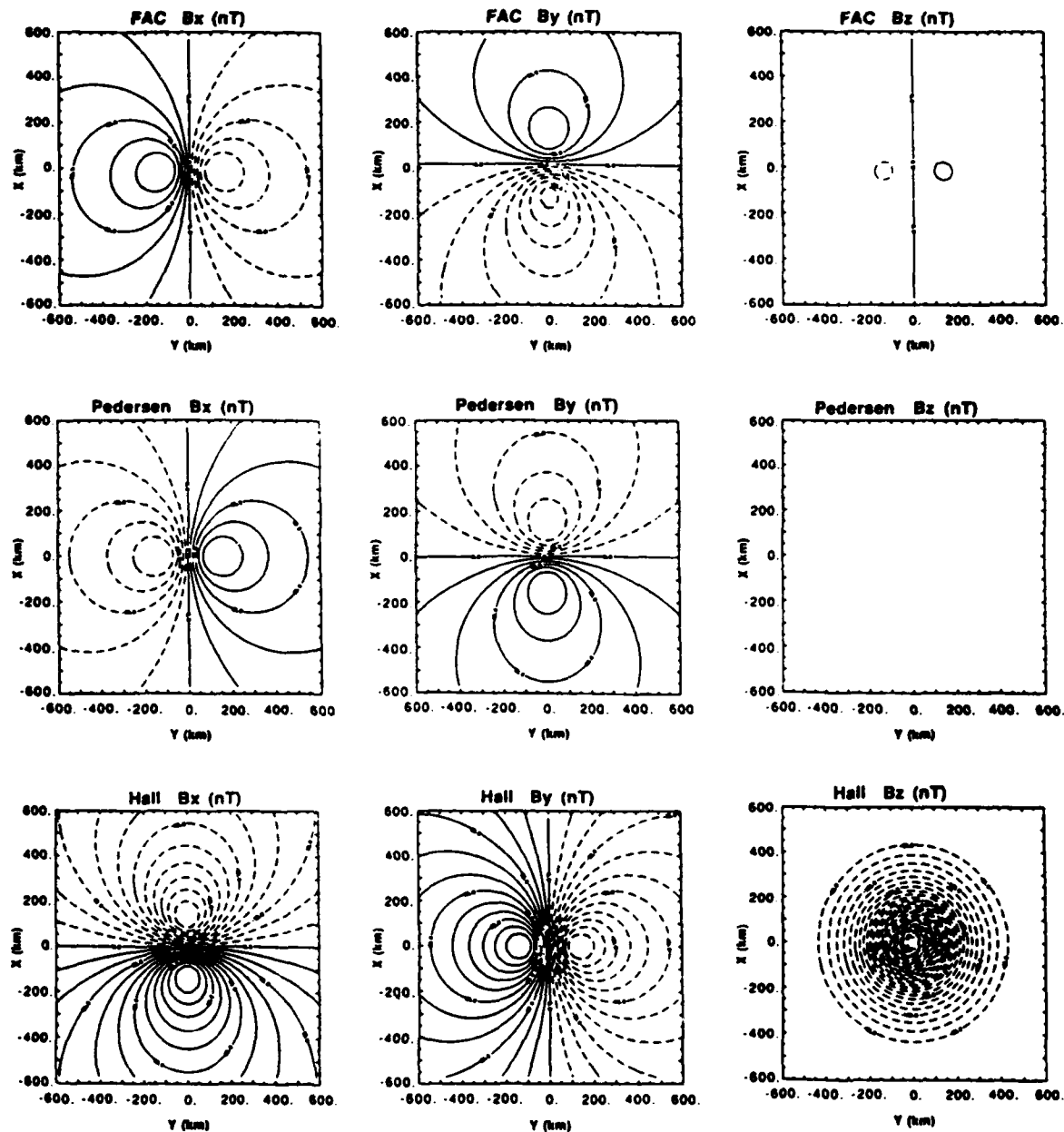


Fig. 3. Magnetic field strength on the ground due to a single field-aligned current filament of 2×10^5 A interacting with the ionosphere. The X axis measures ground distance in the north direction, and the Y axis measures ground distance in the east direction. Each contour represents 10 nT, with the dashed contours for negative values. The ground magnetic field perturbations are shown separately for (top row) the field-aligned current portion, (middle row) the ionospheric Pedersen current, and (bottom row) the ionospheric Hall current. Each row shows contours of magnetic perturbation in the X (magnetic northward), Y (eastward), and Z (downward) components of the magnetic field as a function of ground distance from the field-aligned current filament. The background magnetic field is in the $X-Z$ plane.

100 km, and a magnetic field change of 100 nT in 60 s. This results in an electric field strength of 0.2 mV/m. A rough estimate of the impressed electric field can be made using equation (5) assuming a current system of two very small filaments separated by 100 km with current in the filaments in opposite directions.

$$E(\mathbf{r}_0) = \frac{\sin \chi}{2\pi \Sigma_p} I \left(\frac{1}{r_1} - \frac{1}{r_2} \right) \quad (14)$$

Here I is the current in each filament, and r_1 and r_2 are the distances from where each filament intersects the ionosphere to some other point in the ionosphere. If $\chi = 90^\circ$, $\Sigma_p = 2$ mhos, $I = 2 \times 10^5$ A, and the net distance term is 50 km, the impressed electric field would be 60 mV/m, which is in the range postulated by Lee [1986]. Hence induction electric fields are negligible for current changes taking place in the order of minutes.

Results for a Single Field-Aligned Current Filament

For a single field-aligned current filament, $j_{\parallel}(\mathbf{r})$ becomes a delta function, and the magnetic field below the ionosphere due to this perturbation is

$$\mathbf{B}_{\text{FAC}} = -\frac{\mu_0 (1 + \cos \alpha_0)}{4\pi r' \sin \alpha_0} I \hat{\phi}_0 \quad (15)$$

$$\mathbf{B}_{\text{Pedersen}} = \frac{\mu_0 (1 + \cos \alpha)}{4\pi r' \sin \alpha} I \hat{\phi} \quad (16)$$

$$\mathbf{B}_{\text{Hall}} = -\frac{\Sigma_h \mu_0}{\Sigma_p 4\pi r'} I \left(\frac{1 + \cos \alpha}{\sin \alpha} \hat{\rho} + \hat{z} \right) \quad (17)$$

where I is the total current in the filament. Figure 3 shows contour plots of the components of the magnetic field in the X , Y and Z magnetic coordinate directions for each constituent part of the current. Here I is 2×10^5 A corresponding to what a FTE might carry [Saunders *et al.*, 1984]. The current is directed toward the Earth and does not close locally but through the ionosphere at $r \rightarrow \infty$. Here $\Sigma_h/\Sigma_p = 2$ and the conducting layer is assumed to be 100 km above the ground. The choice of positive Σ_h is for the northern hemisphere. In the southern hemisphere the field due to the Hall currents would be opposite to the direction shown. If the current in the filament was directed away from the Earth, all the fields would be reversed. The magnetic field lines are tilted 10° from the vertical toward the south or negative X direction corresponding to the edge of the polar cap. The top row of Figure 3 shows plots of the magnetic field on the ground due to the field-aligned current (FAC) alone. Contours are drawn at 10-nT intervals, and negative values are dashed. Note the asymmetry due to the tilt of the field line. The middle row shows the magnetic field due to the ionospheric Pedersen currents. As described above, the Pedersen currents produce a field which cancels that of the field-aligned current when the magnetic field is vertical, and here we see the fields are almost identical and opposite in direction. In the single-filament case shown in Figure 3, the magnetic field due to the Pedersen currents and FAC currents together is less than 10-nT in most areas, with a peak value around 20-nT. Their effect on a FTE current system of similar strength would be only several nanoteslas because of the large cancellation due to local closure of the current. Hence in the remaining portion of this paper, we will assume the contributions of the field-aligned current and Pedersen currents cancel exactly, and only the Hall current's contribution to the ground magnetic field will be considered.

The bottom row of Figure 3 shows the field strength on the ground due to the Hall currents generated by the single field-aligned current filament. The Hall currents are a set of circular loops in a horizontal plane about the point where the field-aligned current intersects the ionosphere. They act like a solenoid, creating a strong vertical field. Because the solenoid is flat, the field lines are not confined and spread outward away from the vertical axis. This creates the outward radial field shown in the first two panels of the bottom row. Underneath the source point we see a peak field strength of 400 nT representing the maximum field strength for a given amount of field-aligned current. Distributed current systems or current systems with local field-aligned closure (positive and negative $j_{\parallel}(\mathbf{r})$) having the same size currents

will have a ground signature reduced depending on the exact distribution of current density.

From the $1-R_E$ size of FTEs at the magnetopause and conservation of magnetic flux between the magnetopause and the ionosphere it is believed FTEs should have current systems on the order of 200 km [Cowley, 1984; Goertz *et al.*, 1985] across at the ionosphere. The size of the Green's function or field-aligned current delta function response shown in Figure 3 is roughly 100 km, indicating that the current distribution which a FTE has at the ionosphere will strongly influence the ground magnetic signature and is as important as the peak current strength.

3. RESULTS FOR POSTULATED FLUX TRANSFER EVENT CURRENT SYSTEMS

Currently, there are two FTE current systems discussed in the literature. One possibility [Southwood, 1985, 1987] is that the field-aligned currents form a cylinder with one side directed upward and the other side directed downward as shown in Figure 1b. Southwood suggests the asymmetry is required to have Pedersen currents create a $\mathbf{J} \times \mathbf{B}$ force which pushes the flux tube through the lower collisional ionosphere. Hence the dividing line between upward and downward currents is parallel to the direction of travel of the disturbance. As a first approximation, we assume this dividing line is in the north/south direction and the FTE moves in a poleward direction. With these assumptions, $j_{\parallel}(\mathbf{r})$ at the ionosphere becomes

$$j_{\parallel}(\mathbf{r}) = \frac{I}{2a} \delta(r - a) \sin(\omega) \quad (18)$$

where I is the integral of the upward (or downward) current, a is the radius of the current system and ω is the azimuthal angle around the inside of the current system. (Motion other than poleward would introduce a $\sin(\omega + \omega_0)$ dependence.) The poleward edge of the current system would have ω equal to zero. The $\sin(\omega)$ dependence and circular shape were chosen for simplicity. The top row of Figure 4 shows the ground magnetic 'footprint' of this current system using equation (13) when $a = 100$ km, $I = 2 \times 10^5$ A, $\Sigma_h/\Sigma_p = 2$, and the conducting layer is 100 km above the ground. The horizontal Y axis measures ground distance in the east direction, and the vertical X axis measures ground distance in the north direction.

A more symmetric current system [Saunders *et al.*, 1984; Lee, 1986] is composed of a central core current with an outside return current shown in Figure 1a. The central core current provides an azimuthal magnetic field which when added to the background field creates a twisted field agreeing with in situ satellite observations. The exact radial distribution of field-aligned current in this model is not known, but for simplicity we consider a simple delta function representation

$$j_{\parallel}(\mathbf{r}) = \frac{I}{a} \delta(r - a) - \frac{I}{r} \delta(r) \quad (19)$$

where I is again the total upward (or downward) current. The direction of the currents could be reversed depending on the Y component of the IMF [Lee, 1986]. The 'footprint' of this case is shown in the bottom row of Figure 4 with I and a the same as the Southwood system. Here the value of the vertical field on the ground directly below the center

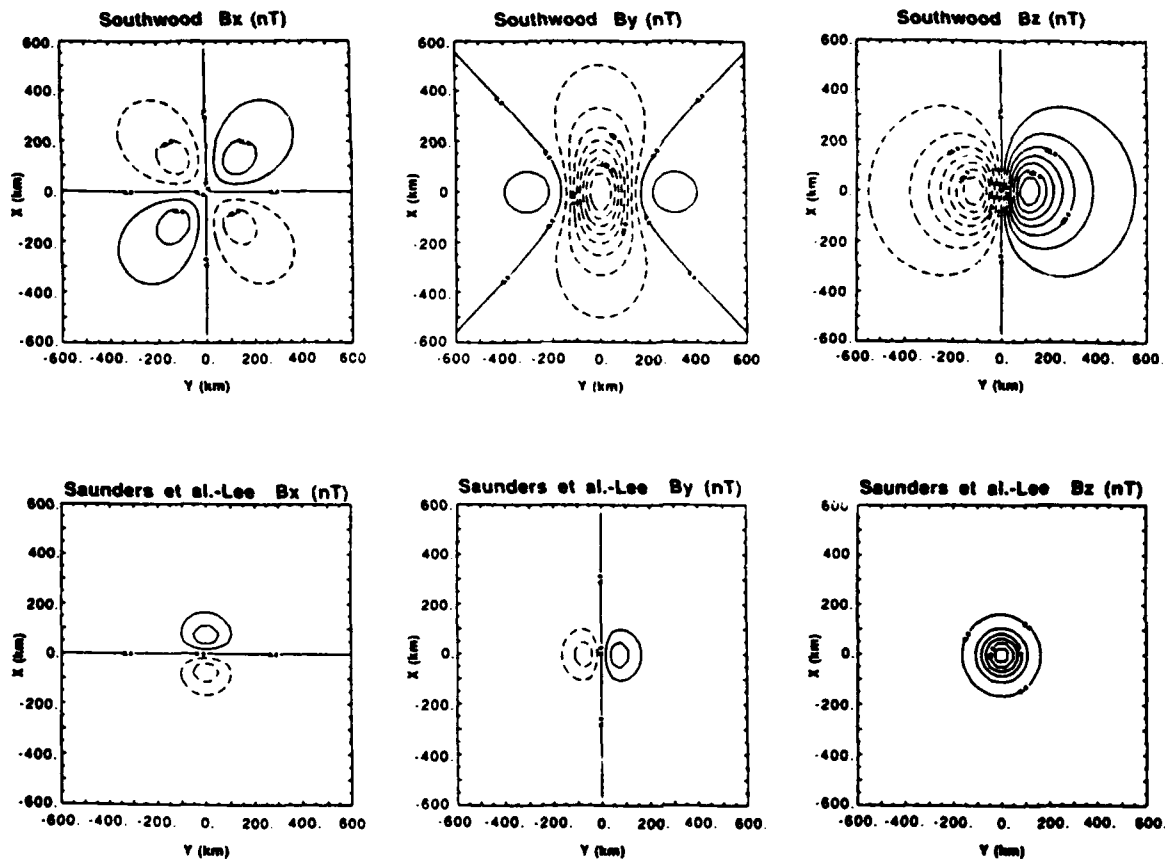


Fig. 4. (Top) Magnetic field strength on the ground due to a FTE assuming the Southwood current configuration with a radius of 100 km at the ionosphere. The X axis measures ground distance in the north direction, and the Y axis measures ground distance in the east direction. The net upward (or downward) current is equal to 2×10^5 A. The contours are dashed for negative values and spaced 20 nT. (Bottom) Magnetic field strength on the ground due to a FTE assuming the Saunders et al.-Lee current configuration with a radius of 100 km at the ionosphere. The net upward (or downward) current is equal to 2×10^5 A.

of the system can be found by direct integration of equation (13) using the current density of equation (19).

$$B_z = \frac{\sum_h \mu_0}{\sum_p 4\pi} I \left(\frac{1}{\sqrt{a^2 + h^2}} - \frac{1}{h} \right) \quad (20)$$

If $h \gg a$, this becomes

$$B_z = \frac{\sum_h \mu_0}{\sum_p 4\pi} I \frac{a^2}{2h^3} \quad (21)$$

which is the result of [Lanzerotti et al., 1986]. However, the assumption of $h \gg a$ is not valid in this situation since h and a are comparable. Using equation (20), we find a peak value of B_z of 120 nT with $\Sigma_h/\Sigma_p = 2$, $a = h = 100$ km and $I = 2 \times 10^5$ A while equation (21) yields 200 nT for B_z in the same situation. The large difference between these estimates is not unexpected, because the Hall current is a distributed current system which is quite different from a current loop when the observer on the ground is relatively close.

To find the magnetic field at an arbitrary location caused by the above FTE field-aligned current models, equation (13) must be numerically integrated using a known field-aligned current system. To obtain the top view of Fig-

ure 4, Southwood's field-aligned current system was used (equation (18)), while for the bottom row of Figure 4, the Saunders et al.-Lee system (equation (19)) was used. Each contour line in these two figures represents a change of 20 nT, and negative values are shown with dashed contours. Comparing the footprints of the two proposed FTE current systems, we see they differ not only in peak value but also in basic configuration. The magnetic perturbation produced by the cylindrically symmetric system proposed by Saunders et al. and Lee has an area less than half that produced by the system suggested by Southwood. It also has a significantly smaller peak value and a smaller horizontal magnetic field at the ground as opposed to Southwood's strong horizontal component. Note that symmetry requires the horizontal magnetic field point toward or away from the center of the Saunders et al.-Lee current system unlike the Southwood system, where the horizontal field points in a roughly uniform direction at all points on the ground. The Z component of the magnetic field of the Southwood system also has regions of strong negative and strong positive values, while the Saunders et al.-Lee system has no sign change in the Z component. If the FTE footprint moved in a direction other than poleward, the Southwood patterns would be rotated corresponding to the angle away from poleward the

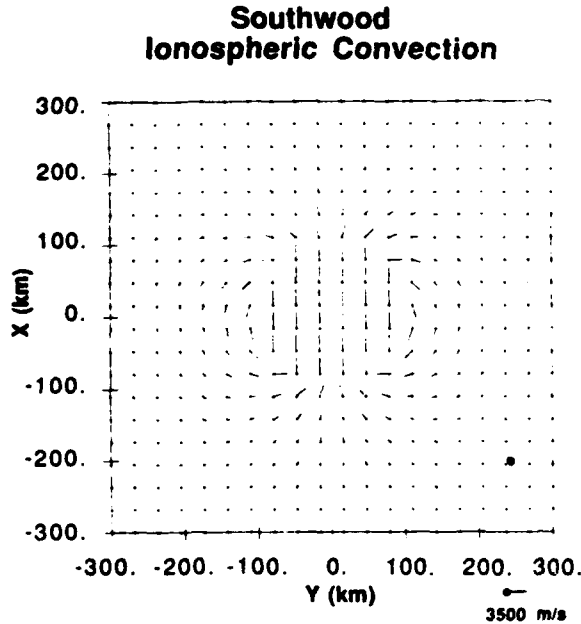


Fig. 5. Ionospheric convection created by the Southwood model of FTE field-aligned currents. The net downward current and upward current is 2×10^5 A. All the field-aligned currents intersect the ionosphere along a 100-km radius circle. The scale vector has length corresponding to a velocity of 3500 m/s.

FTE footprint moved. The Saunders et al.-Lee perturbations would change sign if the direction of the field-aligned currents were reversed.

Perhaps a more realistic version of the symmetric Saunders et al.-Lee field-aligned current system would be to replace the delta function core with a uniform current distribution avoiding singularities in the electric field in the center. Although not shown, the ground magnetic field of this system is similar to the delta function core version shown in the bottom row of Figure 4 with the horizontal field purely radial and with the peak Z perturbation underneath the center. The strength of the field, however, has a slightly different radial dependence. As done in equation (20), the vertical field directly under the center of the current system can be calculated.

$$B_z = \frac{\Sigma_h \mu_0 I}{\Sigma_p 4\pi} \left(\frac{1}{\sqrt{a^2 + h^2}} - 2 \frac{\sqrt{a^2 + h^2} - h}{a^2} \right) \quad (22)$$

Assuming $a \sim h$, this gives a vertical field strength directly under the current system which is approximately half that of the system with a delta function core. The large sensitivity of the ground magnetic field due to the field-aligned current configuration is due to the size of the current system being roughly the same as the height of the ionosphere and the large amount of cancellation when calculating the magnetic field when the field-aligned currents close locally.

Combination of Postulated Flux Transfer Event Current Systems

The field-aligned current system associated with a FTE must be consistent with the flux tube translating in the ionosphere and with twist in the magnetic field inside the tube. Since the two systems studied here each produce only one of the desired effects, it is likely that a combination of

them describe the true FTE situation. First, we require that as the combined field-aligned current system moves across the ionosphere, flux must remain inside the flux tube, and plasma outside must be moved out of the way. To find the ionospheric convection pattern of the Southwood system of field-aligned currents of equation (18) with $I = 2 \times 10^5$ A, we assume $\mathbf{E} \times \mathbf{B}$ drift and use equation (5) to get \mathbf{E} . The result is a large twin-vortex pattern as shown in Figure 5. Inside the 100-km radius ionospheric footprint of the FTE flux tube, the flow is uniform with northward velocity (v_x).

$$v_x = \frac{I \sin^2 \chi}{4a \Sigma_p B} \quad (23)$$

If the field-aligned current system does not move, plasma in the ionosphere circulates with no net motion, since the field-aligned currents cannot apply a net force in a uniform ionosphere. If we now assume the field-aligned current system translates and the plasma inside the flux tube moves with the field-aligned current system, then equation (23) relates the amount of current in the Southwood system to the velocity of the field-aligned current system. Adding field-aligned current in a cylindrically symmetric system such as the Saunders et al.-Lee system, with its radial convection pattern, does not cause flux to leave the inside of the FTE. Second, the observed twist in the magnetic field inside a FTE near the magnetopause adds the requirement that the Saunders et al.-Lee portion of the field-aligned current be much larger than the Southwood portion. We now can use equation (18) along with the observed speed of FTEs (of order 1 km/s [Goertz et al., 1985; Lanzerotti et al., 1986; Todd et al., 1986]) at the ionosphere to estimate the amount of field-aligned current of a FTE assuming a Southwood configuration with 100-km radius. Using a vertical magnetic field of 0.6 G with $\chi = 80^\circ$ and $\Sigma_p = 2.5$ mhos, the net downward field-aligned current (I) would be 0.6×10^5 A. Assuming this current system was added to a Saunders et al.-Lee system of 2×10^5 A, a twisted magnetic field would be expected inside the FTE, although it would be distorted. The contributions of the two current systems to the ground magnetic field, however, would be comparable even though the Southwood current strength is a factor of 3 smaller because of the small ground perturbation of the Saunders et al.-Lee system.

For the remaining analysis, however, the Southwood and Saunders et al.-Lee current systems will continue to be considered separately because estimation of the relative amounts of current in each system in a combined model depends on the total current, the conductivities, and the ionospheric speed of FTEs, which are not well known and possibly variable.

Ground Magnetometer Signatures of Postulated Flux Transfer Event Current Systems

To predict the time record of a ground magnetometer when a FTE passes near by, the current strength as a function of time must be known as well as how fast and in what direction the disturbance propagates. If we assume a FTE's field-aligned current system is stable and moves in a straight line across the ionosphere, its ground magnetic signature at a fixed observatory can be approximated by a cross section of the ground magnetic 'footprint' taken along the overhead track. Figure 6 shows for each current system the compo-

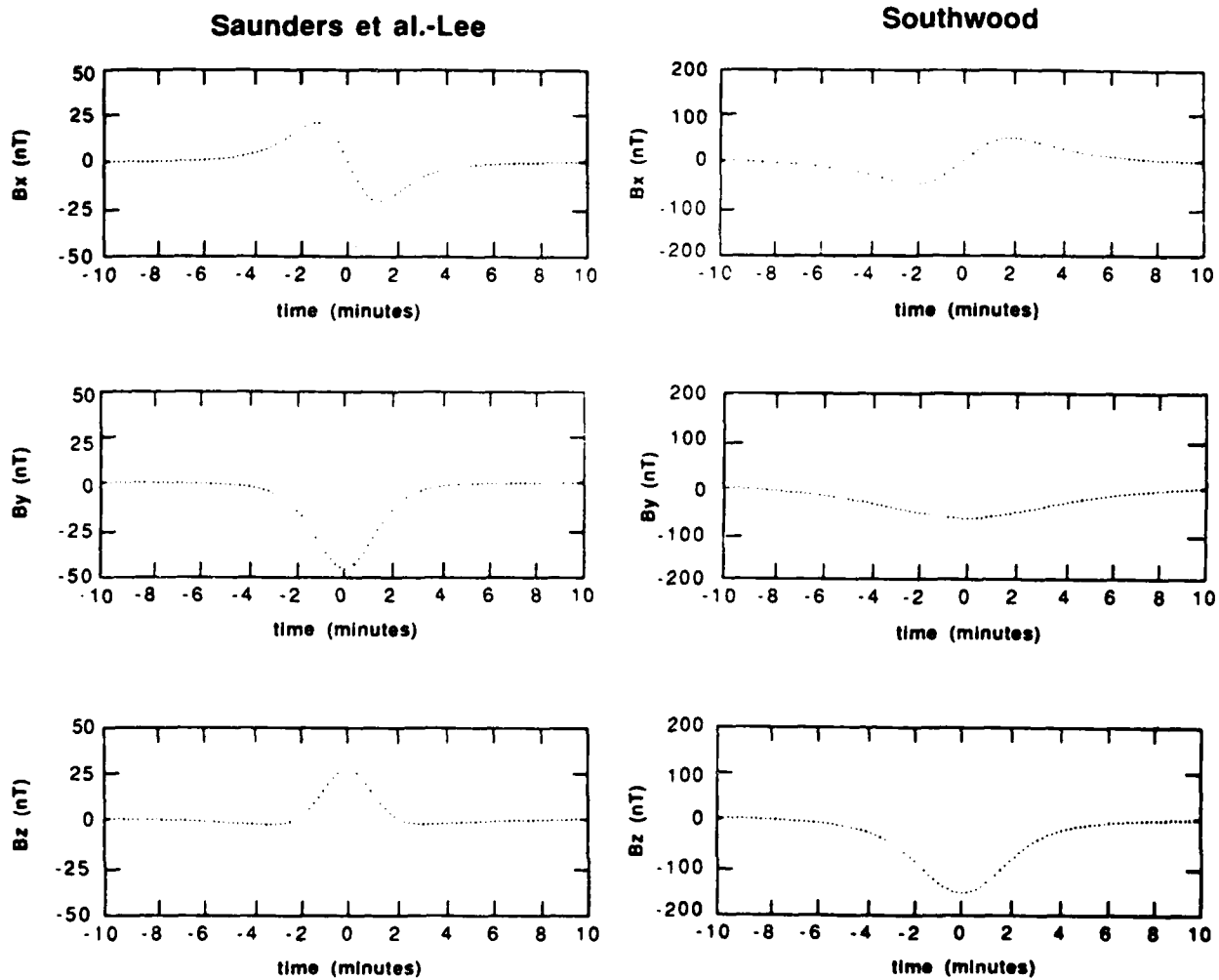


Fig. 6. (Left) Magnetic field versus time of a FTE assuming the Saunders et al.-Lee current system moving poleward at a rate of 1 km/s and passing 100 km ground distance away to the east. The strength and configuration of the field-aligned currents are assumed to be constant. (Right) Magnetic field versus time of a FTE with the Southwood current system moving poleward at a rate of 1 km/s and passing 100 km ground distance away to the east. The strength and configuration of the field-aligned currents are assumed to be constant.

nents of the magnetic field on the ground which would be measured for a FTE moving poleward at 1 km/s and with its center passing 100 km to the east of a ground magnetometer located in the northern hemisphere. The central core current in the Saunders et al.-Lee system was directed away from the Earth. Note the large differences in the basic shape of each component and how the asymmetric Southwood current model has more than twice the peak magnitude of the symmetric Saunders et al.-Lee model for equal field aligned currents.

Unfortunately, there have only been a few possible observations of FTEs in the ionosphere to verify the above assumption of a stable FTE current system moving across the ionosphere with constant velocity [Goertz et al., 1985; Todd et al., 1986; Lanzerotti et al., 1986]. These experiments do indicate that the ionospheric signature of a FTE moves with a speed of 0.5 to 2.0 km/s and has a duration on the order of 4 min. While this 4-min duration could represent the time it took for the FTE to cross the field of view of the experiment, it is possible it could represent the lifetime

of the ionospheric signature. Comparing this 4-min lifetime with the time it takes a FTE to pass a ground station as noted in Figure 6, we see the assumption of constant field-aligned current is only marginally met. The true ground magnetometer signature would be similar to that in Figure 6 during the time period with significant field-aligned currents and greatly reduced during the time intervals when the FTE field-aligned currents cease.

One way to identify a FTE using its ground magnetic signature without assumptions of its ionospheric motion or field-aligned current strength is to use simultaneous measurements using an array of closely spaced magnetometers. The observed horizontal magnetic perturbation vector plotted at the location of the station can then be easily compared to theoretical models. In Figure 7, the horizontal magnetic perturbation is shown for both the Southwood and Saunders et al.-Lee models. The length of the scale vector shown is 200 nT in the Southwood plot but only 100 nT in the Saunders et al.-Lee data. Note the the large Y perturbation normal to the assumed X-directed velocity in the Southwood model!

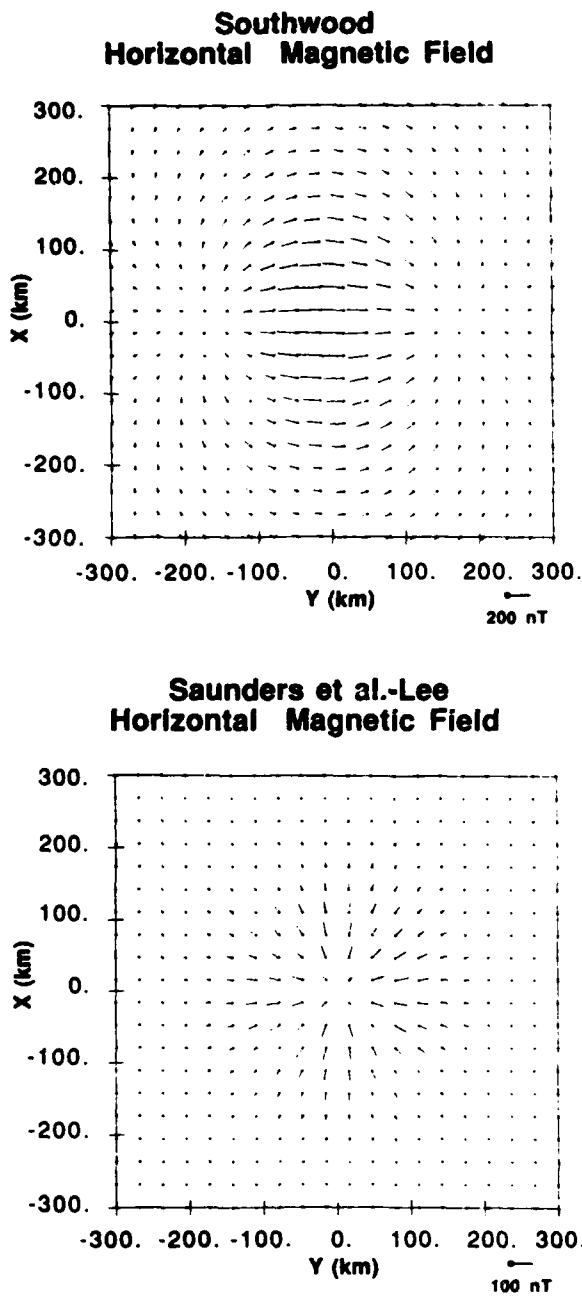


Fig. 7. (Top) Horizontal magnetic perturbation due to a FTE assuming the Southwood field-aligned current system. The length of the scale vector represents a 200-nT perturbation. The field is largely perpendicular to the assumed X -directed motion of the FTE. (Bottom) Horizontal magnetic perturbation due to a FTE assuming the Saunders et al.-Lee field-aligned current system. The length of the scale vector represents a 100-nT perturbation. The field is radial about the center of the field-aligned current system because of symmetry.

while the magnetic perturbation is radial from the center of the Saunders et al.-Lee system. As mentioned above, the true FTE signature will be a combination of the Southwood and Saunders et al.-Lee models, with the ratio depending on the conductivities, the FTE ionospheric speed, and the total amount of current.

Estimate of Ground Magnetometer FTE Detection Rate

An important factor in observing the ground signature of a FTE is the detection rate. A statistical survey [Rijnbeek et al., 1984] of satellite detections near the dayside magnetopause has shown that FTEs exist uniformly over a large region. At a given location in this region, FTEs recur every 7 to 8 min on average. These data are consistent with the idea that the observed FTEs are caused by the antisunward motion of reconnected flux tubes moving along the magnetopause carried by magnetosheath flow.

A fundamental unanswered question regarding FTEs is the global generation rate. A variety of assumptions can be made to estimate this rate. For example, let us consider only the northern hemisphere and assume that each FTE is initially formed near the equatorial magnetopause. Further assume that the reconnected flux tube is pulled tailward across the magnetopause either toward dawn or dusk depending on the orientation of the IMF and the reconnection location. A satellite located at the dayside magnetopause should then detect a large fraction of the antisunward moving FTE flux tubes. If we assume that on average half the reconnected tubes move toward the dawn flank and half move toward the dusk flanks, we might expect a satellite to detect at most half of the globally generated FTEs. If FTEs are generated globally at least every 4 min, what would be the expected detection rate of a ground magnetometer?

To find the ionospheric density of FTEs, their starting location and ground track must be known and we can only speculate on these at present. Estimating that FTEs can be formed on the front third of the magnetosphere, we map this region to roughly the dayside third of the auroral oval. This is a band perhaps 3000 km wide in longitude. The normal dimensions of FTEs at the magnetopause when mapped to the auroral oval give a width of several hundred kilometers, producing a detection band which is 3000 km in longitudinal length and about 300 km in latitudinal width located around the convection reversal boundary. This band forms the most probable area where the ionospheric signature of a FTE would start.

If we define 50 nT to be the minimum ground magnetic field perturbation required to detect a FTE, we find from Figure 4 that the Southwood configuration produces a 600-km detection range, while the Saunders et al.-Lee configuration produces a 100-km detection range. Thus, roughly three observatories suitably distributed over the detection band would be sufficient to observe the global generation of FTEs of the Southwood model, while 15 stations would be required for the Saunders et al.-Lee model. If the ground track of FTEs is composed of a significant longitudinal component, fewer stations may be required. Of course, more stations distributed in latitude will be required, since the detection band will move in latitude as the auroral oval expands and contracts.

It follows from the above estimates that if a station was known to be under the dayside convection reversal boundary and the IMF was southward, FTE signatures should be observed in the data roughly every 12 (60) min on the average for the Southwood (Saunders et al.-Lee) current model. This represents an upper limit on the time between detections because of the conservative global FTE generation rate assumed above. It is also a long-term average, since the location of reconnection could remain steady for some period

of time; hence the ionospheric signatures of the accompanying FTEs could follow nearly the same path repeatedly, allowing a higher detection rate for a given ground station.

4. SUMMARY AND CONCLUSIONS

Making the assumptions of a thin conducting region in the ionosphere, near-uniform conductivity, and small induction electric fields, the ground magnetic field of an arbitrary small-scale field-aligned current system has been reduced to a simple integral over the field-aligned current filaments. This approximation includes the tensor nature of the conductivity of the ionosphere. These results have been applied separately to two models of FTE field-aligned current systems. The resulting ground magnetic fields are of the order of 100 to 150 nT depending on the size and strength of the current systems at the ionosphere. The two models have significantly different vertical and horizontal magnetic fields on the ground as indicated in Figure 4. To meet the requirements of twist in the magnetic field inside the FTE near the magnetopause and movement of the FTE footprint in the ionosphere, the most likely field-aligned current arrangement is a combination of the Southwood and Saunders et al.-Lee models. By comparing the calculated velocity of the ionospheric convection to the observed FTE speed, we find the fraction of total current in the Southwood model roughly a factor of 3 less than in the Saunders et al.-Lee model, but because the Southwood system has a much larger magnetic signature, the ground magnetic effects are comparable.

From the above detection rate estimates, it appears that using ground magnetometers is a plausible method to study FTEs if an area underneath the convection reversal could be monitored with a chain of magnetometers. It is likely that the relatively strong magnetic signature produced by the Southwood asymmetric configuration would be easily detected. If, however, FTE currents are predominantly of the Saunders et al.-Lee symmetric configuration, the smaller magnetic effects are much less likely to be detected, and a more dense magnetometer array will be required.

If FTEs could be reliably identified from the ground, not only could the current configuration and time history be studied using the results of this paper, but the field line where reconnection started could be found as well as checking the above estimates on the total worldwide FTE rate. Since a single FTE does not transfer enough flux to explain the existing magnetospheric potential [Rijnbeek et al., 1984], their rate of occurrence is critical in deciding their overall importance.

Acknowledgments. This research has been supported by the National Science Foundation through grant ATM-8503105 and by the Air Force Geophysics Laboratory through contract F19628-85-K-0001. Mark A. McHenry was partially supported by the NASA Student Researchers Program through grant NGT 50016. We would like to thank Eigil Friis-Christensen for helpful comments on earlier versions of this manuscript. We also appreciate the care which the referees gave to this paper and their helpful suggestions.

The Editor thanks S. W. H. Cowley and Y. Kamide for their assistance in evaluating this paper.

REFERENCES

Berchem, J., and C.T. Russell, Flux transfer events on the magnetopause: Spatial distribution and controlling factors. *J. Geophys. Res.*, **89**, 6689, 1984.

- Cowley, S.W.H., The causes of convection in the Earth's magnetosphere: A review of developments during the IMS. *Rev. Geophys.*, **20**, 531, 1982.
- Cowley, S.W.H., Evidence for the occurrence and importance of reconnection between the Earth's magnetic field and the interplanetary magnetic field, in *Magnetic Reconnection in Space and Laboratory Plasmas*, *Geophys. Monog.*, Vol. 30, edited by E. W. Hones, Jr., p.375, AGU, Washington, D.C., 1984.
- Dungey, J.W., Interplanetary magnetic field and the auroral zones, *Phys. Rev. Lett.*, **6**, 47, 1961.
- Fukushima, N., Equivalence in ground geomagnetic effect of Chapman-Vestine's and Birkland-Alfvén's electric current-systems for polar magnetic storms, *Rep. Ionos. Space Res. Jpn.*, **23(3)**, 1969.
- Goertz, C.K., E. Nielsen, A. Korth, K.H. Glassmeier, C. Haldoupis, P. Hoeg, and D. Hayward, Observations of a possible ground signature of flux transfer events, *J. Geophys. Res.*, **90**, 4069, 1985.
- Kamide, Y., and S. Matsushita, Simulation studies of ionospheric electric fields and currents in relation to field-aligned currents, 1, Quiet periods, *J. Geophys. Res.*, **84**, 4083, 1979.
- Kisabeth, J.L., and G. Rostoker, Modelling of three dimensional current systems associated with magnetospheric substorms, *Geophys. J. R. Astron. Soc.*, **49**, 655, 1977.
- Lanzerotti, L.J., L.C. Lee, C.G. MacLennan, A. Wolfe, and L.V. Medford, Possible evidence of flux transfer events in the polar ionosphere, *Geophys. Res. Lett.*, **13**, 1089, 1986.
- Lee, L.C., Magnetic flux transfer at the Earth's magnetopause, *Solar Wind-Magnetosphere Coupling*, edited by Y. Kamide and J. Slavin, Terra, Tokyo, 1986.
- Morse, P.M., and H. Feshbach, *Methods of Theoretical Physics*, McGraw-Hill, New York, 1953.
- Paschmann, G.B., B.U.Ö. Sonnerup, I. Papamastorakis, N. Sckopke, G. Haerendel, S.J. Bame, J.R. Asbridge, J.T. Gosling, C.T. Russell, and R.C. Elphic, Plasma acceleration at the Earth's magnetopause: Evidence for reconnection, *Nature*, **282**, 243, 1979.
- Ratcliffe, J.A., *An Introduction to the Ionosphere and Magnetosphere*, Cambridge University Press, New York, 1972.
- Rijnbeek, R.P., S.W.H. Cowley, D.J. Southwood, and C.T. Russell, A survey of dayside flux transfer events observed by ISEE 1 and 2 magnetometers, *J. Geophys. Res.*, **89**, 786, 1984.
- Robinson, R.M., D.S. Evans, T.A. Potemra, and J.D. Kelly, Radar and satellite measurements of an F-region ionization enhancement in the post-noon sector, *Geophys. Res. Lett.*, **11**, 899, 1984.
- Russell, C.T., and R.C. Elphic, Initial ISEE magnetometer results: Magnetopause observations. *Space Sci. Rev.*, **22**, 681, 1978.
- Russell, C.T., and R.C. Elphic, ISEE observations of flux transfer events at the dayside magnetopause, *Geophys. Res. Lett.*, **6**, 33, 1979.
- Saunders, M.A., C.T. Russell, and N. Sckopke, Flux transfer events: Scale size and interior structure, *Geophys. Res. Lett.*, **11**, 131, 1984.
- Sonnerup, B. U. Ö., G. B. Paschmann, I. Papamastorakis, N. Sckopke, G. Haerendel, S.J. Bame, J.R. Asbridge, J.T. Gosling, and C.T. Russell, Evidence for magnetic field reconnection at the Earth's magnetopause, *J. Geophys. Res.*, **86**, 10,049, 1981.
- Southwood, D.J., Theoretical aspects of ionospheric-magnetosphere-solar wind coupling, *Adv. Space Res.*, **5**, 7, 1985.
- Southwood, D.J., The ionospheric signature of flux transfer events, *J. Geophys. Res.*, **92**, 3207, 1987.
- Stenzel R.L., and J.M. Urrutia, Laboratory model of a tethered balloon - electron beam current system, *Geophys. Res. Lett.*, **13**, 797, 1986.
- Todd H., B.J.I. Bromage, S.W.H. Cowley, M. Lockwood, A.P. van Eyken, and D.M. Willis, EISCAT observations of bursts of rapid flow in the high latitude dayside ionosphere, *Geophys. Res. Lett.*, **13**, 909, 1986.

C. R. Clauer and M. A. McHenry, STAR Laboratory, Stanford University, Durand 335, Stanford, CA 94305.

(Received February 18, 1987;
revised June 19, 1987;
accepted July 1, 1987.)

The U.S. Government is authorized to reproduce and sell this report.
Permission for further reproduction by others must be obtained from
the copyright owner.

Solar Wind-Magnetosphere Coupling, edited by Y. Kamide and J. A. Slavin, 507-518.
Copyright © 1986 by Terra Scientific Publishing Company (TERRAPUB), Tokyo.

IMF B_z Control of Ionization and Electric Fields Measured by the Sondrestrom Radar

R. M. ROBINSON¹, C. R. CLAUSER², O. DE LA BEAUJARDIERE³, J. D. KELLY¹,
and D. S. EVANS^{1,*}

¹*Space Sciences Laboratory, Lockheed Palo Alto Research Laboratory, Palo Alto
California 94304, U.S.A.*

²*STAR Laboratory, Stanford University, Stanford, California 94305, U.S.A.*

³*Radio Physics Laboratory, SRI International, Menlo Park, California 94025, U.S.A.*

The pattern of ionization and electric fields measured in the dayside auroral zone by the Sondrestrom incoherent scatter radar has been compared with interplanetary magnetic field (IMF) data from the IMP-8 spacecraft. The electric field configuration is most sensitive to the B_z component of the IMF. For $B_z < 0$ there is a strong reversal in convective flow between 1300 and 1600 MLT with a region of enhanced F region ionization associated with low energy particle precipitation at the reversal. For $B_z > 0$ the convection reversal is most apparent on the morning side. Ionization produced by particle precipitation for $B_z > 0$ is much less conspicuous than that observed on the afternoon side for $B_z < 0$. We show radar measurements of ionization, electric fields and electron temperatures associated with two distinct types of particle precipitation in the pre-noon local time sector for $B_z > 0$. The patterns of precipitation for $B_z < 0$ and $B_z > 0$ are consistent with the distribution of field-aligned currents, in that precipitation occurs primarily in the upward current regions. With this interpretation, only the precipitation associated with the cusp field-aligned currents on the dawn side may be intense enough to produce ionospheric signatures observable from the ground.

1. Introduction

The large-scale pattern of electric fields and field-aligned currents in the auroral zone and its response to changes in the interplanetary magnetic field have been studied extensively in past years (see, for example, HEPPNER, 1972; FRIIS-CHRISTENSEN *et al.*, 1972; IJIMA and POTEMRA, 1978; HEELIS, 1984). BURCH *et al.* (1985) have shown that the electric field pattern can be understood in terms of the superposition of several cells referred to as either merging, viscous or lobe cells. Each cell responds differently to changes in the interplanetary magnetic field. Precipitation is expected in various parts of the convection pattern depending on the connection of these field lines to various plasma regimes.

Since operations began in Greenland in February, 1983, numerous experiments were performed in which the Sondrestrom radar was used to measure the distribution of ionization and electric fields at very high latitudes. The radar data provide a

*Permanent address: Space Environment Laboratory, NOAA, Boulder, Colorado, U.S.A.

complimentary view to that obtained with polar orbiting satellites, because patterns of ionization and electric fields can be constructed from measurements made at different local times. However, the interpretation of these observed patterns must be done carefully because electric fields may change substantially during the time over which the measurements are made. Interplanetary magnetic field data are presently available for many of the radar experiments so that variations of electric fields in response to IMF conditions can be identified.

In this paper we describe the results of a study in which we examined radar measurements in the dayside auroral oval and polar cap made during 24 experiments. After describing the data used in the study, we present a short, qualitative description of the observed electric field patterns and their dependence on the IMF. We then discuss the ionization that occurs in association with these patterns and look in detail at two examples of ionization enhancements produced by particle precipitation in the morning sector.

2. Data Base

The radar data used in this study were obtained during experiments on 24 days chosen on the basis of the availability of IMF data. Some of these experiments were performed as part of the World Day observations; others were performed as part of campaigns to study electrodynamic in the polar cusp. Preliminary results of these experiments have been described in a number of papers (see, for example, JORGENSEN *et al.*, 1984; CLAUER *et al.*, 1984; KELLY and VICKREY, 1984). For the present study, we examined the data set for the specific purpose of identifying IMF B_z -dependent patterns of particle precipitation and electric fields in the prenoon and postnoon local time sectors. The radar operating mode for most of the 24 days consisted of some combination of fixed-position measurements and scans. The fixed-position measurements at a sequence of elevation angles and azimuths provided electric field data over a broad latitudinal range, while the scans yielded high time- and spatial-resolution measurements of ionization and drifts over a more limited region.

Table 1 shows the number of times different orientations of B_z occurred during radar measurements in the morning and afternoon sectors. All IMF components given in this paper refer to the GSM coordinate system. To be counted as an occurrence, B_z had to maintain the same sign for longer than an hour, which is greater than the 15 minutes to one-half hour required for electric fields on the dayside to

Table 1. Occurrence frequency of various orientations of IMF B_z in morning and afternoon sectors for the data set used in this study.

	$B_z > 0$	$B_z < 0$
Morning	14	8
Afternoon	9	11

respond to changes in the IMF at the location of IMP-8 (CLAUER *et al.*, 1984). No sorting according to the magnitude of B_z was performed and the data include cases of both positive and negative values of B_z . Although B_z was highly variable, there were many days when this component of the IMF remained fairly constant over long time intervals. Out of the 24 days there were eight in which B_z was positive throughout the morning and afternoon sectors, while there were five in which B_z remained negative during this local time interval.

3. Large-Scale Electric Fields and Their Relation to IMF B_z

In general, the electric fields measured by the radar during the local times between 0600 and 1800 are quite consistent with the results of previous studies based on satellite data. Of particular note is the strong dependence of the electric field on the y component of the IMF (DE LA BEAUJARDIERE *et al.*, this volume). For $B_z < 0$ the radar measures predominantly eastward drifts in the morning sector, while in the evening sector both eastward and westward convecting plasma is observed. The westward (sunward) drifting plasma is confined to the equatorward part of the oval, with the eastward (antisunward) drifting plasma poleward of it. The antisunward drifting plasma is typically quite strong and confined to the region immediately poleward of the convection reversal. As pointed out by JORGENSEN *et al.* (1984) the convection reversal is typically rotational; however, the change in the east-west component of the velocity is particularly large and is thus an easily identifiable feature in latitudinal plots of electric field in the post-noon sector (ROBINSON *et al.*, 1984).

For $B_z > 0$ the convection reversal in the afternoon sector disappears and westward drifts dominate at all latitudes. A corresponding reversal appears, however, on the morningside with, again, sunward drifts on the equatorward side and antisunward drifts on the poleward side. The reversal in velocity on the morning side is not as dramatic as on the afternoon side, but is still quite obvious in the radar data.

The convection observed near noon is highly variable, but tends to be dominated by westward drifts for $B_z > 0$ and eastward drifts for $B_z < 0$. Occasionally, antisunward drifting plasma at noon can be observed, especially when B_z is large and negative.

These general statements about the patterns of electric fields and their dependence on B_z underscore the importance of IMF data in the interpretation of radar measurements. Under conditions when B_z is changing rapidly, radar measurements through the prenoon to postnoon local time sector reveal multiple reversals in the zonal convection of plasma. Fortunately, there are enough periods of fairly stable IMF conditions to allow unambiguous mapping of the local time and latitudinal distribution of electric fields from radar measurements. These studies are currently in progress.

4. Ionization Produced by Particle Precipitation and Its Dependence on IMF B_z

Because much of the electron precipitation that occurs in the dayside oval and polar cap is very soft, ionization is predominantly produced at altitudes above 200 km. At these altitudes, ionization has lifetimes from several tens of minutes to hours

and can be transported great distances from the location at which it is produced. Thus, the appearance of ionization enhancements does not necessarily indicate the presence of local production by particle precipitation. Although there are other measurable indicators of local production that can be used, we show here only ionization that can be definitely attributed to particle precipitation, either because the precipitation was hard enough to ionize at altitudes below 200 km, or because simultaneous satellite data were available to confirm the association. Because we limited ourselves to these obvious indicators of particle precipitation, we may have overlooked regions of precipitation in which the energy of the particles was too low to produce measurable enhancements in ionization. KOFMAN and WICKWAR (1984) and WICKWAR (this volume) describe a method based on solving the electron heat balance equation by which regions of local production can be identified regardless of the accompanying ionization. This technique may prove useful for future studies.

The most obvious region of particle precipitation observed with the radar at Sondrestrom is that associated with the convection reversal in the afternoon sector when $B_1 < 0$ (FOSTER, *et al.*, 1983; CLAUER *et al.*, 1983). ROBINSON *et al.* (1984) presented radar and satellite measurements in this precipitation region to show that it is associated with the region 1 Birkeland current and precipitating electrons accelerated through parallel potential drops of about 1 kV from a source of density 3.5 cm^{-3} and temperature 350 eV. EVANS (1984) studied precipitation in this local time sector using data from the NOAA satellites and confirmed the persistence of this feature even in periods of very low magnetic activity. The ionospheric signature and induced effects of this precipitation have been examined by WICKWAR (this volume). For $B_1 < 0$ on the morning side no localized region of enhanced ionization was identified in the radar data that could be attributed to particle precipitation.

For $B_1 > 0$, a reversal in the convective flow of plasma appears on the morning side. In examining the fourteen periods of measurements during which B_1 was positive in the morning hours we were able to identify two examples of ionization produced by particle precipitation. Figure 1 shows data obtained on 13 July 1983 while the radar was performing an elevation scan in the plane of the magnetic meridian. At the time of these measurements, B_1 was +10 nT and B_2 was -10 nT. The top panel in Fig. 1 is a contour plot of electron density in the meridian plane constructed from the radar measurements. The center of the plot corresponds to the location of the radar which is at 74 degrees invariant latitude. Directly above the radar a region of ionization was observed with a peak density of about $3 \times 10^5 \text{ cm}^{-3}$ at an altitude of 200 km. Because this region of ionization extends downward to altitudes well below 200 km, we can be reasonably sure that local production by precipitating particles was occurring at this location. The second panel in Fig. 1 shows the latitudinal profile of electric field measured during the scan. The eastward electric field is small to the south and increases gradually to the north. The meridional electric field is southward with a peak value of about 75 mV m just poleward of the ionization enhancement. Assuming no significant gradients in the east-west electric field in the zonal direction and uniform ionospheric conductivity, the north-south gradients in the meridional electric field are consistent with the presence of upward field-aligned currents within the ionization enhancement and downward field-aligned currents poleward of the

J. Geophys. Res., 1984, Vol. 89, No. 3, P. 510-518

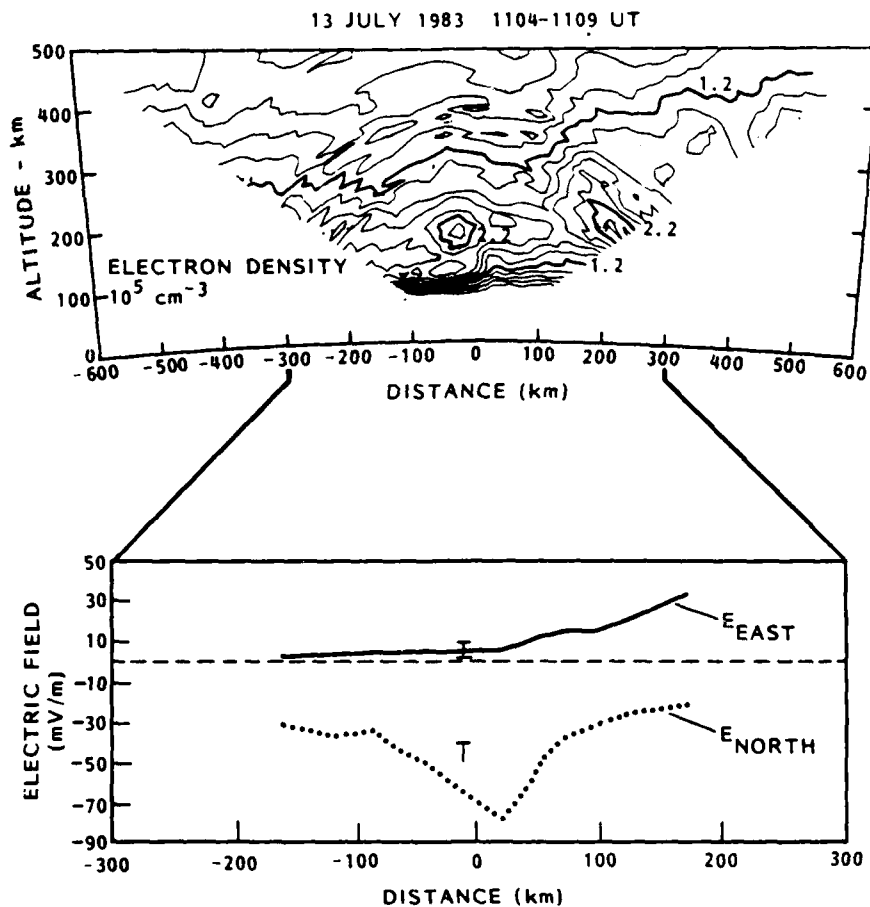


Fig. 1. Radar data obtained during a 5-minute scan in the magnetic meridian on 13 July, 1983. Distances are in km magnetically north and south from the radar.

enhancement. The sense of these currents is consistent with that of the region 1 and region 2 Birkeland currents (IJIJIMA and POTEMRA, 1976). The ionization feature at 74 degrees latitude was apparent at the same location in the data from the subsequent radar scan (not shown) which was made about a half hour later. Thus, the precipitation producing this ionization was probably extended at constant invariant latitude along the auroral oval over about one-half hour in local time and persisted for at least this long in Universal Time. The latitudinal structure of electric field observed during the second scan was somewhat different. The precipitation was associated with a local perturbation in a wide region of fairly uniform southward fields. However, the gradient in electric field associated with the perturbation was, as before, consistent with the presence of upward field-aligned currents. In summary, the observations on

13 July are consistent with arc-like precipitation embedded in sunward drifting plasma and associated with upward field aligned currents.

The second type of precipitation identified in the morning sector for positive IMF B_z is shown in Plate 1. The top panel shows a color plot of electron density in the magnetic meridian plane observed on 13 April 1983 at about 1000 magnetic local time. At this time B_z was about +8 nT and B_y was about -5 nT. The radar data show several regions of latitudinally confined ionization enhancements with electron densities of about $3 \times 10^5 \text{ cm}^{-3}$. Because these enhancements were situated at altitudes of about 400 km, they cannot definitively be associated with particle precipitation. Electron temperature measurements from the same scan are shown in the second panel. These data show that the electron temperature between 73 and 74 degrees invariant latitude was higher than that in the surrounding plasma, reaching temperatures of over 4000 K. This suggests local production of heat and ionization by precipitating particles. This conclusion was confirmed by data from the NOAA-6 satellite during a north polar pass between 1137 and 1154 UT. Radar and satellite data at this time are shown in Fig. 2. The top panel is a plot of the total energy flux carried into the atmosphere by precipitating ions and electrons. These data show a region of enhanced precipitation within the same latitude range as the ionization enhancement detected by the radar. The peak energy flux exceeded $10 \text{ ergs cm}^{-2}\text{-s}$ and was carried almost exclusively by precipitating electrons. Spectral information about the precipitating electrons indicated average energies less than about 300 eV. Electric fields measured by the radar at about the time of the NOAA-6 pass are shown in the bottom panel of Fig. 2. Latitudinal profiles of the northward electric field at two different times are shown. The similarity between the two sets of electric field measurements confirms the constancy of the electric field pattern over the duration of the observations. The electric field over most of the region scanned by the radar was strong and northward indicating antisunward drifting plasma. The particle precipitation is located just poleward of where the electric field maximizes. The gradient in the electric field assuming uniform ionospheric conductivity is consistent with the presence of upward field-aligned currents. The location of these currents is well within the polar cap as determined by the direction of the plasma drift. Thus, the ionization shown in Plate 1 was probably the ionospheric signature of a polar cap arc. Note that, as pointed out by WICKWAR and KOFMAN (1984), the high electron temperatures along with the enhanced ionization can lead to substantial thermal excitation of the O^1D state of atomic oxygen, so that 630.0 nm emissions probably exceeded a few kR in intensity from this source alone.

5. Discussion

By examining Sondrestrom radar measurements made during the morning and afternoon hours, we have attempted to relate ionization produced by particle precipitation to boundaries of the convective flow and to the y component of the IMF. The most obvious signature of electron precipitation is the F region ionization enhancement associated with the afternoon sector convection reversal during times when IMF B_z is negative. EVANS (1984) showed that this precipitation probably

13 APRIL 1983

1213 - 1223 UT

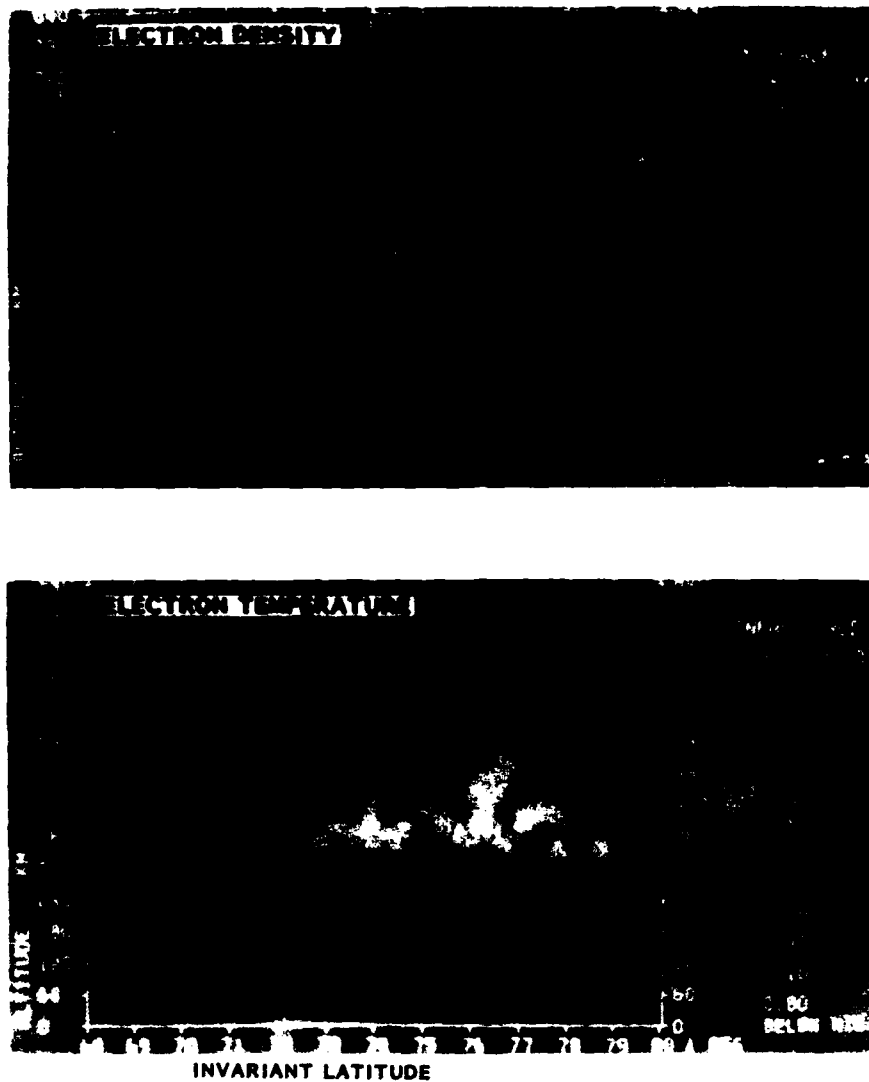


Plate 1. Color plots of electron density and electron temperature measured during an elevation scan on 13 April, 1983, at about 1000 magnetic local time.

consists of electrons from the low latitude boundary layer accelerated through parallel potential differences of about a kV.

In contrast to the afternoon sector, ionization enhancements in the morning

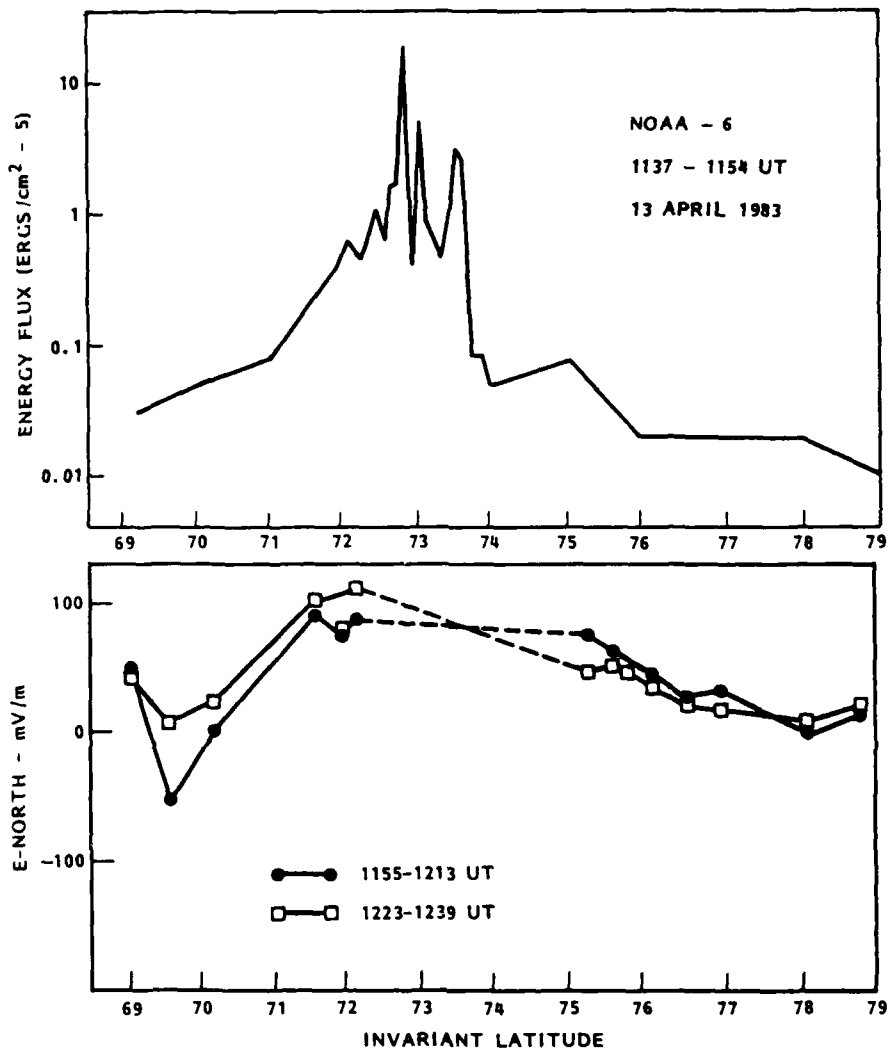


Fig. 2. NOAA-6 measurements of total energy flux and Sondrestrom radar measurements of the northward electric field obtained on 13 April 1983 at about 1000 magnetic local time.

sector that are obviously produced by discrete particle precipitation are rare. In examining the radar data for the 22 mornings during which IMF data were available, we found only two examples of ionization produced by particle precipitation. The absence of such ionospheric enhancements at this local time may be due to several effects. First, as noted above, the precipitating electrons may be very low in energy, thus depositing most of their energy at high altitudes where ionization production is

slow. Second, the precipitation may be weak and diffuse so that it is indistinguishable from ionization produced by solar illumination which is a significant source at these local times. Finally, the discrete precipitation at these local times may occur outside of the radar field of view.

In this paper we have shown two cases of ionization in the morning sector traceable to discrete particle precipitation. Both occurred between 1000 and 1200 MLT during times when B_z was positive and B_y was negative. One was observed in the region of sunward convecting plasma while the other was observed in the region of antisunward convecting plasma.

While the event in the sunward convecting plasma can probably be identified as a morning sector auroral arc, the precipitation in the region of antisunward moving plasma must have been situated within the polar cap. The presence of discrete aurora at very high latitudes in the morning sector has been noted by LASSEN and DANIELSEN (1978) and GUSSENHOVEN (1982). That these features are not observed more often from Sondrestrom may be a result of the size of the auroral oval relative to the latitude range within which the Sondrestrom radar can make measurements. On April 13 the K_p index for the three-hour period from 0900 to 1200 UT was 6 so that the oval was probably greatly expanded at this time. For most of the other mornings included in our data set, K_p was between 2 and 4. When a convection reversal was present on these days ($B_z > 0$) it was usually located between 74° and 76° invariant latitude. Thus, the radar field of view only extended a few hundred km into the polar cap. On 13 April, the convection reversal was located at 71° invariant latitude and a greater portion of the polar cap was observed.

In trying to account for the precipitation features that have been observed from Sondrestrom, it is significant to note that all are associated with gradients in the electric field that are consistent with upward field-aligned currents. In the case of the afternoon precipitation, this corresponded to the region 1 Birkeland current. For the precipitation occurring in the sunward drifting plasma on the morning side, we associated the upward current with region 2 Birkeland current. The precipitation observed on antisunward drifting field lines probably coincided with the polar cusp currents. These currents have been studied by IJIMA *et al.* (1978) and MCDIARMID *et al.* (1978) and were found to depend on the B_z component of the IMF.

With these considerations we can predict the locations at which intense particle precipitation is likely to occur based on the convection patterns that have been observed. Figure 3 shows the general pattern of convection for $B_z < 0$ and $B_z > 0$. Upward field-aligned currents occur where the divergence of the electric field is negative (LYONS, 1978). These regions on the dayside are shown by shading in Fig. 3. Each of the regions of particle precipitation thus far identified from the radar measurements can be associated with one of these shaded areas. In the nomenclature of BURCH *et al.* (1985), the precipitation at the convection reversal in the afternoon for $B_z < 0$ and equatorward of the convection reversal in the morning for $B_z > 0$ are both associated with the viscous cell. The poleward region of precipitation for $B_z > 0$ on the morning side is associated with the merging cell.

It should be noted that although we did not sort our data by B_z , this component of the IMF was never large and positive for a sustained period for any of the data sets

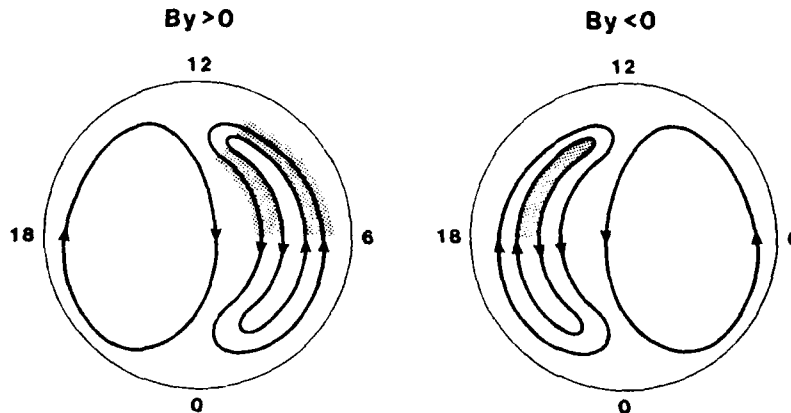


Fig. 3. Relationship between observed precipitation and the large-scale convective flow of plasma. The shaded regions show the locations on the dayside where ionospheric effects of particle precipitation were observed.

and there were no examples in which the convection at very high latitude was sunward. Thus, the type of polar cap arcs that appear under sustained B_z north conditions were not observed on these days. On the other hand, the data shown for April 13 clearly indicates precipitation in the polar cap. The distinction between these two types of polar cap arcs may be that the former is associated with the lobe convection cell, while the latter is associated with the merging cell (BURCH *et al.*, 1985).

6. Conclusion

Many claims have been made about identification of polar cusp precipitation from ground observations. An identification of a precipitation feature as originating from the polar cusp cannot be made solely on the proximity of the feature to local noon. One should instead consider the possible sources of the precipitation. The precipitation associated with the post-noon convection reversal boundary appears to originate from the low latitude boundary layer, and thus is not polar cusp precipitation. However, the precipitation observed on 13 April in a region of antisunward convecting plasma is probably associated with the merging cell (BURCH *et al.*, 1985). For $B_z < 0$, a corresponding region of antisunward drifting plasma exists on the afternoon side of the polar cap. However, as the polar cusp currents are downward in this region, we should not expect the precipitation to be as intense as on the dawnside for $B_z > 0$. Because the polar cusp field-aligned currents change direction on opposite sides of the polar cap, it follows that the fluxes of precipitating electrons associated with the polar cusp must exhibit a corresponding asymmetry. This may account for the results of studies of the distribution of polar cap arcs which show that these precipitation features appear more often on the dawn side in the northern

hemisphere (see, for example, LASSEN and DANIELSEN, 1978).

We thank N. Ness and J. King of NASA-Goddard space flight Center for providing IMP-8 data. The site crew of the Sondrestrom radar maintained and operated the radar during the experiments. This work was supported at Stanford by AFGL contract F19628-85-K-0001 and National Science Foundation grant ATM-82-10562, at SRI by National Science Foundation cooperative agreement ATM-81-17792 and at Lockheed by the Lockheed Independent Research Program.

REFERENCES

- BURCH, J. L., P. H. REIFF, J. D. MENIETTI, R. A. HEELIS, W. B. HANSON, S. D. SHAWHAN, E. G. SHELLEY, M. SUGIURA, D. R. WEIMAR, and J. D. WINNINGHAM, IMF B_z -dependent plasma flow and Birkeland currents in the Dayside magnetosphere. I. Dynamics Explorer observations, *J. Geophys. Res.*, **90**, 1577, 1985.
- CLAUER, C. R., P. M. BANKS, E. FRIIS-CHRISTENSEN, T. S. JORGENSEN, and V. B. WICKWAR, Ion convection in the dayside cleft measured by the Sondre Stromfjord radar, *EOS Transactions, American Geophysical Union*, **64**, 820, 1983.
- CLAUER, C. R., P. M. BANKS, A. Q. SMITH, T. S. JORGENSEN, E. FRIIS-CHRISTENSEN, S. VANNERSTROM, V. B. WICKWAR, J. D. KELLY, and J. DOUPNIK, Observation of interplanetary magnetic field and of ionospheric plasma convection in the vicinity of the dayside polar cleft, *Geophys. Res. Lett.*, **11**, 891, 1984.
- DE LA BEAUJARDERE, O., V. B. WICKWAR, and J. H. KING, Sondrestrom radar observations of the effect of the IMF B_z component on polar cap convection, this volume, 1986.
- EVANS, D. S., The characteristics of a persistent auroral arc at high latitude in the 1400 MLT sector, *Proceedings from NATO Conference on the Polar Cusp in Lillehammer, Norway, 7-11 May, 1984*, 1984.
- FOSTER, J. C., V. B. WICKWAR, and J. D. KELLY, Dayside patterns of plasma convection and density, *EOS Transactions, American Geophysical Union*, **64**, 819, 1983.
- FRIIS-CHRISTENSEN, E. K. LASSEN, J. WILHELM, J. M. WILCOX, W. GONZALEZ, and D. S. COTBURN, Critical component of the interplanetary magnetic field responsible for large geomagnetic effects in the polar cap, *J. Geophys. Res.*, **77**, 3371, 1972.
- GUSSENHOVEN, M. S., Extremely high latitude auroras, *J. Geophys. Res.*, **87**, 2401, 1982.
- HEELIS, R. A., The effects of interplanetary magnetic field orientation on dayside high-latitude ionospheric convection, *J. Geophys. Res.*, **89**, 2873, 1984.
- HEPPNER, J. P., Polar cap electric field distributions related to the interplanetary magnetic field direction, *J. Geophys. Res.*, **77**, 4877, 1972.
- IJIMA, T. and T. A. POTEMRA, The amplitude distribution of field-aligned currents at northern high latitudes observed by Triad, *J. Geophys. Res.*, **81**, 2165, 1976.
- IJIMA, T., R. FUJII, T. A. POTEMRA, and N. A. SAFLEKOS, Field-aligned currents in the south polar cusp and their relationship to the interplanetary magnetic field, *J. Geophys. Res.*, **83**, 5595, 1978.
- JORGENSEN, T. S., E. FRIIS-CHRISTENSEN, V. B. WICKWAR, J. D. KELLY, C. R. CLAUER, and P. M. BANKS, On the reversal from "sunward" to "antisunward" plasma convection in the dayside high latitude ionosphere, *Geophys. Res. Lett.*, **11**, 887, 1984.
- KELLY, J. D. and J. F. VICKREY, F -region ionospheric structure associated with antisunward flow near the dayside polar cusp, *Geophys. Res. Lett.*, **11**, 907, 1984.
- KOFMAN, W. and V. B. WICKWAR, Very high electron temperatures in the daytime F -region at Sondrestrom, *Geophys. Res. Lett.*, **77**, 919, 1984.
- LASSEN, K. and C. DANIELSEN, Quiet-time pattern of auroral arcs for different directions of the interplanetary magnetic field in the $y-z$ plane, *J. Geophys. Res.*, **83**, 5277, 1978.
- LYONS, L. R., Generation of large-scale regions of auroral currents, electric potentials and precipitation by the divergence of the convection electric field, *J. Geophys. Res.*, **85**, 17, 1980.

- MCDIARMID, I. B., J. R. BURROWS, and M. D. WILSON, Magnetic field perturbations in the dayside cleft and their relationship to the IMF, *J. Geophys. Res.*, **83**, 5753, 1978.
- ROBINSON, R. M., D. S. EVANS, T. A. POTEIRA, and J. D. KELLY, Radar and satellite measurements of an F-region ionization enhancement in the post-noon sector, *Geophys. Res. Lett.*, **11**, 899, 1984.
- WICKWAR, V. B. and W. KOFMAN, Dayside red auroras at very high latitudes: The importance of thermal excitation, *Geophys. Res. Lett.*, **1**, 923, 1984.
- WICKWAR, V. B., The polar cap boundary observed in the early afternoon, this volume, 1986.